MODELING AND CONTROL ISSUES ASSOCIATED WITH SCALED VEHICLES

BY

SEAN N. BRENNAN

B.S., New Mexico State University, 1997
B.S., New Mexico State University, 1997

THESIS

Submitted in partial fulfillment of the requirements
for the degree of Master of Science in Mechanical Engineering
in the Graduate College of the
University of Illinois at Urbana-Champaign, 1999

Urbana, Illinois

Acknowledgments

This material is based upon work supported under a National Science Foundation Graduate Fellowship. Any opinions, findings, conclusions or recommendations expressed in this publication are those of the author and do not necessarily reflect the views of the National Science Foundation. Legal stuff aside, I really do want to thank NSF for the opportunities they have provided in my life. I hope this thesis meets their expectations.

There are probably three types of people who will read this thesis: future employers who are reviewing my work as consideration for some future position; future experimenters who are sifting through my work to learn how to do it themselves; and finally my friends and family who have supported me throughout my stay at UIUC and want to know what all the fuss was about. To those who are seeking some useful knowledge out of this thesis, try to get the bad as well as the good out of this work. I made a point of documenting every mistake so that it will not be repeated.

To my future employers: I purposely chose a thesis that was not trivial. As a result, I learned more than I thought I would about how to get things to work, finding the right people to talk to, and the limits I can push myself. You will be the benefactor of this, and you have professor Alleyne to thank for the motivation… "All I ask is that you work as hard as I do".

Thank you Dr. Alleyne for having enough patience with me to let me make my own mistakes, and for always having an open door. You have taught me as much about myself as you have about control: how to listen, how to think about things as other people would best see them.

To my friends, thank you. Thank you Dan Block for taking the time to show me how to do things right, the first time. Thanks to all the drivers who were exceedingly patient while spending their lives watching me tweak things to get them …. just ………. right.

To my familiy: mom, Jesse, Roy, Andy, and even Terry. Thank you.

To my wife Rachel, I love you. It is hard to say in words how much I feel that you are part of me, and how lucky I feel to have found you. Thank you for loving me. Thank you for warm afternoon lunches, for late night talks, for the way your hands fit, the way your voice sounds, for being you. I love you.

Table of Contents

List of Symbols and/or Abbreviations

4WS4WD – An acronym for one of the vehicles used in the IRS that has 4 wheel steering capability and a standard 4 wheel drive system.

ABS (Automatic Braking System) - A system using computer actuated brakes such that maximum braking is achieved without skidding.

DIL (Driver In the Loop) - A control system where the driver's steering input is directly transferred to the front wheels. Hence, any modeling of the vehicle must incorporate the driver as participating in the control loop.

DOF (Degrees of Freedom) - The number of independent motions utilized by a model. For instance, a vehicle model that only examines lateral motion and longitudinal motion is a 2 DOF model.

DOL (Driver Out of the Loop) – A control system where the driver's steering input is transferred to a controller, which then steers the front wheels. The modeling of the control loop can hence ignore the driver input (but use the driver input as a reference signal).

DYC (Direct Yaw Control) – The use of wheel torque to generate a yaw moment and hence steer the vehicle.

IRS (The Illinois Roadway Simulator) – Abbreviation for the experimental testbed used to study vehicle dynamics

LQR (Linear Quadratic Regulator) – A type of control utilizing a cost function whose minimization guarantees an optimal control.

MRC (Model Reference Control) – A feedforward and feedback control method where the design specifications are given as a reference model.

PWM (Pulse Width Modulation) – The use of a variable pulse length to transmit information. This type of system is often used for motor control because of its simplicity and immunity to noise.

Uberquad – A name for one of the vehicles used in the IRS. This vehicle has 4 wheel steering capability and uses an independent motor for each wheel to simulate torque control or braking maneuvers.

1 Introduction

This thesis details the hardware/software integration, dynamic modeling, and control of a scale vehicle system. The complete system, known as the Illinois Roadway Simulator (IRS), provides a means by which vehicle dynamics and vehicle control strategies can be studied on scale vehicles before implementation on full-sized vehicles. A research facility in the area of vehicle dynamics and controls that is able to provide simulation work in combination with industrial data has been lacking: the Illinois Roadway Simulator is the first of its kind to address this need. The purpose of the IRS is to bridge the gap between industrial experimentation and academic simulation research. Lateral control, stability, sensor placement for intelligent control, and intelligent cruise control are just a few of the topics studied on this system. However, the scope of this thesis will be in detailing the technical issues associated with scale vehicle testing and in describing a single area of advanced vehicle control currently under study on the IRS: yaw rate control (spin control) of a vehicle.

The organization of this introductory chapter is as follows. First, a motivation for vehicle research is given, with specific emphasis on safety and performance. Second, a short literature review of the area of vehicle control is given. The specific goals of this thesis are described, including a motivation for using scale vehicles as well as the history of scale vehicle testing. Finally, a summary of the remaining chapters in this thesis is provided.

1.1 Motivation for Vehicle Research

There is a strong motivation to make vehicles “smarter”: that is, the vehicle will partially or completely control its motion to improve safety and/or performance. However, the goals of “safety” do not always align with those of “performance”, and hence a discussion of each is presented separately below. In addition, the implementation of vehicle controllers generally falls into two arenas: full automation, and human driver assistance (Peng et al. 1994). Automation attempts to replace the driver with intelligent control systems, while driver assistance attempts to monitor the driver behavior, provide warnings, assist, and interfere the steering control of the driver when necessary. Technically, the issues involved with each are the same. However, driver assistance must account for driver behavior, which is complex and often unpredictable. As a consequence, driver-assistance is often more difficult to achieve than full vehicle automation. However, driver-assist controllers seem to be the most promising route of research activity and a natural prelude to complete automation.

The goal of this thesis therefore is not to develop an automated vehicle, but to instead assist the driver using a controller. A simple justification for this goal is that it is difficult to create a controller that is as adaptive and intelligent as a human. Until an automated controller can verifiably outperform a human under all circumstances (and drivers are comfortable relinquishing control of their vehicles and lives to a computer), there will likely be strong resistance to vehicle automation despite arguments for increased safety, efficiency, or economy. Arguments against implementing complete vehicle automation as a first step toward automated driving can be found in the literature. Chen and Evrin (Chen and Ervin 1990) note that there are three separate communities capable of funding and implementing complete vehicle automation: the automotive industry, the electronics industry, and the highway community. These three areas are unlikely to join their efforts and budgets to develop the hardware and infrastructure simultaneously for full automation. For the automotive and electronics industries, it is difficult to justify the need to spend their R & D dollars on vehicle-centered automated systems, especially when these markets are outside their 3-5 year research horizon. The highway community is not in a position to support this research, especially when the needs of highway maintenance and operation outstrip authorized tax revenues (Chen and Ervin 1990). Without the equipment or infrastructure, vehicles will not "suddenly" be autonomous. Instead, the beginnings of automation must start by developing controllers that make the vehicle perform better under human guidance.

A question central to the study of vehicle controllers is whether an automated vehicle can outperform a human driver. This question is valid, but the answer (if there is one) depends on the driver. To determine how well a human can drive, a model must be obtained of how the human actually controls the vehicle. Many authors include models of a driver to examine handling characteristics of the vehicle system with the interaction of the human driver model (Cho and Kim 1996; Legouis et al. 1986; MacAdam 1981; Tousi, Bajaj, and Soedel 1988; Tousi 1991). In the above papers, as well as (Weir and McRuer 1970), the driver is modeled as a feedback controller with an error estimation scheme. In general, the driver is modeled as a function containing gains and a time delay (Cho and Kim 1996). A preview error is obtained by using a look-ahead point and comparing it to a desired vehicle trajectory. The distance between the vehicle and the look-ahead point is often called the look-ahead distance. Thus, the major parameters in most driver models are the driver gain, the driver delay, and the look-ahead distance. Since these parameters are largely psychological, they are quite difficult to measure.

From published work, the primary focus on using an automated controller for vehicle emergency driving is to improve the delay related to the time the driver takes to respond to an impending collision or instability. It is well known that the vehicle will become unstable in certain situations if the driver does not react within a certain time frame. It is also well known that the delay in emergency responses in general is the biggest distinction between a poor and expert driver. This reaction delay may include actuator dynamics or human response time (Cho and Kim 1996). Again, we foresee situations where computer intervention or assistance in driving may improve the vehicle response significantly.

Finally, it is currently in the realm of university-sponsored research to bridge the gap between theory and marketable product. Considering funding limitations, vehicle automation will most likely begin gradually in the form of human assistance and improvements in performance rather than complete one-step automation. For this reason, the vehicle controllers developed in this thesis focus on methods to assist, rather than replace, the driver. The following sections outline different arenas where this focus may lie, and the motivation for study in each area.

1.1.1 Safety

The modern automobile is one of the most complex and dangerous machines mankind has yet developed. It was in 1769 that Nicholas Joseph Cugnot made history by constructing and driving the first road vehicle. He also made history by having the world's first road vehicle accident (Nwagboso 1993). Traffic accidents are one of the largest public health problems in the United States: more pre-retirement years of life are lost due to traffic accidents than the combined deaths due to cancer and heart disease (Evans 1991). From 1928 through 1988, more than 2.5 million Americans were killed from vehicle accidents. To put this in perspective, traffic deaths from 1977 to 1988 exceeded all US battle deaths in all the wars in American history (Evans 1991). The annual cost for vehicle crashes in 1998was estimated to be 70 billion dollars, and worldwide 500,000 people are killed annually from automobile accidents (Evans 1991). In the United States, there are an estimated 4.34 million injuries per year due to vehicle accidents, with 94 injuries per fatality (Evans 1991). That is, approximately 2% of Americans are injured due to automobile accidents EACH YEAR, and roughly 30% of people are injured by an automobile accident sometime in their life.

If we examine fatal accidents, more than half of all fatal accidents involve only one car (1986). Consider that in 1988, 44.73% of fatalities were from vehicles colliding with inanimate, stationary objects not found on the road (trees were the primary culprit) (Evans 1991). Vehicle safety does not only extend to the driver, but also it extends to others who may share the highway. A German study conducted in 1985 of 12,000 injury causing accidents revealed that more than half the injuries and half of the deaths involving vehicles were pedestrians, bicyclists, and motorcyclists (Danner, Langwieder, and Schmelzing 1985).

The focus on vehicle crashworthiness generally examines four aspects of a vehicle: crash energy management, car size, occupant volume (a.k.a. “Flail Space”), and human factors (Hyde 1992). What is often neglected, or lumped into “human factors”, is the ability of the crash to be avoided or lessened by faster or “smarter” driver inputs. If we consider the use of a computer to continually evaluate and intercede when dangerous situations arise, we may foresee situations where a small amount of intervention results in a significant improvement in safety. While improvements in the crashworthiness of vehicles is at a point of diminishing returns, the field of automated collision warning and avoidance is in its infancy (Chen and Ervin 1990). An example of this type of work would be the automatic road-departure warning system for motor vehicle drivers (LeBlanc et al. 1996).

1.1.2 Performance

The motivation for vehicle control lies not only in improved safety, but also in improved performance. To examine the motivation for using control to enhance vehicle performance, one simply has to examine modern vehicle control systems. These motivations include improved engine performance (idle, throttle, emissions), transmission control, suspension, traction control (ABS), longitudinal control (cruise control, automated handling systems), and improved directional stability (yaw rate control, spin control, automated driving, and automated handling systems) (Nwagboso 1993). There is some overlap between safety-related control and performance-improving controllers. For instance, an ABS system improves braking performance in icy conditions, which clearly improves vehicle safety. As another example, Smith and Benton (1996) reduced the distance needed to change lanes in an emergency maneuver by 17% by using a controller to steer the rear wheels of a vehicle. The ability of a computer to control an aggressive lane-change maneuver may be important for performance and for safety.

1.1.3 Improved Vehicle Measurements

An often neglected but increasingly utilized area of vehicle control is to simply monitor the status of the vehicle and/or driver and "passively" feedback the situation to the driver. The controller is not “actuating” anything other than the human (or another controller), but the structure in terms of feedback / estimation / sensing etc. are very similar to a controller that actually has some type of physical actuation. An example of this measurement type of controller would be one that simply calculates fuel usage (or miles/gallon) as the vehicle is driving. The intent would be that the driver satisfaction (and hopefully fuel economy) is improved. Another example using a more advanced measurement controller would be one presented by Pasterkamp and Pacejka, where the tire is used in conjunction with a neural network to sense the road friction as the vehicle is driving. The driver is then alerted if dangerous road conditions are detected (Pasterkamp and Pacejka 1997b). Based on this type of measurement, a dashboard type alert system could be developed that notifies the driver of possible skidding, lane change obstacles, impending collisions, and unsafe headway conditions (Kamal 1990).

1.2 Summary of Dynamic Ranges to Motivate Controller Design

The dynamic range of a vehicle is very dependent on its velocity. As an example, it is well understood that aerodynamic forces begin to become significant between 40-50 m/s (Doniselli, Mastinu, and Gobbi 1996). The non-uniform stiffness of an ordinary tire causes the longitudinal dynamics to have much faster pole locations than the dynamics associated with steering input. By examining the dynamic range of each effect, it becomes clear not only what obstacles each controller will face, but also the limitations and the most likely sources of disturbances and unmodeled dynamics. If we examine the frequency range of the vehicle, tires, and aerodynamic forces previously discussed, we obtain the following diagram.

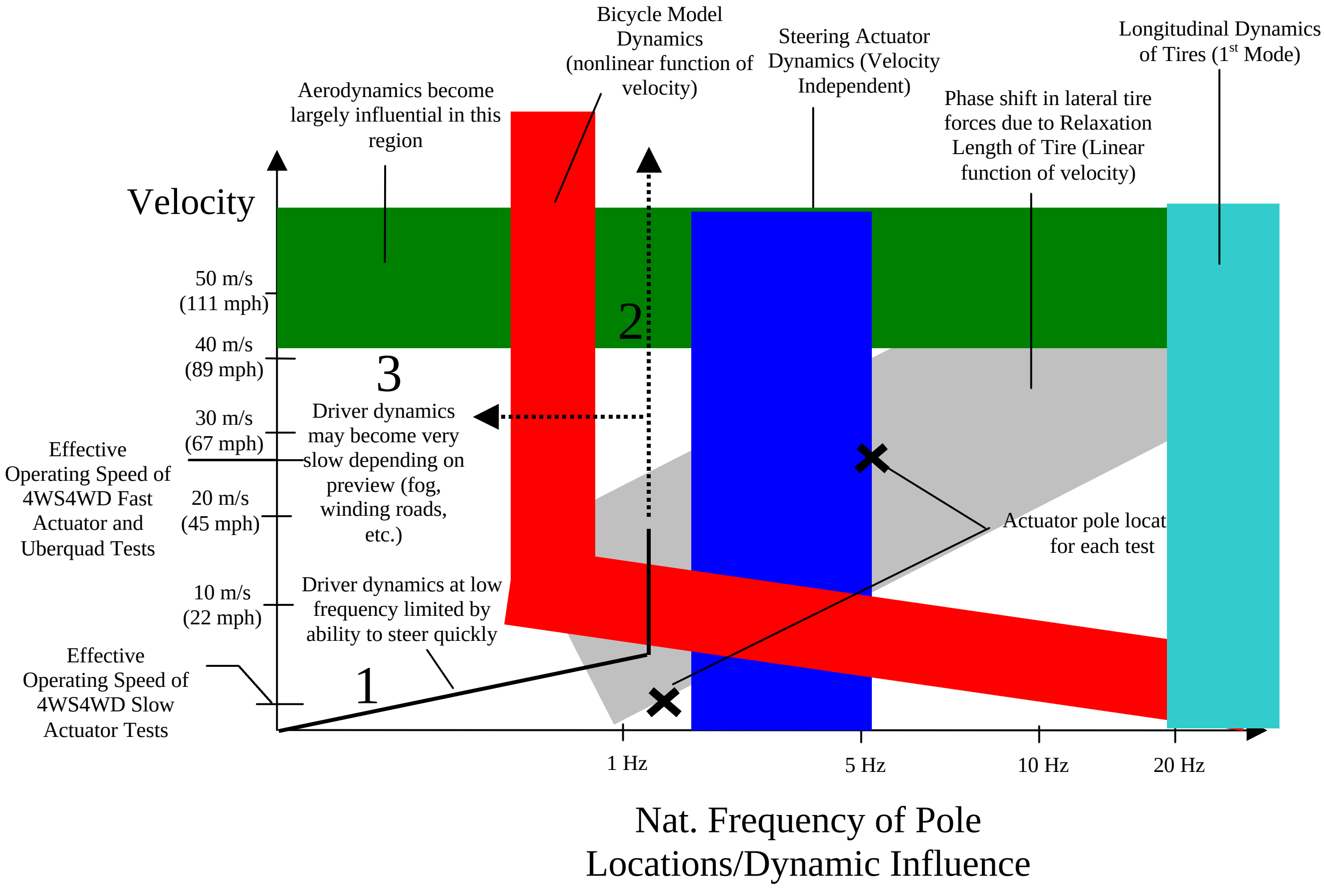

Figure 1.1: Frequency range of driver inputs, lateral dynamics, longitudinal dynamics, actuator dynamics, and aerodynamics.

The above chart shows three regions of interest in terms of vehicle control. Region 1 is where the vehicle is traveling slowly, and the intent of the controller is to improve the vehicle response. This is often achieved by the use of rear-wheel controllers at low speeds that effectively reduce the turning radius of the vehicle. Region 2 represents non-emergency highway driving, where comfort and performance is more important than safety in terms of the controller approach. Region 3 represents the regime where emergency maneuvers may be necessary because driving conditions or emergency situations may impair the driver. The focus of controller development for this thesis is Region 2 and to a small extent Regions 1 and 2. In Region 3, nonlinear dynamics may become significant, while in Region 1 there are very little dynamic or slip contribution.

1.3 Literature Review on Vehicle Dynamics

The following section is a brief overview of the field of lateral vehicle control. A more in-depth analysis of specific control algorithms is provided in the "Controller Development" section of Chapter 4.

1.3.1 Survey Articles

For the interested reader, a short list of survey articles outlining the areas of vehicle control is presented. A good overview of general vehicle control systems is provided in Tomizuka and Hedrick (1995) where the focus is given on engine/transmission modeling and control, suspension systems, traction control and ABS, cruise control and vehicle longitudinal control, and steering systems including vehicle lateral control. There are several books that themselves serves as broad overviews of the field of automotive research. A useful book regarding the basics of vehicle dynamics is written by John Ellis (1989). The book by Nwagboso (1993) is a good introduction to vehicle systems and instrumentation used in vehicles. For vehicle automation, a key issue is feedback of vehicle position. A good article reviewing the state-of-the-art in vehicle sensing can be found in (Peng and Tomizuka 1990a). The merits, drawbacks, and robustness of vision based, magnetic marker, magnetic rod, radar, laser, beacon, reflective, ultrasonic and other guidance systems are discussed. Finally, a broad overview of 4WS steering strategies is presented in the paper by Furukawa and others (1989).

1.3.2 Published Methods for Yaw or Lateral Control of a Vehicle

The published control approaches can be divided topically in many different ways: by method of control input (2WS, 4WS, DYC), by controller design methods (optimal, neural network, parameter space design), or by controller implementation structure (feedforward, feedback, or combinations). For this section, the controller structure (feedforward versus feedback) is chosen as the metric of comparison. Although the use of feedback will make a system more robust to unmodeled dynamics and disturbances, the same feedback may increase system cost and lead to worse performance in the event of sensor/actuator failures. Many authors, notably Inoue and Sugasawa (1993), recognize that this tradeoff is central in the choice of vehicle controllers. To simplify the presentation of the control methods, the figure below is taken from the above authors to outline the different control approaches presented in the literature.

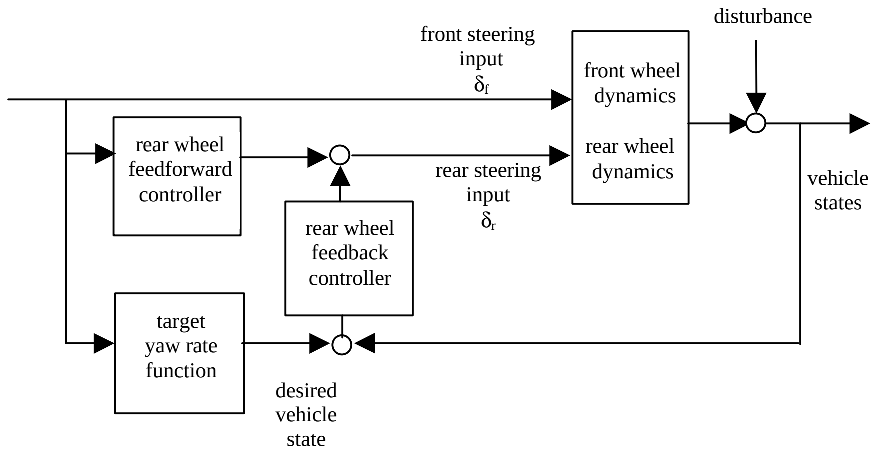

Figure 1.2: A block diagram of a general 4WS-vehicle control system.

If not stated otherwise, it can be assumed in the controllers described below that the driver retains control over the front wheels. There are vehicle control designs, however, where this may not be the case (Okuno, Kutami, and Fujita 1990). These systems are often referred to as drive-by-wire controllers because the steering is controlled directly by the computer, and indirectly by the driver who sends steering signals to the steering computer. Other types of control include safety-monitoring and driver assist. A safety-monitoring controller is one where the driver steers the vehicle, and the controller has no control over steering. A driver assist controller is one where the driver maintains direct control over the vehicle, but the controller can augment the steering by some other control input such as the rear wheels or brake and torque input. Throughout this literature review, special note is given to controllers that remove the driver's direct input by including a controller for the front wheels.

Additionally, we can divide the controller methods by the acceleration region for which they were designed (Nagai, Hirano, and Yamanaka 1997). In general, the more acceleration forces on the vehicle, the more non-linear the vehicle behavior and consequently the more complex the controller structure required for appropriate vehicle control. Referring to Figure 1.3 below, we can see that a system that provides good performance in one region may not provide good performance in another. For instance, a Direct Yaw Controller (DYC) that utilizes brake input to aggressively correct a vehicle in Region 6 would not be suited to Region 1, where only minor steering corrections are needed. Table 1.1 gives a summary of the regions, along with descriptions of the maneuvers encountered in each region and the types of controllers used. It should be stated beforehand that the acceleration regions are not strictly defined and that the performance and slip of a tire is a more appropriate metric. For instance, a controller suited for Region 10 may be more suited to a wheel that is skidding over gravel with a deceleration of 0.1 g's, even though the diagram above may not suggest this. In extreme cases or under changing operating conditions, the best metric will nearly always be the relationship between available forces from the tire and steering angle/torque input.

Unfortunately, it is very difficult to determine the tire model on-line, and hence acceleration may be a more feasible, but less precise, metric.

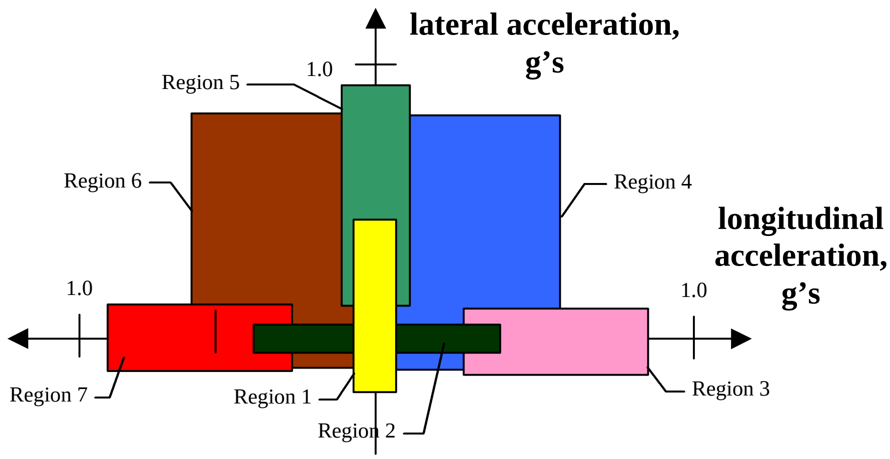

Figure 1.3: An acceleration plot describing general areas of research activity.

Table 1.1: A summary of regions of operation.

Region	Behavior	Situation	Controller
1	Lat. vehicle dynamics are linear, long. dynamics are negligible	Steady highway driving	AHS Controllers
2	Linear long. dynamics and lat. dynamics	Highway accelerations	Adaptive Cruise Control
3	High long. acceleration, nonlinear long. tire models	Skidding or "Peeling Out"	ABS, TCS
4	Nonlinear long. deceleration, nonlinear lateral accelerations	Skidding AND Spinning	None
5	Negligible or linear long. dynamics, non-linear lat. dynamics	Spinning	DYC
6	Nonlinear long. acceleration, nonlinear lat. Accelerations	"Peeling Out" AND Spinning	None

A description of each region in the above diagram follows. Region 1 is the area where control systems based on linear vehicle models have demonstrated good performance in experimental testing (Peng et al. 1994; Smith and Starkey 1994; Smith and Starkey 1995). This area, with lateral accelerations less than 0.3 g's (Lee 1997), is where the vehicle velocity is approximately constant and there is little acceleration in the longitudinal direction. This region would characterize non-emergency highway driving, and is the focus of the vast majority of vehicle automation research. Region 2 is the area where a linear tire model remains valid for acceleration and deceleration and the lateral acceleration is small (very little steering). This area would be where adaptive cruise control systems usually perform. Most highway-type driving remains in Regions 1 and 2. Region 3 refers to an area where there is very aggressive acceleration to the point where a linear tire model is no longer valid. The non-linear tire effects such as traction come into play in this region, and hence Traction Control Systems (TCS) often operate in this region. It should be noted that on roads where the tire friction is low (gravel, snow, etc.), the vehicle behavior may be best controlled by systems suited for Region 3 even though the formal acceleration criteria are not met. Region 4 refers to the area where there is very aggressive longitudinal and lateral acceleration. This area is usually not encountered on the roadway, and very little published data describing controllers for this region have been encountered. Region 5 refers to situations where very aggressive steering maneuvers are performed such that the vehicle model is no longer governed by a 2 DOF model. Examples would include a severe avoidance maneuver or unintended roadway departure. Several authors describe this region to begin around 0.3 g's (Lee, Mariott, and Le 1997; Peng and Tomizuka 1990a; Peng and Tomizuka 1990b; Smith and Benton 1996; Smith and Starkey 1994; Smith and Starkey 1995) and continue up to the tractive limit of the tire (usually about 0.8 g's). Again, this region is not strictly determined by acceleration, and is assumed to start where the tire model is no longer linear. The speed in this region can be assumed approximately constant, but there is more variation than Region 1 due to harsher maneuvers.

1.3.3 Publishing Authors and their Vehicle Research Institutions

The authors and institutions presented here in no way represent all of the publishing authors worldwide. Instead, it is a list of publishing authors encountered while conducting literature searches in the field of vehicle dynamics. It is divided between overseas and domestic research institutions.

The leader in vehicle controls in terms of new methods that are being implemented in commercial vehicles remains the Mercedes-Bosch group led by Robert Bosch GmbH. This group currently has a commanding lead in the field of interactive chassis systems, and was the first group to feature commercial yaw-rate control systems (Sherman 1995b). Authors associated with this group include E. Zabler, F. Heintz, R. Dietz, among others. The Delft Institute in the Netherlands has conducted a volume of very practical vehicle research by the Road-Vehicles Research Institute. This work has been published under the authors Besselink, Higuchi, Jansen, Van Oosten, Palkovics, Pacejka, Pasterkamp, J. van der Weide, R.F. Wolffenbuttel, J.A. Foerster, and Zegelaar among others.

Other foreign vehicle research centers include the Honda Research and Development group, whose articles are generally published originally in Japanese journals and translated to English. Authors publishing with Honda include Yoshimitsu Akuta, Nobuyoshi Asanuma, O. Furukawa, Manabu Ikegaya, Y. Shibahata, K. Shimada, T. Tomari, and Kiyoshi Wakamatsu. Toyota sometimes publishes work under Yutaka Hirano, who works closely with Tokyo University with Masao Nagai and Sachiko Yamanaka, among others. Additional Toyota authors include Katsutoshi Horinouchi, Takashi Yonekawa, M. Mutoh, Tamio Kanou, Seisyu Utsumi, and Yoshihisa Nagahara. Mazda has published work through its Technical Research Center by Kenji Fujita, Atsushi Kutami, and Akihiro Okuno. Their particular focus in recent years has been the development of automated cruise control systems that utilize vision sensing (Okuno, Kutami, and Fujita 1990). Mitsubishi Motors Corporation has released vehicle dynamics articles associated with riding comfort under the authors Kazuya Hayafune and Hiroaki Yoshida. Nissan (a.k.a. Nippondenso Co. Ltd.) has developed recently a variable dynamic vehicle called the Simulator Vehicle that is capable of varying yaw rate and lateral acceleration response characteristics independently via software (Sugasawa, Irie, and Kuroki 1992). Authors publishing from Nissan include F. Sugasawa, N. Irie, and J. Kuroki. In their IC Engineering Department, publishing authors include O. Ina, Y. Yoshino, and M. Iida among others. In Europe, articles are presented by the ITT Automotive Europe by B. Lammen, F. Kemmler, U. Judaschke, and S. Muller.

In the United States, domestic manufacturers have published a significant amount of vehicle research. E. Ahring has published vehicle dynamics articles at Ford A.G. in Germany. Tom Pilluti of Ford has published several articles related to differential brake steering (direct yaw control). General Motors Research Laboratories publishes vehicle control articles through Mounir M. Kamal and others. The two most significant academic institutions currently conducting vehicle research in the United States are the University of California, Berkeley with the PATH project, and the University of Michigan, under the University of Michigan Transportation Research Institute (UMTRI). U.C. Berkeley's California PATH program (Partners for Advanced Transit and Highways) was developed with a long-term implementation and application of automated vehicle controllers in mind. The university currently maintains the Richmond Field Station where vehicle controllers are tested. The objective of this program is to develop a system that is not only high-performance, but also platform independent. The ultimate goal is to develop systems suitable for large-scale implementations with minimal lead-time in the development and implementation phase (Peng et al. 1994). Authors associated with the PATH program are: Huei Peng, Masayoshi Tomizuka, Weibin Zhang, Steven Shladover, S. E. Desoer, J.K. Hedrick, J. Walrand, W. D. McMahon, S. Sheikholeslam, N. McKeown and others. At the University of Michigan, vehicle research papers are often presented under the authors Kan Chen, Robert D. Ervin, Gregory Johnson, W.B. Ribbens, and Charles MacAdam among others. Research on vehicle dynamics has been conducted for decades at this research institution; the extent of their studies is too extensive to list in this short discussion. During the 70's and 80's, Fenton and colleagues at the Ohio State University conducted a long term and large-scale project. Work is still being published at their Center for Automotive Research under Young Cho, Dennis A. Guenther, G. Rizzoni, Bong-Choo Jang, Matthew Y. Rupp, and Charles M. Woodburn among others. The well-published authors Smith and Starkey conduct vehicle dynamic research at their respective universities. Dr. Smith's research was formerly conducted by the Integrative Modeling Research Laboratory at Louisiana State University before his leaving the university. Dr Starkey conducts research at Purdue, where the authors Anthony Will, Stanislaw Zak have also published papers.

1.4 Goals of This Study

The intent of this research is to demonstrate new techniques for vehicle control that improve vehicle performance and safety. For the work discussed in this thesis, the specific goal is to improve vehicle handling and stability. As will be shown in later sections, there are many controller methods available to achieve this goal; however, a Model Reference Controller (MRC) approach is selected for this study due to the "intuitive" nature of the performance specifications, and the "standard" form of implementation. When a driver wishes to improve vehicle performance, they usually do not specify that the pole locations be moved, or that the rise-time or overshoot be changed. Instead, the performance is described in terms of other vehicles. For instance, a driver may wish that their station wagon behaved like a Porsche while in the city, but handle like a Lincoln Towncar on the highway. Each vehicle can be represented dynamically by a different reference model, thus suggesting a model-reference type of controller structure.

A primary purpose of the Illinois Roadway Simulator is simply to validate the performance of vehicle controllers. Thus, ease of implementation, adaptability, and evaluation are important considerations. From the beginning, the primary intent in selecting MRC methods was to maintain a simple controller structure that is easily adaptable so that the driver may change performance specifications "on-the-fly". In terms of implementation, MRC methods in the transfer-function domain are relatively easy to implement. In terms of adaptation, Model Reference Controllers are used in adaptive situations as Model Reference Adaptive Control, so the structure developed in this thesis can easily be extended to adaptive situations. In terms of evaluation, the performance of the resulting control is easily evaluated because of the use of a reference model. As a comparison, the performance measures for some control techniques such as LQ, optimal control, neural networks, or fuzzy logic are not always clear. It is easy to obtain good vehicle performance when the evaluator chooses the metric of performance measurement. For this thesis, it is relatively simple to evaluate the performance of the vehicle controller. If the vehicle tracks the reference model, the controller is probably working well.

One final goal of this thesis is to validate the use of scale automobiles for dynamics and control studies. Scale testing as a science is usually applied to capital-intensive situations such as cargo ships, aircraft, and spacecraft. However, the advantages of using a "real-life" system instead of a simulation become obvious in the implementation stages of the controller. To restate this goal, this thesis is an attempt to unify the results of what today seems to be three separate fields of vehicle dynamics study: simulation based studies using theoretical equations of motion, full-sized vehicle testing based on semi-empirical analysis, and the third method based on scale vehicle testing. The following section is intended in part to motivate the use of scale vehicles to refine performance before risking capital, drivers, and time transferring a control method from simulation to full-scale vehicles.

1.4.1 Motivation for Using Scale Vehicles

From a research standpoint, the primary advantage of using scale vehicles over full-sized vehicles is cost. The use of a full-sized vehicle testing is prohibitively expensive to most academic institutions. The few research sites conducting vehicle testing require very sizable grants to conduct their research, and most of this capital goes simply to infrastructure development such as equipping the vehicles. The cost of the entire Illinois Roadway Simulator to date is well under $30,000, which includes the cost of 5 vehicles (2 of the 3 vehicles have been completely rebuilt twice), three computers (also upgraded twice), the treadmill, the transmitter system, the amplifier systems, and motors including spare parts. This price tag also includes operating costs for 4 years. For comparison, it is estimated that the cost of equipping a full-sized vehicle for autonomous control is in excess of $100,000 (Note: this cost does not include any research). This price tag is simply out of the range of ordinary research institutions. In comparison to scale testing, the intellectual return on each research dollar spent cannot be very large for full-sized vehicles when the majority of the allocated money is spent simply on equipment and road usage. Although these costs buy "realism", this realism is sacrificed by the cost intensity. Full-sized autonomous vehicles at research universities are rarely put in real-world situations that push vehicle performance to its limits.

There is an additional economy of time using a scale vehicle system. The time required to change or modify a scale vehicle is very small compared to full-scale vehicle testing. From the standpoint of commercial vehicle development, a primary cost consideration is the start-up and turn-around time needed to attempt a new control idea. If all the parts are at-hand, it is quite easy for a single student to build an entire scale vehicle "from scratch" in a single day. The variety of commercially available parts means that, if a novel part is needed, only small modifications of an existing part are usually required. The durability of the R/C vehicles and the ability to physically intervene during an accident mean that the downtime due to vehicle breakage is small. The use of a treadmill system means that no scheduling of roadway usage is needed, and on-site real-time evaluation of vehicle performance can be conducted at any time or any hour in the day. More importantly, the road conditions remain as constant as required by controller testing. Frequency responses requiring a full day of testing can be conducted continuously on the vehicle using swept-sine techniques. This feat would not be achievable with full sized vehicles unless very expensive GPS systems were employed.

The final motivation for scaled vehicles is the most important: they are simply safer than full-sized vehicles to test. No drivers are put at risk as the computer drives the car at scaled highway speeds. There are no pedestrians or roadside traffic to worry about. The treadmill surface can be varied quickly and easily to simulate various road surfaces that may be dangerous for a driver to be on, and the treadmill itself is designed for consumer safety (finger guards, belt protection, and pinch guards). The use of the treadmill surface as a driving road makes testing safe, consistent, and repeatable. Because of the increased safety, more aggressive vehicle testing can be conducted on the IRS than will likely ever be tested with a full sized vehicle with a passenger inside. New controller ideas and techniques can be tuned "on-the-fly" without a significant worry for safety (and sometimes stability). It is not uncommon to "crash" the vehicle a half dozen times in a single day of aggressive testing, with no adverse effects on the vehicle. In fact, the biggest safety hazard encountered thus far is the tendency of the author to forget that the treadmill is moving after a long night of testing, lean against the moving surface, and be quickly "scooted" to the floor.

1.4.2 History of Using Scale Vehicles

As stated earlier, there are two distinct methodologies to examine vehicle dynamics. The first is to establish the governing equations of motion and conduct a simulation-based study, and assume that the vehicle is strictly governed by the theoretical differential equations and the parameters used in those equations. The resulting controllers are in general solved in terms of these parameters. Fundamental to the controller is the assumption that the unmodeled dynamics are insignificant enough to be compensated by feedback. Well over 90% of the controllers encountered in literature are based on this methodology. The second methodology is to test a full-sized vehicle and conduct semi-empirical analysis (black-box approach) of the full-sized vehicles using input/output modeling. The use scale vehicles generally allows both approaches. An advantage of scale vehicles is that they encourage both methodologies: the theoretical analysis is used to validate scale dynamic similitude, but the use of a physical model ensures that critical dynamics will not likely be neglected.

Before the advent of simulation-based modeling, nearly all vehicle testing was conducted using scale or full-sized vehicles. Naturally, the use of scale vehicles was preferred because of cost reasons, and consequently there was extensive use of scaled vehicles through the mid-1960’s due to cold-war military research and space-race sponsored studies. Although the traditional association of scaled vehicles is with wind tunnels, the use of scale vehicles has extended to automobiles in the areas of crash reconstruction, vehicle-soil interaction (tire forces), suspension analysis and dynamics, and roll dynamics.

Scale testing of amphibious vehicles was conducted extensively at the Army’s Land Locomotion Laboratory in Detroit (Bekker 1969). Studies conducted using these scaled vehicles led to the development of shrouded tires on amphibious vehicles (Rymiszewski 1965) (Bekker, 1969) (p. 636).

To begin discussing land vehicles, it should be noted that the primary likelihood of disagreement between scale vehicles and full-size vehicles at higher speeds is in the tire-road interaction. Extensive scale model studies were conducted in the 1960’s that specifically examined tire forces of scale models and their scaling, and showed that scale vehicle testing was the best way to determine the vehicle turning radius (Bekker 1969) (p. 671). These studies, although likely motivated by the first use of a vehicle on the moon, demonstrated themselves as very good analysis tools for the use of experimental determination of overall vehicle dynamics. An example would be the use of a scaled vehicle to analyze vehicle performance over rough terrain (Bekker 1969). Ironically, the vehicle used in this study and others (Pavlics 1966) to examine full-sized vehicle motion on extraterrestrial surfaces seems to be the inspiration for replacing those same vehicles. Today, small robotic vehicles dominate over "man-sized" robotic rovers. The scale, wheel placement, and climbing motions of the scale vehicles of the 1960's are nearly identical to the full sized Mars Sojourner robot used for exploration today. This is a good example where the use of scale vehicles eventually became a separate field of study.

In the field of automobile accident reconstruction, detailed analysis was conducted examining automobile crashes of scale vehicles before the advent of computer simulation based studies. Conditions for dynamic similitude between scale and full sized vehicles governed by similar crash forces have been derived and examined historically. Experiments have been conducted that demonstrate experimental agreement between scale and full-sized automobiles in non-crush dynamics of automobile accidents (Emori 1969).

Scaled vehicles have been used to study dynamic behaviors of complex multi-body vehicle systems. This work has focused especially tractor-trailer combinations, with specific focus on trailer snaking. As far back as 1930’s, Huber and Dietz (1937) used a “running roadway” (a treadmill) to conduct experimental work with small-scale models of tractor-trailer combinations (Bekker, 1969) (p. 538). This method of using a treadmill to study vehicle dynamics was also used by Zakin (1959) to study trailer stability (Bekker, 1969)(p. 538). A comprehensive study during the 1960's by the U.S. Army Land Locomotion Laboratory was conducted examining the turning behavior of two-unit, tracked, articulated locomotion using scale vehicles (Clark 1960) (Bekker, 1969)(p. 539). This study included nonlinear turning behaviors as well as steady-state turning for a variety of vehicle configurations. A validation of the turning radius was conducted for tracked vehicles using scale vehicles in the 1950's by Nuttal and others (Nuttal) (Bekker,1969) (p. 539). Nuttal's tests were conducted at very low speeds and low slip angles.

For very complex multi-mode vehicle behavior, it has been suggested that the use of scale vehicles may be limited (Bekker 1969). An example provided by Bekker would be the use of scale vehicles to tune the suspension systems of vehicles over very rough terrain (obstacles larger than the vehicle itself). Marquard conducted preliminary work using scale vehicles in this manner. His research suggests that scale vehicles might, in fact, scale correctly *even in this usage*, although dynamic similitude is difficult to prove (Marquard 1937) (Bekker, 1969) (p. 558).

Today, there currently very little use of scale vehicles when compared to previous research institutions. However, there has been a recent revival in the use of full-sized vehicles where each vehicle is "tuned" beforehand to express variable dynamics. The concept of using a single vehicle with varying parameters was first considered by General Motors Corporation in the 1970's (McKenna 1974). The Nissan Motor Company has followed this example in 1992, developing a vehicle capable of independent yaw and lateral acceleration response characteristics (Sugasawa, Irie, and Kuroki 1992). Recently, researchers at the California Institute of Technology in conjunction with the National Highway Safety Administration and NASA developed a vehicle with variable dynamics and have used it for model-following controllers as well as dynamic evaluations (Lee 1997; Lee, Mariott, and Le 1997).

1.5 Overview of Remaining Chapters

The remaining chapters are organized as follows. In Chapter 2, a system description is given of the Illinois Roadway Simulator (IRS), including the vehicles, computer systems, and control loops. Chapter 3 discusses modeling and system identification covering treadmill dynamics, longitudinal vehicle control, theoretical vehicle dynamics, and measured vehicle dynamics. In Chapter 4, a control strategy using Model Reference Control (MRC) is introduced, and alternative methods of control are discussed. Chapter 5 details the results of using this control strategy. Conclusions and future work are discussed in Chapter 6.

2 IRS System Description

2.1 A General Description of the System

The focus of this research has been to develop a scale version of a vehicle and a roadway for safe and economic testing of vehicle controllers. To that end, the Illinois Roadway Simulator (IRS) has been developed. The IRS is an experimental testbed consisting of scaled vehicles running on a simulated road surface, and can be thought of as a vehicle counterpart of a wind tunnel. Instead of moving wind around a stationary scale aircraft, a roadway (treadmill surface) is moved under a scale vehicle.

As discussed earlier, there are several advantages of the IRS over full scale vehicle testing. First, the availability of scale vehicle components makes construction simple and very cheap. The durability of these vehicles and the ability to intervene during an accident makes testing safe and repeatable. The scheduling and use of public or private roadways is not an issue. No drivers or pedestrians are put at risk during testing of aggressive vehicle controllers. The roadway surface can be varied quickly and easily to simulate changing road conditions. The simulator is dynamically realistic in that it includes actuator, sensor, tire, and communication dynamics and nonlinearities that are seen in actual vehicles, but often neglected in computer simulations. Finally, testing and theoretical analysis has shown that scale vehicle dynamics follow the same trends as full-scale vehicles under certain operating conditions.

The Illinois Roadway Simulator (IRS) testbed begins with the scaled roadway surface, which consists of a 4 x 8-ft. steel-framed treadmill capable of top speeds of 15 mph. The belt is kept in place by a plywood running board underneath the surface with 1/4" channels down the length of the board. These channels provide a path for two small rubber-toothed belts that run the inside length of the belt to keep the belt straight. The belt itself has a very smooth surface and was constructed to not have a seam or notch to affect the testing of a vehicle. Two rollers support the treadmill surface, where one roller is geared to a DC motor drive by a timing belt. Some modifications were made to the original simulator as precautionary measures. A barrier was originally built around the belt of the simulator to prevent a vehicle from running off the side of the treadmill. However, in the case of an accident where the car impacted the barrier, the car would bounce back onto the moving treadmill often at the wrong orientation, thus resulting in an even larger collision. For this reason, the barriers were later removed. Also, the "hood" of the treadmill was altered to provide easy access to the drive and sensors.

Scale vehicles are run via a standard transmitter on this treadmill. The remainder of the IRS consists of a driver console, a 400 MHz Pentium II computer (formerly a 75 MHz Pentium), a transmitter/receiver system, and a vehicle position sensor system. Each of these subsystems is described in great detail later in this chapter.

The controller/hardware loop begins with a reference signal. The signal can come from either the driver console or from a function imbedded in the controller code. The entire system is sampled at 1 kHz. The computer then applies the desired vehicle controller, and outputs control commands to the vehicle via a transmitter (for the 4WS4WD vehicle) or amplifier system (for the Uberquad vehicle). If a transmitter is used, a receiver system on the vehicle transforms the transmitter's FM signals into a pulse-width modulated signal, which are then sent to the vehicle actuators. Each actuator has a built-in controller that converts the pulse-width-modulated signals into reference commands.

To maintain the vehicle on the treadmill, a longitudinal controller uses the vehicle's inertial position as feedback and sends an output voltage signal to the treadmill. The treadmill uses an industrial motor controller that converts the input voltage level to a reference speed, and adjusts the DC drive motor current to match this speed accordingly. The diagram below gives an overview of the entire system:

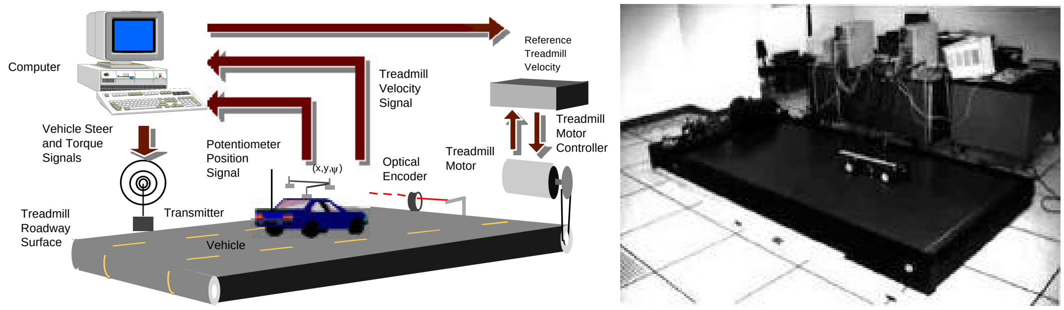

Figure 2.1: Diagram of the control loop used on the IRS (left), and a picture of the IRS system in its early stages (right).

The feedback loop begins with a position sensor mounted on the vehicle. The sensor consists of a 3-bar linkage with potentiometers or encoders at each joint. The angles from each joint are then used to determine the position of the vehicle on the treadmill. The treadmill speed is monitored through an encoder wheel mounted on the drive shaft of the motor. Depending on the vehicle, wheel velocities can also be measured via encoders.

There are currently three vehicles in use on the IRS, each with different operating capabilities. The simplest car is a 2WD vehicle with front wheel steer, and is used to test following strategies and sensors. The second is a 4WD vehicle with independent front and rear steering. This vehicle is used to conduct basic vehicle dynamics and controller analysis. The most advanced vehicle is a custom built, independent wheel torque vehicle. It has a separate motor on each wheel, is front and rear steerable, and has encoders on each wheel monitoring wheel velocity. This vehicle is used to test ABS and integrated chassis controller strategies.

2.2 *Types of Vehicles*

There are currently three scale vehicles in use on the IRS: the follow car, the 4WS4WD vehicle, and the Uberquad. The follow car is a 1/10-scale rear-wheel-drive vehicle with front wheel steering. It is used to test following strategies and vehicle roadway sensing. It is equipped with four optical sensors that are used to sense a light source in front of the vehicle. By measuring the resistance change across the photoresistors, the location of the light source can be determined and used for tracking another vehicle.

Professor Alleyne of UIUC presented work on this follow vehicle at the 1998 IEEE Transactions on Mechatronic Systems.

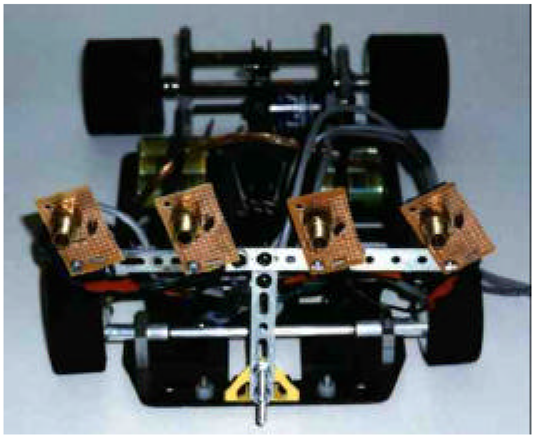

Figure 2.2: The follow vehicle.

A second vehicle, referred to in this thesis as the 4WS4WD vehicle, has been the focus of most of the vehicle testing to date. This vehicle has front and rear steering capability and is driven by a single motor via a standard 4 Wheel Drive (4WD) type system. The vehicle is 27 cm long (front to rear axle) with a track of 19.5 cm. Early versions of this vehicle utilized a bar mounted on top of the vehicle that allowed the position sensor to be moved laterally along the vehicle. This was used for studies of vehicle dynamics and its dependence on sensor placement. As shown theoretically in later sections of this thesis, the sensor placement was shown to be a type of feedback. After reaching this conclusion, the author remounted the position sensor for the vehicle to the top of the center-of-gravity (CG) of the vehicle. In addition, encoders were mounted coaxial to the actuators to monitor actuator angles. This allows studies of the actuator dynamics in the closed-loop system. The first actuators used were Futaba S9304 series, and were found to have dynamics that were slower in bandwidth than the vehicle dynamics. Modifications were made to the vehicle to make its dynamics slower (primarily by increasing the mass and moments of inertia), and faster Futaba S9402 servos were substituted to improve performance. The dynamics of the vehicle and actuators under both configurations is discussed in great detail in later sections.

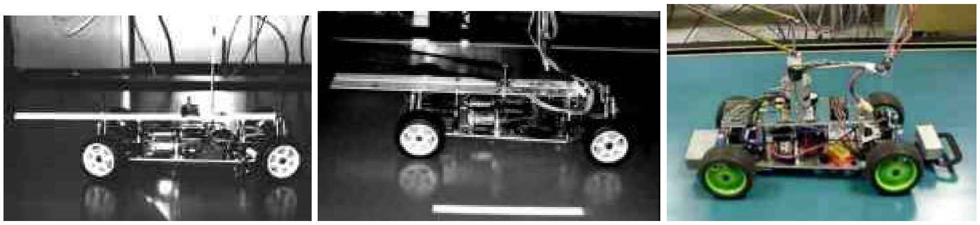

Figure 2.3: The 1997 4WD4WS vehicle (left), the 1998 version (center), and 1999 version (right).

The most advanced vehicle is known as the Uberquad and is completely custom-built. It has a separate motor to drive each wheel, and has front and rear steering capability. Each wheel and steering actuator utilize coaxial encoders to monitor wheel rotation and steering angle. To overcome limitations encountered with an R/C transmitter system, the Uberquad was modified to utilize direct-drive DC motors for the wheel torque and steering actuation rather than servos and RC-drive motor controllers. Also, unlike the previous two vehicles the Uberquad was designed from the beginning to dimensionally scale very close to a real vehicle with a track of 1.5 meters and length of 2.7 meters. The track and length of the Uberquad is 0.21 meters and 0.39 meters, maintaining a ratio from scale to full-size vehicles of approximately 1 to 7.1. The Uberquad is used to study torque control of the vehicle's yaw rate and lateral position, as well as more advanced control techniques. These controllers are presented in Chapter 5 of this thesis.

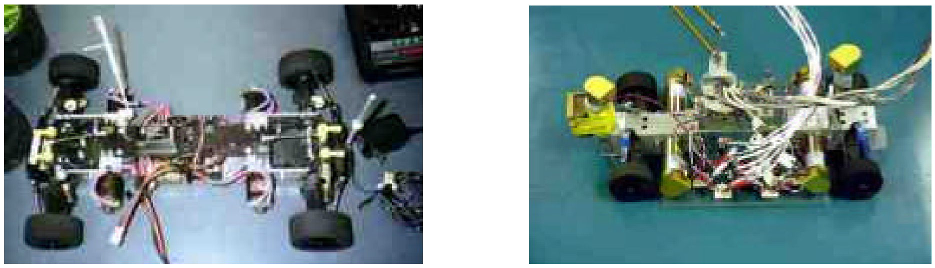

Figure 2.4: The 1998 versions (left) and 1999 versions (right) of the Uberquad vehicle.

2.3 The Computing System

2.3.1 The Performance Limits of a Non-Dedicated CPU System

Because of cost and implementation reasons, it was decided that a non-dedicated CPU system would be used for data-acquisition. The term "non-dedicated" refers to the use of a PC based I/O system, rather than a microcontroller or a DSP to control the vehicle. Because the PCs CPU must in part run the software associated with background tasks, disk access, etc., it is not capable of the same sampling and performance capabilities as a dedicated DSP. Hence, the performance capabilities of this system are more limited. However, the PC-based system is much more affordable, easier to upgrade, and provides a better platform for rapid-prototyping of control systems. In addition, the current system provides real-time graphing capabilities that are ordinarily not affordable on a DSP system.

The original design of the IRS used two 75-MHz Pentium computers to control the vehicle. The concept was to use one computer to control the vehicle and another to control the treadmill. A network system was developed where the computers communicated control and feedback information between each other utilizing digital I/O and flags to coordinate timing. This network system proved difficult and unwieldy to use in practice and the full computational capabilities of each computer were being used more for communication than control. Eventually, the entire I/O system was consolidated onto one computer, with the resulting system being much easier to debug and much easier to code.

As the speed of commercial PCs increased, the system was eventually upgraded to the current computing platform. Currently, a 400 MHz system is being used with 128 Megabytes of RAM. One problem with the upgrade to the new system was the need to maintain ISA slots for the I/O cards. The PC industry is phasing out the use of ISA slots; however, the controller boards previously used were completely based on the ISA bus. As a consequence, one of the previous 4 ISA boards was replaced with its PCI bus counterpart in order to be implemented on the new system.

2.3.2 Data Acquisition Boards

For the PC based system used in these experiments, the central limitation to the data acquisition speed of the control loop is the I/O boards. The time it takes the computer to read an external voltage, send a voltage out, read an encoder, or read digital inputs and outputs depends primarily on the hardware used by the computer. The following time-loading values were obtained by doing 1,000,000 consecutive samples on the 75 MHz Pentium and timing the length of time needed to complete each of the following:

1 Channel Analog Read on the 815 board	75.46 micro sec
1 Channel Analog Write on the 802 board	8.62 micro sec
1 Encoder Channel Read	19.39 micro sec
Reset the timer on the 800 boards (with error checking)	60.36 micro sec
Reset the timer on the 800 boards (w/o error checking)	58.49 micro sec
Read the timer on the 800 boards	34.44 micro sec

These times represent the minimum time needed to perform each reading of external voltages, and are limited primarily by the I/O boards. These sampling times place hard limitations on the speed of the controller used. Unless otherwise stated, all inputs and outputs are conducted at a 1 kHz sampling frequency.

There are currently 4 boards used in the PC system: two Western Digital ISA 4-channel encoder boards, one Computer Boards RTI-802 ISA analog output board, and one Computer Boards RTI-815 PCI board. With the use of an encoder-sensing arm, a minimum of 4 encoder measurements is needed: 3 from each arm joint and one to monitor the treadmill velocity. With the addition of actuator or wheel position encoder measurements, another encoder board is needed. The RTI 802 board has the capability of outputting 8 analog channels. The RTI 815 board can input 16 analog channels, output 2 analog channels, and can input or output 24 digital channels.

2.3.3 Software

In the original system, DOS-based C-code was used for the implementation of the control loop. When the author took over the vehicle implementation from the previous student, it was relatively easy to code simple controllers; however, complex high-order controllers required a conversion to state-space formulations and consequent coding and debugging. The timing of the system was conducted by polling the RTI timer located on the 815 board. This process turned out to be very computationally intensive and wasteful. Consequently, there was no effective method to analyze in real-time the performance of the system graphically or numerically.

Later versions of the software retained the use of the C-code, but the author moved the system to a Windows platform. The use of timer polling was replaced by the use of the interrupt vector chip on the CPU to call an interrupt service routine to implement the controller code. This system allowed real-time display of controller performance in the form of screen-printing; however, Windows software and hardware interrupts were disabled and thus disk I/O and real-time graphics were not available.

In the final version of the system, the author adopted and modified the commercial software produced by Wincon® for MATLAB®. This software uses the MATLAB's Real-Time Workshop® compiler to compile a Simulink diagram into c-code. The c-code is then compiled into an executable and downloaded to the CPU. The Wincon software provides the time polling capability, graphics, and disk I/O. However, the Wincon system assumes that the user is utilizing the Wincon I/O board. With the help of Dan Block, the control systems lab technician at UIUC, the Wincon and MATLAB compiler routines were modified by this author to create new I/O software driver routines to support the RTI-802 ISA, RTI-815 ISA, RTI-815 PCI, and U.S. Digital Encoder board input and outputs. These drivers are currently available to UIUC students.

2.4 The Transmitter and Communication System

For the experimental testing discussed in this thesis, two communication loops were used to control the two different vehicles. For the 4WS4WD vehicle, a modified R/C transmitter/receiver system was used to control the vehicle. For the Uberquad, a standard DC-motor/amplifier system was used for the control.

The 4WS4WD vehicle used a modified off-the-shelf R/C transmitter system for communication. The figure below shows the transmitter system used from a joystick command on a hand-held transmitter to servo or motor motion. The signal begins with the handheld transmitter, where the user normally moves a joystick or switch to change the voltage produced by a potentiometer. The potentiometer signal for each channel is converted into a pseudo-PWM signal, which is then modulated by R/C electronics into a FM signal. An R/C receiver demodulates this signal, and sends the appropriate pulse commands to each servo and to the motor controller. The motor controller provides power to the receiver and to each servo, and converts the PWM signal into a voltage command to each motor.

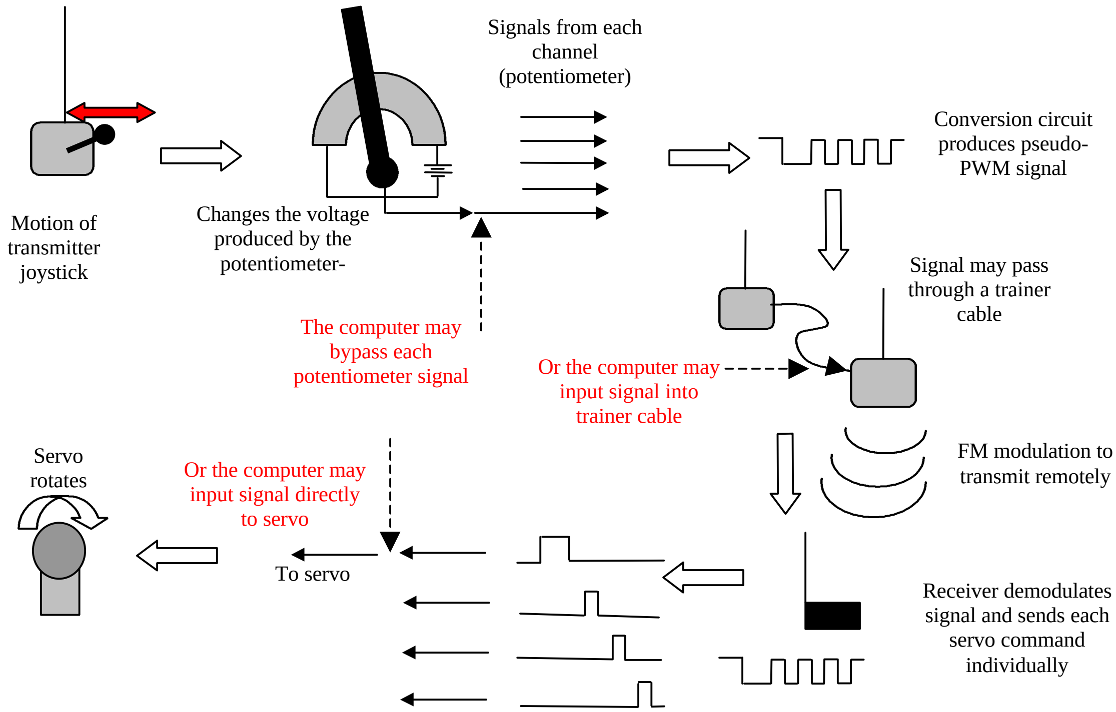

Figure 2.5: A schematic of the communication system used for the 4WS4WD vehicle.

The original motivation for the IRS was to utilize off-the-shelf components for as much of the system as possible; thereby minimizing cost and setup time. Although this did allow fast implementation of control techniques, the transmitter system and servos were ill suited for control applications from a dynamics and electronics standpoint. The primary issue was that the transmitter system by design had a large variable-delay in the transmission. Electronically, the voltage range needed to produce the full range of actuation was very small (0.2 volts), and hence noise, voltage drift on the I/O boards, and digitization all introduced noticeable and sometimes significant effects in the control loop. From a dynamics standpoint, it was discovered that the R/C servo pole locations were close to those of the vehicle dynamics. Furthermore, the actuator had a rate limiting term due to the torque limits on the motor. Later sections address actuator dynamics and the methods used to measure them.

2.4.1 The Pseudo – PWM Servo Control Signal

Shown in the figure below is an R/C servo. The servo connects to the receiver and is the actuator that steers the vehicles. For the work conducted in this thesis, two different kinds of servos were used: the Futaba S9304 servos and the Futaba S9402 servos. The performance of each type of servo is discussed in more detail in later sections of this thesis.

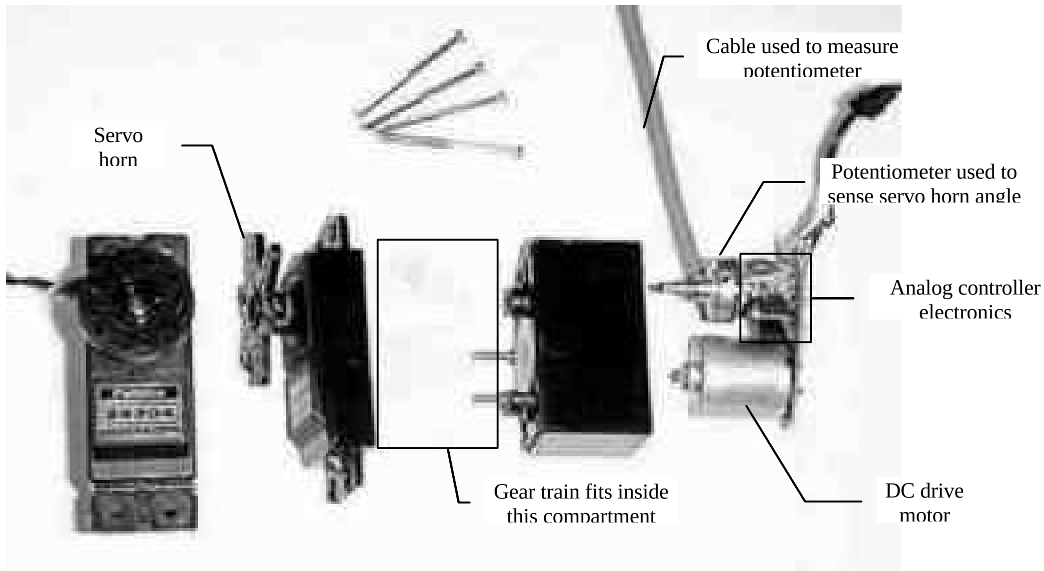

Figure 2.6: The servo used for the 4WS4WD vehicle.

Each servo is connected to the receiver by three wires. Two of the wires are high voltage (red) and ground (black). The supply voltage is generally between 5 and 7.5 volts DC, but depends on the battery system. The third wire (white or yellow) is used to transmit a control signal. The control signal received by the servos is best described as pseudo Pulse-Width-Modulation (PWM). Classic PWM signals consist of a square wave whose duty cycle is varied from 0 to 100 percent to control the speed, position, or toque of a motor. The servo signal, using the same concept, is also a square wave that is repeated every 20 to 30 milliseconds, with a pulse height approximately the same voltage as the "high" voltage line (whose numerical value depends on the battery supply voltage, typically between 5 and 7.5 volts). The position of the motor is transmitted via the pulse length. The pulse length is varied from a minimum of 1 millisecond to a maximum of 2 milliseconds, where 1 millisecond pulse length would represent full counterclockwise motion, and 2 milliseconds represents full clockwise motion. Thus, the center pulse-length would be approximately 1.5 milliseconds (Note: some servos can actually utilize pulse lengths outside of this range, but the above values represent the "standard" for the R/C industry). The figure below shows a sample pulse-train to an R/C servo and how the pulse-length may be varied to change the rotation of the servo-horn. For further information on servo systems, refer to Scott Edward's book where computer control of servo systems is discussed in detail in Chapter 9 (Edwards 1998).

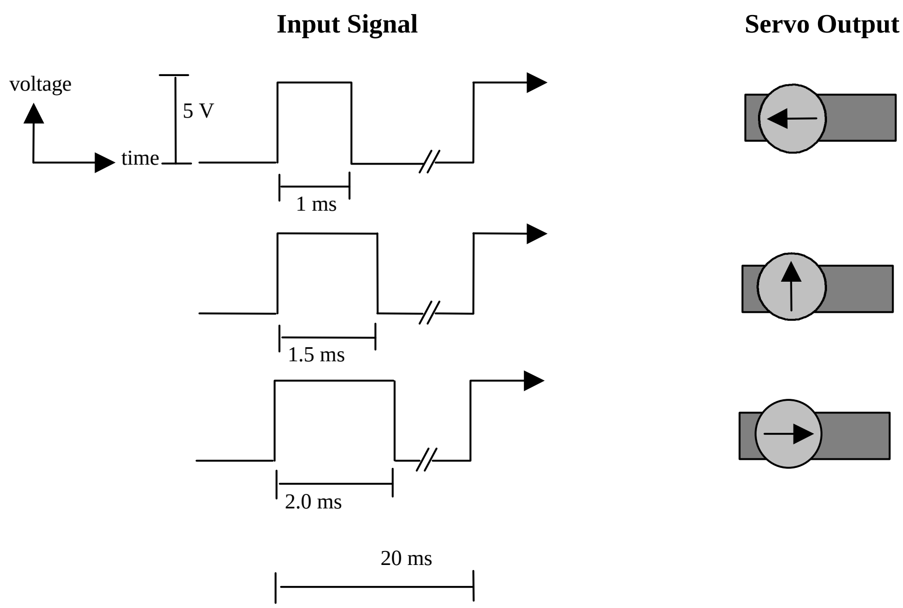

Figure 2.7: The relationship between the pulse command and the servo output.

An important drawback to the servo controller is that there is a small dead-zone built into the controller. If the servo-horn is within approximately a degree of the desired reference angle, but not exactly on the reference value, the servo will not respond. The intent of this feature is to prevent the servo from responding to noise and thus allow the servo to remain "off". If the servo did not have a dead-zone, it would continually "jitter" about a nominal position in response to noise when not actively being used. In commercial R/C systems, this would rapidly wear down the batteries, which already have a very short life span (Note: there is no battery system for this project since an external power supply is used). The impact of this dead-zone on the dynamics of the system will be discussed in more detail in later sections.

In order for the servo to receive the signal from the receiver, the receiver must first obtain a signal from the transmitter. To determine the nature of this signal, the trainer port of the transmitter was used. Regarding the trainer port, scale aircraft transmitters often are equipped with a port that is used to connect an instructor's handheld transmitter to a student's transmitter. The plane is set up to only accept signals from the instructor's transmitter. Once the instructor flies a plane into in the air with sufficient altitude, the instructor can flip a switch on his/her transmitter to allow the student to fly the plane via a cable connection to the student's transmitter. The student's control inputs then fly the aircraft as long as the instructor has the switch depressed. If the student looses control of the plane, the instructor can release the trainer switch to regain control of the aircraft. Note that the trainer cable also provides power from the instructors' transmitter to the student's transmitter, because the student's transmitter does not even need to be on to fly the aircraft.

There are two advantages to using the trainer port: it allows the servo signals to be examined directly and it allows us the computer to be directly connected into the transmitter without any rewiring of the transmitter system. Examination of the wires inside the trainer cable reveals that there are four main wires. These wires consist of a high and a low power line that connect the power systems of the two transmitters, the line that transmits the instructor's servo controls to the student, and a line that transmits student's servo controls to the instructor. If we examine the signal lines from a 4-channel transmitter with an oscilloscope, we might find a signal that looks like the following:

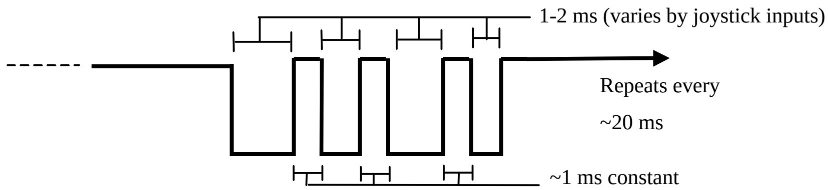

Figure 2.8: A sample servo signal on the trainer cord.

If we move the flight joystick relating to servo 3, the signal would change like the following:

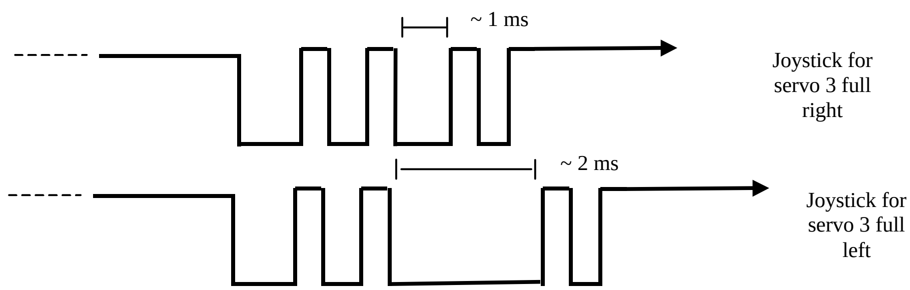

Figure 2.9: How the transmitter signal changes with joystick input.

Examination of this signal reveals that the transmitter and the receiver "communicate" via a pulse-type modulation similar to that used to control the individual servos. The signal for servo 2 is simply appended to the signal for servo 1; the signal for servo 3 is appended to signal 2, etc. This creates a single chain of pulses, where the number of "troughs" is equal to the number of channels the transmitter transmits. The chain repeats itself every 20 milliseconds. The transmitter very likely takes this low-frequency signal and modulates a fixed frequency (by a crystal) FM signal and transmits it to the receiver. The receiver then demodulates the signal and de-multiplexes the signal to send a single pulse to each servo during each 20-millisecond cycle. Once point to note about this method is that the signal is very immune to noise by the its' digital nature. The figure below shows how the demodulation might be done:

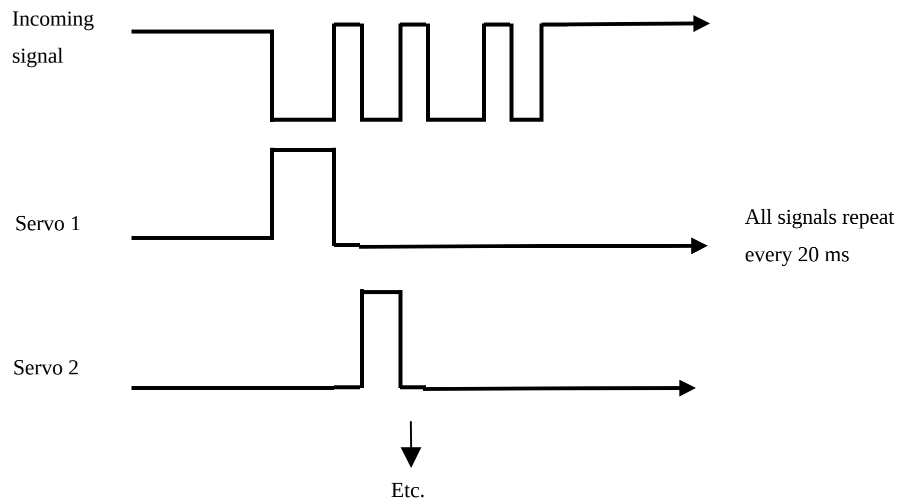

Figure 2.10: The demodulation of the transmitter signal at the receiver.

On a normal R/C transmitter, the human sends driving/flight commands to the vehicle by moving joysticks or knobs connected to a potentiometer. The transmitter reads the voltage produced by the potentiometer, and produces a pulse train (described above) that is proportional to each potentiometer voltage. The potentiometer voltages usually vary between 1.9 to 2.1 volts over the entire range of input. That is, if the driver pushes a joystick full right, the potentiometer might read 1.9 volts, while full left may read 2.1 volts. Experimentally, we have found that the “center” voltage may vary between joysticks from 1.9 to 2.5 volts. The small voltage range, about 0.2 to 0.3 volts between full servo on and full servo off, means that any small voltage drift or noise significantly affects the servo performance.

At this point, there are three clear methods to drive a scale vehicle by a computer using an R/C transmitter. To describe these methods, assume that there are 6 different servo systems (or channels) that are to be controlled on the vehicle. The first method of control is to use the computer to generate the servo pulses directly to each servo. The computer would then need to change the pulse length of each of the six pulses separately, and output the pulses on 6 separate digital or analog lines that are connected directly to the vehicle. No transmitter or receiver would be needed, the car would not be autonomous, and a timer board or conversion circuit would be needed by the computer to generate the pulses. The second method is to use the computer to generate a single pulse train using digital or analog output that would be input into the trainer port: i.e. the computer would act as the “student” on the trainer cord. This method would require only one line and allow "autonomous" cord-free vehicles, but again a timer board or conversion circuit would be needed. This method was actually used experimentally for a short period of time by using a conversion circuit build on cascaded 555 timers to convert voltages to pulse-length. The third and final method is to bypass the potentiometer used to measure the joystick position inside of each handheld transmitter, and use the computer to input its own potentiometer voltage into the transmitter via analog output. This is the method utilized in current system for the 4WS4WD vehicle. This system is very simple, but suffers from the noise and voltage drift drawbacks previously mentioned. These drawbacks are discussed in greater detail in the next section.

2.4.2 Delays, Variation in Communication Intervals, and Noise

Using the joystick-voltage approach has caused significant difficulties in controlling the vehicle remotely. For instance, attempting to control the vehicle at a nominal speed of 2 m/s may be quite difficult because the voltage difference between 2 m/s and 3 m/s may be only 0.05 volts. In some cases, this voltage change used by a controller may be within the range of background noise and hence the servos may act erratically. A larger problem is that the base voltage from the computer board and the voltage supplied to the vehicle may drift very slightly, causing small changes in the servo output. These small changes may require re-calibration of the servos and speed every several hours during testing in the presence of an electrically noisy environment. Extensive work was done to ensure adequate shielding and drift prevention, including shielding of source wires, prevention of grounding loops, and ground isolation between signal and power supply lines. This significantly improved performance, but did not completely eliminate the problem.

Another inherent problem in using the above transmitter system is the communication delay. Because the transmitter signal is essentially only updated every 10 ms at maximum, faster vehicle responses are quite difficult to obtain. To make matters worse, the delay itself is not constant. For instance, if a step response on actuator 3 takes place immediately before the pulse train starts, then the delay associated with this step response is simply the amount of time needed for the pulses of actuator 1 and 2 to pass. If the step response on actuator 3 happens after the pulse train reaches actuator 3, then the delay is the entire 10-20 milliseconds of the pulse cycle in addition to the delay from actuators 1 and 2. The effect is a "quantized-like" delay, where step responses may appear to start only on set intervals of 10 ms, rather than a true "random" delay. This non-random delay is seen quite clearly in a series of step responses conducted on the front steering actuator of the vehicle, as seen below:

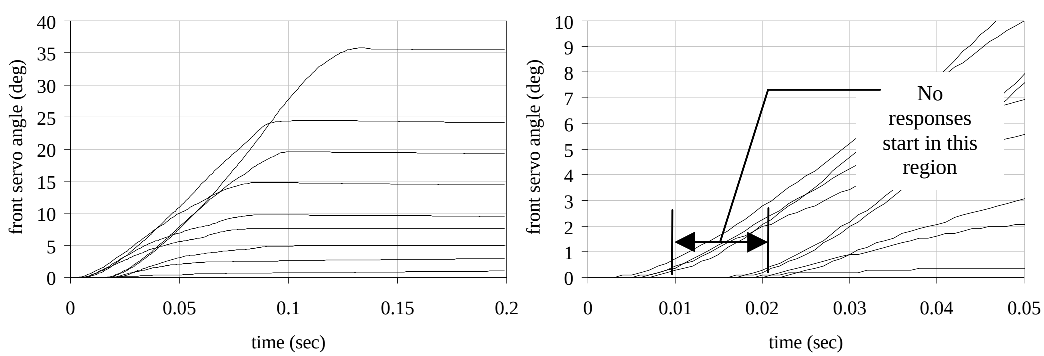

Unfortunately, there is no method to determine beforehand the specific delay of the system because the delay determined by the transmitter itself instead of the computer. This creates nightmarish problems in modeling fast vehicle dynamics or servo dynamics because the starting time of the control input can vary over a range of 20 milliseconds (as seen above). As a compromise in modeling, this delay can be approximated as a constant delay of 0.012 – 0.015 seconds. This delay problem is inherent in the use of the pseudo PWM signal used by the servo actuator controller itself. Hence, the same delay problems will occur if the vehicle control signal is sent into each servo directly, into the trainer cord, or into the joystick voltage. Dan Block here at the University of Illinois has developed a method where the controller internal to the servomotor is bypassed, thus producing a system that can be sampled and controlled without time-delay limitations. Basically this required "gutting" the analog controller used by the servo system. As a consequence, a feedback loop must be created for each servo system. With this amount of complexity, the only advantage of the servo system is that it is a small, packaged motor and sensor. If we compare the cost of a quality (high-bandwidth) servo system to a DC motor and integrated encoder with the same bandwidth, the costs are comparable. The DC system, however, will not likely be rate limited to the extent exhibited by the servo system.

2.4.3 Alternative Implementation Methods – Direct Motor Control

The “standard” method to control the position of a motor without using a transmitter system is to utilize an amplifier on a DC motor with position or velocity feedback. The computer outputs a voltage to the amplifier, which then converts it usually into a standard PWM signal whose current (or voltage) is proportional to the source voltage. The motor’s position is then monitored to complete the feedback loop.

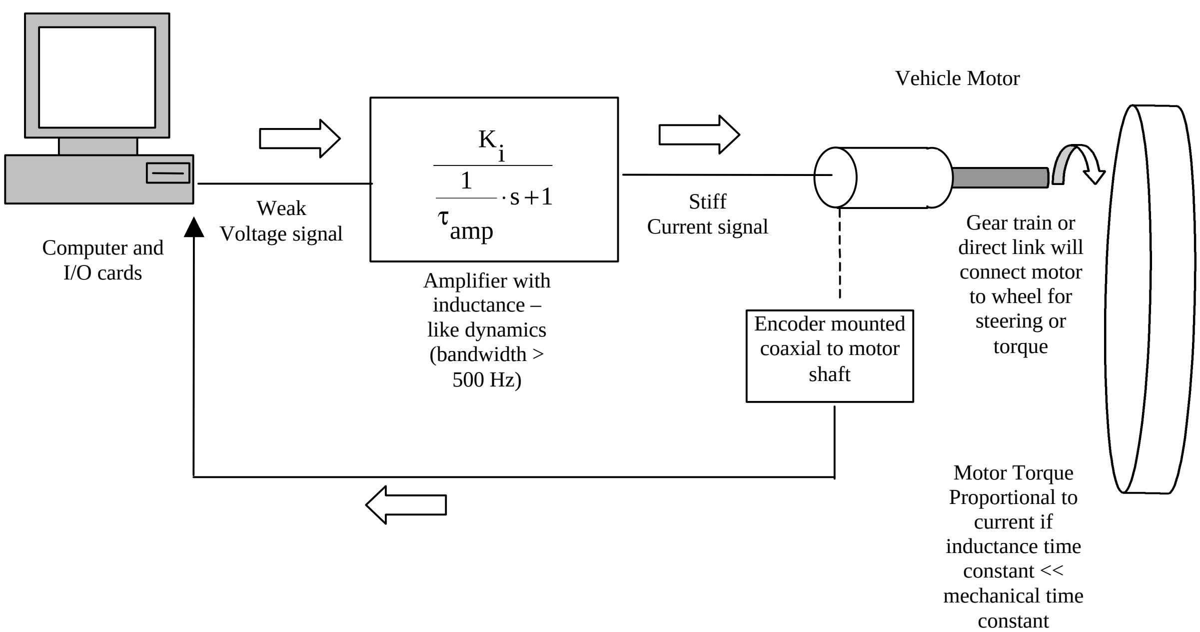

Figure 2.12: A block-diagram of the DC-amplifier circuit.

There are several advantages and disadvantages to using a tethered DC-amplifier system. The biggest disadvantage is the cost: each amplifier costs approximately $200 and requires a dedicated power supply (about $150). The motors, although high performance, cost as much as a high-quality servo. In addition, the vehicle is no longer capable of being "untethered" by cables or power supplies. Because the amplifiers are bulky and require a 120-volt power source, it is simply not feasible for the 1/8 scale car to carry amplifiers onboard the vehicle. The advantage of using the "standard" system is primarily that they are well-known well-identified systems and remarkably linear. The DC motor control is a standard plant examined in beginning controls laboratories. The motors can provide high-bandwidth actuation with very little non-linearities. If non-linearities or lower bandwidth are desired in the actuators at a later point, they can be added by software without any hardware changes.

2.5 The Driving Console

To include a human driver in the control implementation, the Illinois Roadway Simulator is equipped with a driving console. The console is a modified video-game driving unit, and consists of a steering wheel, a shift bar, two buttons, a gas pedal, and a brake pedal. The shifter and two buttons are simply digital switches that connect to ground. Hence, there are a total of 4 outputs available (2 on the shifter and one for each button). The steering wheel, brake, and gas pedals use potentiometers to measure incremental changes. Thus, three analog outputs are available. A picture of the driving console is shown below:

Figure 2.13: A picture of the driving console.

The steering wheel is used in several ways. When the vehicle is autonomously driving, the steering wheel is used to input a reference lateral position. The steering voltage is scaled by some factor to correspond to some lateral position. When a Driver Assist Controller is being tested, the steering wheel is used to input a steer input into the front tires. For each steering wheel measurement, the centered steering wheel voltage is subtracted off the measured voltage to obtain the steering input.

2.6 The Method of Sensing Vehicle Position

The Illinois Roadway Simulator is somewhat unique in that the vehicle position can be measured absolutely from a fixed ground position. As discussed in the literature review section of this thesis, full-size vehicles can sense their position on the road by a number of techniques including radar, vision systems, magnetic markers, laser telemetry, and GPS. During the design of the IRS, many different sensing systems were considered including optical, magnetic, and vision systems. However, the cost of the fixed-arm sensing and the simplicity of implementation were significant factors in the selection of the arm system. This section details how the arm is used to measure the vehicle states.

2.6.1 Arm Configuration

The position of the vehicle is determined via an arm attached to the vehicle. The arm has two segments, with three potentiometers or encoders attached at the ends of the segments. From the potentiometers or encoders, the angle of each segment can be determined. Given the length of the arms, the position of the vehicle can then be found. The diagram below shows the angle conventions used to determine vehicle position from the arm angles:

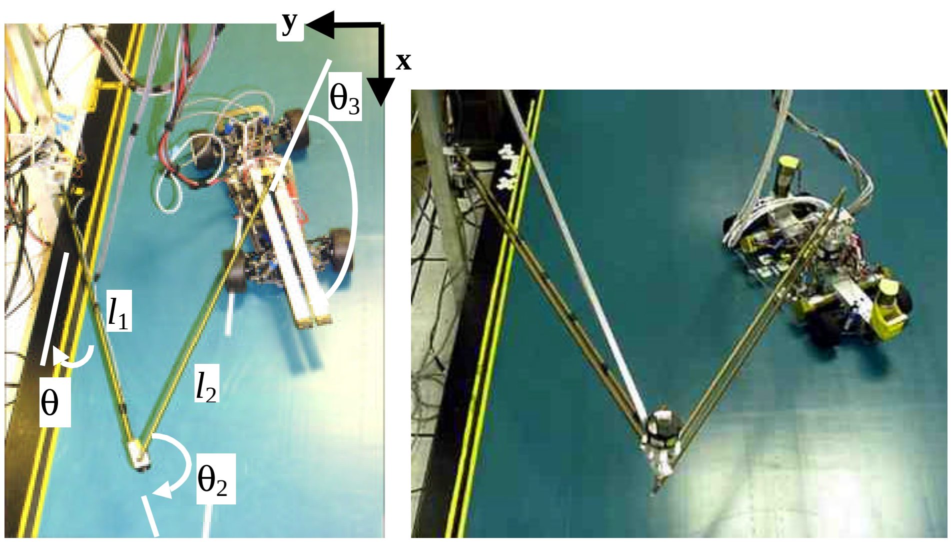

Figure 2.14: The angle conventions used to determine vehicle position using link angles on old arm (left) and new arm (right).

The arm has two segments, with three sensors attached at the ends of the segments. From the sensors, the angle of each segment can be determined. Given the length of the arms, the 3 planar degrees of freedom of the vehicle can then be found. The figure above shows the angle conventions used to determine vehicle position from the arm angles. From these angles, trigonometric relations give the vehicle's position:

$$
\begin{aligned}
x &= L_1 \cdot \cos(\theta_1) + L_2 \cdot \cos(\theta_1 + \theta_2) \\
y &= L_1 \cdot \sin(\theta_1) + L_2 \cdot \sin(\theta_1 + \theta_2) \\
\psi &= \theta_1 + \theta_2 + \theta_3
\end{aligned} \tag{2.1}
$$

The vehicle velocities in the plane are determined via numerical differentiation instead of using analytical derivatives of Equation (2.1). The resolution is approximately the same. The measurement of the linkage angles has been tested using two different methods: potentiometers and encoders. The following is a discussion of the advantages and disadvantages of each measurement technique.

2.6.2 Digital versus Analog Position Sensing

Over the course of this thesis work, there has been some contention whether encoders or potentiometers should be used for vehicle position feedback. The original vehicle feedback system utilized low-resolution incremental encoders that were unsuitable for yaw-rate feedback and very prone to breakage. For these reasons, the encoders were replaced with potentiometers. Initially, the performance improvement was substantial. However, the performance of the potentiometers deteriorated rapidly, and the system was then upgraded to high-resolution impact-resistant encoders. The intent of this section is to outline the methodology used to design the feedback system, with specific focus on the mistakes made during each design iteration.

In selecting between encoders and potentiometers to measure angular rotation, one must realize that both systems have limited resolution. The resolution of the encoder is simply the digital number of counts per revolution multiplied by the encoder multiplication factor (usually 4), which is determined via software. The multiplication factor increases the counts of the encoder by using a second pulse detector to measure the location of each edge. This is often called “edge detection”. Using software, the information from each pulse counter is combined to increase the encoder resolution. The resolution of the potentiometer is limited theoretically by the resolution of the A/D conversion of the Analog-to-Digital Converter (ADC) chip. Considering that most boards have a 12 bit resolution with inputs ranging from 10 to –10 volts, the number of increments per revolution of the potentiometer is roughly 7000 “counts”/revolution. In actual practice however, the analog inputs are very prone to noise, and hence the working resolution is much less. It is clear that an “average” encoder with 2000 counts per revolution (8000 counts with the 4 times multiplication available from the encoder board) will have equal or better performance to a potentiometer using a 12-bit ADC to input the voltage signal. It is important however to ensure that the software multiplication is used. In the original system, encoders were used without edge-detection, and hence the maximum resolution of the encoders was limited to 1000 counts/revolution.

If an encoder is selected with poor resolution (as in the original system), the position signal becomes so quantized as to introduce a large amount of noise, especially when the derivative of the position signal is obtained numerically. An example of this can be found in Mark DePoorter's thesis, where yaw-rate control was attempted and abandoned due to poor yaw-rate feedback. The original encoder system, because of poor resolution, had a significant amount of noise in the yaw rate measurement. To compound the problem, the frequency of the "noise" generated by taking the derivative was in the same frequency band as the dynamics being measured. Initially, filtering was attempted by Mark DePoorter to correct this problem, but the phase lag introduced by the filtering was too significant. Further discussion regarding this problem, as well as plots showing the poor signal conditioning, can be found in Mark DePoorter's thesis (DePoorter 1997a).

When the encoder system was replaced with potentiometers, it was found that calibration of the system became significantly more difficult. First, the potentiometer was calibrated to find the voltage/angle ratio. Afterwards, an offset angle dependent on the mounting of the potentiometer to the arm was subtracted. It was discovered that care must be taken with potentiometers not to pass into the non-linear resistive sensing area. Also, if the source voltage to the potentiometers changes slightly, the potentiometer response will also change. In summary, calibration of the potentiometers must be conducted on the assembled arm, and is quite difficult. Experience showed that the easiest way to calibrate the arms was to mark roughly a dozen known locations on the treadmill surface, and then use the arms to measure the potentiometer voltages with the arm centered at each of these locations. A search routine was then conducted in code that found the correct slope and intercept on EACH potentiometer that matched the predicted arm position with the known arm positions. Even with this method, manual refinement was often required afterward to obtain quality position feedback.

One of the first problems discovered in using the potentiometers was the possibility of having a non-linear response from a potentiometer. Often a new potentiometer will exhibit a non-linear response. A calibration setup was constructed that connected a potentiometer to an encoder; the potentiometer shaft was connected to an encoder, and then the potentiometer was swept back and forth through the appropriate operating angles. The voltage was recorded from the potentiometer at each angle, and the resulting data was plotted. The figure below shows a comparison between linear and non-linear potentiometers.

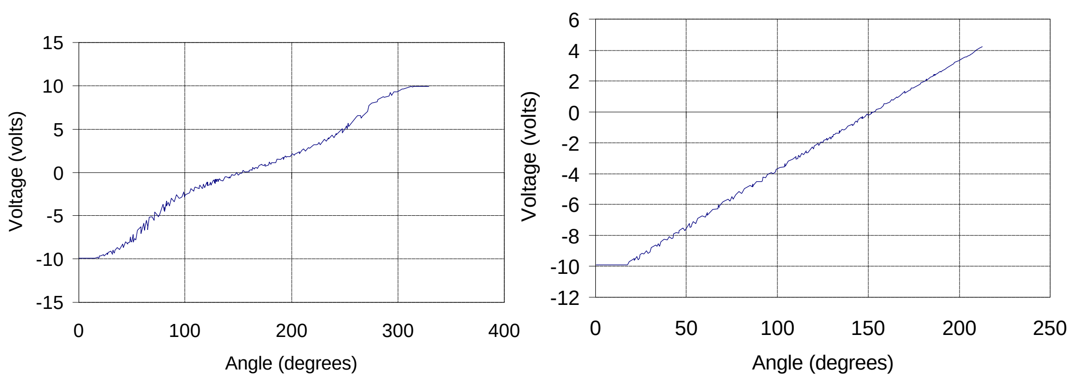

Figure 2.15: The calibration curves non-linear (left) and linear (right) potentiometers.

After being calibrated on the above stand, potentiometers were then selected for use on the arm based on their observed linearity.

The resolution of an encoder in practice never changes with time; however, repeated use of a potentiometer causes wear and hence change in resolution. It was found that after repeated use, the calibration would change and the potentiometer response would become non-linear. An example of how this drift can affect the response can be seen in the plots below, which compare the encoder and potentiometer arms. Both responses were made by using the end of the arm to follow a circle traced out on the track.

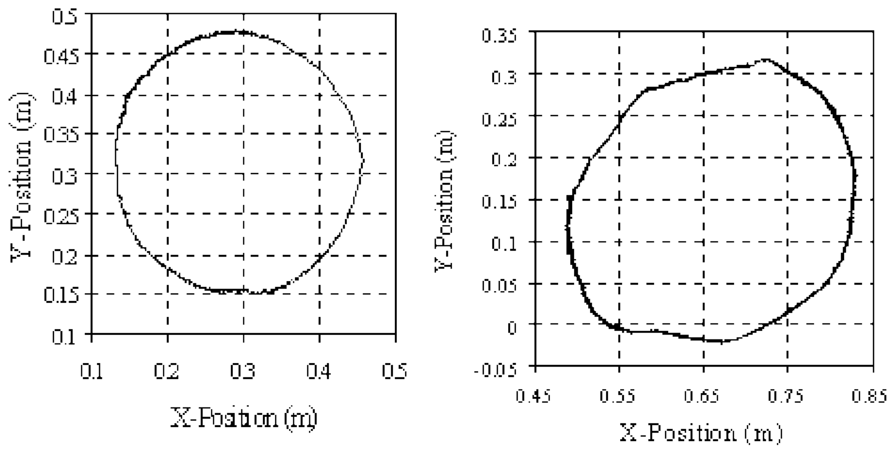

Figure 2.16: responses of each arm tracking a circular path (encoder left, pot right).

When the calibration drift was first encountered, it was thought that the original potentiometer calibration was incorrect. When feedback of the yaw rate signal was examined, the yaw rate response was found to have large spikes that made the signal unsuitable. Suspecting that arm-bounce may be causing this error, the arms were shortened by a factor of 2. The two different yaw rate responses from each arm (using potentiometers at each joint) are compared below.

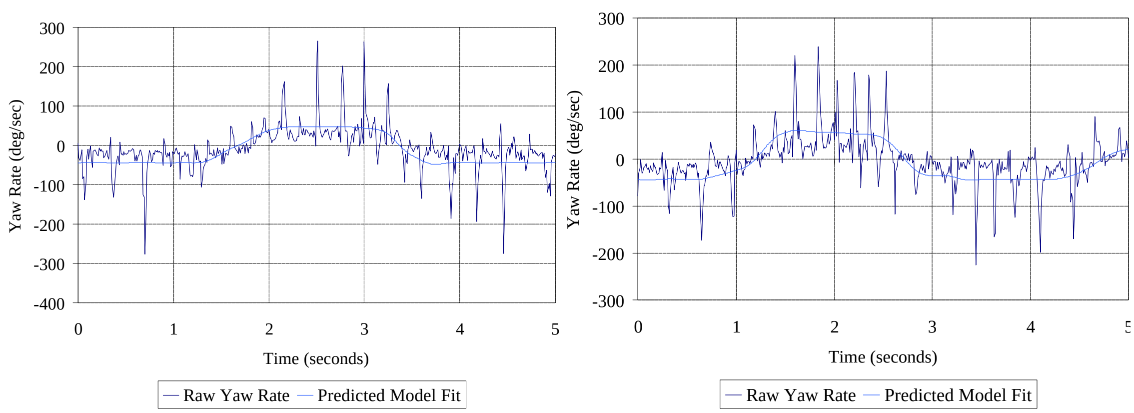

Figure 2.17: The open-loop response of the long arm (left) and short arm (right) at a speed of 1.2 m/s.

Although this change made the arm physically much stiffer which decreased the vibration amplitude and increased the frequency of vibration, no significant change in the amplitude or frequency of the feedback spikes was observed. Concluding that the spikes are unrelated to the bounce motion, it was hypothesized that the potentiometers may be the cause of the error.

During calibration of the potentiometers for the shorter arm, it was noticed that the calibration coefficients (such as the slope and intercept of the regression fit) changed significantly with each calibration. Examining the potentiometers with an oscilloscope during a constant motion of the potentiometer shaft, the voltage response was clearly non-linear and showed a stair-step tendency. It appeared there were small regions, approximately evenly spaced, where the voltage did not change with angle. It was then suspected that the potentiometer element wore away at these points due to repeated use such that the voltage response was no longer linear. To test this theory, the potentiometers in the arm were replaced by encoders one-at-a-time, as shown below. The encoder resolution was 1000 counts/rev.

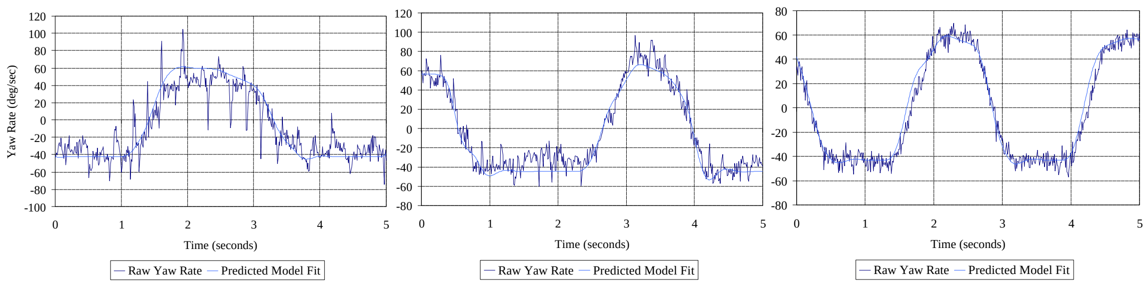

Figure 2.18: The open loop responses of the short arm at a speed of 1.2 m/s using one encoder at the vehicle (left), two encoders at the vehicle and middle joint (center), and all encoders (right).

After realizing the potentiometers were the cause of this error, one of the "used" potentiometers was recalibrated to observe if it was causing the error.

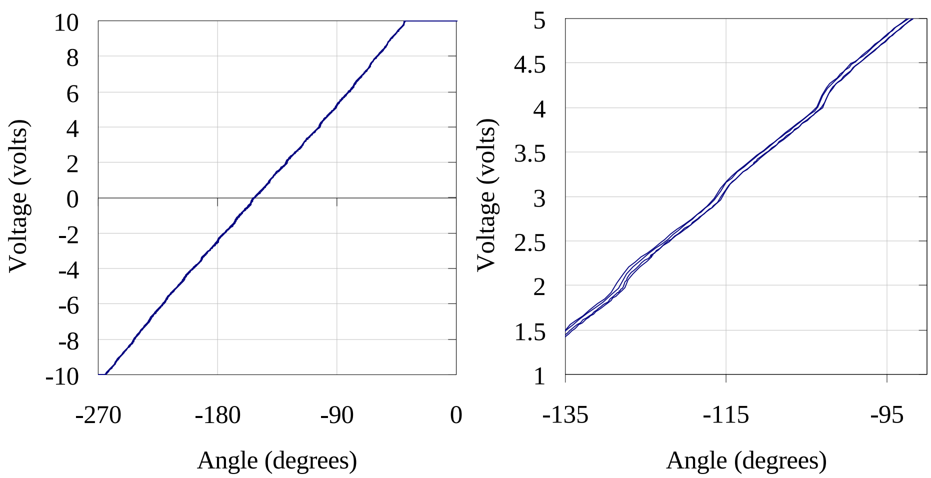

Figure 2.19: Non-linear potentiometer response due to excessive wear. Note that the figure on the right is a zoomed-in portion of the left plot.

Overall, the resulting calibration was deceptively linear; however, closer examination revealed step-like nonlinearities in the response. These nonlinearities are likely due to uneven wear in the potentiometer path due to fretting. Fretting occurs when there is constant rubbing between two surfaces that are moving only slightly with respect to each other. It is possible to purchase potentiometers that have a higher immunity to this kind of wear (by using precious metals as conductors), but the price of these potentiometers is equivalent to their encoder counterparts.

After replacing the potentiometers with newer, higher-quality encoders, a primary concern was that the shaft load on these more-expensive encoders would not bend the shaft as with previous encoders. The previous low-cost potentiometers were very impact resistant (in fact, the arms themselves would most likely break before a potentiometer would fail). Encoders, on the other hand, will readily break upon impact. Fortunately, one of the specifications provided by encoder manufacturers is the amount of torque and normal load the encoders will sustain without breaking. Examining these specifications revealed that the first type of encoders purchased had a normal force limit of 5 oz., which is much less than the weight of the vehicle. Consequently after one severe crash, one of the encoder shafts bent during a test rendering the encoder unusable. New encoders were chosen with a rating of 5-lbs. impact force, which is approximately the weight of the vehicle. In addition, the mounting of the encoders was redesigned to incorporate a flexi-coupling to the encoder shaft to isolate impact damage away from the encoder. Additionally, a bearing system was added to the encoder arm to prevent force or moment transmission to the encoder arm.

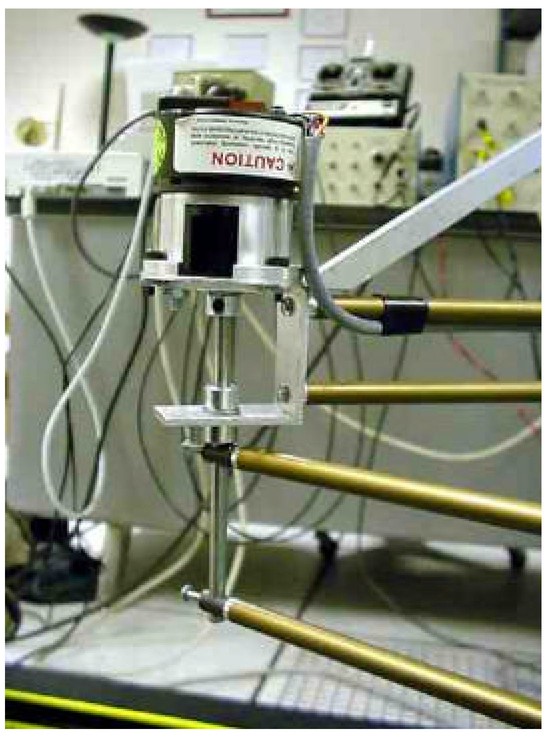

Figure 2.20: The new encoder mountings showing how the encoder shaft was isolated.

The resulting system proved to be very reliable and impact resistant, and was used for the vehicle tests discussed in this thesis.

3 Modeling And System Identification

This chapter is intended to provide a complete dynamic description of the systems, and includes the methods used to obtain this description. The chapter begins with a description of the treadmill dynamics, useful for understanding the limits of the treadmill system to track an accelerating or decelerating vehicle. The next section deals directly with the longitudinal control of the vehicle, and provides results for this control. Lateral control is then begun in the next section, with the introduction of the theoretical bicycle model. Afterwards, scaling issues are discussed using the bicycle model as the dynamics of comparison. The methodology used to obtain the vehicle transfer functions is then presented, followed by the specific results of the dynamic fit for the three vehicle conditions examined in this thesis. Finally, a summary of the vehicle dynamics encountered experimentally and measured in this thesis is given.

3.1 Treadmill Dynamics

To monitor the treadmill velocity, an encoder was mounted on a wheel that “rode” on top of the treadmill surface.

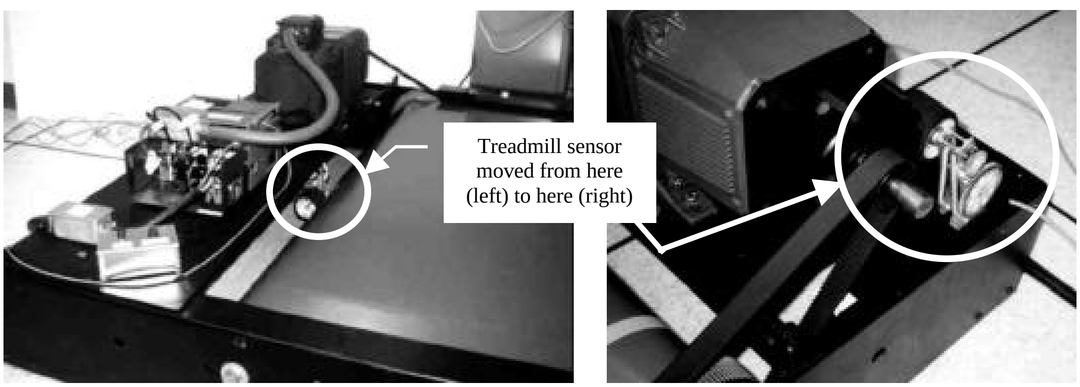

Figure 3.1: The original location of the treadmill speed sensor (left), and the modified location of the sensor (right).

Originally the encoder was mounted by Mark DePoorter to be in the middle of the treadmill. However, after a catastrophic bearing failure, it was decided that the encoder should be mounted somewhere less obtrusive. The above pictures show the “before” and “after” location of the treadmill speed sensor.

To obtain the relationship between treadmill velocity and encoder measurement, the treadmill was then moved through 10 complete rotations, and the number of encoder counts was recorded. There were 4000 encoder counts per encoder revolution, and 47.048 (average) encoder revolutions per complete track revolution. The length of each treadmill revolution (i.e. the “circumference” of the treadmill surface) was also measured to obtain a distance per unit encoder count. The measurement revealed a length of exactly 205.5 inches. Thus, by knowing the number of encoder counts that have passed per unit time, the treadmill velocity can be determined. One problem with this technique is that the encoder-determined velocity is inherently quantized. Originally, running averages of 10 samples were used to measure the encoder velocity (before the author learned about causality and phase lag in sampled systems). Later, a true low-pass filter was used (4^{th} order) to obtain the treadmill velocity. It was found that the error between the averaged responses and the filtered responses was in actuality quite small. Figure 3.3 shows the "smooth" response of the averaged responses, while Figure 3.6 shows the more "jagged" filtered response obtained by true low-pass filtering of the signal. This last signal is the one currently used on the treadmill velocity control.

In order to understand the treadmill response, the treadmill dynamics were determined. Before introducing the dynamics, an important aspect of the treadmill must be presented: the motor used on the treadmill does not allow negative control torque. Acceleration of the treadmill is accomplished by a DC motor that applies torque to the treadmill belt, while deceleration is accomplished by shutting off the motor and allowing friction to slow the treadmill down. Hence, two separate models can simulate the treadmill dynamics: a torque-friction model for acceleration, and a friction-only model for deceleration. We begin by examining the friction-only modeling.

The governing equation used to find the treadmill dynamics is given by:

$$J \cdot \frac{d\omega}{dt} = -B \cdot \omega - F + T_{controller} \tag{3.1}$$

where J is the treadmills rotational moment of inertia, B is the treadmills viscous damping, and F is the sliding friction term. We can rewrite this as

$$\frac{d\omega}{dt} = -\frac{B}{J} \cdot \omega - \frac{F}{J} + \frac{T_{controller}}{J} \tag{3.2}$$

To solve for the various coefficients of this equation, we examine in the time-domain the separate responses to step decrements, steady-state changes, and step increments in the reference velocity that the treadmill is attempting to track.

To obtain the treadmill velocity, the treadmill position was differentiated at each time increment by simply dividing the change in encoder counts in the past time sample by the time sample. The treadmill position in meters was determined by measuring the length of the treadmill surface for one revolution, and measuring the number of encoder counts to complete the revolution. The number of counts was found to be 47048 counts per revolution, and the track length was found to be 205.5 inches. Because the treadmill velocity is measured using an encoder, the velocity signal is quantized and hence has a significant high-frequency component. Initially, a running average filter was used to filter the signal. The signal was very smooth, but the delay produced by this technique made it difficult to model the treadmill dynamics very accurately. The design of the treadmill filter, as with any causal filter, was a tradeoff between phase lag and signal smoothness.

3.1.1 Step Decrement Treadmill Responses

To solve for B/J and F/J, the treadmill was allowed to reach a steady-state operating speed, and then the reference speed was suddenly set to zero. Because the treadmill cannot apply any reversing torque, the dynamic response to this input provides information regarding the amount of friction present in the system. The response of the system can then be fitted to the linear ordinary differential equation

$$\frac{d\omega}{dt} = -\frac{B}{J}\cdot\omega - \frac{F}{J} \tag{3.3}$$

Which can be rewritten as by taking the Laplace transform,

$$s\cdot\Omega(s) - \omega_0 + \frac{B}{J}\cdot\Omega(s) = -\frac{F}{J\cdot s} \tag{3.4}$$

or

$$\Omega(s) = \frac{\omega_0}{s+\frac{B}{J}} - \frac{F}{J\cdot s\cdot\left(s+\frac{B}{J}\right)} \tag{3.5}$$

Which becomes in the time domain

$$\omega(t) = \omega_0 \cdot e^{\frac{-B}{J}\cdot t} - \frac{F}{B}\cdot\left(1 - e^{\frac{-B}{J}\cdot t}\right) \tag{3.6}$$

or

$$\omega(t) = \left(\omega_0 + \frac{F}{B}\right)\cdot e^{\frac{-B}{J}\cdot t} - \frac{F}{B} \tag{3.7}$$

In order to obtain the values F/B and B/J, we guess

$$C = \frac{F}{B} \tag{3.8}$$

and do least-squares regression on the linearized form of Equation (3.7) to obtain best fits to Figure 3.3 below:

$$\ln(\omega(t) + C) = \ln(\omega_0 + C) - \frac{B}{J}\cdot t \tag{3.9}$$

Using the fit of this above equation, we can determine the difference between the actual data and the fit data, which then defines an error. We then can iterate on estimates of F/B to minimize this error. This minimum-error value of F/B is assumed to be the best fit. A graph of the curve fits to this equation using this process is shown below for various initial speeds. Note that treadmill velocity is used instead of rotational speed in the equation fit. The treadmill speed is determined from an encoder mounted on the treadmill. As mentioned, the treadmill length is 205.5 inches, and the encoder records an average of 47048 counts per treadmill length. Hence, it is simply a linear gain to change angular velocity coordinates to treadmill linear velocity coordinates.

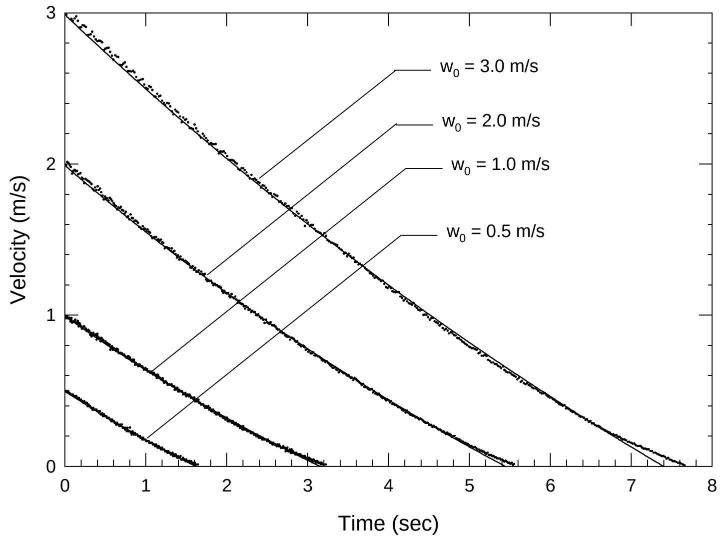

Figure 3.2: The velocity decay of the treadmill showing experimental data and theoretical fit.

There were 5 curves generated for each step-down speed shown above, for a total of 20 different estimates for F/J and B/J. The values found for these curves are given in the table below and plotted.

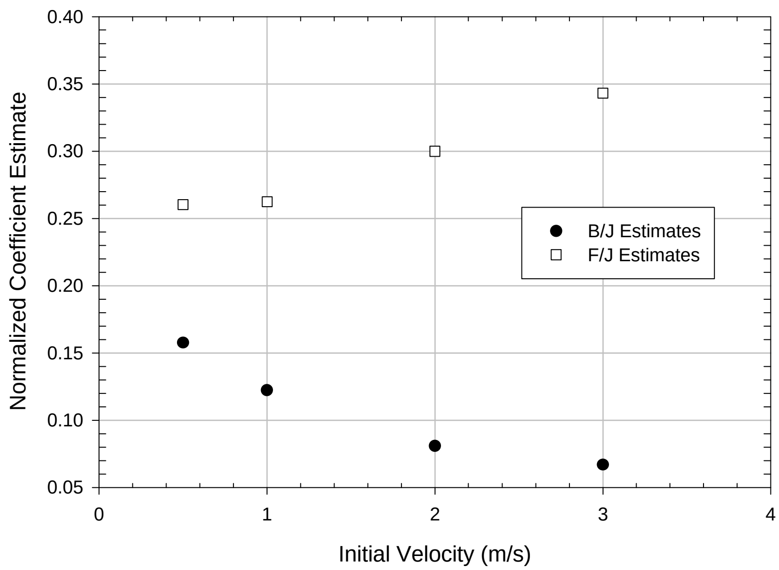

Figure 3.3: The dynamic equation coefficients determined for the treadmill theoretical fit.

The coefficients obtained for the treadmill have minor velocity dependence. For simulation purposes, the experimenters assume constant parameter values at all velocities. However, as will be shown in simulation results (presented later), this assumption does create some error during the velocity decay portion of the treadmill response. This error is acceptable in terms of vehicle experimentation and modeling. Based on the treadmill performance at different velocities, we suspect that the parameter velocity dependence is primarily due to the changing nature of the treadmill belt friction. As the belt speed increases, the torque contribution due to viscous drag decreases, since the sliding surface tends to float on a small air surface at higher velocities. This explanation remains simple conjecture, since further friction analysis is at this point unnecessarily exact. Shown below are values obtained for the parameters of the governing differential equation at several initial velocities:

Table 3.1: The values obtained for F/B, B/J, and F/J for various steps.

Data File	Start Speed (m/s)	Stop Speed (m/s)	F/B Estimate (rad/s)	B/J Estimate (rad/sec)	F/J Estimate (unitless)	Average Estimate B/J (rad/s)	Average Estimate F/J (unitless)
stpdwna1.dat	0.5	0.00	1.80	0.1508	0.2715		
stpdwna2.dat	0.5	0.00	2.01	0.1334	0.2682		
stpdwna3.dat	0.5	0.00	1.33	0.1900	0.2528		
stpdwna4.dat	0.5	0.00	1.30	0.1888	0.2455		
stpdwna5.dat	0.5	0.00	2.11	0.1250	0.2637	0.157632	0.260343
stpdwnb1.dat	1.0	0.00	2.11	0.1226	0.2586		
stpdwnb2.dat	1.0	0.00	2.47	0.1113	0.2749		
stpdwnb3.dat	1.0	0.00	2.15	0.1211	0.2605		
stpdwnb4.dat	1.0	0.00	2.46	0.1090	0.2682		
stpdwnb5.dat	1.0	0.00	1.69	0.1475	0.2494	0.122324	0.262326
stpdwnc1.dat	2.0	0.00	3.28	0.0871	0.2859		
stpdwnc2.dat	2.0	0.00	4.55	0.0704	0.3205		
stpdwnc3.dat	2.0	0.00	3.98	0.0767	0.3053		
stpdwnc4.dat	2.0	0.00	3.48	0.0851	0.2962		
stpdwnc5.dat	2.0	0.00	3.43	0.0851	0.2919	0.080899	0.299933
stpdwnd1.dat	3.0	0.00	4.93	0.0640	0.3157		
stpdwnd2.dat	3.0	0.00	4.95	0.0641	0.3172		
stpdwnd3.dat	3.0	0.00	4.77	0.0755	0.3601		
stpdwnd4.dat	3.0	0.00	5.74	0.0638	0.3663		
stpdwnd5.dat	3.0	0.00	5.30	0.0673	0.3568	0.066947	0.343211

Clearly the parameters show some variation. For simulation fitting, the parameters were varied to best fit the model: F/J ~ .24 (unitless) and B/J ~ 0.30 (rad/sec).

3.1.2 Steady-State Treadmill Response

With the values for F/J and B/J known, the steady state response of the system can be modeled as (from Equation 1).

$$0 = -B \cdot \omega - F + K \cdot V \tag{3.10}$$

or

$$\omega = -\frac{F}{B} + K \cdot V \tag{3.11}$$

Setting the treadmill at a particular velocity and recording the voltage, velocity becomes the dependent variable and a line is obtained where F/B is the intercept of the line and K is the slope. This determination was done for five different ramps of velocity from 0 to 3 m/s at .01 m/s increments, and the values obtained are shown below.

Table 3.2: The determination of F/B and K from steady-state response

data file	slope	intercept (F/B)
ss_tred1.dat	0.416820	-0.060806
ss_tred2.dat	0.416510	-0.063346
ss_tred3.dat	0.410120	-0.072563
ss_tred4.dat	0.418712	-0.063298
ss_tred5.dat	0.418396	-0.063955

A graph of a sample run is provided below

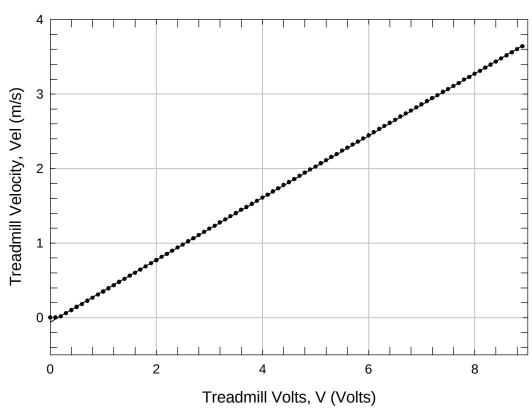

Figure 3.4: The steady state velocity with respect to applied motor voltage showing experimental data and linear fit.

3.1.3 Step Increment Treadmill Responses

The treadmill has a built-in motor controller pack that makes system identification difficult. As discussed in the earlier section, we can model the treadmill quite well at steady state and with the motor off, but the addition of a motor controller to the system adds an additional torque term which is unknown. If we assume that the controller controls the current, then the voltage command in essence initiates a current (and hence torque) response from the controller. The motor used on the treadmill is a DC motor, so we would expect a first order system from input reference voltage to treadmill velocity.

Experimentally, several responses were obtained on the treadmill after a step-up and step-down reference voltage command was sent. These responses were then fit to a simple first order system when the reference velocity is larger than the treadmill velocity, and fit to the previously determined 'decay' system when the reference velocity was less than the treadmill velocity. We noted that the treadmill controller pack contained a time-delay likely to be caused by the velocity sensor. The experimental and fit data are shown below for the treadmill system. Sampling took place at 100 Hz. The filter used here was a 3rd order Butterworth at a cutoff frequency of 10 Hz. The following SIMULINK diagram shows the treadmill model currently used.

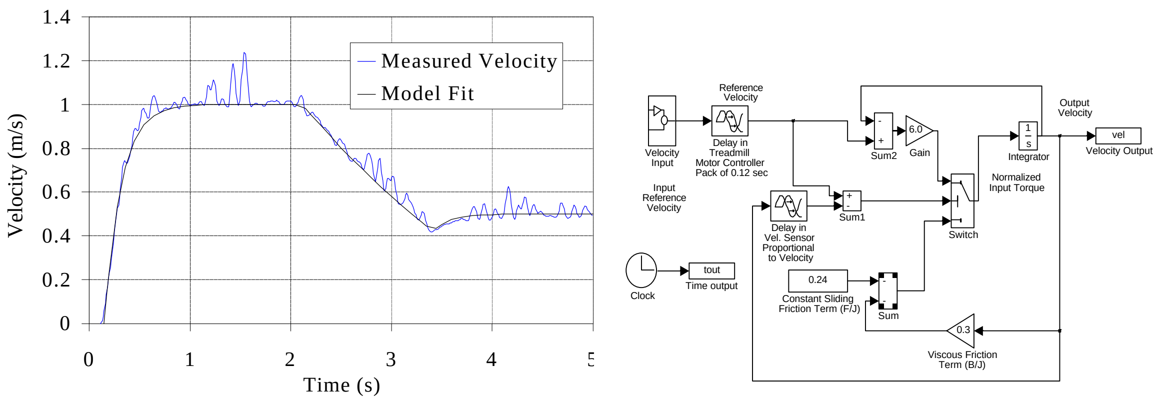

Figure 3.5: Step-up treadmill responses (left), and the resulting model (right).

3.2 *Longitudinal Vehicle Control*

There are two methods to run a vehicle at a particular velocity on the treadmill. The first method is to set the vehicle motor at some speed which is approximately the correct velocity, and the treadmill can be forced to track the vehicle. The second method is to set the treadmill at some speed and the car can be forced to track the treadmill. The choice between the two methods depends on the experiment being run, but the basic difference is between which piece of hardware is the "leader", and which piece of hardware is the "follower".

3.2.1 4WS4WD Vehicle (R/C system) Longitudinal Control

The longitudinal control of the 4WS4WD vehicle was made difficult by the DC motor controller in the loop. This controller is apparently designed to have a non-linear response to have the most sensitivity at low speeds and little throttle sensitivity at high speeds. If not otherwise stated, the longitudinal speed of the vehicle is measured from the base of the measurement arm, where it attaches to “ground”.

3.2.1.1 Repeatability and Adjustment of R/C DC Motors

To drive the car at a set velocity, a constant voltage can be sent to the vehicle motor. Initial testing sought to find the voltage/velocity relationship, and its repeatability. The vehicle was driven on a straight line on the treadmill, and the treadmill speed was monitored over a long period of time. This test was repeated over many voltages to obtain a calibration curve relating voltage to car speed. To test the repeatability of this curve, the curve was generated several times. The results of this test are shown below. Given a set velocity, it is of interest to note how much the car varies in speed over a single test. The figure below shows the average, highest, and lowest velocities recorded while obtaining one calibration curve.

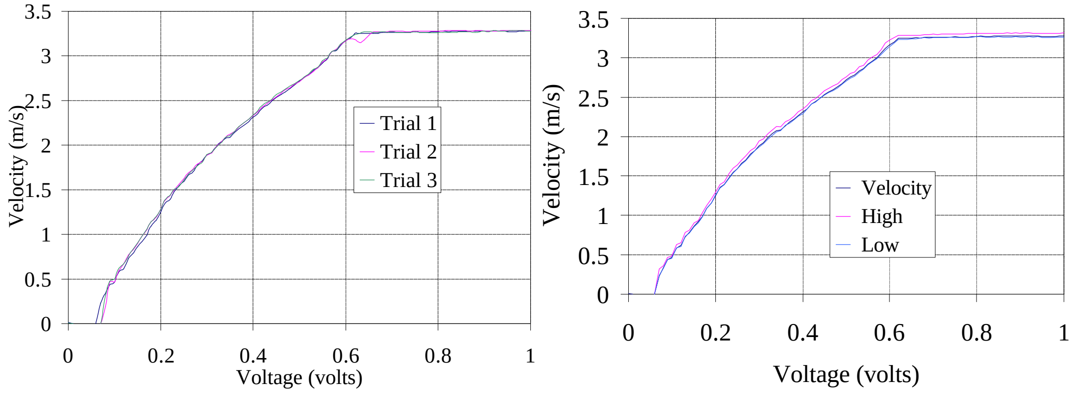

Figure 3.6: The repeatability of the motor voltage/velocity relationship (right), and the variation in speed of the vehicle at a constant voltage (right).

There are three switches available on the motor controller pack labeled "Reverse Time Delay", "Neutral", and "Throttle". The effects of these switches are as follows: the reverse time delay sets the time that the motor controller pack will wait before activating reverse. This was set to be infinite time, thus preventing the vehicle from ever going into reverse on the treadmill. The effect of the other two buttons is not as clear, but can be seen easily in the following figures.

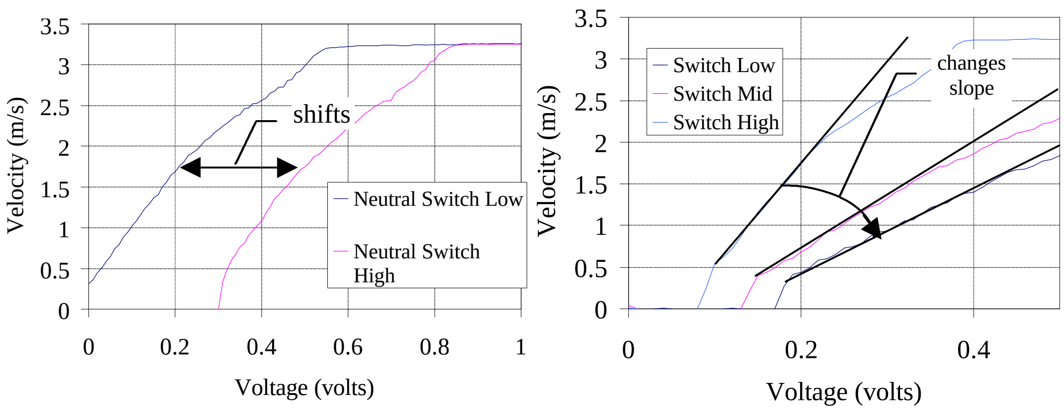

Figure 3.7: The change in the calibration curve with changes in the "Neutral" position setting (left) and the change in the calibration curve with changes in the "Throttle" position setting.

3.2.1.2 Steady-State Motor Voltage/Velocity Relationship

We can see from the above plots that the relationship between voltage and velocity is certainly not linear, and appears to be a power relationship. Using a non-linear solver routine to minimize the sum-of-squares error, the data was fit to the following relationship:

$$(V - V_0) = A \cdot (S - S_0)^n \tag{3.12}$$

Where the terms and best fits were found to be

V	=	Applied Motor Voltage	
V_0	=	"Zero Speed" Motor Voltage	0.089867
S	=	Motor Speed	
S_0	=	"Zero Voltage" Motor Speed	-0.059285
A	=	Power Coefficient	0.12858
n	=	Order	1.5698

3.2.1.3 Treadmill Tracking the Vehicle

The performance of the longitudinal controller is strongly dependent on the gains chosen for the controller. The following plots show the performance of a controller with very tight gains of P–gain: 1.5 m/s per m, I–gain: 0.0001 m/s per m-s, D–gain: 2.0 m/s per m/s.

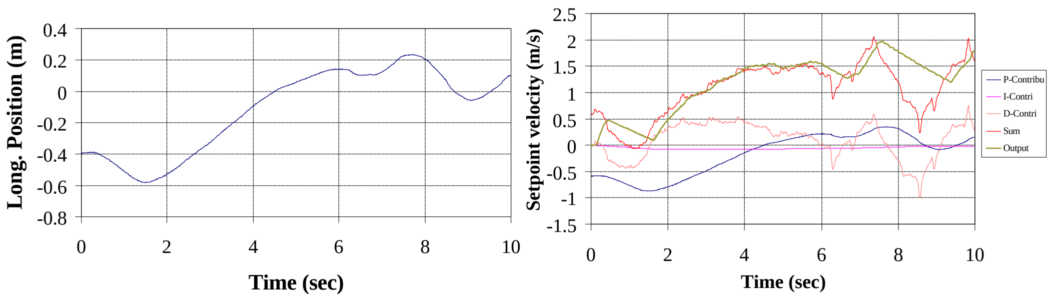

Figure 3.8: Time responses showing the performance of the longitudinal controller.

The following plots show the performance of a controller with medium gains of:

P–gain: 1.50 m/s per m, I–gain: 0.0001 m/s per m-s, and D–gain: 0.150 m/s per m/s.

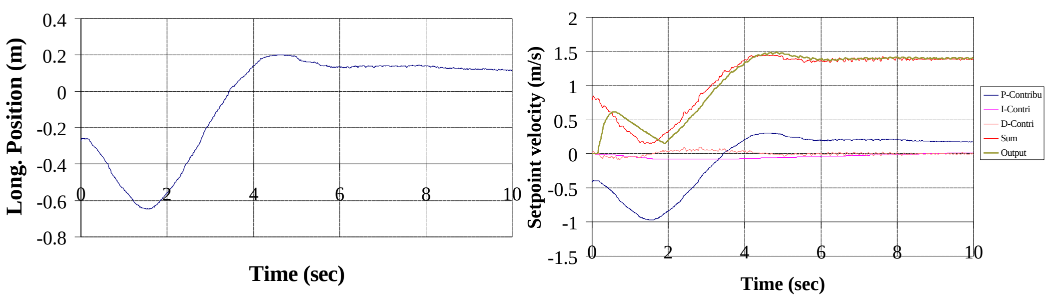

Figure 3.9: Time responses showing the performance of the longitudinal controller.

In general, the treadmill is not used to track the vehicle, simply because the treadmill surface or belt is much more difficult to replace than the vehicle motors or tires. In general, the treadmill is run at a constant velocity and the vehicle is used to track the treadmill, as detailed in the next section. When situations arise where the treadmill must track the vehicle, in general the medium gains shown above rather than the "tight" gains are used to save on wear-and-tear on the treadmill.

3.2.1.4 Vehicle Tracking the Treadmill

The longitudinal controller can be designed so that the vehicle tracks the treadmill. This requires an accurate open-loop model of the relationship between motor voltage and velocity. This relationship is described in detail in the previous section "Motor Dynamics", and it is assumed at this point on that the relationship is well known. The design of the controller is straightforward PID controller design. The results of the controller using gains P–gain: 1.5 m/s per m, I–gain: 0.0001 m/s per m-s, D–gain: 0.15 m/s per m/s is as follows:

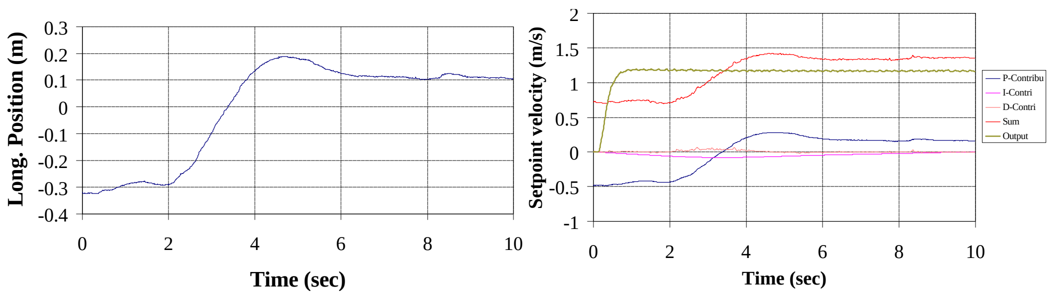

Figure 3.10: The control effort used to have the vehicle motor track the treadmill.

3.2.2 Uberquad (DC Motor system)

The Uberquad has the capability of direct torque input into each wheel. As a consequence, the longitudinal control of the Uberquad is quite simple. A PID control with unagressive gains is used to make the Uberquad track the treadmill. The controller outputs the same torque command to the drive motors (2 or 4, depending on choice of the user) and this torque command is added to the differential torque steering command (if any) that is sent to the wheels.

3.3 Theoretical Vehicle Lateral Dynamics

The intent of this section is to describe the vehicle dynamics from a theoretical approach. First, the history of the modeling of vehicle dynamics is discussed. The vehicle notation used throughout this thesis is then presented. The equations of motion are obtained by resolving the acceleration components for the vehicle in terms of a coordinate system centered on the moving vehicle. Tire forces are then discussed. Linearization of the tire and body dynamics is then performed to obtain the bicycle model. A specific case of this model, the steady-state solution, is then discussed. Transfer functions relating vehicle input to output are then given, and general vehicle dynamic trends are then deduced from these functions.

Finally, a comparison is made between the bicycle model and other methods of modeling, including higher order simulations and experimental results.

3.3.1 History of the Bicycle Model

Vehicle lateral dynamics has been studied since the 1950's. To describe a vehicle's roll, yaw, and lateral motions at a constant velocity, Segel developed a 3 DOF vehicle model (Segal 1956). If the roll motions are ignored, a simpler model is obtained that is known as the bicycle model (Whitcomb and Milliken 1956). At the Royal Military College of Science in 1960, Professor W. Steeds published Mechanics of Road Vehicles presenting Newton's equations applied directly to the bicycle model. A conflicting model was later published by one of Steeds associates at the college, Dr. John R. Ellis. This model used a path deviation model that approximated Newton's equations for a vehicle in motion. This approximated model has become the standard method of modeling vehicle dynamics (even seemingly applied to situations directly in conflict with the assumptions made in developing the model) (Smith and Starkey 1995). The bicycle model has been widely used for control purposes (Fenton 1976; Shladover 1978). For small angles and accelerations, the approximated Newtonian and full Newtonian methods give identical transfer functions.

3.3.2 Vehicle Diagram and Notation

We will first consider a three degree-of-freedom (3 DOF) model, for purposes of establishing notation as well as a physical system of equations. The notation used is the standard notation used by the Society of Automotive Engineers (SAE). We consider the car to be a rigid mass, with a coordinate system centered on the center of mass of the car. The figure below shows the convention to be used throughout regarding vehicle dimensions.

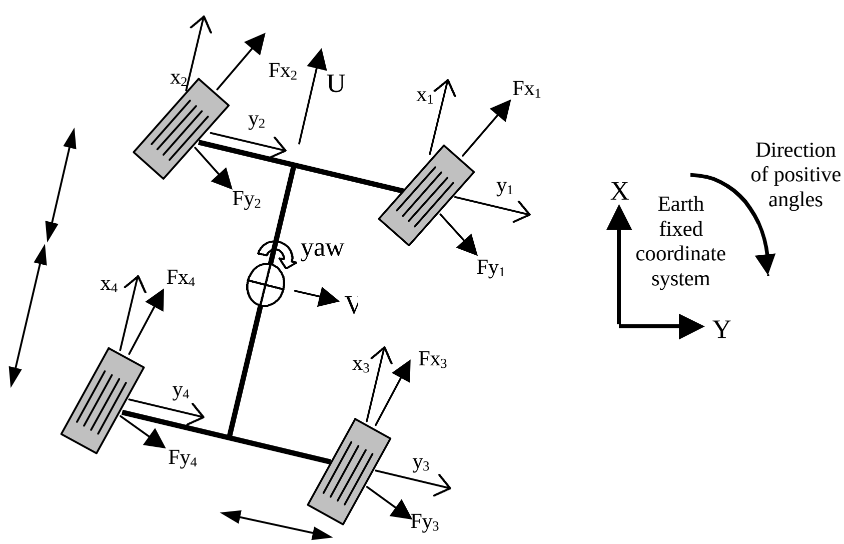

Figure 3.11: A diagram showing the definition of the dimensions used to obtain the bicycle model.

The notation associated with the above diagram is consistent throughout this thesis. The meaning of each term is as follows:

a	Distance from C.G. to front axle
b	Distance from C.G. to rear axle
d	Distance from car centerline to each wheel (1/2 the Track)
X, Y	Earth-fixed coordinates
U	Vehicles longitudinal velocity
V	Vehicle’s lateral velocity

3.3.3 Methods of Dynamic Tire Modeling

The number of tire models that are presented in literature is quite large. In this thesis, we use the linear Dugoff tire model without exception. However, the Magic Tire Model by Pacejka is introduced because of its use in controller design. In addition, neural networks are increasingly being used to estimate both friction potential and friction usage for each tire. An example would be the neural network developed by Pasterkamp and Pacejka to create an input/output model of tire dynamics (Pasterkamp and Pacejka 1997b).

3.3.3.1 The Dugoff Tire Model

The Dugoff tire model is one of the simplest tire models used in simulation. It states that the force exerted by a tire is proportional to the slip angle of the tire. The slip angle is the angle that the tire is making relative to the direction the tire is moving. A diagram defining the slip angle is given below.

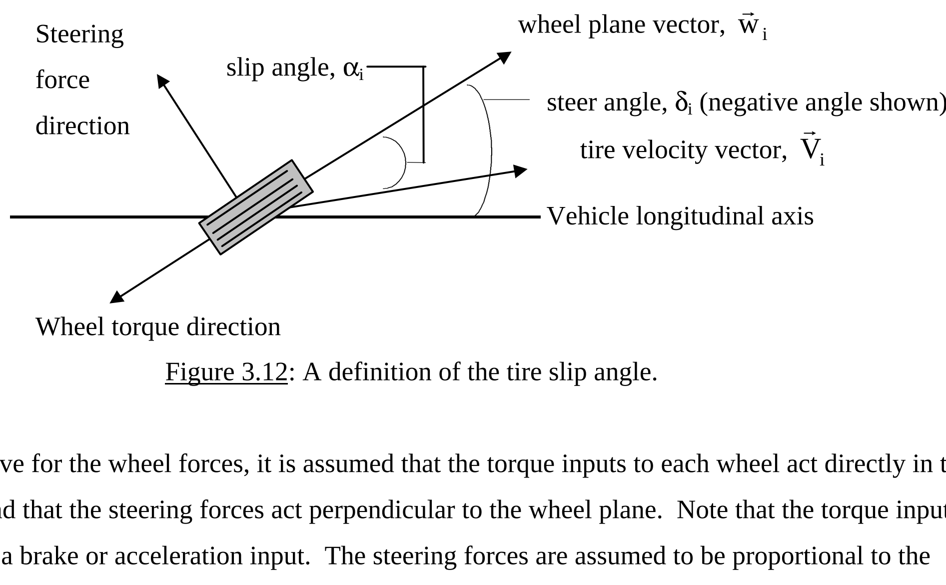

Figure 3.12: A definition of the tire slip angle.

To solve for the wheel forces, it is assumed that the torque inputs to each wheel act directly in the wheel plane, and that the steering forces act perpendicular to the wheel plane. Note that the torque input could either be a brake or acceleration input. The steering forces are assumed to be proportional to the wheel slip angle. The wheel forces then become:

$$F_{xi} = \frac{T_i}{r_i}$$
$$F_{yi} = C_{\alpha i} \cdot \alpha_i \tag{3.13}$$

where α_i is the slip angle of the i[th] wheel (Will and Zak 1997), (Cho and Kim 1996), (Alleyne 1997b). The slip angle of a wheel is defined to be the angle between the tire's velocity vector and the wheel plane. If we assume that the unit vectors $\hat{i}$ and $\hat{j}$ are directed along the vehicle's longitudinal axis and lateral axis respectively, then the velocity of the i[th] tire is given by:

$$\begin{aligned} V_i &= V_{C.G.} + \omega \times r_i \\ &= U \cdot \hat{i} + V \cdot \hat{j} + \dot{\psi} \cdot \hat{k} \times r_i \end{aligned} \tag{3.14}$$

where r_i is the radius vector from the C.G. to the tire. The radius vectors for each tire are as follows:

$$\begin{aligned} r_1 &= a \cdot \hat{i} + d \cdot \hat{j} \\ r_2 &= a \cdot \hat{i} - d \cdot \hat{j} \\ r_3 &= -b \cdot \hat{i} + d \cdot \hat{j} \\ r_4 &= -b \cdot \hat{i} - d \cdot \hat{j} \end{aligned} \tag{3.15}$$

Knowing the i[th] wheel's velocity in the vehicles lateral direction, V_i, and longitudinal direction, U_i, the slip angle of the wheel is simply:

$$\alpha_i = \delta_i - \tan^{-1}\left(\frac{V_i}{U_i}\right) \tag{3.16}$$

where V_i and U_i are the velocity vectors of the i[th] tire in the vehicle coordinate system. Thus, the slip angles for each tire are as follows:

$$\begin{aligned} \alpha_1 &= \delta_1 - \tan^{-1}\left(\frac{V + a \cdot \dot{\psi}}{U - d \cdot \dot{\psi}}\right) \\ \alpha_2 &= \delta_2 - \tan^{-1}\left(\frac{V + a \cdot \dot{\psi}}{U + d \cdot \dot{\psi}}\right) \\ \alpha_3 &= \delta_3 - \tan^{-1}\left(\frac{V - b \cdot \dot{\psi}}{U - d \cdot \dot{\psi}}\right) \\ \alpha_4 &= \delta_4 - \tan^{-1}\left(\frac{V - b \cdot \dot{\psi}}{U + d \cdot \dot{\psi}}\right) \end{aligned} \tag{3.17}$$

(Alleyne 1997a; Alleyne 1997b) (Will and Zak 1997) (Smith and Starkey 1995) (Note that Alleyne's sign convention on the slip angle is non-standard, but this is corrected later by his use of negative cornering stiffness coefficients). For small angles, each slip angle can be simplified like the following:

$$\alpha_1 \approx \delta_1 - \frac{V + a \cdot \dot{\psi}}{U}$$
$$\alpha_2 \approx \delta_2 - \frac{V + a \cdot \dot{\psi}}{U}$$
$$\alpha_3 \approx \delta_3 - \frac{V - b \cdot \dot{\psi}}{U}$$
$$\alpha_4 \approx \delta_4 - \frac{V - b \cdot \dot{\psi}}{U} \tag{3.18}$$

Again, these results agree with (Will and Zak 1997), (Cho and Kim 1996). The use of this model is explained in detail in (Will and Zak 1997) and (Dugoff, Fancher, and Segel 1970).

3.3.3.2 Transient and Non-Linear Tire Dynamics: The Magic Tire Formula

It is important to note that the above discussion of tire dynamics neglects any non-linear dynamics between the tire and the road. It is well known that the tire itself is best modeled as a transfer function under light loading conditions, but that the model rapidly becomes nonlinear when significant tire forces are generated. The frequency range where this transition occurs is important because it represents the limits of frequency analysis of the vehicle and the transition from a linear tire model to a non-linear system. The linear tire dynamics are critical, simply because they are invariant with respect to the vehicle controller. The controller cannot change the pole locations of the tire without changing the physical properties of the tire as the vehicle is driving. First, the linear dynamics of the tire, i.e. the pole locations, are examined in the literature. Secondly, the non-linear dynamics are examined. Combining this information reveals the dynamic range over which a linear vehicle model should be valid.

The linear dynamics of a tire can be inferred by frequency domain tests conducted on full-sized tires. These tests have been conducted experimentally by several researchers with different motivations (tire testing for manufacturing, vehicle dynamics, emergency maneuvering, etc.) and their results can be summarized as follows. For lateral tire motions (steering inputs) the phase change between 1 and 15 Hz for a 205/60 R15 tire is given as 90 degrees, with a magnitude drop of 15 dB. This suggests a tire “pole” location between 3 and 5 Hz (Mastinu et al. 1997). Several authors represent this pole as a distance-dependent tire “lag” due to the distance needed for the tire to deform to develop lateral forces and moments. This distance is referred to as the relaxation length of the tire. This concept is supported by experimental results indicate that the tire pole becomes faster as a linear function of tire velocity (Higuchi and Pacejka 1997). This lateral force transient has also been observed in truck tires (Fancher et al. 1997).

The non-linear dynamics of tires have been fit with semi-empirical modeling. The magic tire model is an empirical model developed by Pacejka and colleagues at Delft University that has been verified experimentally to be quite accurate (d'Entremont 1997). In the formula (Pacejka and Besselink 1997), some constants can be inferred by examine physical tire characteristics. However, as noted by some authors (Leister 1997), this model is updated almost annually, resulting in many versions of the formula. The focus of this model is for use on simulation studies of vehicle dynamics. Because of its complexity and non-linearities, it is rarely used to design controllers, and is almost solely used for validation of controller codes in simulation.

At a constant velocity, therefore, the tire's lateral forces can be considered in the linear case as an approximate 2nd order system from steering input. The pole locations associated with longitudinal forces (braking, torque) have been experimentally shown to be much faster than the lateral modes, and demonstrate a fourth order, double mode of vibration with modes at 33 and 77 Hz (Zegelaar and Pacejka 1997). For basic approximation of tire slip alone in the longitudinal direction, several authors suggest a 1st order model for both the lateral and longitudinal directions (Salaani, Chrstos, and Guenther 1997). It is important to emphasize that each tire model depends on a tradeoff between complexity and model accuracy. The complexity of tire lag and its influence on vehicle stability and control is addressed by (Heydinger, Garrot, and Christos 1991; Heydinger, Garrot, and Christos 1994).

3.3.4 Equations of Motion

Before discussing the equations of motion, the notation used for vehicle control is introduced:

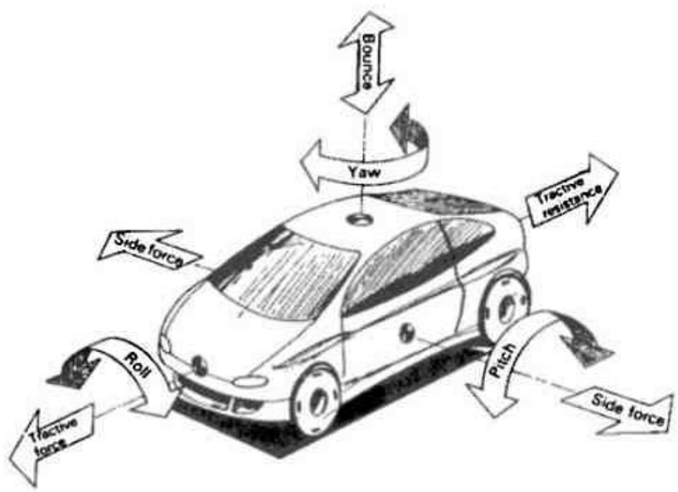

Figure 3.13: A diagram showing the notation for vehicle motions (scanned from (Nwagboso 1993)).

The vehicle dynamic equations can be obtained from Newton's law,

$$\sum \vec{F} = m \cdot \vec{a} \tag{3.19}$$

by substituting the appropriate expression for acceleration (Will and Zak 1997). Given the forces, $F_x \hat{i} + F_y \hat{j}$, that can be generated at the i^{th} tire, the moment of the i^{th} tire is given by

$$\vec{M}_i = \vec{r}_i \times \vec{F}_i \tag{3.20}$$

Substituting,

$$\vec{M}_i = \left(x_i F_{yi} - y_i F_{xi}\right) \cdot \hat{k} \tag{3.21}$$

The sum of moments for the vehicle must be equal to

$$\sum \vec{M}_i = I_z \frac{d^2\psi}{dt^2} \tag{3.22}$$

There is some contention over the best coordinate system to use to model vehicle dynamics, and the answer to this question depends too strongly on the application to allow an answer. For the "in-plane" dynamics under study, moving coordinate systems are most often utilized that are fixed to the vehicles' center-of-gravity. This allows the equations of motion to be re-written so that the dynamics are studied in relation to the car (which in fact is the location that they are most measured from). It is important to note that if the coordinate system is not fixed to the body, then the angular velocity of the vehicle is not the angular velocity of the coordinate system (Steeds 1960).

To fix this problem, the preferred method is to orient the coordinate system along the vehicle's longitudinal axis so that the moments of inertia of the body are constant. If a fixed (stationary) coordinate system were used, the moments of inertia would vary as the body changes orientation to the fixed axes (Steeds 1960).

The first difficulty is in defining the acceleration of the moving coordinate system. It is often necessary to transform a vector from one coordinate system to another. The transformations between a vector in the moving frame, $A \cdot \hat{i}_{moving} + B \cdot \hat{j}_{moving}$, and a vector in the stationary frame, $C \cdot \hat{i} + D \cdot \hat{j}$, are as follows:

$$A \cdot \hat{i}_{moving} + B \cdot \hat{j}_{moving} = [A \cdot \cos(\phi) + B \cdot \sin(\phi)] \cdot \hat{i} + [-A \cdot \sin(\phi) + B \cdot \cos(\phi)] \cdot \hat{j} \tag{3.23}$$

$$C \cdot \hat{i} + D \cdot \hat{j} = [C \cdot \cos(f) - D \cdot \sin(f)] \cdot \hat{i}_{moving} + [C \cdot \sin(f) + D \cdot \cos(f)] \cdot \hat{j}_{moving} \tag{3.24}$$

where ϕ is the angle between the moving and the stationary frame, measured with respect to the x-axis of the stationary frame (Alleyne 1997b). These transformations can be written in matrix form as:

$$\vec{X}_{moving} = \begin{pmatrix} \cos(\phi) & \sin(\phi) \\ -\sin(\phi) & \cos(\phi) \end{pmatrix} \cdot \vec{X} \tag{3.25}$$

and

$$\vec{X} = \begin{pmatrix} \cos(\phi) & -\sin(\phi) \\ \sin(\phi) & \cos(\phi) \end{pmatrix} \cdot \vec{X}_{moving} \tag{3.26}$$

To obtain the acceleration components in the fixed-body coordinate system, a perturbation along the path is examined as the vehicle undergoes a change in orientation (see the figure below).

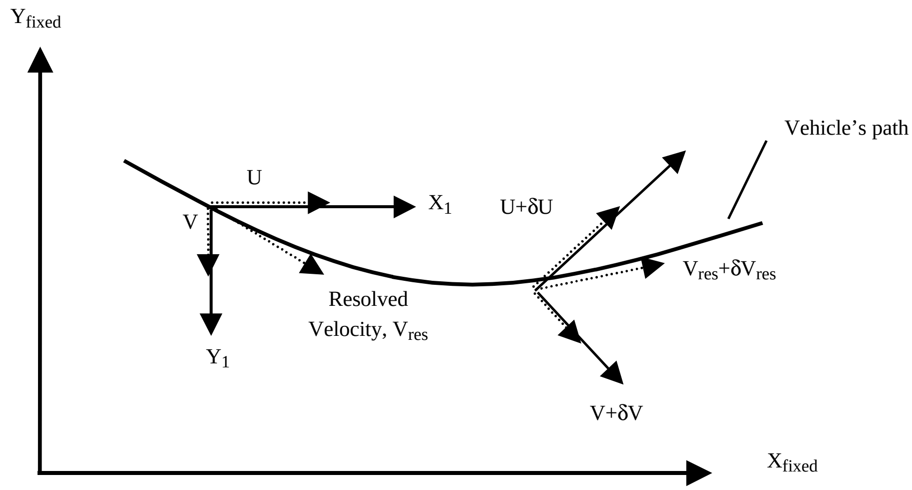

Figure 3.14: Coordinate axes rotation and translation used to derive acceleration components in body-fixed coordinates.

Let U and V represent the velocity components at time t of the vehicle along the longitudinal and lateral directions of the vehicle when the axis of measurement is fixed to the vehicle's body. Note that these velocity components are sometimes referred to as the components of the vehicle velocity relative to the moving axes. This is misleading, since there is no motion of the vehicle with respect to the vehicle's axes. The motion is of the axis itself relative to a fixed coordinate frame (Steeds 1960). To derive the acceleration, the change in velocity is determined in the moving coordinate system in the directions X_1-Y_1 when U, V, and the orientation are incremented by a differential amount. Note that the change in resolved velocity depends not only on the change in velocities U and V, but also on the change in orientation. The change in velocity parallel to X_1 is:

$$\begin{aligned}\delta V_{res,\,X1} &= (U+\delta U)\cdot\cos\delta\Psi - U + (V+\delta V)\cdot\sin\delta\Psi \\ &= U\cos\delta\Psi + \delta U\cos\delta\Psi - U + V\sin\delta\Psi + \delta V\sin\delta\Psi\end{aligned} \tag{3.27}$$

(Steeds 1960). The acceleration is obtained by dividing by δt. In the limiting case as δt goes to zero, the acceleration in this direction becomes:

$$\begin{aligned}a_X &= \frac{dU}{dt} + V\frac{d\Psi}{dt} \\ &= \dot{U} + V\cdot\omega_Z\end{aligned} \tag{3.28}$$

The component dU/dt is due to the changing velocity, while the remaining term is due to the rotation of the axes. Similarly, the acceleration component parallel to Y_1 is:

$$a_Y = \dot{V} - U\cdot\omega_Z \tag{3.29}$$

These planar accelerations agree with published data from (Will and Zak 1997), (Cho and Kim 1996).

These accelerations represent the planar accelerations of the vehicle, and neglect any bounce, pitch, or roll motion. If this perturbation analysis is continued into all three dimensions, then the acceleration component in vehicle body coordinates becomes:

$$\begin{aligned} a_X &= \dot{U} + \omega_Y \cdot W - \omega_Z \cdot V \\ a_Y &= \dot{V} + \omega_Z \cdot U - \omega_X \cdot W \\ a_Z &= \dot{W} + \omega_X \cdot V - \omega_Y \cdot U \end{aligned} \tag{3.30}$$

(Horinouchi et al. 1997) (Steeds 1960). Note that if the angular acceleration components are much larger than the positional acceleration components, the moment equation will also require a transformation (Steeds 1960). For this thesis, we will be assuming that the spin of the vehicle will be small enough that the modified moment equation is not needed. We next assume that the vehicle travels at a constant velocity, U, as measured in the vehicle's frame. For these simple studies, only a 2 DOF model is used (lateral position and yaw angle). Higher-order modeling such as roll, pitch, deceleration, or suspension dynamics will require additional acceleration components. Assuming a 2 DOF model, we can now write the equations of motion as:

$$\dot{\bar{x}} = A_X \bar{x} + B_X F \tag{3.31}$$

where

$$\begin{aligned} \bar{x} &= [V \quad \dot{\psi}]^T \\ F &= [x_1 \quad x_2 \quad x_3 \quad x_4 \quad y_1 \quad y_2 \quad y_3 \quad y_4]^T \\ A_X &= \begin{bmatrix} 0 & -U \\ 0 & 0 \end{bmatrix} \\ B_X &= \begin{bmatrix} 0 & 0 & 0 & 0 & \frac{1}{m} & \frac{1}{m} & \frac{1}{m} & \frac{1}{m} \\ -\frac{d}{Iz} & \frac{d}{Iz} & -\frac{d}{Iz} & \frac{d}{Iz} & \frac{a}{Iz} & \frac{a}{Iz} & \frac{-b}{Iz} & \frac{-b}{Iz} \end{bmatrix} \end{aligned} \tag{3.32}$$

(Alleyne 1997b). It is rare to see a controller where all four wheels are steered independently. At this point it is assumed that the two front wheels are steered by the same angle, δ_f, and the two rear wheels are steered by the same angle, δ_r. It is then assumed that the Dugoff tire model applies, then the lateral forces are determined solely by the steering input, and both front wheels produce the same lateral force. By summing the forces produced in the front two tires as y_f and the rear tires as y_r, the dimension of the force states can be reduced to:

$$\begin{aligned} F &= [x_1 \quad x_2 \quad x_3 \quad x_4 \quad y_f \quad y_r]^T \\ B_X &= \begin{bmatrix} 0 & 0 & 0 & 0 & \frac{1}{m} & \frac{1}{m} \\ -\frac{d}{Iz} & \frac{d}{Iz} & -\frac{d}{Iz} & \frac{d}{Iz} & \frac{a}{Iz} & \frac{-b}{Iz} \end{bmatrix} \end{aligned} \tag{3.33}$$

The forces, x_i and y_i, can be resolved from the wheel forces, F_{xi} and F_{yi}, by the following expression:

$$
\begin{aligned}
x_i &= Fx_i \cdot \cos(\delta_i) - Fy_i \cdot \sin(\delta_i) \\
y_i &= Fx_i \cdot \sin(\delta_i) + Fy_i \cdot \cos(\delta_i)
\end{aligned}
\tag{3.34}
$$

(Alleyne 1997a; Alleyne 1997b), (Smith and Starkey 1995). This is simply a rotation from wheel coordinates to body coordinates, where the rotation angle is the steering angle of the wheel.

For the dynamics under study, the x-direction forces are used solely to produce a moment on the system. As a simplification, we can assume that the x-forces produced by lateral steering forces, represented by the term $Fy_i \cdot \sin(\delta_i)$, produce moments that cancel each other. This term is neglected hereafter. In addition, for small steering inputs the cosine and sine terms may be approximated. Thus,

$$
\begin{aligned}
x_i &\approx Fx_i \\
y_i &\approx Fx_i \cdot \delta_i + Fy_i
\end{aligned}
\tag{3.35}
$$

Substituting the tire forces from the Dugoff Tire Model, we obtain:

$$
\begin{aligned}
x_i &\approx \frac{T_i}{r_i} \\
y_i &\approx \frac{T_i}{r_i} \cdot \delta_i + C\alpha_i \cdot \alpha_i
\end{aligned}
\tag{3.36}
$$

Using the linear representation of the slip angles:

$$
\begin{aligned}
y_f &\approx \left(\frac{T_1}{r_1} + \frac{T_2}{r_2}\right) \cdot \delta_f - \frac{2 \cdot C\alpha_f}{U} \cdot V - \frac{2 \cdot a \cdot C\alpha_f}{U} \cdot \dot{\Psi} + 2 \cdot C\alpha_f \cdot \delta_f \\
y_r &\approx \left(\frac{T_3}{r_3} + \frac{T_4}{r_4}\right) \cdot \delta_r - \frac{2 \cdot C\alpha_r}{U} \cdot V + \frac{2 \cdot b \cdot C\alpha_r}{U} \cdot \dot{\Psi} + 2 \cdot C\alpha_r \cdot \delta_r
\end{aligned}
\tag{3.37}
$$

where $C_{\alpha f} = (C_{\alpha 1} + C_{\alpha 2})/2$, $C_{\alpha r} = (C_{\alpha 3} + C_{\alpha 4})/2$.

It is clear from the above formulation that the control inputs between torque and front steering are coupled. To decouple these control inputs, some simplifying assumptions are made. First, we assume that the torque input consists of two terms, a steady-state term and a transient term that represents the torque control effort sent to each wheel.

$$
T_i = T_{nom,\,i} + \Delta T_i
\tag{3.38}
$$

Note that the torque input into the x-direction on each axle is now only affected by the transient term because the steady-state terms generate equal and opposite moments.

$$
x_i \approx \frac{\Delta T_i}{r_i}_{\;i}
\tag{3.39}
$$

Finally, it is assumed that the differential torque multiplied by the steering control input is much smaller than the steady-state torque multiplied by the steering control input. In essence, this is assuming that the control torque input into the wheels does not produce significant **lateral** forces even if the wheel is being steered while a torque is being applied. It is also assumed the tires have (approximately) the same radius. The lateral forces are:

$$y_f \approx \frac{2 \cdot T_{nom,f}}{r} \cdot \delta_f - \frac{2 \cdot C\alpha_f}{U} \cdot V - \frac{2 \cdot a \cdot C\alpha_f}{U} \cdot \dot{\Psi} + 2 \cdot C\alpha_f \cdot \delta_f$$
$$y_r \approx \frac{2 \cdot T_{nom,r}}{r} \cdot \delta_r - \frac{2 \cdot C\alpha_r}{U} \cdot V + \frac{2 \cdot b \cdot C\alpha_r}{U} \cdot \dot{\Psi} + 2 \cdot C\alpha_r \cdot \delta_r \tag{3.40}$$

With this last assumption, the control inputs are completely decoupled and the tire forces are now linear in the inputs and states. We can now conclude the model development by representing the system in state-space format as:

$$F = A_F \cdot \bar{x} + B_F \cdot \bar{u} \tag{3.41}$$

where:

$$F = \begin{bmatrix} x_1 & x_2 & x_3 & x_4 & y_f & y_r \end{bmatrix}^T \tag{3.42}$$

$$\bar{x} = \begin{bmatrix} V & \dot{\psi} \end{bmatrix}^T \tag{3.43}$$

$$\bar{u} = \begin{bmatrix} \delta_f & \delta_r & \Delta T_1 & \Delta T_2 & \Delta T_3 & \Delta T_4 \end{bmatrix} \tag{3.44}$$

$$A_F = \begin{bmatrix} 0 & 0 \\ 0 & 0 \\ 0 & 0 \\ 0 & 0 \\ -\frac{2 \cdot C\alpha_f}{U} & -\frac{2 \cdot a \cdot C\alpha_f}{U} \\ -\frac{2 \cdot C\alpha_r}{U} & \frac{2 \cdot b \cdot C\alpha_r}{U} \end{bmatrix} \tag{3.45}$$

$$B_F = \begin{bmatrix} 0 & 0 & \frac{1}{r} & 0 & 0 & 0 \\ 0 & 0 & 0 & \frac{1}{r} & 0 & 0 \\ 0 & 0 & 0 & 0 & \frac{1}{r} & 0 \\ 0 & 0 & 0 & 0 & 0 & \frac{1}{r} \\ \frac{2 \cdot T_{nom,f}}{r} + 2 \cdot C\alpha_f & 0 & 0 & 0 & 0 & 0 \\ 0 & \frac{2 \cdot T_{nom,r}}{r} + 2 \cdot C\alpha_r & 0 & 0 & 0 & 0 \end{bmatrix} \tag{3.46}$$

The linear vehicle dynamics can now be derived by substituting the above expression into (3.31):

$$
\begin{aligned}
\dot{\bar{x}} &= \underbrace{A_X}_{2X2} \cdot \underbrace{\bar{x}}_{2X1} + \underbrace{B_X}_{2X6}\left(\underbrace{A_F}_{6X2} \cdot \underbrace{\bar{x}}_{2X1} + \underbrace{B_F}_{6X6} \cdot \underbrace{\bar{u}}_{6X1}\right) \\
&= \left(A_X + B_X A_F\right) \cdot \bar{x} + B_X B_F \cdot \bar{u} \\
&= A \cdot \bar{x} + B \cdot \bar{u}
\end{aligned}
\tag{3.47}
$$

where:

$$
A = \begin{bmatrix} -2\dfrac{C_{\alpha f} + C_{\alpha r}}{m \cdot U} & -U - 2\dfrac{a \cdot C_{\alpha f} - b \cdot C_{\alpha r}}{m \cdot U} \\ -2\dfrac{a \cdot C_{\alpha f} - b \cdot C_{\alpha r}}{I_z \cdot U} & -2\dfrac{a^2 \cdot C_{\alpha f} + b^2 \cdot C_{\alpha r}}{I_z \cdot U} \end{bmatrix}
$$

$$
B = \begin{bmatrix} \dfrac{2}{m} \cdot \left(\dfrac{T_{nom,f}}{r} + C_{\alpha f}\right) & \dfrac{2}{m} \cdot \left(\dfrac{T_{nom,r}}{r} + C_{\alpha r}\right) & 0 & 0 & 0 & 0 \\ \dfrac{2 \cdot a}{I_z} \cdot \left(\dfrac{T_{nom,f}}{r} + C_{\alpha f}\right) & -\dfrac{2 \cdot b}{I_z} \cdot \left(\dfrac{T_{nom,r}}{r} + C_{\alpha r}\right) & -\dfrac{d}{I_z \cdot r} & \dfrac{d}{I_z \cdot r} & -\dfrac{d}{I_z \cdot r} & \dfrac{d}{I_z \cdot r} \end{bmatrix}
\tag{3.48}
$$

and:

m = the vehicle mass

V = the vehicles velocity (assumed to be primarily in longitudinal direction)

δ_i = the steer input into the i^th vehicle

a, b = the longitudinal distance from the C.G. to the front and rear axle

ψ = the yaw angle of the vehicle, measured w.r.t. the ground

I_z = the moment of inertia about the z-axis

C_{af}, C_{ar} = front and rear wheel cornering stiffness (see definition in text above)

$T_{nom,F,R}$ = the nominal torque produced by the front and rear tires

ΔT_i = the controlled torque input into the i^th tire

If the torque input is ignored, the resulting linear state-space model agrees with published dynamics from (Smith and Starkey 1994), (Cho and Kim 1995), (Alleyne 1997b), and (Will and Zak 1997) among others. This linear model is referred to as the bicycle model, because the dynamics represented by this model are equivalent to those of a bicycle whose motions are restricted to a single plane. The importance of the bicycle model requires further discussion.

In some instances, such as tracking problems where the coordinate system is fixed to the reference path, it is more convenient to use a fixed coordinate system to resolve the state positions rather than the state velocities. The dynamics of the fixed system are the same, except that the slip angles are defined as follows:

$$
\begin{aligned}
\alpha_1 &\approx \delta_1 + \psi - \frac{V + a \cdot \dot{\psi}}{U} \\
\alpha_2 &\approx \delta_2 + \psi - \frac{V + a \cdot \dot{\psi}}{U} \\
\alpha_3 &\approx \delta_3 + \psi - \frac{V - b \cdot \dot{\psi}}{U} \\
\alpha_4 &\approx \delta_4 + \psi - \frac{V - b \cdot \dot{\psi}}{U}
\end{aligned}
\tag{3.49}
$$

The remaining modifications become:

$$
\begin{aligned}
y_f &\approx \frac{2 \cdot T_{nom,f}}{r} \cdot \delta_f - \frac{2 \cdot C\alpha_f}{U} \cdot V + 2 \cdot C\alpha_f \psi - \frac{2 \cdot a \cdot C\alpha_f}{U} \cdot \dot{\Psi} + 2 \cdot C\alpha_f \cdot \delta_f \\
y_r &\approx \frac{2 \cdot T_{nom,r}}{r} \cdot \delta_r - \frac{2 \cdot C\alpha_r}{U} \cdot V + 2 \cdot C\alpha_r \psi + \frac{2 \cdot b \cdot C\alpha_r}{U} \cdot \dot{\Psi} + 2 \cdot C\alpha_r \cdot \delta_r
\end{aligned}
\tag{3.50}
$$

With this last assumption, the tire forces are now linear in the inputs and states, and can be written in state-space format as:

$$F = A_F \cdot \bar{x} + B_F \cdot \bar{u} \tag{3.51}$$

$$F = \begin{bmatrix} x_1 & x_2 & x_3 & x_4 & y_f & y_r \end{bmatrix}^T \tag{3.52}$$

$$\bar{x} = \begin{bmatrix} y & \dot{y} & \psi & \dot{\psi} \end{bmatrix}^T \tag{3.53}$$

$$\bar{u} = \begin{bmatrix} \delta_f & \delta_r & \Delta T_1 & \Delta T_2 & \Delta T_3 & \Delta T_4 \end{bmatrix} \tag{3.54}$$

$$
A_F = \begin{bmatrix}
0 & 0 & 0 & 0 \\
0 & 0 & 0 & 0 \\
0 & 0 & 0 & 0 \\
0 & 0 & 0 & 0 \\
0 & -\dfrac{2 \cdot C\alpha_f}{U} & +2 \cdot C\alpha_f & -\dfrac{2 \cdot a \cdot C\alpha_f}{U} \\
0 & -\dfrac{2 \cdot C\alpha_r}{U} & +2 \cdot C\alpha_r & \dfrac{2 \cdot b \cdot C\alpha_r}{U}
\end{bmatrix}
\tag{3.55}
$$

Thus, the A and B matrices become:

$$
A = \begin{bmatrix}
0 & 1 & 0 & 0 \\
0 & -2\dfrac{C_{\alpha f} + C_{\alpha r}}{m \cdot U} & 2\dfrac{C_{\alpha f} + C_{\alpha r}}{m} & -2\dfrac{a \cdot C_{\alpha f} - b \cdot C_{\alpha r}}{m \cdot U} \\
0 & 0 & 0 & 1 \\
0 & -2\dfrac{a \cdot C_{\alpha f} - b \cdot C_{\alpha r}}{I_z \cdot U} & 2\dfrac{a \cdot C_{\alpha f} - b \cdot C_{\alpha r}}{I_z} & -2\dfrac{a^2 \cdot C_{\alpha f} + b^2 \cdot C_{\alpha r}}{I_z \cdot U}
\end{bmatrix}
\tag{3.56}
$$

$$B = \begin{bmatrix} 0 & 0 & 0 & 0 & 0 & 0 \\ \frac{2}{m}\cdot\left(\frac{T_{nom,f}}{r}+C_{\alpha f}\right) & \frac{2}{m}\cdot\left(\frac{T_{nom,r}}{r}+C_{\alpha r}\right) & 0 & 0 & 0 & 0 \\ 0 & 0 & 0 & 0 & 0 & 0 \\ \frac{2\cdot a}{I_z}\cdot\left(\frac{T_{nom,f}}{r}+C_{\alpha f}\right) & -\frac{2\cdot b}{I_z}\cdot\left(\frac{T_{nom,r}}{r}+C_{\alpha r}\right) & -\frac{d}{I_z\cdot r} & \frac{d}{I_z\cdot r} & -\frac{d}{I_z\cdot r} & \frac{d}{I_z\cdot r} \end{bmatrix} \quad (3.57)$$

This agrees with (Peng and Tomizuka 1993).

3.3.5 Linearized Vehicle Dynamics – The Bicycle Model

Today, the bicycle model is one of the most widely used for purposes of vehicle lateral controllers. A derivation of this model is based on the assumption that the two front tires and two rear tires can be lumped together effectively as one tire in front and in back of the vehicle, like a bicycle. To obtain the 2 DOF vehicle model (yaw and lateral vehicle motion), several aspects of the vehicle dynamics are ignored; specifically, any dynamics associated with vehicle roll, bounce, or pitch are neglected. Included in the neglected dynamics are those associated with suspension, weight shift due to braking or acceleration, and other out-of-plane motions. Depending on the tire model chosen, a linear or non-linear 2 DOF model is obtained. The major inputs into this system are the front and rear steering angles, while the throttle angle and brake forces act as secondary inputs (Tomizuka and Hedrick 1995). Studies conducted on full sized vehicles and high-order models (LeBlanc et al. 1996; Smith and Starkey 1994; Smith and Starkey 1995) show that the bicycle model matches relatively well to a full sized vehicle and to high-order simulations for low-g (0.3) cases.

Higher-order models are sometimes used both for design and for validation of vehicle controllers. A sample development of these models can be found in (Lugner 1977; Lugner 1982; Peng and Tomizuka 1990b). The higher complexity of these models usually arises from examining increasing number of vehicle states and more complex tire forces. Since the forces for vehicle motion must arise from the contact of the tires to the ground, the tire model is a critical element of any vehicle dynamics model (Bakker, Nyborg, and Pacejka 1987; Bakker, Pacejka, and Lidner 1989). As discussed earlier, non-linear tire dynamics arise under high loading and high frequency conditions. However, it is important to note that the bicycle model ignores tire nonlinearities, and hence should not be expected to fit the measured vehicle responses under aggressive conditions.

3.3.6 Vehicle Transfer Functions

The transfer functions for the vehicle dynamics can be obtained by the standard state-space conversion: $C*(s*I-A)^{-1}*B$, where A is the state matrix, B is the control input matrix, and C is the output matrix. From this approach, it is clear that the pole locations will not change with the state under control or with method of control input or placement of the sensor. Using MATLAB's symbolic solver, the characteristic equation for the 2 state model was obtained (Note: L = a+b).

$$\text{poles} = s^2 + \left(\frac{2\left(C_{\alpha f} + C_{\alpha r}\right)}{mU} + \frac{2\left(C_{\alpha f} a^2 + C_{\alpha r} b^2\right)}{I_z U} \right) \cdot s + \frac{4C_{\alpha f} C_{\alpha r} L^2}{mI_z U^2} - \frac{2}{I_z}\left(aC_{\alpha f} - bC_{\alpha r}\right) \tag{3.58}$$

The transfer functions become:

$$\frac{V(s)}{\delta_f(s)} = \frac{\frac{2}{m}\left(\frac{T_{nom,f}}{r} + C_{\alpha f}\right) \cdot s + \frac{2}{mUI_z}\left(\frac{T_{nom,f}}{r} + C_{\alpha f}\right) \cdot \left[2bLC_{\alpha r} - amU^2\right]}{\text{poles}} \tag{3.59}$$

$$\frac{V(s)}{\delta_r(s)} = \frac{\frac{2}{m}\left(\frac{T_{nom,r}}{r} + C_{\alpha r}\right) \cdot s + \frac{2}{mUI_z}\left(\frac{T_{nom,r}}{r} + C_{\alpha r}\right) \cdot \left[2aLC_{\alpha f} + bmU^2\right]}{\text{poles}} \tag{3.60}$$

$$\frac{\dot{\psi}(s)}{\delta_f(s)} = \frac{\frac{2a}{I_z}\left(\frac{T_{nom,f}}{r} + C_{\alpha f}\right) \cdot s + \frac{4C_{\alpha r} L}{mUI_z}\left(\frac{T_{nom,f}}{r} + C_{\alpha f}\right)}{\text{poles}} \tag{3.61}$$

$$\frac{\dot{\psi}(s)}{\delta_r(s)} = \frac{-\frac{2b}{I_z}\left(\frac{T_{nom,r}}{r} + C_{\alpha r}\right) \cdot s - \frac{4C_{\alpha f} L}{mUI_z}\left(\frac{T_{nom,r}}{r} + C_{\alpha r}\right)}{\text{poles}} \tag{3.62}$$

An interesting point to note is that both the poles and zeros related to the steering inputs are invariant with respect to the average (nominal) torque input. However, the DC gain of the transfer function increases with increasing torque (assuming the nominal torque is approximately a constant). Thus, the "responsiveness" some drivers associate with front-wheel-drive vehicles is likely attributable to an increased DC gain on these transfer functions. The transfer functions associated with the differential torque input are:

$$\frac{V(s)}{\Delta T_1(s)} = -1 \cdot \frac{V(s)}{\Delta T_2(s)} = \frac{V(s)}{\Delta T_3(s)} = -1 \cdot \frac{V(s)}{\Delta T_4(s)} = \frac{\frac{U \cdot d}{r \cdot I_z} \cdot \left(1 + \frac{2}{mU^2} \cdot \left(a \cdot C_{\alpha f} - b \cdot C_{\alpha r}\right)\right)}{\text{poles}} \tag{3.63}$$

$$\frac{\dot{\psi}(s)}{\Delta T_1(s)} = -1 \cdot \frac{\dot{\psi}(s)}{\Delta T_2(s)} = \frac{\dot{\psi}(s)}{\Delta T_3(s)} = -1 \cdot \frac{\dot{\psi}(s)}{\Delta T_4(s)} = \frac{-\frac{d}{rI_z} \cdot s - \frac{2d}{rmUI_z} \cdot \left(C_{\alpha f} + C_{\alpha r}\right)}{\text{poles}} \tag{3.64}$$

Significant discussion has been given in the literature regarding "optimal" placement of vehicle positions sensors. Using the four-state model just developed, we can obtain the vehicle transfer function to position as long as we have an output equation. If the lateral position is measured from a sensor located a distance d_s (a preview sensor distance) in front of the center of gravity, then the output equation becomes:

$$\text{output} = \underbrace{\begin{bmatrix} 1 & 0 & d_s & 0 \end{bmatrix}}_{\substack{\text{pseudo-gain} \\ \text{vector, K}}} \cdot \begin{bmatrix} y \\ \frac{dy}{dt} \\ \Psi \\ \frac{d\psi}{dt} \end{bmatrix} \tag{3.65}$$

where the states are as shown. If the lateral position is measured at the center of gravity, then the d term in the output matrix becomes zero.

It is clear that the dynamics of the system with a preview sensor distance are the same dynamics as a state feedback feedback controller based on yaw angle and lateral position feedback. The feedback gain on the yaw state is proportional to sensor distance, as shown in the above equation. Conceptually, this is the same framework as a lateral position controller with additional yaw angle feedback, where the feedback gain is proportional to sensor distance, d_s. Because sensor preview gives the same effect as feedback, it is not used in this thesis. The characteristic equation for the 2 state model is then obtained (Note: L = a + b):

$$\text{poles} = s^2 + \left(\frac{2\left(C_{\alpha f} + C_{\alpha r}\right)}{mU} + \frac{2\left(C_{\alpha f} a^2 + C_{\alpha r} b^2\right)}{I_z U} \right) \cdot s + \frac{4C_{\alpha f} C_{\alpha r} L^2}{m I_z U^2} - \frac{2}{I_z}\left(aC_{\alpha f} - bC_{\alpha r}\right) \tag{3.66}$$

Interestingly, the pole locations are the same whether a fixed or a moving coordinate system is used. However, the order of the transfer function for lateral position and velocities are different. The transfer functions become:

$$\frac{\dot{y}(s)}{\delta_f(s)} = \frac{1}{s}\left(\frac{T_{nom,f}}{r} + C_{\alpha f} \right) \frac{\frac{2}{m} \cdot s^2 + \frac{4bLC_{\alpha r}}{mUI_z} \cdot s + \frac{4LC_{\alpha r}}{mI_z}}{\text{poles}} \tag{3.67}$$

$$\frac{\dot{y}(s)}{\delta_r(s)} = \frac{1}{s}\left(\frac{T_{nom,r}}{r} + C_{\alpha r} \right) \frac{\frac{2}{m} \cdot s^2 + \frac{4aLC_{\alpha f}}{mUI_z} \cdot s - \frac{4LC_{\alpha f}}{mI_z}}{\text{poles}} \tag{3.68}$$

$$\frac{\dot{\psi}(s)}{\delta_f(s)} = \left(\frac{T_{nom,f}}{r} + C_{\alpha f} \right) \frac{\frac{2a}{I_z} \cdot s + \frac{4LC_{\alpha r}}{mUI_z}}{\text{poles}} \tag{3.69}$$

$$\frac{\dot{\psi}(s)}{\delta_r(s)} = -\left(\frac{T_{nom,r}}{r} + C_{\alpha r} \right) \frac{\frac{2b}{I_z} \cdot s + \frac{4LC_{\alpha f}}{mUI_z}}{\text{poles}} \tag{3.70}$$

Note that the yaw-rate transfer functions are again invariant with respect to the coordinate system used. The torque-input transfer functions are as follows:

$$\frac{V(s)}{\Delta T_1(s)} = -1 \cdot \frac{V(s)}{\Delta T_2(s)} = \frac{V(s)}{\Delta T_3(s)} = -1 \cdot \frac{V(s)}{\Delta T_4(s)} = \frac{2 \cdot d}{r \cdot m \cdot I_z} \frac{\frac{\left(a \cdot C_{\alpha f} - b \cdot C_{\alpha r}\right)}{U} s - 2 \cdot \left(C_{\alpha f} + C_{\alpha r}\right)}{\text{poles}} \tag{3.71}$$

$$\frac{\dot{\psi}(s)}{\Delta T_1(s)} = -1 \cdot \frac{\dot{\psi}(s)}{\Delta T_2(s)} = \frac{\dot{\psi}(s)}{\Delta T_3(s)} = -1 \cdot \frac{\dot{\psi}(s)}{\Delta T_4(s)} = -\frac{d}{rI_z} \frac{s + \frac{2}{mU} \cdot \left(C_{\alpha f} + C_{\alpha r}\right)}{\text{poles}} \tag{3.72}$$

At this point, 5 separate models were developed to compare the methodologies presented here. The first model was a 2 DOF model where the small angle approximations for each wheel were not made, and the slip angle calculations were determined using inverse tangents rather than a linearization. The remaining four models consisted of two state-space models and two transfer function-based models (which are equivalent theoretically, but treated separately to confirm numerical equivalence in Wincon implementation), where one of each model type represented the dynamics derived using a moving coordinate system, and one set of dynamics represented the fixed coordinate systems. These five models were tested using a step steer input into the front and rear wheels, and a step steer input into each of the tires. Naturally, we expect the moving coordinate systems to provide the same results, and the stationary coordinate systems to provide the same results. However, there should be discrepancy between the two systems for large angles of yaw or steering. The figure below shows the data obtained from a 0.05 radian front steer step input at time t=0. The parameters used in this set of simulations were the measured bicycle parameters for the 4WD4WS vehicle.

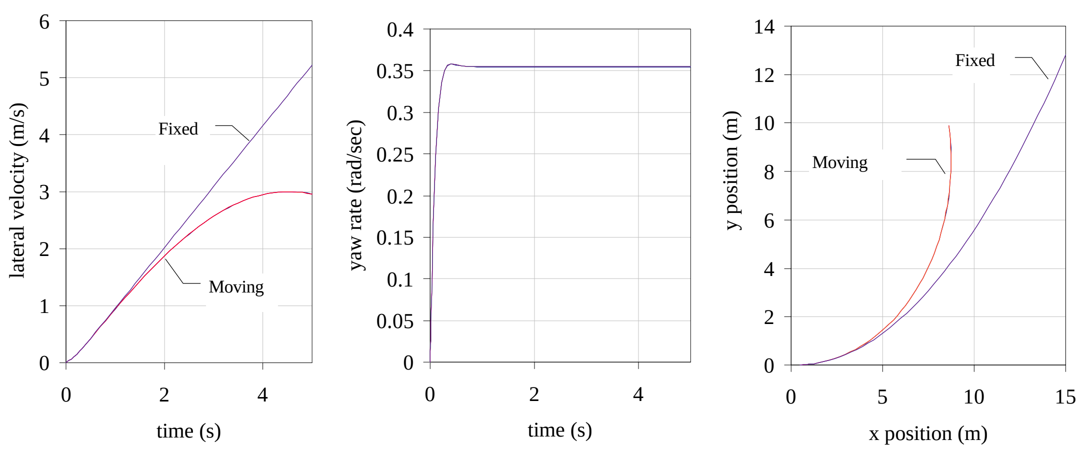

Figure 3.15: Lateral acceleration (left) yaw rate (center) and position (right) responses from 2 different vehicle coordinate frames.

In the model responses, the simulation was allowed to run long enough for the vehicle to begin to turn around. No differences were notable in comparing the nonlinear 2DOF model (utilizing nonlinear rotation and inverse tangent slip angle calculations) and the linear models that utilized body-centered coordinate systems.

In the above simulations, an increasing error is seen between the fixed coordinate system models and the moving coordinate system models. For fixed coordinate systems, it was expected that modeling errors will increase at large yaw angles because the slip angle calculation for these cases assumes that the vehicle is only at a small angle from the fixed axes. As seen in the figure above, the two systems utilizing a fixed coordinate reference frame failed to model the vehicle well as the yaw angle is increased. However, it is clear that at small yaw angles both methods gave identical results. At larger angles, the error due to the slip angle approximation rapidly increases until the velocity responses diverge as expected. In all cases, the yaw angle and yaw rate responses were nearly identical. Again, this result is expected because identical yaw-rate transfer functions were obtained for the above models. The results of the above simulations appear to provide good preliminary evaluation of the modeling approaches.

3.3.7 Steady State Solutions to Bicycle Dynamics

If a vehicle is traveling at a constant velocity around a turn of a constant radius, it is relatively easy to solve for the steady-state vehicle response to the turn because a fixed polar coordinate system can be used. At steady state, the acceleration vector tangent to the vehicle path is zero. A derivation of the relationship between steer angle and turning radius was originally done by R.T. Bundorf in "A Primer on Vehicle Directional Control" in 1968 (Bundorf 1968). The derivation provided in that paper is presented here in more detail. A diagram used in the derivation is shown below.

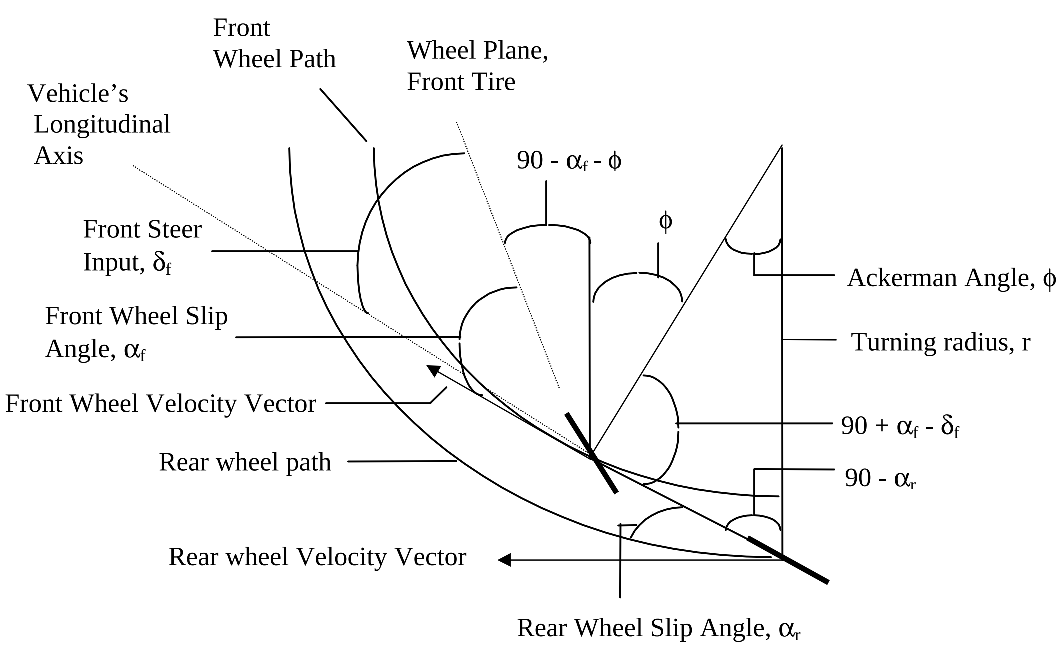

Figure 3.16: A diagram used in the derivation of the relationship between steer angle and turning radius.

When the vehicle is traveling as shown, the vehicle makes a triangle with the wheel axis as one leg, the front radius vector another leg, and the rear wheel radius vector as the final leg. The internal angles to this triangle can summed so that

$$\delta_f = \phi + \alpha_f - \alpha_r \tag{3.73}$$

The forces produced by tire 1 and tire 2 can be approximated to be

$$F_f = 2 \cdot C_{\alpha f} \cdot \alpha_f \cdot \hat{j} \tag{3.74}$$

$$F_r = 2 \cdot C_{\alpha r} \cdot \alpha_r \cdot \hat{j} \tag{3.75}$$

The sum of moments about the center of gravity is zero, so we can solve for F_f in terms of F_r.

$$F_r = -\frac{a}{b} \cdot F_f \tag{3.76}$$

The sum of forces can be written as:

$$\sum F_y = F_f + F_r = \frac{m \cdot V^2}{r} \tag{3.77}$$

Which can be combined with Equations (1) and (4) to solve for r

$$r = \frac{m \cdot V^2}{\delta \cdot 2 \cdot C_{\alpha f} \cdot C_{\alpha r}} \cdot \frac{\left(b \cdot C_{\alpha r} - a \cdot C_{\alpha f}\right)}{(b+a)} + \frac{(a+b)}{\delta} \tag{3.78}$$

This agrees with results presented in (Cho and Kim 1996) The steady-state slip angles are as follows:

$$\begin{aligned} \alpha_{f,s} &= \frac{m \cdot V^2}{\delta \cdot C_{\alpha f}} \cdot \frac{b}{(b+a)} \\ \alpha_{r,s} &= \frac{m \cdot V^2}{\delta \cdot C_{\alpha r}} \cdot \frac{a}{(b+a)} \end{aligned} \tag{3.79}$$

(Cho and Kim 1996). From Equation (3.79), we can see that if a vehicle has a center of gravity moved toward the front of the car, then the vehicle will pitch inside a constant-velocity turn. If the vehicle has a center of gravity toward the rear of the car, then the vehicle will pitch out of the turn. More importantly, Equation (3.78) gives the radius that we should expect a vehicle to turn at steady state if the vehicle dynamics are correct.

We can test the transfer functions we obtained earlier by comparison with this steady-state analysis. For a vehicle traveling around a circular track at steady state with constant steering input, we can assume that the yaw rate is the same as the change in angle of the vehicle about the center of the track. The time for the vehicle to travel around the track is given by:

$$t = \frac{2\pi}{\dot{\psi}} \tag{3.80}$$

where phi dot is the yaw rate at steady state of the vehicle. The distance traveled by the vehicle in this time is simply

$$\frac{2\pi}{\dot{\psi}} \cdot U = \text{circumference} = 2\pi \cdot r \tag{3.81}$$

where r is the radius of the turn. Thus

$$r = \frac{U}{\dot{\psi}_{ss}} \tag{3.82}$$

This equation gives the following insight: any controller attempting to maintain the vehicle on a constant radius turn at a constant velocity is simply attempting to control the inverse of the yaw rate. To compare Bundorf's result with the planer dynamics just derived, note that the steady-state yaw rate given by the DC gain of the yaw-rate transfer functions obtained previously for a front steering input:

$$\dot{\psi}_{ss}(s) = \frac{4ULC_{\alpha f}C_{\alpha r} \cdot \delta}{4C_{\alpha f}C_{\alpha r}L^2 + 2mU^2 \cdot \left(b \cdot C_{\alpha r} - a \cdot C_{\alpha f}\right)} \tag{3.83}$$

The steady state radius given by these transfer functions is thus:

$$r = \frac{4C_{\alpha f}C_{\alpha r}L^2 + 2mU^2 \cdot \left(b \cdot C_{\alpha r} - a \cdot C_{\alpha f}\right)}{4LC_{\alpha f}C_{\alpha r} \cdot \delta} \tag{3.84}$$

$$r = \frac{L}{\delta} + \frac{mU^2}{2\delta C_{\alpha f}C_{\alpha r}} \cdot \frac{\left(b \cdot C_{\alpha r} - a \cdot C_{\alpha f}\right)}{L} \tag{3.85}$$

Which is identical to the value obtained by Bundorf and others using their polar type of analysis and making no small angle assumptions. The fact that each approach (polar coordinates versus fixed body coordinates versus globally fixed coordinates) gives the exact same turning radius at high speeds validates the model development for each method.

3.3.8 Bicycle Model Trends

In the conventional, front-wheel steering systems found on nearly all vehicles, only the front wheels are actively involved in controlling the lateral motion of the vehicle. In the basic vehicle response to a steering input, there are usually two characteristic degrees of freedom: yaw rate and sideslip angle (or lateral velocity). The sideslip angle is related to lateral acceleration by:

$$\ddot{y} = V \cdot \left(\dot{\psi} + \dot{\beta}\right) \tag{3.86}$$

where V is the vehicle velocity, phi is the yaw angle, and beta is the body sideslip angle (Furukawa and Abe 1997). With two wheel steering, the phase lag of the lateral acceleration increases with respect to the yaw rate response. This is caused by the decrease in the steady-state gain of the body sideslip angle with increasing speed. At some velocity, the steady-state gain becomes negative, and the possibility for unstable vehicle motion increases. Several control approaches discussed in the literature review specifically focus on minimizing this effect.

In the studies conducted in this thesis, we were more concerned with the yaw dynamics of the vehicle rather than the sideslip. Because the dynamics for both yaw rate and sideslip share the same pole locations, a discussion of one will serve for both. Hereafter, only yaw dynamics are considered, and specific focus is given to speed related dynamic changes as well as model sensitivity to changes in cornering stiffness.

One of the most common causes for driver (and controller) errors is that the vehicle may be driving on a surface with changing road friction coefficients, such as ice or water. Later testing addresses controller robustness to such variations; however, a theoretical analysis of the effect of parameter changes on the bicycle model is needed. The parameter that most significantly affects the bandwidth vehicle response is the cornering stiffness. As noted in (Jansen and VanOosten 1995), as the cornering stiffness increases, the bandwidth of the system increases, the damping of the system increases (decreasing overshoot). Jansen and VanOosten also outline the model sensitivity to the roll damping and tire relation length.

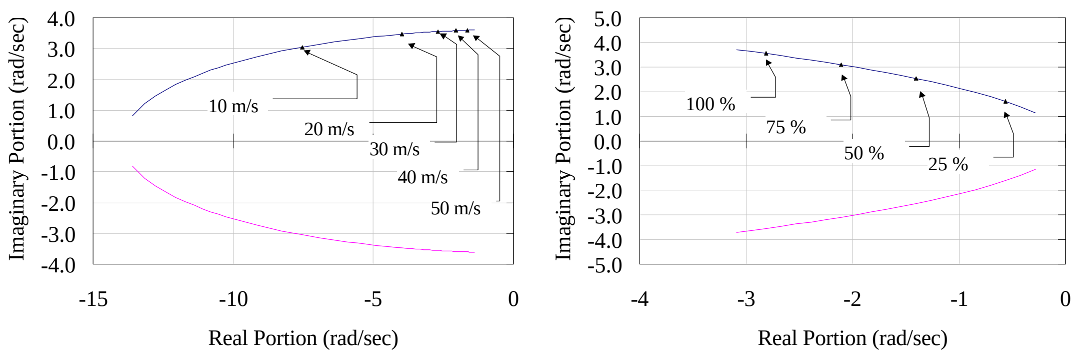

Figure 3.17: A root-locus of the bicycle model (for average full-sized vehicle) with respect to velocity (left) and cornering stiffness (right).

The above root-locus plots, generated using the nominal vehicle parameters presented in (Alleyne 1997a; Alleyne 1997b), illustrate the linear dynamics' pole dependence on velocity and cornering stiffness. Both the speed and cornering stiffness greatly affect the bandwidth, but changes in velocity also affect the damping ratio of the system in addition to bandwidth. Both of these variations have significant implications in controller dynamics of the closed-loop system, and are very difficult to account for. One method is to use robust control theory to create a controller that is robust to all classes of plant changes. Clearly from the above Bode plots, this approach is quite difficult because of the amount of variation in plant dynamics. Another method has been to use gain scheduling; however, this assumes that plant parameters are known exactly and that the model is very closely described by the bicycle model. One final method is to use adaptive algorithms to identify either the plant or the parameters, and then design a controller structure suitable to these dynamics using standard control techniques.

3.3.9 Comparison of Bicycle Model to Full Dynamics

Currently there is a lack of well-documented vehicle response measurements that include all of the required data for accurate simulation (Smith and Starkey 1995). In the paper by Smith and Starkey (Smith and Starkey 1994; Smith and Starkey 1995), a comparison is made between 2D, 5D, and 8D models and experimental vehicle data obtained by other authors. For low-g maneuvers, a good agreement was obtained between all of these models. However, above 0.6 g's, the tire response becomes non-linear and an automated steering control system based on the 2D or 5D models may produce unexpected results (Smith and Benton 1996). The authors demonstrate via controller implementation that ignoring these dynamics can significantly affect the performance (including destabilizing the vehicle) during aggressive maneuvers (Smith and Starkey 1994). The tire lag dynamic was cited in this paper as being the primary cause of modeling error; however, for the validation data used to make this conclusion, the effect of tire lag cannot be separated from actuator dynamics. The authors do note that inclusion of tire dynamics in the linear model results in a linear model that is seemingly valid up to 0.6 g's.

Historically, the question of how well the bicycle model matches measured vehicle responses has been questioned. It is easy to confirm that the model accurately predicts the steady-state behavior of the vehicle, but controller implementation is most concerned with transient performance (drivers usually don't have several minutes to avoid an accident when driving a car!). In recent history, several authors have directly addressed this issue, notably the papers(LeBlanc et al. 1996; Smith and Starkey 1994; Smith and Starkey 1995). The general conclusions of these experimental studies can be inferred by the previous paragraphs: the linear bicycle model (2-DOF) is valid for controller design as long as accelerations do not exceed 0.3 g's and obvious tire saturation (such as black-ice) does not occur. Accepting the conclusions of other researchers, we may now assume that the bicycle model can model full-sized vehicles. However, the question remains of how well do scale vehicles model full-sized vehicle. To develop an answer to this question, we use the bicycle model as the method of comparison.

3.4 Comparing Scale and Full-Sized Vehicle Dynamics

A natural question asked when one system must dynamically match another is what is the quality of the representation? It is not enough to say that a scale vehicle has the same trends, similar dynamics, or about the same performance. What is needed is a method to quantify the exact agreement between scale system and full sized vehicle. The dynamics of the vehicle must be central to this quantification, because the purpose of the control presented here is to determine methods to affect the vehicle dynamics. The method of quantification presented here is the Buckingham Pi Theorem of Dimensional Similitude, dating from 1914. First, an overview of the theorem is presented. After this, the methods of the theorem are applied to vehicle dynamics to determine the testing conditions required for dynamic similitude.

3.4.1 Introduction to the Buckingham Pi Theorem

The Buckingham Pi theorem is based on dimensional analysis whose central idea is to substitute a set of dimensionless numbers for the dimensional physical variables that describe the dynamics of a system. Because the dimensionless numbers are products or ratios of the physical variables, this process always reduces the number of variables needed to physically describe a problem. From a dynamical standpoint, the effect of this reduction is to non-dimensionalize the differential equations describing the dynamics of the system. The Buckingham Pi theorem states that two systems are dynamically similar if both systems, by selection of the same dimensionless numbers, yield the same non-dimensional differential equation (McMahon and Bonner 1983).

To determine the number of dimensionless parameters (known as Pi groups), the fundamental quantities must be determined. The fundamental quantities of a system consist of the minimum number of unit dimensions needed to describe each parameter. For instance, the units of measure for density are mass units/ (length units)^3. The fundamental quantities generally discussed in literature are Mass/Length/Time (MLT) or Force/Length/Time (FLT). Other fundamental quantities include Temperature, Power, Charge, etc. The Buckingham Pi theorem states that for m physical values defined in terms of n independent fundamental quantities, there are (n – m) independent dimensionless groups, known as Pi groups (Buckingham 1914). Before discussing the analysis of Pi groups, a simple example is presented from (McMahon and Bonner 1983) that motivates the discussion.

Consider using the Buckingham-Pi Theorem to predict the period of a pendulum (McMahon and Bonner 1983). Assuming that air resistance does not affect the pendulum dynamics, we may note beforehand (by experiment perhaps) that the period of the pendulum is invariant with the mass, but changes with changing length of pendulum arm. Because the fundamental quantities of the length and period of the arm are L and T, there is no way of combining these two parameters to cancel their units. If we guess that the formula for the period will depend somehow on gravity, we may add the gravitational acceleration as another parameter for our guessed formula. We then would obtain as a possible Pi group the term T^2*g/l. If we conduct experimental studies for various pendulums at small amplitudes, we would find that the above term in fact does remain constant! A derivation of the period from first principles would also confirm this and reveal the numerical value of this constant.

To approach the much more difficult problem of predicting the period of a pendulum at larger amplitudes, it would be natural to use numerical studies or repeated experiments to obtain a prediction for period based on measured parameters. However, by simply guessing that the longer period may additionally depend also on the length of the arc, another Pi group may be formed of a/l, where a is the arc length. Conducting a simple experiment, we would find for a constant a/l for any pendulum that the other pi group remains constant! The use of the Buckingham Pi theorem is demonstrated further in later sections where it is applied to the dynamics of scale automobiles.

3.4.2 Situations Where Dynamic Analysis May Fail

Dimensional analysis sometimes reveals that multiple pi groups affect the dynamics of a model such that matching one pi group causes mismatch with another. An example would be the testing of a 1/50-scale submarine in a tank of water. The drag on a submarine depends on the Reynolds number (viscous friction) and the Froude number (energy lost to wave propagation). The Reynolds number predicts that the submarine would have to travel at 50 times the full-size speed, while the Froude number predicts 0.14 times the full-size speed. In this case, both conditions cannot be met. To overcome this problem, the surface of the scale model is often roughened to increase the Froude number artificially by gluing a strip of sandpaper to the model near the bow. The same dimensional matching problem is encountered with scale aircraft, where both the Mach numbers and Reynolds numbers must be matched. To change the Reynolds number, a trip wire is often introduced near the leading edges of the wings and body to cause turbulence. This "compensation" is not always exact, yet scale model testing remains a primary method to test aircraft and ship designs. In the next section, it is shown that the dynamic scaling of vehicles is relatively easy to obtain (when compared to aircraft or submarine testing), and yields insightful results into the governing differential equation known as the bicycle model.

3.4.3 Similitude of the Bicycle Model

Originally, the dynamic similitude of the vehicles used in the IRS was validated with the notion that pole/zero equivalence between full sized and scale vehicles justifies dynamic similitude. Experimentally, it was found that the input/output pole/zero locations were similar to those of full-sized vehicles. However, it was later shown by work conducted in this thesis that the dynamic matching was obtained via the actuator dynamics, rather than true vehicle body dynamics. In this section, it is shown that dynamic similitude does in fact guarantee identical pole locations, but that the reverse is not true.

To apply the Buckingham-Pi Theorem to the control of a scale vehicle, the governing dynamic equations are first examined. From analysis of the bicycle model, we assume that the lateral position and yaw rate will be a function dependent on the scaled parameters:

$$Y = f\left(\delta, m, I_z, V, a, b, C\alpha_f, C\alpha_r, T, r\right) \tag{3.87}$$

If we assume that Y exists, then we can always define a function, g(s), where:

$$0 = g\left(Y, \delta, m, I_z, V, a, b, C\alpha_f, C\alpha_r, T, r\right) \tag{3.88}$$

As a reminder, it was assumed in the development of the bicycle model that the net velocity of the vehicle, V, is approximately equal to the longitudinal velocity, V_x.

The Buckingham Pi theorem states that any function that can be written in the above form can be rewritten in a dimensionless form without changing the solution to the differential equation. As discussed earlier, similitude is achieved by grouping the parameters into (n – m) independent dimensionless parameters, where n is the number of parameters and m is the dimension of the unit space occupied by the parameters. The parameters with units used above, along with their primary unit dimensions, are:

$$
\begin{aligned}
&m = kg = [M] \\
&V = V_x = V_y = m/s = \left[\frac{L}{T}\right] \\
&Y = L = a = b = d = r = [L] \\
&C_{\alpha f} = C_{\alpha r} = \left[\frac{kg \cdot m}{s^2}\right] = \left[\frac{ML}{T^2}\right] \\
&I_z = \left[kg \cdot m^2\right] = \left[ML^2\right] \\
&T = \left[\frac{kg \cdot m^2}{sec^2}\right] = \left[\frac{ML^2}{T^2}\right]
\end{aligned}
\tag{3.89}
$$

Note that the angles such as the steer angle and slip angle are unitless and thus form their own Pi groups (all angles are unitless because they represent the ratio of an arc length to the radius of the arc). It is clear that the basic unit dimensions are time, length, and mass. Thus, there are 3 primary dimensions in the unit space, and 6 parameters in question (assuming consistent length scaling throughout the vehicle). If we choose m, V, and L as repeating parameters, we can express the remaining 3 parameters as dimensionless groups, to create 3 pi groups. First, a dimensional equation is formed in powers of the repeating parameters.

$$
C\alpha_f \cdot m^a \cdot V^b \cdot L^c = \left[\frac{ML}{T^2}\right] \cdot [M]^a \cdot \left[\frac{L}{T}\right]^b \cdot [L]^c = [MLT]^0 \tag{3.90}
$$

Equating the powers, three equations are obtained:

$$
\begin{aligned}
&\text{mass} && 1 + a = 0 \\
&\text{time} && -2 - b = 0 \\
&\text{length} && 1 + b + c = 0
\end{aligned}
\tag{3.91}
$$

Solving the equations gives a = -1, b = -2, and c = 1. Hence, the first pi group is $C_{\alpha 1}L/mV^2$. Solving for the second Pi group:

$$
I_z \cdot m^a \cdot V^b \cdot L^c = \left[ML^2\right] \cdot [M]^a \cdot \left[\frac{L}{T}\right]^b \cdot [L]^c = [MLT]^0 \tag{3.92}
$$

Equating the powers, three equations are obtained:

$$
\begin{aligned}
&\text{mass} && 1 + a = 0 \\
&\text{time} && -b = 0 \\
&\text{length} && 2 + b + c = 0
\end{aligned}
\tag{3.93}
$$

Solving the equations gives a = -1, b = 0, and c = -2. The second pi group is Iz/mL^2. Solving for the third Pi group:

$$
T \cdot m^a \cdot V^b \cdot L^c = \left[\frac{ML^2}{T^2}\right] \cdot [M]^a \cdot \left[\frac{L}{T}\right]^b \cdot [L]^c = [MLT]^0 \tag{3.94}
$$

Equating the powers, three equations are obtained:

$$
\begin{aligned}
&\text{mass} && 1 + a = 0 \\
&\text{time} && -2 - b = 0 \\
&\text{length} && 2 + b + c = 0
\end{aligned}
\tag{3.95}
$$

Solving the equations gives a = -1, b = -2, and c =0. The third pi group is T/mV^2. A summary of all pi groups:

$$\Pi_1 = \frac{a}{L}, \Pi_2 = \frac{b}{L}, \Pi_3 = \frac{r}{L}, \Pi_4 = \frac{C_{\alpha f}L}{mV^2}, \Pi_5 = \frac{C_{\alpha r}L}{mV^2}, \Pi_6 = \frac{Iz}{mL^2}, \Pi_7 = \frac{T}{mV^2} \tag{3.96}$$

The Buckingham Pi theorem states that if two dynamic systems are described by the same differential equations, then the solution to these differential equations will be the same if the pi groups are the same. This becomes clear during non-dimensionalization of the governing non-linear differential equations. To perform the non-dimensionalization, note that the differential equations are performing derivatives of velocity, time, and yaw angle. By using the repeating parameters chosen above, we can select:

$$\begin{aligned} t^* &= t \cdot \frac{V}{L} \\ Vy^* &= \frac{Vy}{V} \end{aligned} \tag{3.97}$$

Note that the yaw angle measured in radians is non-dimensional and needs no parameter transformations. Examining small perturbations of each parameter, we obtain the differential relationships between the above parameters.

$$\begin{aligned} \frac{L}{V} \cdot dt^* &= dt \\ V \cdot dVy^* &= dVy \end{aligned} \tag{3.98}$$

Note that substitution of the above values into the differential equations representing the bicycle model yield a non-dimensional bicycle model.

To determine the validity of the use of scaled vehicles on the IRS, originally the pole locations of the scale vehicle were compared to the full sized vehicles. These pole locations are determined by the eigenvalues of the 'A' matrix for the bicycle model. These eigenvalues are the solution to the polynomial equation in the Laplace variable, s:

$$s^2 + \left(\frac{1}{mV}\left(C_{\alpha f} + C_{\alpha r}\right) + \frac{1}{I_z V}\left(a^2 C_{\alpha f} + b^2 C_{\alpha r}\right) \right) s + C_{\alpha f} C_{\alpha r} \frac{L^2}{I_z m V^2} - \frac{1}{I_z}\left(aC_{\alpha f} + bC_{\alpha r}\right) = 0 \tag{3.99}$$

Note that the s term has units of (sec^{-1}), so we may make a scale transformation to non-dimensional coordinates:

$$s^{*2} + \left(\left(\frac{C_{\alpha f}L}{mV^2} + \frac{C_{\alpha r}L}{mV^2} \right) + \frac{mL^2}{I_z}\left(\left(\frac{a}{L}\right)^2 \frac{C_{\alpha f}L}{mV^2} + \left(\frac{b}{L}\right)^2 \frac{C_{\alpha r}L}{mV^2} \right) \right) s^* + \frac{C_{\alpha f}L}{mV^2}\frac{C_{\alpha r}L}{mV^2}\frac{mL^2}{I_z} - \frac{mL^2}{I_z}\left(\frac{a}{L}\frac{C_{\alpha f}L}{mV^2} + \frac{b}{L}\frac{C_{\alpha r}L}{mV^2} \right) = 0 \tag{3.100}$$

$$s^{*2} + \left(\left(\Pi_4 + \Pi_5\right) + \frac{1}{\Pi_6}\left(\Pi_1^2 \Pi_4 + \Pi_2^2 \Pi_5 \right) \right) s^* + \Pi_4 \Pi_5 \frac{1}{\Pi_6} - \frac{1}{\Pi_6}\left(\Pi_1 \Pi_4 + \Pi_2 \Pi_5\right) = 0 \tag{3.101}$$

Clearly, if the pi groups exactly match between two systems governed by the bicycle model, then both characteristic equations will be the same and the normalized pole locations will be the same. If we compare the relationship between pi groups and pole locations in the above equation, five pi groups are used to match two coefficients. Although the five pi groups uniquely characterize the two coefficients of the characteristic equation, clearly many different combinations of pi-groups can achieve the same characteristic equation. Thus, the characteristic equation does not uniquely characterize the pi groups.

To test for dynamic similitude of the IRS, full sized and scale vehicle parameters, pole locations, and pi groups were compiled (see Appendix 1) (compare.xls). Discussion of the agreement between scale and full-sized vehicles is discussed in detail in later sections of the thesis. To summarize these results, analysis shows experimentally and theoretically that exact agreement can be achieved between scale and full sized vehicle dynamics if testing conditions are chosen correctly.

3.4.4 Measured Vehicle Parameters

The transfer function previously derived for the lateral dynamics behavior of a vehicle was previously derived via bicycle model parameters. We can note that these parameters consist of many values that are experimentally measurable, such as vehicle speed, mass, and moment of inertia. If these values are measured and substituted into the transfer function given above, then a reasonable approximation of the vehicle's transfer function should be obtained. Although the measurement of the vehicle mass is trivial, measuring the other values is not obvious. This section describes the measurement of these parameters and the resulting parameter trends determined by these measurements. A summary of these parameters is then provided.

3.4.4.1 Vehicle Weight and Center of Gravity Location

Determination of the vehicle weights and location of the center of gravity was almost trivial. The vehicles were weighed using a postal scale. The center of gravity, by definition, is the point where the net force vector on an object would pass through if the object were acted upon by a gravitational (or inertial) force. To determine the vehicle's center of gravity, the vehicle was suspended at various angles and it was noted where the suspension line passed through the vehicle. The center of gravity is the point at which these lines cross. The picture shown below shows this being done for the vehicle.


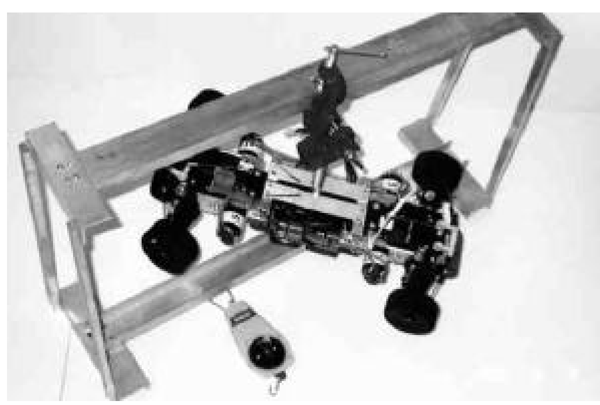

Figure 3.18: A picture of the hang method used to find the center of gravity (left) and the oscillation test stand with car (right).

Once the center of gravity was determined, the wheel displacements from the center of gravity (x_i) were measured, and the vehicle length was determined from these measurements. Note that X_1 is the distance from the C.G. to the front axle and X_2 is the distance from the C.G. to the rear axle. In addition, the normal forces produced from the front and rear axles was measured separately, and a force/moment balance was used as a second method to verify the C.G. location.

3.4.4.2 Measurement of the Z-Axis Moment of Inertia

To determine the z-axis moment of inertia, each vehicle was suspended by a spring (shown above), and the period of oscillation about the z-axis was measured. For a mass that is suspended by a spring whose force is proportional to angle, the governing equation is given by the equation:

$$\sum M_z = I_z \ddot{\theta} = -\beta\dot{\theta} - k\theta \tag{3.102}$$

where β is a damping term [N*m*sec/rad], I_z is the z-axis moment of inertia [kgm^2] and k is a spring constant [N*m/rad]. If we take the Laplace transform of the equation and set it equal to zero (our input), we obtain:

$$\left(I_z s^2 + \beta s + k\right)\theta(s) = 0 \tag{3.103}$$

If we solve for s, we obtain

$$s = -\frac{\beta}{2I_z} \pm \sqrt{\left(\frac{\beta}{2I_z}\right)^2 - \frac{k}{I_z}} \tag{3.104}$$

If the system is underdamped, the terms inside the square root will be imaginary, and the system will be a sinusoid with exponentially decaying amplitude. The time constant of the decay, $-\beta/(2\cdot I_z) = \lambda$, can be measured as well as the spring constant k and the frequency of the response. From these measurements, note that

$$\omega^2 = -\lambda^2 + \frac{k}{I_z} \tag{3.105}$$

$$I_z = \frac{k}{\lambda^2 + \omega^2} \tag{3.106}$$

Thus, a measurement for I_z is obtained. To measure the torque spring constant, a scale was applied on the suspended vehicle at a known distance from the pivot point. The force required to maintain a displaced spring angle was then measured. The graph below shows a sample data run.

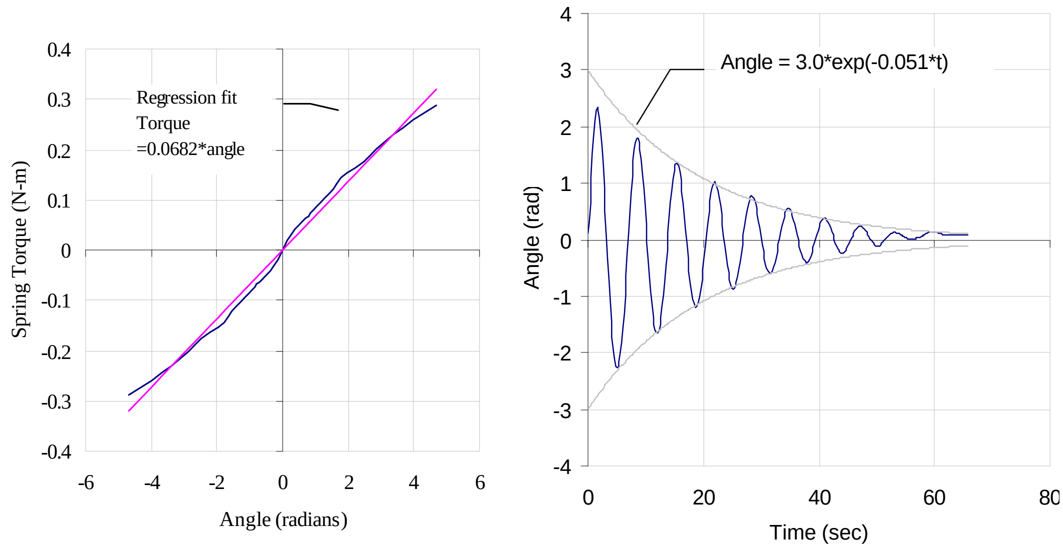

Figure 3.19: The experimental determination of the spring torque constant (left), and oscillatory response of the system suspended from the spring(right).

After the spring constant is determined, a time response of the system is obtained (shown above). This response is then examined to determine an exponential fit to determine lambda. In the above figure, lambda is approximately 0.051 rad/sec and the period of 6.51 seconds. The frequency of the system is hence 0.965 rad/sec. From the moment equation previously developed, the moment of inertia is calculated in this case to be 0.0730 [kg-m^2]. Note that the inclusion of the damping term only affects the I_z determination by 0.2 percent. Hence, the system can be approximated as a simple harmonic oscillator with no damping.

The measured I_z value can be verified by approximating the vehicle as a solid block and then calculating the z-axis moment of inertia. The equation for the moment of inertia for a block is:

$$Iz = 1/12\ M * (a^2+b^2) \tag{3.107}$$

where a and b are the length and width of the block, and M is the mass. If the density of the block is known, then the equation can be rewritten as:

$$Iz = 1/12 \cdot \rho \cdot a \cdot b \cdot h \cdot (a^2+b^2) \tag{3.108}$$

(Serway 1990). If the vehicle is approximated as a slab of aluminum (density 2.7×10^3 kg/m^3) with dimensions of 1.5-cm height, 40-cm length, and 20-cm width, then I_z is 0.054 kg·m^2. Note that the weight of this theoretical slab is 3.24 kg, which is in rough agreement with the measured vehicle weights, and the I_z moments also approximately agree.

3.4.4.3 Cornering Stiffness

Before beginning an explanation of the experimental testing, it is assumed that the reader is familiar with the Dugoff tire model and the corresponding importance of the cornering stiffness, C_α . A discussion of this model is provided in the previous "tire forces" sections of this thesis work.

The tire forces produced by the wheels of the scale vehicles were determined in two methods: holding the slip angle constant and measuring the wheel force, and by applying a known force to the system under feedback control, and measuring the steady-state wheel angle. The setup used to experimentally measure the cornering stiffness via known slip angles is shown in the test stand shown below.

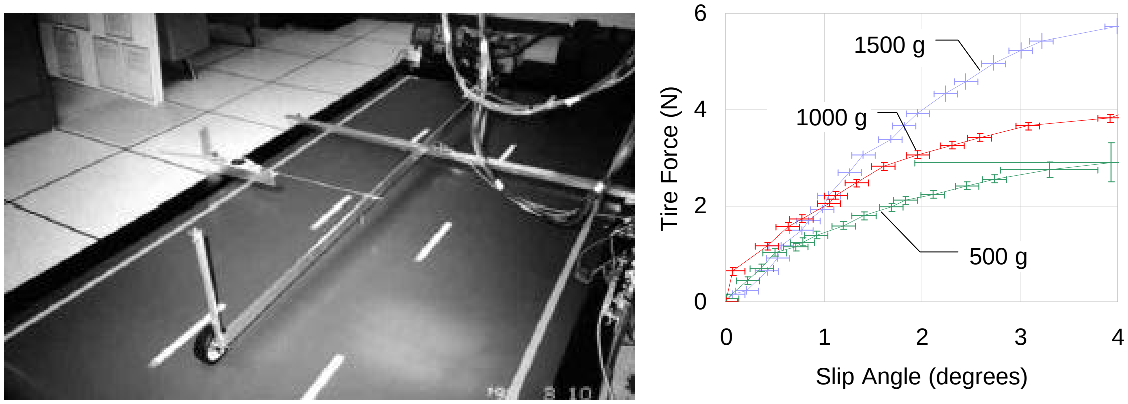

Figure 3.20: The cornering stiffness measurement stand (left) and sample cornering stiffness runs using this stand (right).

Initial testing of the vehicle focused on the effect of changing loads on the tire cornering stiffness. As seen in the above graph, the normal force on the tire primarily affect the roll-off of the tire forces. The cornering stiffness was obtained by conducting a linear regression on the above curves at small slip angles (where the plots were approximately linear). Some slight variation in the cornering stiffness were observed: at 500 g, C_α of a single tire measured to be 1.5 N/deg., 1000 g measured 1.60 N/deg., and at 2000 g measured to be 2.09 N/deg. At high slip angles (above 4 degrees slip), the tire forces increased slightly, but the tire tended to "roll" under the axle of rotation. At extreme angles, above 8 to 10 degrees of slip, the rubber rolling under the tire would begin to show stick-slip effects, and would rapidly deform under the hub of the wheel and bounce back onto the hub, causing the wheel and stand to literally bounce. At higher angles, this bouncing actually caused loss of contact with the road surface and a consequent decrease in measure forces.

Depending on the tire model used, the cornering stiffness is usually assumed to be independent of wheel loading. To investigate this assumption, the slip angle was held constant at an aggressive turning angle of 3 degrees, and the load on the tire was varied. The forces were measured, producing the relationship shown in the figure below on the left. The tire forces seem to scale linearly with normal force on the tire. To determine any velocity dependence, the load was held constant on the tire, and the velocity was varied at constant slip angles. Two slip angles were tested, 1 degree and 3 degrees. The resulting relationships are shown below in the figure on the right. Clearly, at constant normal load and cornering stiffness, the tire forces seem to be independent of vehicle velocity.

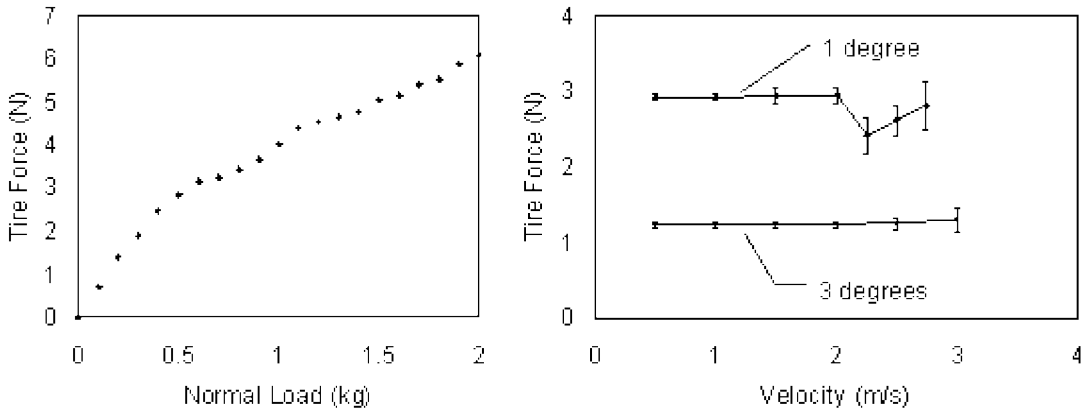

Figure 3.21: The variation of tire force with normal force (left) and velocity (right).

The angle at which the tire forces saturate was assumed to be the point where the tire roll-under becomes significant. This was assumed to be the point where notable wheel oscillation was observable due to the rubber stick-slip cycle. The change in critical slip angle with respect to velocity and normal force was examined, and the relationship is shown below in the figure on the left.

To determine how sensitive the cornering stiffness was to tire make and type, an experiment was conducted where two tires are compared: one with slick tread and one with knobby tread. The slick tire was the tire used for low-speed (1.2 m/s) testing where dynamic matching was not yet considered. The knobby tire was the tire used for high speed (3.0 m/s) testing, where emphasis was placed on dynamic matching. The choice of a knobby tire was not a random one. Previous researchers have reported that the cornering stiffness of scale vehicles tends to be too high for comparison with full-sized vehicles, and as a compensation knobby tires were used. Naturally, the ability to change cornering stiffness is important with respect to dynamic matching of full-sized vehicles. The cornering stiffness relationships are shown below in the figure on the right.

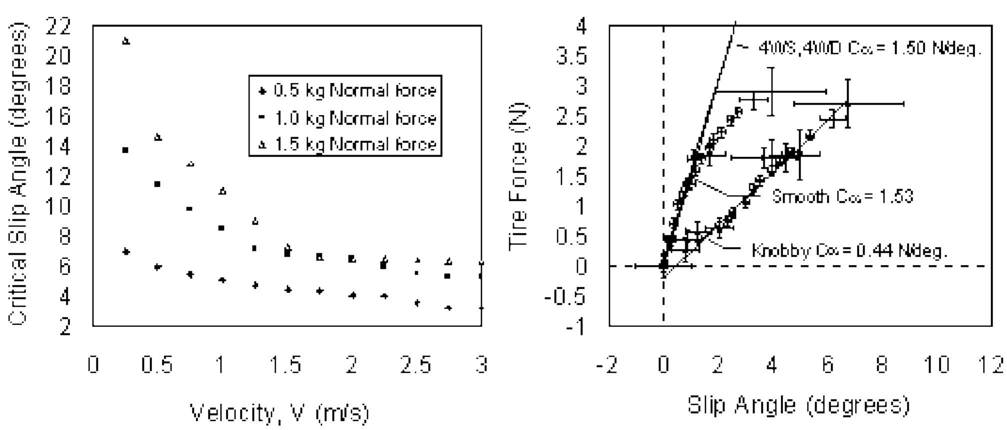

Figure 3.22: The variation of the critical slip angle with velocity for the 4WS,4WD tires (left), and a comparison of each tire type (right).

With the Uberquad vehicle, the cornering stiffness was measured in the closed-loop as previously described. Thus, the normal forces and operating conditions on the vehicle are identical to those of the experimental testing. The following figure summarizes the cornering stiffness experiment results. To measure the slip angle, the steering motor angle was recorded. This angle is simply a constant (approximately 1.3 for the front wheels, 1.1 for the rear wheels) larger than the wheel angle. Note that the closed-loop identification provided a much better "quality" of data. The linearity at small cornering angles AND roll-off of the tire forces at large angles is quite evident. At very large angles, the force/slip-angle relationship levels off to a nearly horizontal line.

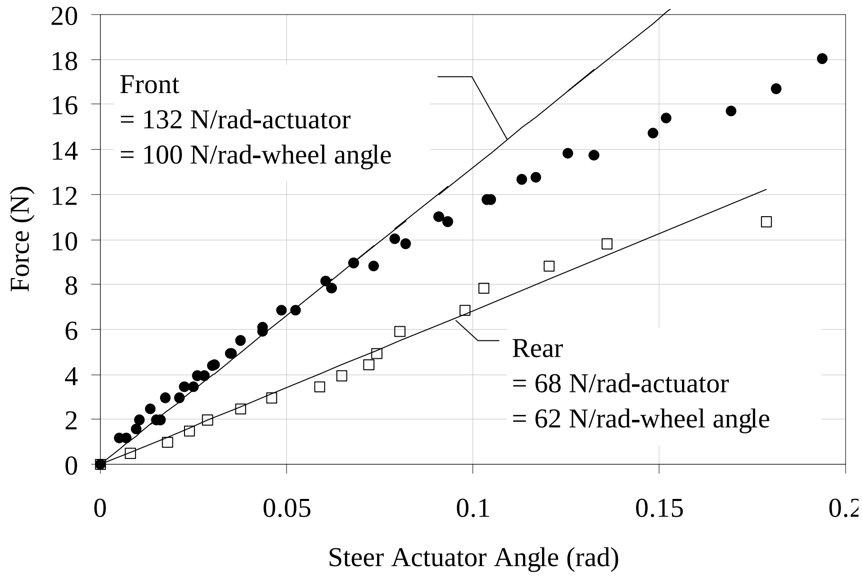

Figure 3.23: The cornering stiffness for the Uberquad vehicle at 3.0 m/s.

For the Uberquad, the rear cornering stiffness was approximately 2/3 less than the front cornering stiffness. Most published values for cornering stiffness make the assumption that both the front and rear cornering stiffness values are the same. However, those publications that report two separate measurements (implying that each was measured separately) show that the rear cornering stiffness on full-sized vehicles are approximately 2/3 the cornering stiffness of the front tires. In the comparison below between the "average" full-sized pi groups and the vehicle's cornering stiffness, it should be noted that the full-sized cornering stiffness "average" is biased by those data that assume the same cornering stiffness for both tires. Noticeable exceptions are the data presented by Lee and Pillutti. For instance, (Lee 1997) report the following values for (front, rear): Ford Escort, (72,500,49600); Buick Skylark (80790,58300); and Ford Taurus (120400,90980).

Note that the above tire analysis does not include any transient dynamic effects in the tire model as discussed in earlier sections. In the testing of full-sized vehicles, several authors have noted that the transient effects on tires can have a significant effect at higher frequencies on the model fit (Jansen and VanOosten 1995). Smith and Starkey go further and demonstrate that linear models that do not include tire dynamics will severely underestimate the distance needed to perform emergency lane changes (Smith and Starkey 1994). These authors cite tire lag as the primary cause for discrepancies between linear models and experimental data during high-g maneuvers. One note must be said of this result: based on the data the authors use to validate their conclusions, the effects of tire lag cannot be separated from actuator dynamics.

3.4.4.4 Summary of Measured Values

Table 3.3: Summary of the Measured Physical Values

Parameter	Follow Vehicle	4WS4WD at 1.2 m/s testing	4WS4WD at 3.0 m/s testing	Uberquad at 3.0 m/s testing
Mass (kg)	1.47	2.61	4.02	6.52
Iz (kg-m2)	0.0236	0.66	0.13	0.183
a (m)	0.13	0.15	0.1387	0.155
b (m)	0.18	0.185	0.1893	0.235
Caf (N/rad)	87.7	85.9	20.00	96.00
Car (N/rad)	87.7	85.9	45.00	65.00

The parameters on the 4WS4WD are intentionally changed during the second test (at 3.0 m/s) to obtain better dynamic matching. This vehicle was originally designed and tested at 1.2 m/s without knowledge of dynamic scale matching (which is evident in the poor pi matching shown below). The following table shows the pi-group matching conducted on the 4WS4WD vehicle between the 1.2 m/s and 3.0 m/s experiments. Clear improvement is seen in the pi-group matching between.

Table 3.4: Summary of the Pi-matching for the 4WS4WD vehicle

4WS4WD Vehicle Summary	Smooth Tires No Added Mass (Original Configuration)	Knobby Tires No Added Mass	Knobby Tires Added Mass (Final Configuration)	Ave. Full
Speed (m/s / mph)	1.2/2.61	3/6.52	3/6.52	23.8/51.8
Poles	-55.7,-73.5	-9.0+/- 1.7j	-4.8+/- 3.5j	-4.6+/- 3.3j
a/L	0.4878	0.4878	0.4229	0.4203
b/L	-0.5122	-0.5122	-0.5771	-0.5797
$C_{\alpha f} \cdot L/(mV^2)$*	7.5293	0.4176	0.2698	0.2698
$C_{\alpha r} \cdot L/(mV^2)$*	7.5293	0.4176	0.2698	0.2622
$I_z/(mL^2)$	0.1859	0.1859	0.2755	0.2593

* These two values can be matched by varying car speed

From the above chart, it is clear that there is a significant change in the bandwidth of the system due to the changing cornering stiffness. Results have been published supporting a similar bandwidth dependence on the cornering stiffness of the vehicle (Jansen and VanOosten 1995). The following table shows a similar summary for the Uberquad vehicle.

Table 3.5: Summary of the Pi-matching and poles for the Uberquad vehicle

Uber Pi Groups		Uber	"Average"	2 sigma
Pi 1	a/L	0.40	0.40	0.086
Pi 2	b/L	0.60	-0.60	0.086
Pi 3	Caf*L/(mU^2)	0.64	0.64	0.295
Pi 4	Car*L/(mU^2)	0.43	0.60	0.272
Pi 5	Iz/(m*L^2)	0.18	0.23	0.080

Uber Poles	Uber	Average	Min	Max
Real	-9.49	-7.40	-13.68	-4.53
Im	0.76	3.55	1.14	5.77

A more complete comparison is given in the Appendix showing a comparison of scale and Full-sized vehicles.

3.4.5 Methods of Obtaining Dynamic Similitude

The following procedures outline the method used to obtain dynamic similitude in the second and third experimental vehicle tests described in this thesis:

1) Build a vehicle to a predetermined scale.
2) Pick an operating velocity (full-scale) to match. This numerically fixes the pi-groups for the full-sized vehicles and provides a “goal” for matching the scale-vehicle parameters.
3) Add additional mass to the vehicle until dimensional matching is obtained for the length related pi groups a/L and b/L.
4) Measure the I_z moment and determine the related pi group. If the I_z moment is too small, add mass symmetrically about the C.G. until it is near the required value.
5) Measure the cornering stiffness of the scale vehicle tires.
6) Determine the operating velocity of the scale vehicle by finding the velocity matches the cornering stiffness pi-groups with those of the full-sized vehicle.

7) Ensure that at this velocity the remaining pi-groups agree. If not, select different tires or add additional mass to the system, and repeat steps above.

3.5 Experimental Methods to Verify the Dynamic Model

For control purposes, it is not enough to develop a theoretical model of a system without some type of verification that the theory indeed matches the physical system. Traditionally, two methods are used in engineering practice to confirm system dynamics: time-domain and frequency-domain measurements. This section details the use of each of these methods, among others, to determine the vehicle dynamics.

3.5.1 Frequency Domain Measurements

This subsection outlines the background of frequency-domain methods used to measure the vehicle dynamics. The vehicle system from a lateral control standpoint is assumed to be linear with justification presented in earlier sections. In addition, the vehicle dynamics are unstable. As a result, the determination of the OPEN-LOOP dynamics is not trivial, and considerable effort was expended developing and confirming the following methodology to measure these dynamics.

3.5.1.1 Frequency Range of Fits

If a vehicle model, linear or nonlinear, is to be obtained from frequency response data, then consideration must be given to the range at which the frequency fitting should occur. As a reference, the range used by several authors is presented. (Jansen and VanOosten 1995)obtain a fit of a full-sized vehicle model shown on plots of the frequency domain (linear in frequency, rather than logarithmic) up to 3 Hz. (Nagai, Ueda, and Moran 1995) perform model validation and fitting again using a linear scale from 0 to 3 Hz. Vehicle fits including a tire model were obtained up to 2 Hz by Roos et al (Roos, Rollet, and Kriens 1997). In validating the National Advanced Driving Simulator models (NADSdyna) with an experimental vehicle (Ford Taurus), bode plot fits were attempted up to 20 rad/sec for yaw rate, and magnitude matching up to 10 rad/sec (1.5 Hz) was achieved. The predicted phase at this frequency (3.5 Hz) was too high by approximately 30 degrees (experimentally, the phase was about –100 degrees at this frequency) (Salaani, Heydinger, and Guenther 1997).

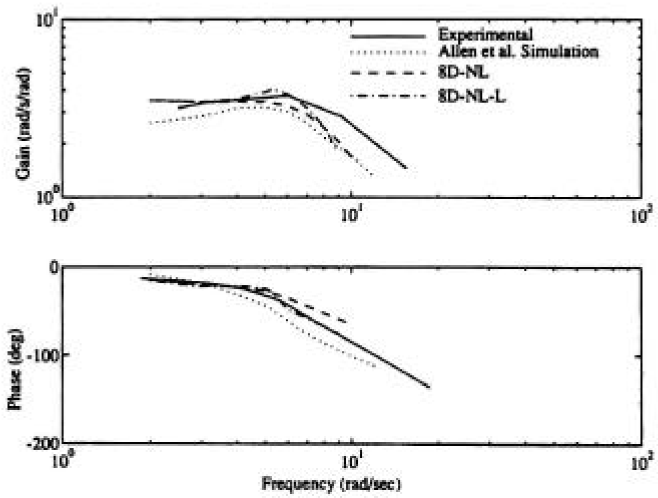

Figure 3.24: A sample frequency response reported in Steeds, 1995 for a full-sized vehicle.

A note must be made in comparing frequency domain to time-domain modeling. Jansen and Van Oosten note that validation using time responses can give ambiguous results, and that frequency response functions are much more usable in validation (Jansen and VanOosten 1995). Although this conclusion is debatable (and depends on testing conditions), in general the author has found that frequency-response testing yields consistently better model matching than time domain. In this thesis, an effort has been made to combine the two methodologies as appropriate (for instance, the rate-limited servo actuator modeling).

3.5.1.2 Initial Tests

3.5.1.2.1 Repeatability Tests

Before obtaining any system Bode plots, it was first determined if a Bode plot, once measured, is repeatable. The following responses were conducted on the 4WS4WD vehicle with slow servos and at low speed (i.e. before consideration was given to pi matching). The frequency responses are of the CLOSED-LOOP system. The DSA was used to generate a reference sinusoid trajectory, and the lateral P-controller was made to follow this trajectory, and the measured lateral position was fed back to the DSA.

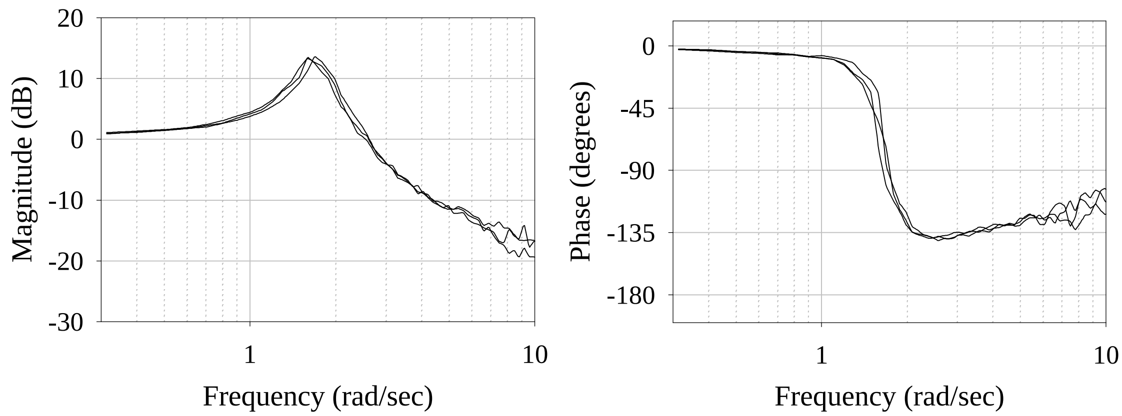

Figure 3.25: The reproducibility testing done on the vehicle being pulled by the treadmill at 1.2 m/s using P-control tracking a reference lateral position input from DSA of a 15-cm amplitude sinusoid.

As expected, some discrepancy is observed between each trial, especially at high frequencies. For controller design purposes, it is clear that the system identification performed on each plot is consistent.

3.5.1.2.2 Longitudinal Controller Sensitivity

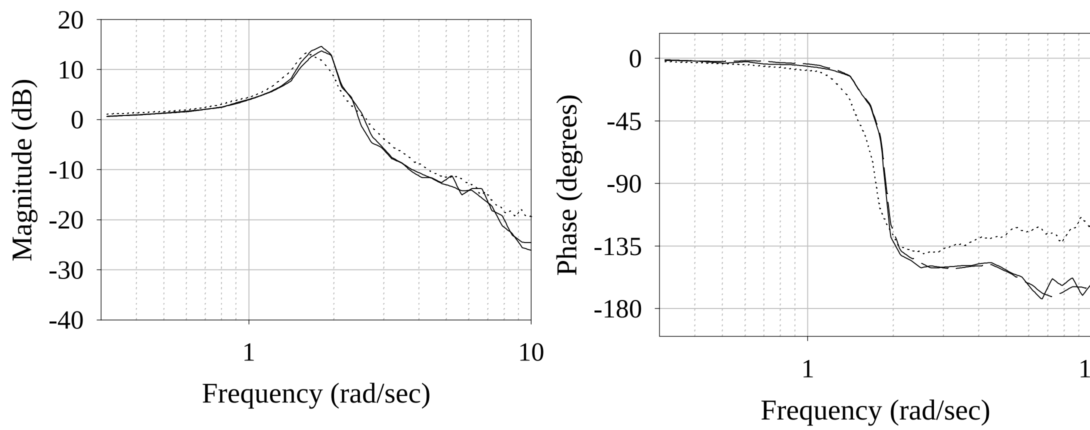

Figure 3.26: Bode plots for the same testing conditions (1.2 m/s, 15 cm amplitude) using different longitudinal controllers. The dotted line is the treadmill tracking the vehicle. The remaining two are for the car tracking the treadmill and for the car being pulled on the treadmill.

3.5.1.2.3 Sensitivity to Amplitude of Frequency Sweep

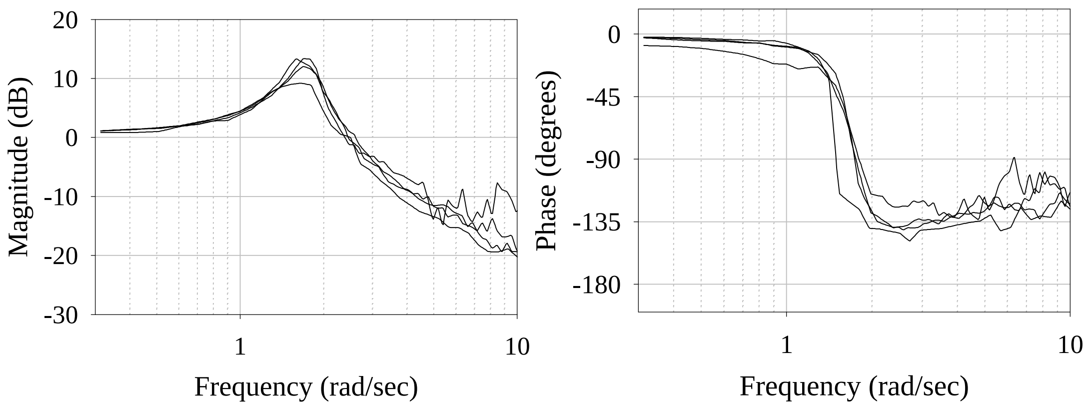

Figure 3.27: The amplitude reproducibility testing done on the vehicle being pulled by the treadmill at 1.2 m/s using P-control to track reference lateral position on sinusoid amplitude 15-cm.

We can see that the system responses are relatively insensitive to the amplitude of input. This is fortunate, because it indicates that the lateral dynamics (and as a result the yaw dynamics) are in quite linear with respect to amplitude of the lane change maneuver. This also reveals that the rate-limit of the servo is not very active at these lower velocities, even when attempting to track a large-amplitude sinusoid signal.

3.5.1.2.4 Velocity Trends

The bicycle model is highly dependent on the vehicle's velocity. This is easily seen in the Bode plots of the system at various velocities:

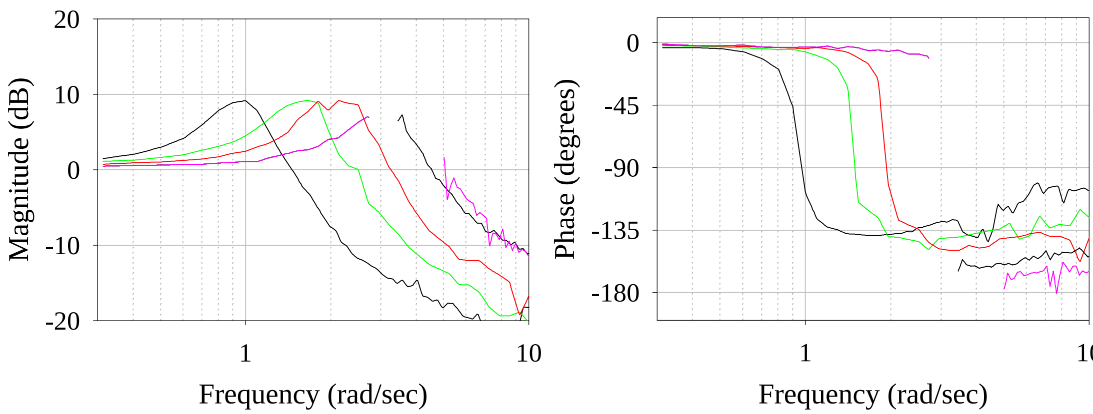

Figure 3.28: The velocity effect on the system Bode plots.

3.5.1.3 Methods Of Obtaining Open-Loop Frequency Responses from Closed Loop Data

As stated earlier, there is a significant difficulty in determining the open-loop frequency response from closed-loop testing. This section details various methods that have been attempted to determine open-loop dynamics from closed-loop data.

3.5.1.3.1 Using Complex Number Theory

To convert the closed loop bode plots of the system response into those of an open-loop response, we begin by examining a block diagram of the system. The following can represent the system:

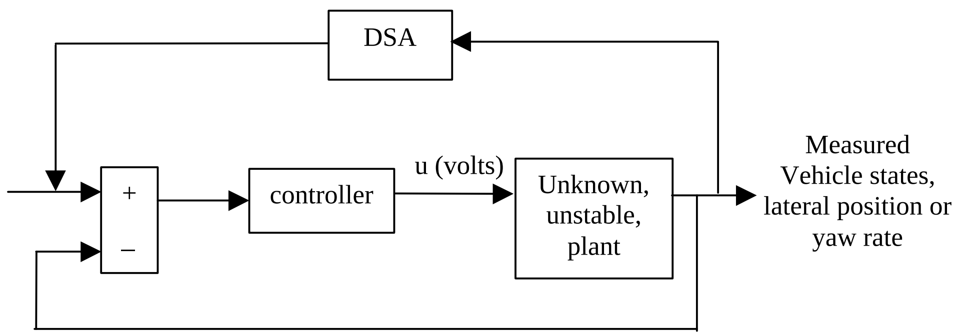

Figure 3.29: The block diagram used to measure the vehicle lateral dynamics via complex number theory.

To obtain the transfer function of the unknown plant, we note that the output of the plant can be represented as:

$$Y(s) = P(s) \cdot V_\delta(s) \tag{3.109}$$

Solving for the Plant

$$P(s) = \frac{Y(s)}{V_\delta(s)} \tag{3.110}$$

The closed loop system response is given by

$$\frac{Y_{out}(s)}{Y_{ref}(s)} = \frac{K \cdot P(s)}{1 + K \cdot P(s)} \tag{3.111}$$

Solving for P

$$P(s) = \frac{\frac{Y_{out}(s)}{Y_{ref}(s)}}{K \cdot \left(1 - \frac{Y_{out}(s)}{Y_{ref}(s)}\right)} \tag{3.112}$$

The magnitude and phase of Y_{out}/Y_{ref} is recorded by the DSA. We can then find P(s) by noting that the magnitude and phase create an imaginary number, which can be represented as:

$$\frac{Y_{out}(s)}{Y_{ref}(s)} = R \cdot e^{i\theta} \tag{3.113}$$

$$= R \cdot (\cos(\theta) + i \cdot \sin(\theta)) \tag{3.114}$$

Substituting into above:

$$P(s) = \frac{R \cdot e^{i \cdot \theta}}{\left(K - K \cdot R \cdot \cos(\theta)\right) + K \cdot R \cdot \sin(\theta) \cdot i} \tag{3.115}$$

The magnitude of P is given by

$$|P| = \frac{R}{K \cdot \sqrt{1 + R^2}} \tag{3.116}$$

And the phase is

$$\angle P = \theta - \tan^{-1}\left(\frac{R \cdot \sin(\theta)}{1 - R \cdot \cos(\theta)}\right) \tag{3.117}$$

A code was written to perform the above conversion from closed to open systems. To test this theory, the open-loop vehicle dynamics were inferred from the closed-loop system responses using several different gains. The following plots reveal the different "open-loop" dynamics determined for four different controller gains:

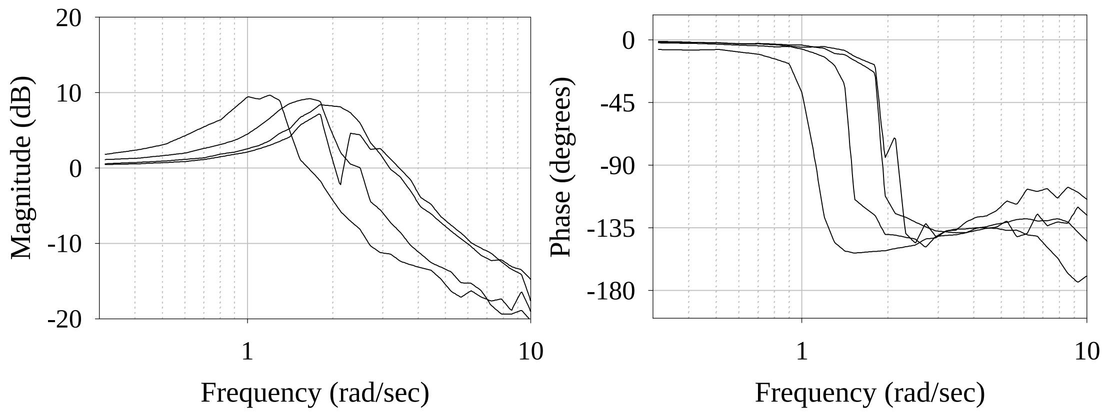

Figure 3.30: The effect of gain on the closed loop responses, at 1.2 m/s and 9 cm peak to peak change in reference lateral position.

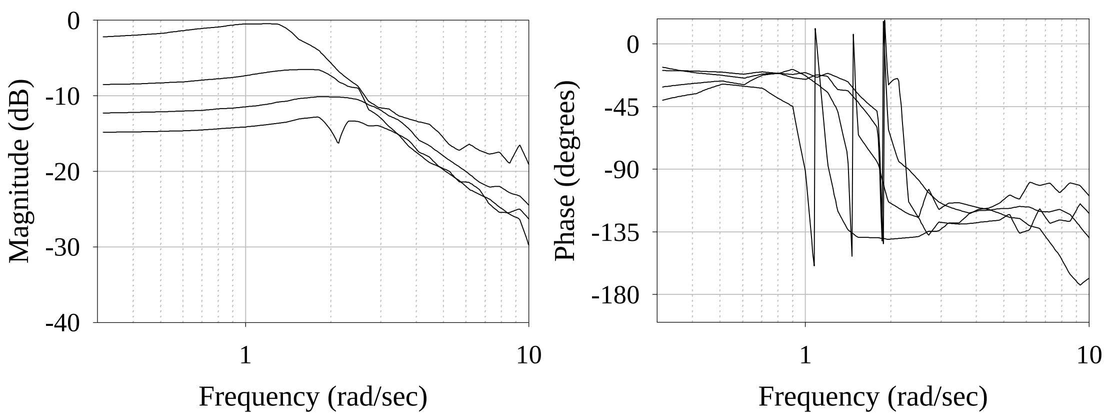

Figure 3.31: The effect of gain on the open loop responses, at 1.2 m/s and 9 cm peak to peak change in reference lateral position.

From the above plots, it is clear that the open-loop system ID depends strongly on the gain used in the closed-loop system. This implies that the open-loop identification is sensitive to closed-loop parameters, i.e. the open-loop identification is not entirely decoupled from the closed-loop dynamics. Because this is the intent of this method, clearly this method is inadequate to transform closed-loop responses into open-loop responses. Consequently, other methods are considered.

3.5.1.3.2 Using Input Feedback

The 35670A HP Dynamic Signal Analyzer used by this lab has the capability of inputting both the input signal AND the output signal into a system. The DSA has the capability of analyzing the correlation between the input and output and thus form a frequency response of the system. To use this feature to identify the open-loop dynamics of the system under closed-loop control, the front steer command was used as the input feedback to the DSA on the input line. The yaw angle was then fed back to the DSA as a response. The sine wave from the DSA was used to create a sine wave reference position that the lateral controller was made to track.

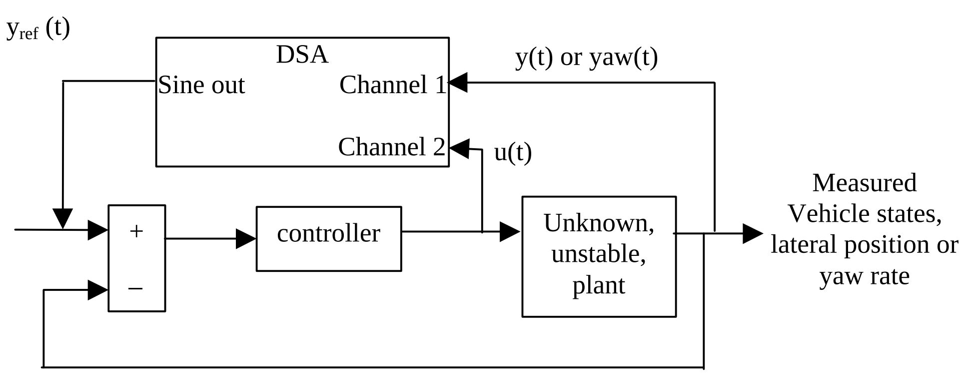

Figure 3.32: The block diagram of the frequency response measurement technique used to determine open-loop dynamics via correlation between plant inputs and outputs.

Initially, the input/output correlation technique was tested on the vehicle directly, with results shown below:

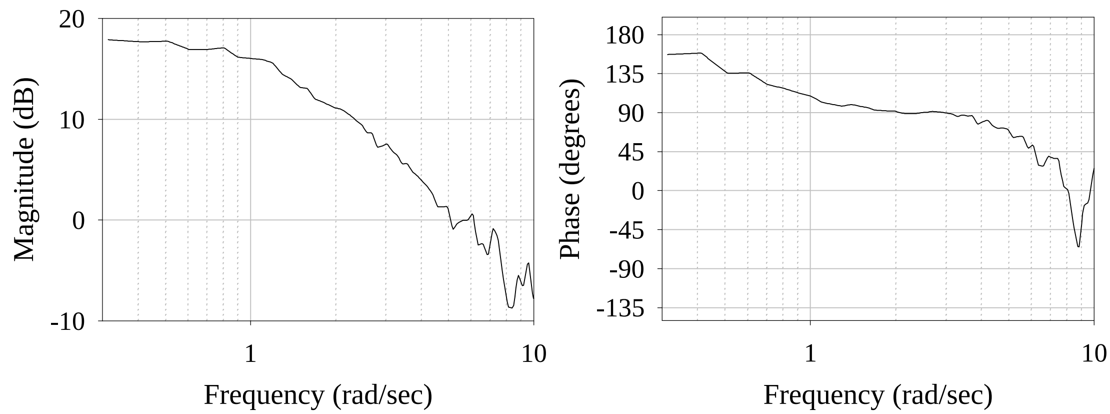

Figure 3.33: The Bode plots for the yaw angle dynamics using input/output correlation.

From the above plots, it is clear that the approach seems to work significantly better than the previous method, but suffers to some extent. The expected yaw angle dynamics were that the system had a free integrator. The yaw angle dynamics, because of the 1/s free integrator term, should start out at a phase angle of -90 degrees. The above plots indicate that the phase is off by 180 degrees, indicating that a sign is missing somewhere in the system identification. If this error is included, it is seen that the frequency response does begin at approximately –90 degrees as expected. However, there is a significant amount of error at low frequencies. This suggests that the results at very low frequencies, and possibly high frequencies, are probably erroneous. As a result, this method was abandoned for use in system identification for the 4WS4WD vehicle.

By the time frequency testing was needed for the Uberquad, computing capabilities had improved to where input/output correlation could be adequately tested. By using the SIMULINK-based code generation, we were able to simulate an artificial plant in code to determine the viability of the I/O approach. The dynamics were chosen to represent the bicycle model yaw-rate dynamics and lateral dynamics. The closed-loop controller normally used for the vehicle was then implemented on this artificial system, and the inputs and outputs to the system were sent to the DSA as described above for correlation. The following figure shows both the model and the resulting identification:

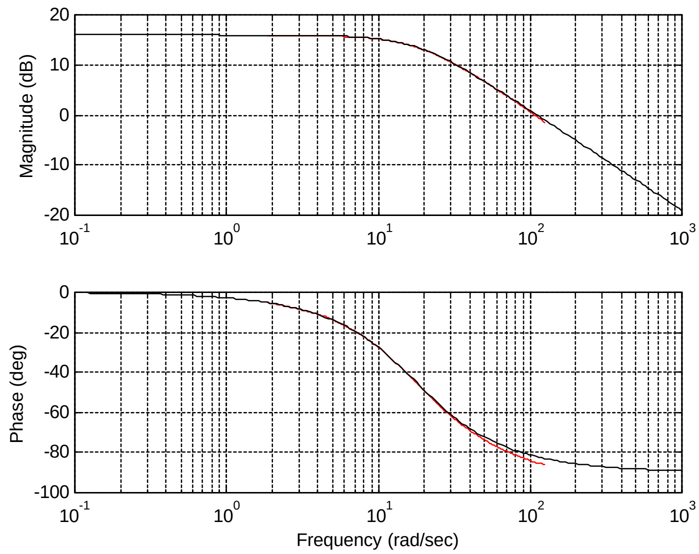

Figure 3.34: The Bode plots for the artificial yaw angle dynamics and resulting open-loop model determined from closed-loop input/output correlation.

Continued thought into why the original attempt would correlate so poorly on the original 4WS4WD system revealed a possible cause to the poor low-frequency correlation: at low frequencies, the vehicle is basically tracking a constant signal. Thus, the controller is not exciting the system in a sinusoidal manner but instead is regulating itself about some slowly varying setpoint. The primary system excitation is not a result of the input reference signal as intended but rather system disturbances. Thus, the correlation between control input and plant output would be very poor at these frequencies, simply because the signal-to-noise ratio is very small in this region. Knowing this, the controller used on the Uberquad system was made to be as "tight" as possible: that is, the controller was made to track the reference input very closely and reject disturbances VERY quickly. The resulting frequency identification on the actual system proved to work quite well, as will be shown in later sections.

3.5.1.3.3 Frequency Domain Identification Using Multiple Bode Plots

The third and final system ID approach attempts to correct the miscorrelation of the sinusoid input by examining the transfer function from change in reference lateral position, y_{ref} (t) to the command voltage u(t), and the transfer function from y_{ref} (t) to the output yaw angle, $\psi(\tau)$.

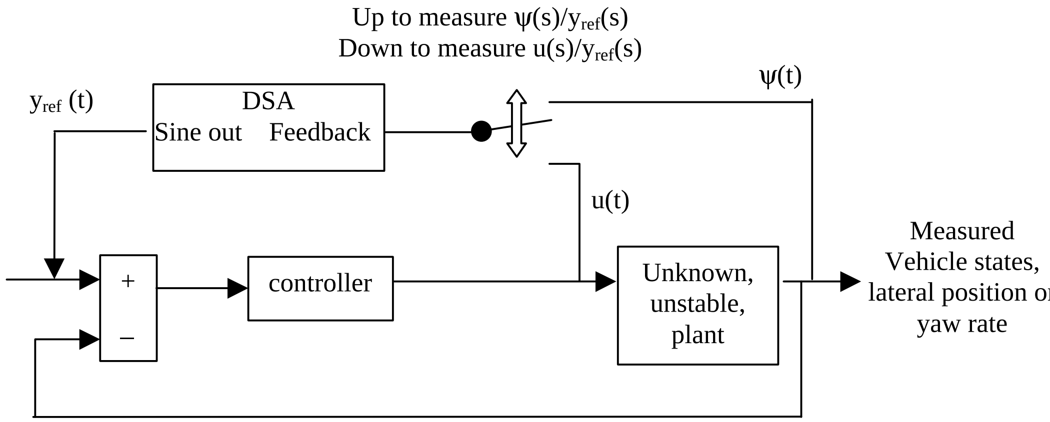

Figure 3.35: The block diagram of the frequency response measurement technique used to determine open-loop dynamics using multiple bode plots.

The transfer functions $\psi(s)/y_{ref}(s)$ and $u(s)/y_{ref}(s)$ can be measured directly using the DSA. However, the transfer function of interest is the open loop dynamics, $\psi(s)/u(s)$. If the system is linear, this would simply be:

$$\frac{\psi(s)}{u(s)} = \frac{\dfrac{\psi(s)}{y_{ref}(s)}}{\dfrac{u(s)}{y_{ref}(s)}} \tag{3.118}$$

Since frequency domain is in general presented in logarithmic form, division in the above expression can in actuality be obtained by subtraction of the logarithmic measurements of the frequency plot (Note: another researcher has also used this method for a closed-loop system by saving the frequency response in complex notation. Division was conducted in the complex space and the magnitude and phase were simply the mag and phase of the resulting complex number). After subtracting the Bode plot for $u(s)/y_{ref}(s)$ from the Bode plot for $\psi(s)/y_{ref}(s)$, Bode plots were obtained that represent the open-loop response.

To test this concept, the following open-loop bode plots were obtained using this method for the yaw dynamics using the front wheel as input. These plots show responses that agree very well with the expected yaw state dynamics. Based on the magnitude plot, it would appear that the plant (open-loop) behaves almost exactly like a free integrator (as theory predicts). The phase begins at a constant –90 degrees, which also agrees with the theoretical expectation. One aspect of the yaw dynamics system identification was that the previous graduate student, Mark DePoorter, identified a system pole at a location of s = 10 rad/sec. Since this location is at the limits of the above plot, a refinement was added to increase the resolution of the plot at high frequencies in an attempt to determine the location of the faster pole. To do this, the amplitude of the input reference tracking signal was increased to +/- .1 meters (from +/- .075 meters) and the integration and settling times were increased to 30 cycles each. Originally, the frequency was swept from 0.05 Hz to 3 Hz, but to refine the higher frequencies, the frequencies were swept from 1 Hz to 10 Hz. The two plots were then combined and plotted. The results of this refinement are included in the above plots.

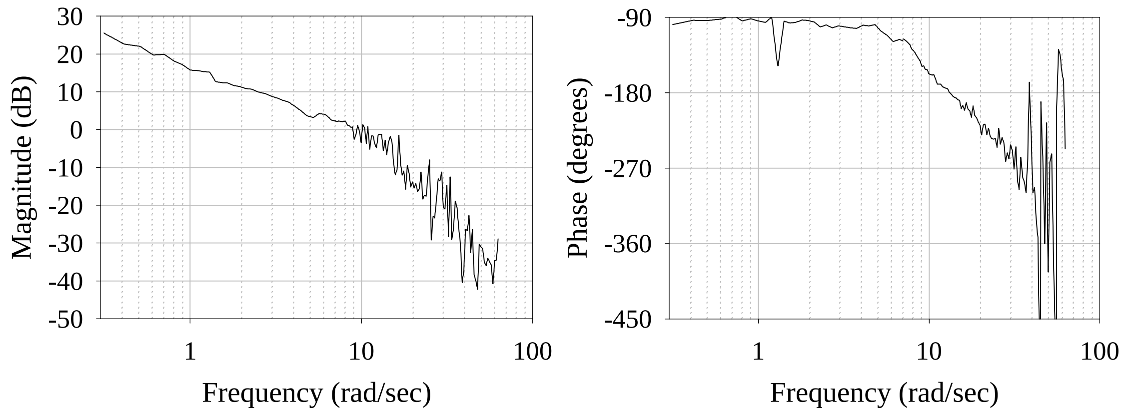

Figure 3.36: The yaw angle bode plots obtained from the transfer function subtraction approach, with an additional refinement at high frequencies to determine these pole locations.

3.5.2 Time Domain Modeling

Often, vehicle dynamics are obtained using time domain methods alone. As an example of the common usage of time domain tests for vehicle testing, there is an international standard on methods of conducting step steering input tests on vehicles (ISO 7401). A natural question arises as to what trajectory to use for validation. Naturally, some obvious choices are sinusoid and ramp maneuvers (referred to as J-turn maneuvers because of the vehicles trajectory follows a J when conducting a ramp steering input). However, each maneuver emphasizes different aspects of the vehicle dynamics, and nonlinear effects can dominate parameter tests, such as step-inputs. A particular question often addressed in literature is the question and theoretical determination of the "best" maneuver to use to change a lane (Sledge and Marshek 1997).

3.5.3 Random Steering Tests

One final method to obtain a frequency domain fit is called the Random steering test (ISO 7401 and ISO/TR 8726). This method attempts to correlate the input and output of a plant that is under open-loop or closed-loop control by introducing a random input into the system. This method was not used in this thesis, but is detailed here for completeness. The use of this technique for full-scale vehicle testing is described in (Jansen and VanOosten 1995). As noted in this paper, the advantages of this test are listed as follows:

- it is an open-loop test
- it is easy to perform
- preparation and execution time are short

- the results are statistically most accurate since the measurement time is long
- for model validation purposes the resulting transfer functions are very suitable to use. The transfer function of the system is obtained by obtaining a correlation between the inputs and the outputs via spectral analysis. Based on results published by other authors, this method may be a valid alternative to the lengthy and difficult swept-sine approach used in this thesis.

This paper does not note the disadvantages of using random steering inputs.

- they are more susceptible to errors and depend strongly on data "quality"
- it is difficult to determine if the random input has provided enough excitation such that the frequency response is representative of the true system.

For these reasons, the random input testing is NOT used in this thesis, but may be considered later as a comparison to (not a replacement for) swept-sine testing.

3.6 Vehicle Model Fits

This section can be divided into two major sub-sections: a discussion of actuator dynamics and a discussion of vehicle dynamics. With regard to vehicle dynamics, three major system identifications were performed. The first was on the 4WS4WD vehicle at a velocity of 1.2 m/s using low-bandwidth Futaba S9304 servos. The second was on the 4WS4WD vehicle at a faster velocity of 3.0 m/s using high-bandwidth Futaba S9402 servos. The third was on the Uberquad using DC motors as the steering actuator. Each vehicle test displayed noticeably different dynamics (by design); hence, a separate discussion of each test is necessary.

3.6.1 Actuator Dynamics

Typical controllers developed for full-sized vehicles using bicycle model dynamics often do not include the dynamics related to the steering actuator. Because the steering command must be directed through a motor, gears, and other actuators whose response may not be immediate or exact, resulting in a response far different than predicted by the bicycle model

Previous work using R/C scale vehicles on the Illinois Roadway Simulator (IRS) (DePoorter, Brennan, and Alleyne 1998) has shown that neglecting these dynamics can lead to invalid design models, and hence invalid controller design. In the paper by Smith and Starkey, a large amount of mismatch was observed in the phase and magnitude of the frequency responses of actual vehicles above frequencies of 6 radians/second (Smith and Starkey 1995). This suggests that either tire dynamics or actuator dynamics may be present. Studies conducted by other researchers discussed in this thesis note that tire dynamics are significant above 20 Hz, so it is quite likely the phase drop and magnitude drop seen beginning at 6 rad/sec are due to steering actuator dynamics. Research conducted by other research institutions supports this concept. The bandwidth of the actuation for the Pontiac 6000 vehicle used by the California PATH program was found to be about 2 Hz with load for a +/- 2 degree amplitude steering angle (Peng et al.

1994). Clearly, for actual vehicle systems with actuator poles around 1-2 Hz, the actuation bandwidth presents a serious constraint on the possible system performance.

Previous work performed on the IRS identified the actuator as first order based on the difference between the expected vehicle response and the experimentally obtained vehicle response from input to output analysis (driver steer command to yaw rate). This work did not isolate the actuator itself, and instead inferred the actuator response by assuming it was the fastest pole location identified. Closer examination discussed in this section revealed that this assumption was not valid, and that the actuator dynamics for the servo used by previous researchers (the Futaba S9304) was much slower than previously thought.

3.6.1.1 Actuator Dynamics of Full-Scale Vehicles

It is difficult to find published data regarding full-sized vehicle actuators for several reasons: first, measurement of the actuator dynamics requires non-standard sensing capabilities (such as measurement of wheel angles) generally not found outside of research institutions. Secondly, most vehicle researchers ignore actuator dynamics as a first approximation of the dynamics of the entire vehicle. Finally, car manufacturers likely do not want to publish vehicle limitations such as actuator limits that may benefit their competition or agitate their customers.

The rate limiting effect previously identified on the steering actuator of the 4WS4WD vehicle may also been seen in full-sized vehicle actuators. Although published data on this subject has been lacking from industry (for obvious reasons), the possible presence of a rate limiter on steering systems can be inferred. The actuators commonly used on full-sized vehicles for automated or driver assisted vehicle control are electric motors mounted on the steering column or modified power-steering hydraulic systems. Regardless of the system, very fast actuation can saturate the hydraulic or the DC motor system because of rational design limits on actuator size. For hydraulic systems, if the required rate of volume change of the actuator piston is larger than the available flow rate through the valve opening, the system will become rate-limited. For DC motors, a motor large enough to move the wheels directly would be impracticably large; thus, gearing systems are used. With gearing systems coupled with DC motors, rate limiting effects commonly are seen (such as in the servo motor on the R/C systems!). Without verification from industry or direct measurement of full-sized vehicle systems, the presence of this type of non-linearity in full-scale vehicle systems remains a question. Without a doubt, such nonlinearities could become a large obstacle in the implementation of vehicle automation on full-sized vehicles.

From the previous arguments, it is clear that there is a large discrepancy between the actuators that actually exist on today’s vehicles and the actuators control engineers would like to use. In a paper by TU Delft and Volvo, an actuator with damping ratio of 0.6 and natural frequency of 65 rad/sec is specified by the control engineers for rear steering applications (Roelofsen 1995). This corresponds to approximately a 10 Hz actuator (in practice, vehicle actuators are in the 1-2 Hz range). In research conducted by (Lee, Mariott, and Le 1997), it was found that steering actuators with a bandwidth of 4 Hz gave a much larger rise time in a J-turn maneuver. These researchers also specify an actuator bandwidth of at least 10 Hz.

The drawbacks of electric motor torque limits or hydraulic saturation and bandwidth can be overcome with large actuators. In fact, this is partially the approach with the Uberquad redesign: using high-torque motors to achieve the desired bandwidth. A problem with this approach (other than cost) is that large actuators decrease vehicle efficiency and add weight to a vehicle. From an efficiency standpoint, it may not be good economics to use a big motor or pump that gives slightly better vehicle performance at the tradeoff of fuel economy. As pushes toward more fuel-efficient or electric vehicles continue, actuator dynamics will play an increasing role in vehicle dynamic studies.

3.6.1.2 Slow Servos – Futaba S9304

The first method to identify the steering actuator dynamics was to remove a servo actuator from the vehicle and identify the servo dynamics separately. Initially, a swept-sine frequency response was conducted on the servo at different amplitudes, and it was revealed that the response was very dependent on the amplitude of the swept sine. Close examination of servo step responses revealed that the system is rate limited. A swept-sine frequency response was then conducted using very small steering inputs that do not saturate the actuator at the frequencies corresponding to the pole locations. Using this frequency response, a linear model was obtained for the servo for small-amplitude inputs. Finally, a second-order, rate-limited Simulink model of the steering actuator was developed, and the model results were compared to experimental results using step responses.

To determine the actuator dynamics, some method of angular feedback was necessary. The servo actuator was connected with an encoder mounted coaxial along its output shaft so that the shaft angle could be measured. Because the particular encoder had a low resolution, it was not suited for system identification at low frequencies. Noting that the servo contained a potentiometer inside, the potentiometer voltage was measured with respect to the encoder, and the angle of the servo was monitored with respect to the voltage input into the transmitter. The figures below show the functional relationship between measured voltage and servo angle, and transmitter voltage and servo angle.

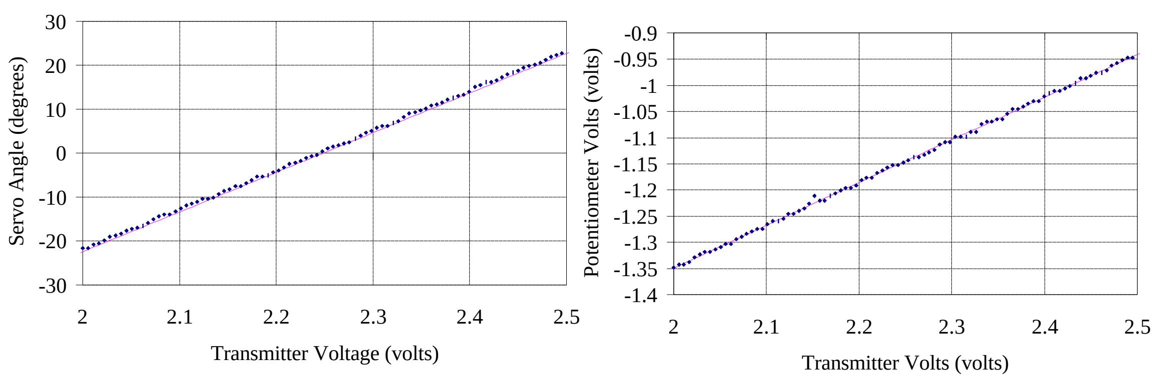

Figure 3.37: The relationship between transmitter voltage and servo angle.

Clearly the above relationships suggest a linear relationship between transmitter voltage and servo angle. Accordingly, five trials were conducted and a linear regression was performed on each trial to fit the slope for these two relationships. The results of these trials are presented in the table below. Using these relationships, either encoder or potentiometer feedback could be used to obtain the frequency response of the servo.

Table 3.1: The regression fit between servo angle, applied transmitter voltage, and measured servo potentiometer voltage.

Trial	Slope Servo Angle (deg.)/ Transmitter Volts (volts)	Slope Pot Voltage (volts)/ Transmitter Voltage (volts)
1	90.3 deg./volt	0.816 volt/volt
2	90.2 deg./volt	0.822 volt/volt
3	87.2 deg./volt	0.785 volt/volt
4	89.7 deg./volt	0.820 volt/volt

Using commercial DSA equipment (HP 45670A Dynamic Signal Analyzer), the frequency response of the system was measured as the following:

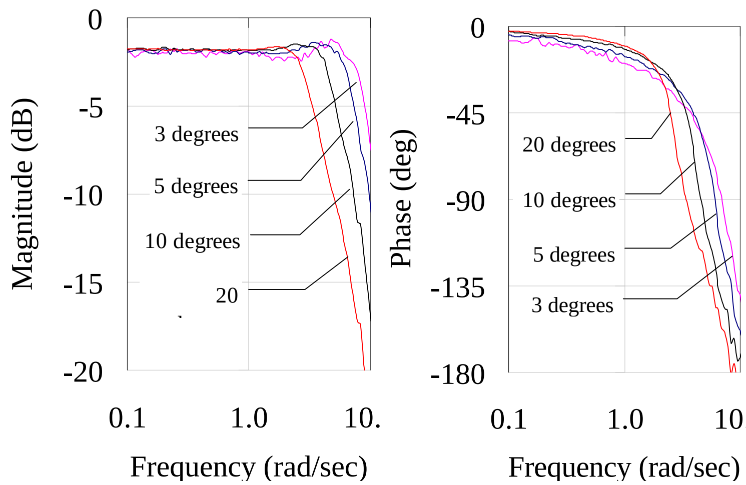

Figure 3.38: The initial frequency responses obtained for the servo actuator.

The above responses clearly reveal amplitude dependence in the frequency response. Because the servo utilizes a DC motor for shaft motion, a second-order fit of the system was expected. However, we note that the DC motor does not have infinite torque, and instead is geared significantly to magnify the available torque from the motor. A consequence is that the resistance of the gearing limits the servo to a maximum speed corresponding to the point where the gear torque is equal to the maximum torque available from the motor. This results in a rate-limited response. To obtain the numerical value of the rate-limited, time-domain step-responses were conducted. The following plot summarizes the results:

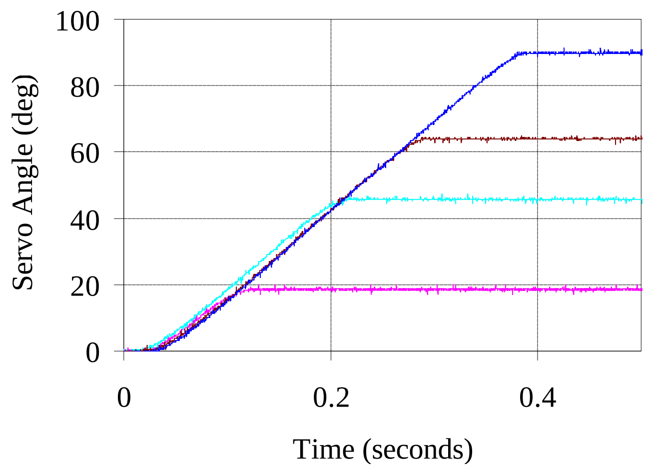

Figure 3.39: The step responses obtained for the Futaba S9304 servo actuator.

From the above plots, a rate limit on the response is clearly present. Because of this rate-limited dynamic, frequency domain analysis was conducted at very small amplitudes to identify the linear non-rate-limited actuator dynamics. Because of the uncertainty of how "small" an amplitude is necessary to correctly identify the system, frequency responses were conducted at decreasing amplitudes until convergence was seen in the bode plots. Convergence was seen at amplitudes less than 5 degrees. A discussion on the measurement of the rate-limit follows in a later section. The resulting linear model was obtained as:

$$\frac{V_{pot}(s)}{V_{transmitter}(s)} = \frac{10000}{s^2 + 170 \cdot s + 10000}\left[\frac{\text{rad}}{\text{volt}}\right] \tag{3.119}$$

After obtaining a dynamic model of the servo system experimentally, this model was tested by creating a Simulink model of the system and comparing it with experimental step-responses. It should be noted that the experimental data could not be fit with reasonable error without including a time delay on the transmitter. Based on the nature of the communication system discussed earlier, a small delay was expected between 10 and 20 milliseconds. The time delay was found experimentally to be approximately 0.015 to 0.02 seconds.

Combining the time delay, rate limit, conversion and transfer functions, the following Simulink model was obtained representing the servo dynamics:

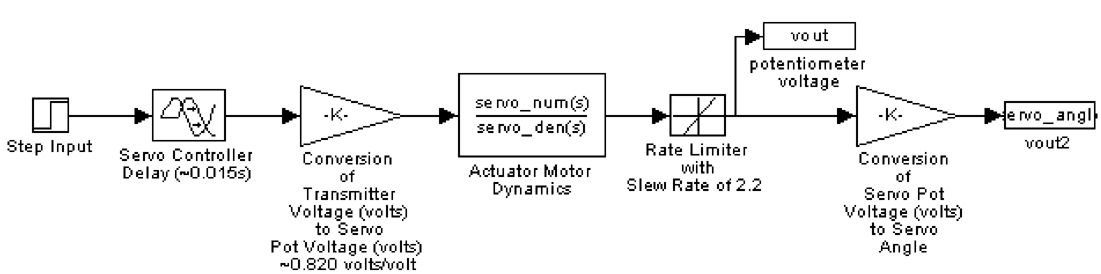

Figure 3.40: The Simulink model of the servo actuator.

This model was used to compare simulated actuator responses to measured responses in the time domain using step inputs. Note that this model was formed after the controller design and implementation to validate that the servo pole locations were much faster than the vehicle dynamics. However, this was not the case, and new servos were selected that would give a higher bandwidth. Consequently, the exact “fit” of the above servo is unimportant because it was never used to design or evaluate any vehicle controllers presented in this thesis.

3.6.1.3 Fast Servos – Futaba S9402

The dynamic modeling of the faster Futaba S9402 series servos follows that of the previous servo, except that the servo angles were measured via an encoder rather than the internal potentiometer. Hence, the results are presented below, with a side-by-side comparison with the slower Futaba S9304 servo where appropriate.

Initial testing was conducted to confirm that there was approximately a linear relationship between the command voltage and the servo horn angle at steady state. This relationship was obtained by slowly varying the servo voltage and measuring the horn angle after a long settling time. After establishing the steady-state relationship for the servo, the dynamic transient relationship between the voltage sent through the transmitter and the output of each servo was sought.

Knowing that the system was likely to be rate-limited (as was the previous servo), frequency-domain testing was again conducted on the front servo where the amplitude of the swept-sine was decreased until convergence was observed. The figure below shows a clear non-linearity in the system (the rate-limited effect). A linear model-fit for the servo dynamics was again obtained by fitting the curves for very small amplitudes of input (where the system will not likely be rate-limited). The below frequency responses also clearly show an increased bandwidth of the actuator (by approximately an order of magnitude).

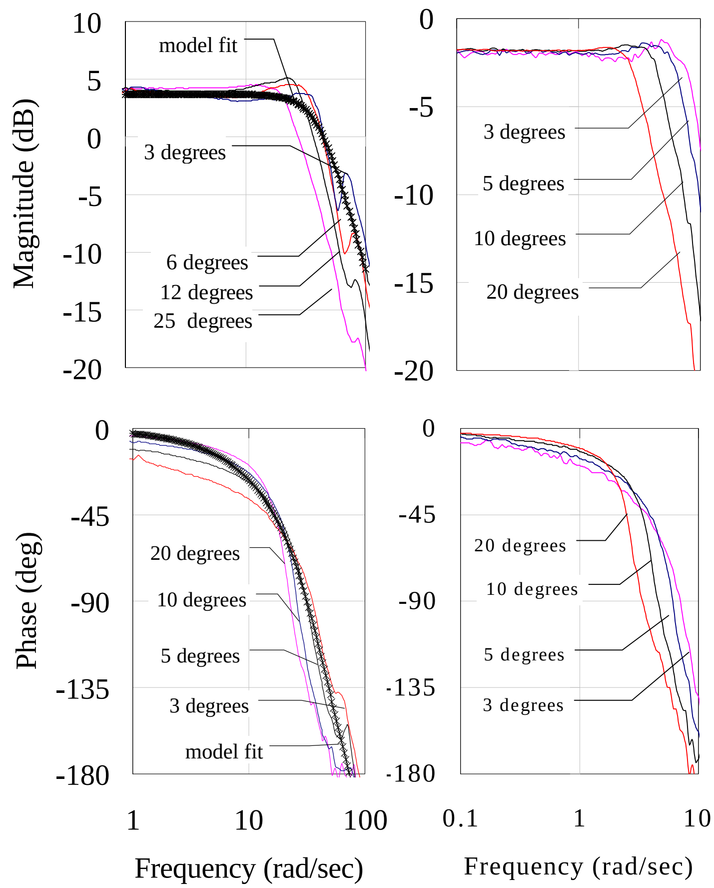

Figure 3.41: A comparison of the frequency responses of the Futaba S9304 (right) and S9402 (left) actuators showing an order-of-magnitude improvement in actuator bandwidth.

The servo dynamic model identified from the above frequency responses is given by the following second-order transfer function:

$$\frac{\theta_{front-servo}(s)}{V_{transmitter}(s)} = \frac{2700}{s^2 + 60.5 \cdot s + 1764}\left[\frac{rad}{volt}\right] \tag{3.120}$$

Again, a second-order transfer function is expected because the servo utilizes a DC motor for actuation, and a DC motor is theoretically represented by second order transfer function from voltage to position. The poles of this transfer function are:

$$\text{Poles} = -30 \pm 29 \cdot i \quad [rad/sec] \tag{3.121}$$

It is interesting to note that the bandwidth of the actuator presented in (3.120) is in fact slower than that of the actuator represented by (3.122), even though the frequency responses of the new actuator clearly show an increased bandwidth. It is important to note that the model fit for the slow actuator was obtained using time-domain analysis of the step responses; the transfer function was chosen to give the best fit of the system WHEN THE SYSTEM IS NOT RATE-LIMITED. When comparing the rate limit of the two actuators, the newer actuator is clearly faster. If we fit the slower actuator dynamics of the slow actuator in the same manner as the fast actuator by INCLUDING the rate limiter by fitting the frequency domain data alone, we would obtain the pole locations identified by the previous student Mark DePoorter for the slow actuator: -8 rad/sec and –20 rad/sec. Hence, from a linear input/output standpoint, the pole locations confirm a higher actuator bandwidth. It does agree with intuition that the “slower” actuator may have faster LINEAR dynamics than the faster, higher-torque actuator. The higher torque actuator uses a larger motor with metal gearing, causing the motor to have a higher effective rotational inertia. For very small angles, the smaller motor may in fact have a faster response than the larger motor.

The above tests were conducted with the vehicle stationary and the front wheels lifted off the track. Because there is relatively little load on the servos, a question arises of how the linear fit might degrade when the wheels actually have an operating load acting upon them (as with driving). Two validation tests were conducted: a stationary test where the actuator dynamics are obtained with the wheels down, and a moving test where the actuator dynamics are identified in the closed-loop with the vehicle operating. The stationary test with the wheels down very likely represents the largest load the wheels will encounter, and hence present a "worst-case" fit. The intent of the closed-loop fit is to verify that the system, in closed-loop, actually acts more like the linear "best-case" rather than worst case (high load) scenario. The closed-loop tests will naturally show some large errors at low frequencies due to the low signal-to-noise ratio mentioned in earlier sections of this thesis. At high frequencies, the actuator dynamics will be dominated by the rate-limiter.

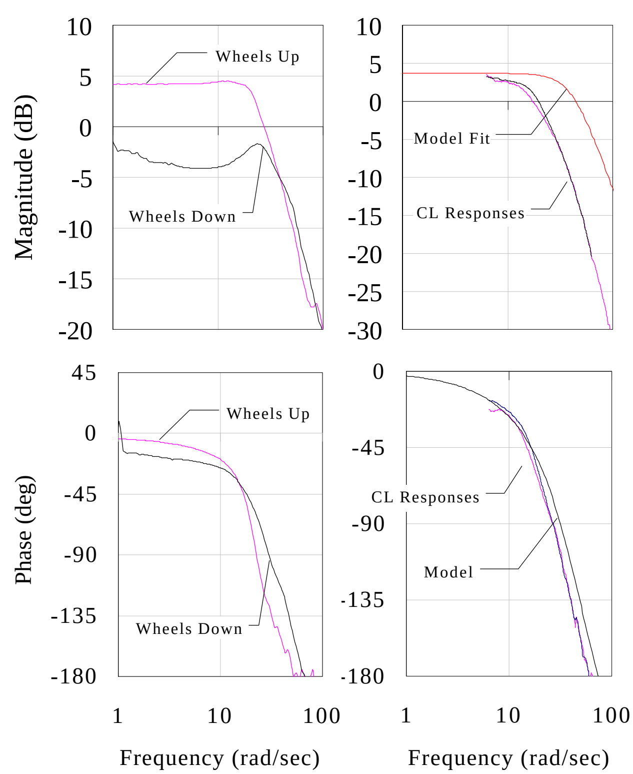

Figure 3.42: A linearity test where the frequency response is compared to heavy wheel loading (left) and closed-loop (right) operating conditions.

Similar tests were conducted to obtain the open-loop, up/down, and closed-loop frequency responses for the rear actuator, shown below. Note that the model fit for the rear servo was obtained using the open-loop, "wheels up" plot shown below.

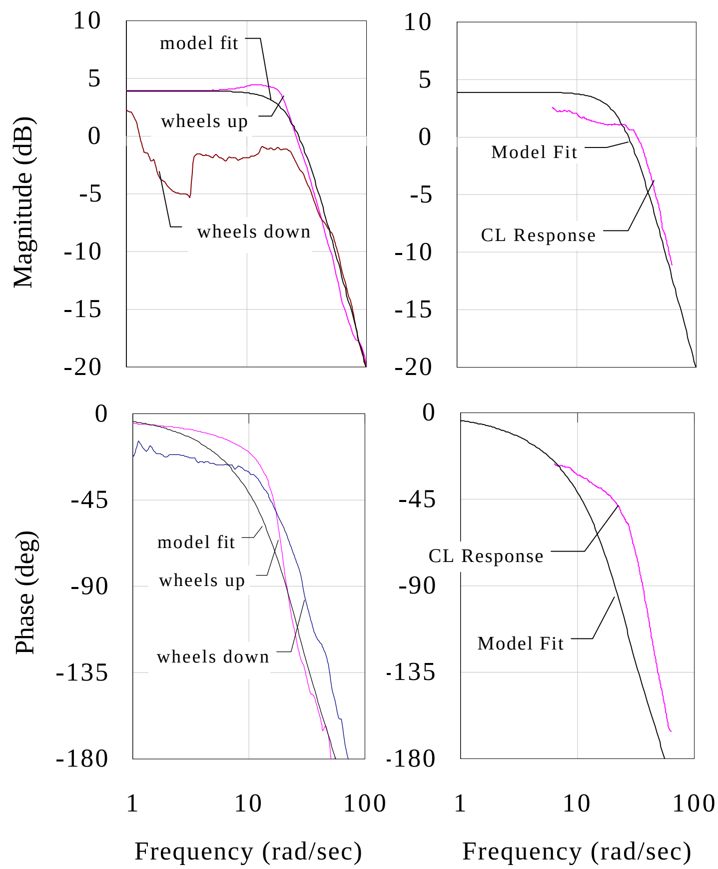

Figure 3.43: A linearity test where the frequency response is compared to heavy wheel loading (left) and closed-loop (right) operating conditions.

The linear rear servo dynamics were found to be:

$$\frac{\theta_{rear-servo}(s)}{V_{transmitter}(s)} = \frac{981}{s^2 + 36 \cdot s + 625}\left[\frac{rad}{volt}\right] \tag{3.123}$$

whose poles are:

$$\text{Poles} = -18 \pm 17 \cdot i \quad [rad / sec] \tag{3.124}$$

Note that the rear servo is slightly slower in bandwidth than the front servo. The physical design of the 4WS4WD vehicle is such that the rear servo must actuate over a longer and more complicated steering mechanism to move the rear wheels. As a consequence, the load torque on the servo motor may be higher thus resulting in a lower bandwidth.

After determining the linear dynamics of the system, the non-linear rate-limiter slope was determined experimentally via step responses, and the resulting fit was incorporated into the model. The newer, higher-torque actuators were expected to have a much higher rate-limiting slope, and this is clearly seen in the figures below:

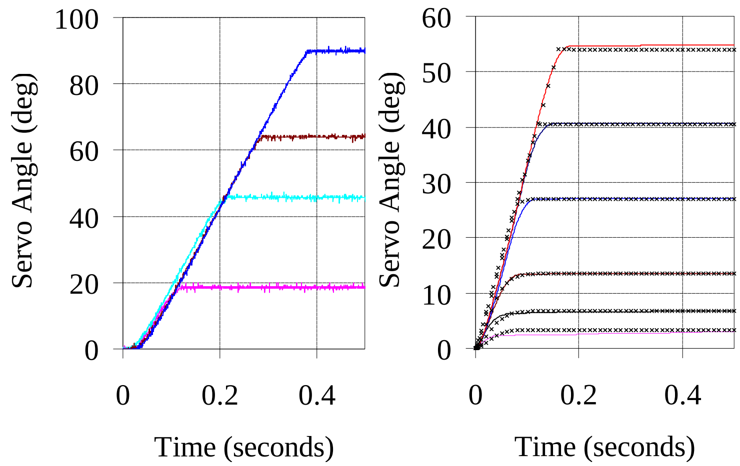

Figure 3.44: A comparison of the step responses of the slower Futaba S9304 (right) and high-speed S9402 (left) actuators.

The rate-limited slope was modeled for the front and rear actuators to be:

$$m_{max, front} = 300 \quad [deg/sec] \tag{3.125}$$

$$m_{max, rear} = 300 \quad [deg/sec] \tag{3.126}$$

The above step responses of the high-speed S9402 servo includes the model fit (dots) and have had the time delays subtracted off the response. The quasi-random time-delay discussed in the previous section made modeling of the system in the time domain quite difficult. Consequently, time-domain confirmation of the servo dynamic response should be conducted with the expectation of some error regarding this delay and a consequent error in the phase of the closed-loop system.

3.6.1.4 Limitations of Control Systems Using R/C Servos for Actuation

There are four primary limitations in the use of servos to steer scale vehicles. In order of influence, these are the rate-limited nonlinear dynamics, the dead-zone and flexibility in the steering linkages, the time-delay associated with the transmitter, and the nonlinear kinematic relationship between servo output and wheel angle. A separate discussion is given to each topic below.

The rate limited actuator dynamics previously discussed are likely the most detrimental in obtaining a linear approximation of the system. The rate-limit is due to a torque limit on the motor. It is unknown what torque the steering actuator will need to steer the vehicle at high speeds, so the modeling was conducted on the steering actuator with the actuator separated from the vehicle or on a stationary vehicle. Consequently, the rate limiter slope used in this model is probably not very accurate. The error is probably a non-linear relationship with respect to steering angle and speed, because it is strongly dependent on tire forces. The rate-limit effect can clearly be seen in the actuator time and frequency responses. For the frequency responses, the rate-limiter is probably responsible for the shift at high frequencies to lower bandwidths.

In order to measure the rate limit on the actual vehicle, a large frequency and amplitude sinusoid was fed into the vehicle steering actuator such that the actuator was rate limited over nearly the entire wave. The angles the actuator swept through were then recorded, and the time to take one cycle was measured. From this information, the slew rate could be determined. As an example, we measured the Futaba S9304 servo sweeping 200 degrees (100 degrees in each direction) 41 times in 60 seconds. This implies that the slew rate is approximately 135 degrees/second. When the same servo was tested while disconnected from the vehicle, the slew rate was measured to be 2.2 Vpot /sec. To convert this to degrees per second, we note that the conversion from pot voltage to servo angle was obtained from the previous calibration as $\theta/V_{pot} = (\theta/V_{trans})/(Vpot/Vtrans) = 90/0.82 = 110$ deg/volts pot. The model slew rate is then 2.2 Vpot/sec*110 deg/Vpot = 240 deg/sec. Obviously, the addition of the steering linkage significantly affects the rate-limiter and possibly the actuator dynamics, and hence the rate-limit should be measured under conditions as close to running conditions as possible. In summary, the rate limit (tested on the vehicle) found for the S9304 servo was approximately 130 degrees/second, and the rate limit for the S9402 high-speed servo was found to be between 300 and 330 degrees/second.

A second servo non-linearity consists of a deadzone. As mentioned earlier, the controller on the servo motor has a deadzone designed into the system to prevent the servo from constant actuation that would drain the battery on an R/C vehicle. This deadzone on the servo-horn is approximately a degree in size. In addition, the steering linkage itself contains ‘slack’, thus introducing additional deadzone. The sum contributions of the deadzones are difficult to quantify in the frequency responses.

The third servo non-linearity is the random time delay caused by the transmitter system. The delay itself, if constant, can be included in the system model and maintain a linear system. However, the delay of the vehicle system caused by the transmitter is clearly variable and quantized-random (as seen in previous plots). The effect of this non-linearity is not easily seen in the frequency domain responses, but is quite evident in the time-domain step responses shown earlier.

The fourth servo non-linearity arises from the steering linkage. The figure below shows the linkage used to transform the servo angle into the steering angle.

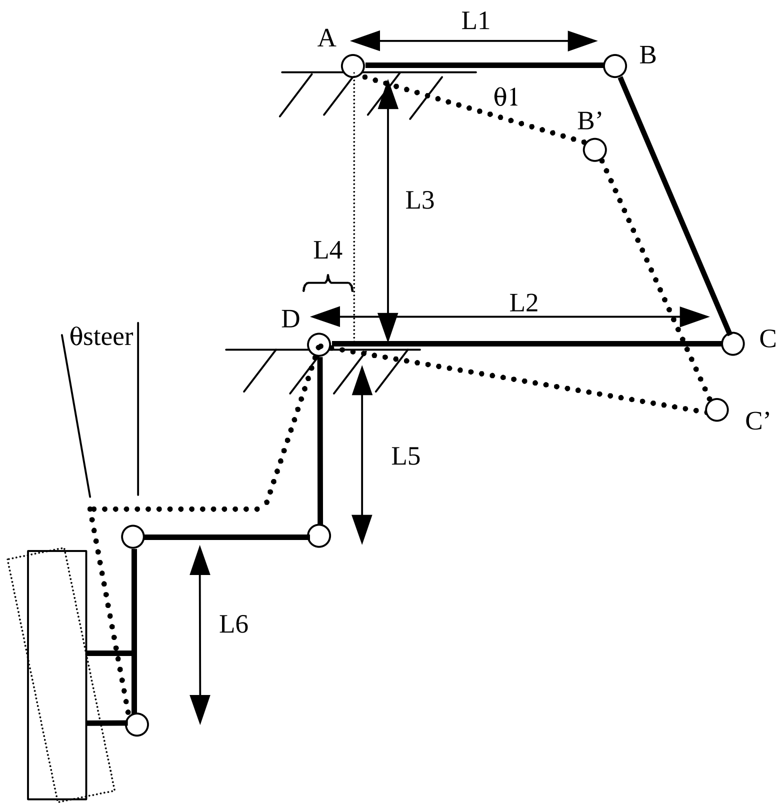

Figure 3.45: The steering linkage of the 4WS, 4WD vehicle used on the IRS.

The lengths of the links in the above steering linkage were originally as follows: L_1 = 8-mm, L_2 = 24-mm, L_3 = 52-mm, L_4 = 3-mm, L_5 = L_6 = 30-mm. Note, because of the following analysis, these lengths were modified between the 1.2 m/s tests and 3.0 m/s tests later to provide a linear relationship between servo angle and wheel angle for both the front and rear linkages. The following equation development therefore only applies to the testing conducted at 1.2 m/s (and a very small subset of data presented at 3.0 m/s).

Examination of the geometric arrangement of the linkages reveals that the steering angle θsteer is equal to the angle ∠CDC'. To solve for ∠CDC', we can examine the system as a four-bar linkage. In standard vector notation,

$$r_1 e^{i\theta_1} + r_2 e^{i\theta_2} + r_3 e^{i\theta_3} + r_4 e^{i\theta_4} = 0 \tag{3.127}$$

We can see that

$$\begin{aligned} r_1 &= L_1 \\ r_2 &= \sqrt{L_3^2 + (L_2 - L_1 - L_4)^2} \\ r_3 &= L_2 \\ r_4 &= \sqrt{L_4^2 + L_3^2} \end{aligned} \tag{3.128}$$

If we solve numerically for r_2 and r_4, we find r_2 = 55.02 mm and r_4 = 52.09 mm. We can also note that θ_4 is the angle of the ground link, and does not change. Solving for θ_4:

$$\theta_4 = \tan^{-1}\left(\frac{L_3}{L_4}\right) \tag{3.129}$$

we find θ_4 = 176.7 degrees numerically. If we continue the vector equation by expanding the imaginary vectors, we can then collect the real and imaginary portions of the vectors to obtain:

$$\begin{aligned} r_2 \sin(\theta_2) &= -r_1 \sin(\theta_1) - r_3 \sin(\theta_3) - r_4 \sin(\theta_4) \\ r_2 \cos(\theta_2) &= -r_1 \cos(\theta_1) + r_3 \cos(\theta_3) - r_4 \cos(\theta_4) \end{aligned} \tag{3.130}$$

If we square both equations and add them, we obtain:

$$\begin{aligned} r_2^{\,2} &= r_1^{\,2} + r_3^{\,2} + r_4^{\,2} - 2r_1r_3[\sin(\theta_1)\sin(\theta_3) + \cos(\theta_1)\cos(\theta_3)] + \\ &2r_1r_4[\sin(\theta_1)\sin(\theta_4) + \cos(\theta_1)\cos(\theta_4)] - 2r_3r_4[\sin(\theta_3)\sin(\theta_4) + \cos(\theta_3)\cos(\theta_4)] \end{aligned} \tag{3.131}$$

Collecting terms relating θ_3:

$$\begin{aligned} r_2^{\,2} - r_1^{\,2} - r_3^{\,2} - r_4^{\,2} - 2r_1r_4\cos(\theta_1 - \theta_4) &= -[2r_1r_3\sin(\theta_1) + 2r_3r_4\sin(\theta_4)]\sin(\theta_3) \\ &- [2r_1r_3\cos(\theta_1) + 2r_3r_4\cos(\theta_4)]\cos(\theta_3) \end{aligned} \tag{3.132}$$

It is easier to solve this if the following substitution is made

$$\begin{aligned} A &= r_2^{\,2} - r_1^{\,2} - r_3^{\,2} - r_4^{\,2} - 2r_1r_4\cos(q_1 - q_4) \\ B &= -[2r_1r_3\sin(q_1) + 2r_3r_4\sin(q_4)] \\ C &= -[2r_1r_3\cos(q_1) + 2r_3r_4\cos(q_4)] \end{aligned} \tag{3.133}$$

The equation then becomes

$$A = B\sin(\theta_3) + C\cos(\theta_3) \tag{3.134}$$

This can be solved using the trigonometric relationships:

$$\begin{aligned} \sin(\theta) &= \frac{2\tan(\theta)}{1 + \tan^2(\theta)} \\ \cos(\theta) &= \frac{1 - \tan^2(\theta)}{1 + \tan^2(\theta)} \end{aligned} \tag{3.135}$$

Substituting, the equation becomes

$$(1 + \tan^2(\theta_3))A = (2\tan(\theta_3))B + (1 - \tan^2(\theta_3))C \tag{3.136}$$

Which is quadratic in $\tan(\theta_3)$,

$$(A + C)\tan^2(\theta_3) - 2B\tan(\theta_3) + (A - C) = 0 \tag{3.137}$$

Solving

$$\tan(\theta_3) = \frac{2B \pm \sqrt{4B^2 - 4(A + C)(A - C)}}{2(A + C)} \tag{3.138}$$

$$\theta_3 = a\tan\left(\frac{B \pm \sqrt{B^2 - A^2 + C^2}}{(A + C)}\right) \tag{3.139}$$

A plot of this relationship reveals the nonlinear relationship between servo angle and wheel angle for the 4WS4WD vehicle. Shown below are the slope and derivative of this relationship:

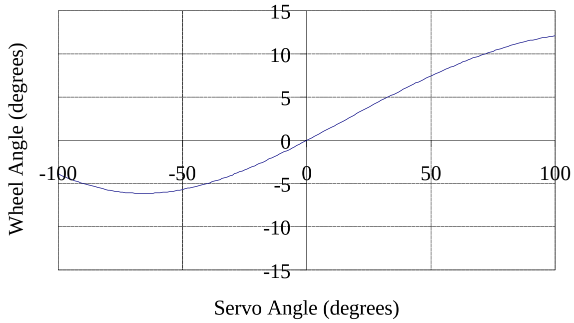

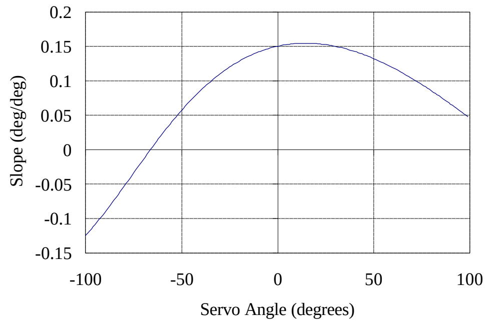

Figure 3.46: Relationship between servo angle and wheel angle (left) and slope of this relationship (right).

The graph of the slope of the system provides insight into the control of the system: a linear controller assumes that the slope is constant. This is similar to fitting the above left plot to a line. Clearly the left plot shows that the slope varies with operating point. Ideally, the system is nominally operated at 0 degrees but in practice there are errors in calibration. The resulting effect on the controller is to change not only the magnitude of the response, but also the phase of the response. The phase is seen if we imagine a point on the curve having to travel over the "hump" on the slope plot to contribute a steering input: the resulting non-linear change would affect the phase of the system as well. In practice, it was found that the frequency domain and time domain fits were VERY sensitive to the initial conditions on the steering actuator angle, and precise alignment of the actuator was needed. In other words, the system dynamics changes significantly with a small error in operating point of the system. Because the vehicle was both front and rear steering, a small error in one steering input would be canceled by control effort in the other input during closed loop operation, so these types of errors were very difficult to remediate and had to be conducted on a trial-and-error basis.

To simulate this linkage in a Simulink model, the following model was created.

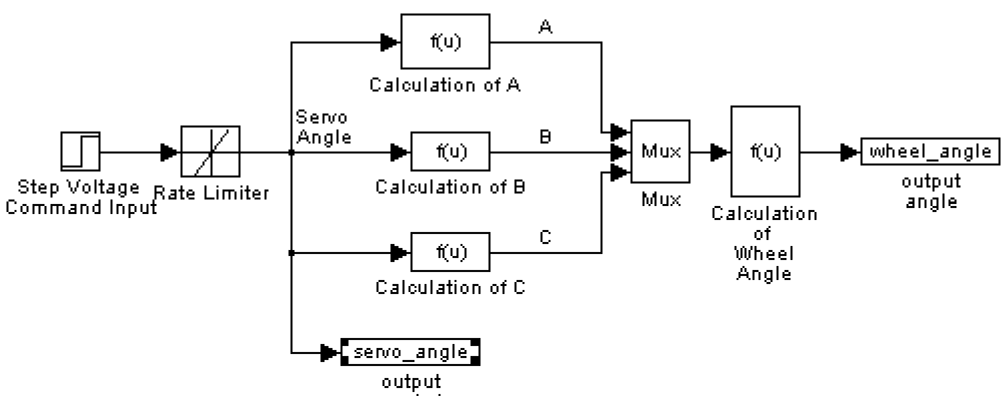

Figure 3.47: The SIMULINK model to determine wheel angle.

In the above figure the A, B, and C terms perform the corresponding calculations developed in the previous equations. The effect of this linkage non-linearity is demonstrated in later sections where the same MRC controller is implemented first on a system with strong steering linkage non-linearities, and secondly on one with minor nonlinearities.

The linkage nonlinearity can be approximated as a DC gain between actuator angle and wheel angle. This DC gain varies strongly with respect to the point where the above non-linear relationship is linearized. This "operating point" depends on the initial transmitter calibration. For the vehicle testing discussed in this thesis, DC values for the front wheels were found to be approximately 1.3 degrees (front wheel) per degrees (front actuator) and 0.76 degrees (rear wheel) to degrees (rear actuator). The resulting transfer functions are as follows:

$$\frac{\delta_f(s)}{V_{transmitter}(s)} = \frac{3510}{s^2 + 60.5 \cdot s + 1764}\left[\frac{rad}{volt}\right] \tag{3.140}$$

$$\frac{\delta_r(s)}{V_{transmitter}(s)} = \frac{751}{s^2 + 36 \cdot s + 625}\left[\frac{rad}{volt}\right] \tag{3.141}$$

These transfer functions were used in the later sections to represent the actuator dynamics of the system.

3.6.1.5 Direct Actuation – DC Motor System

Compared to the difficulties encountering in modeling the non-linear actuator dynamics for the servo systems, the modeling of the DC motor steering system was trivial. A PID controller was created to control the position of the system, and a frequency response was conducted to measure the tracking performance of this controller. The following figure shows the resulting frequency responses at three different amplitudes of steering input: 5 degrees, 10 degrees, and 20 degrees where the angle is measured in servo-motor degrees (as opposed to true wheel angle).

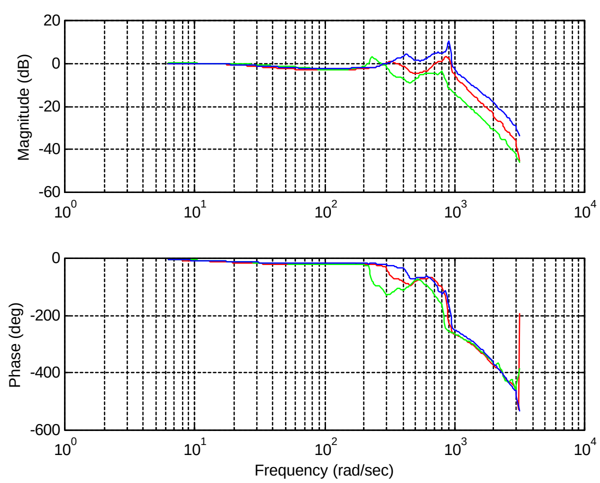

Figure 3.48: The frequency responses of the front steering actuator.

The bandwidth of the above steering actuator is clearly about 300 rad/sec, or between 40-50 Hz. This is nearly another order of magnitude faster than the R/C servo actuators! A small amount of amplitude dependence is seen, however it is unlikely that these differences will be seen simply because the mechanical system, with pole locations around 1-2 Hz, will act as a low pass filter for these actuator dynamics.

If the steering dynamics were used directly for steering of the vehicle, higher performance would be obviously achieved, but at the sacrifice of realism. In reality, the actuators on real full-scale vehicles are in the 5 Hz range (at best). The controller of the DC motor steering actuator was modified to emulate a 5 Hz actuator by placing a filter on the reference input of the controller with two poles at 5 Hz, critically damped. To test how well this tracking method would work, the frequency response of the actuator emulating a 10 Hz actuator (more difficult to track than a 5 Hz actuator) was obtained. The figure below shows the resulting response:

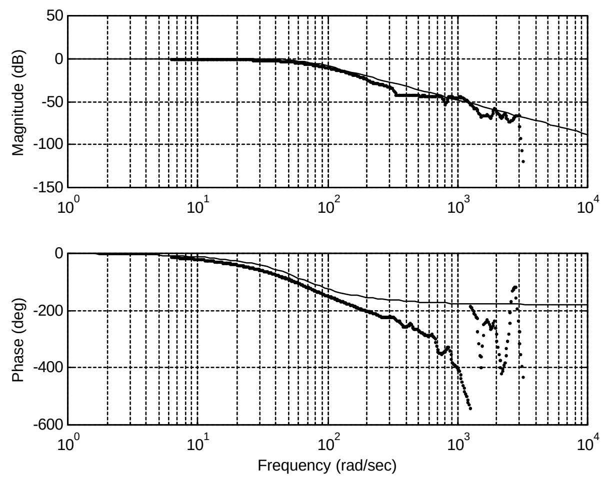

Figure 3.49: The frequency responses of the front steering actuator.

The system displays adequate tracking up to nearly 100 rad/sec, well past the dynamic range we would expect to observe from the vehicle. The 5 Hz, second order, critically damped actuator model was used for both the front and rear steering actuators hereafter.

The Uberquad vehicle can also steer via differential torque input. To approximate the available dynamics from the "torque" motors, again a PID tracking controller was constructed, and the system was made to track a sinusoid input from the DSA. The DSA was then used to obtain the frequency response from reference input to measured steering age to obtain a closed-loop frequency response. The figure below shows the resulting responses for 3 different inputs (again 5, 10, and 20 degrees as measured at the motor):

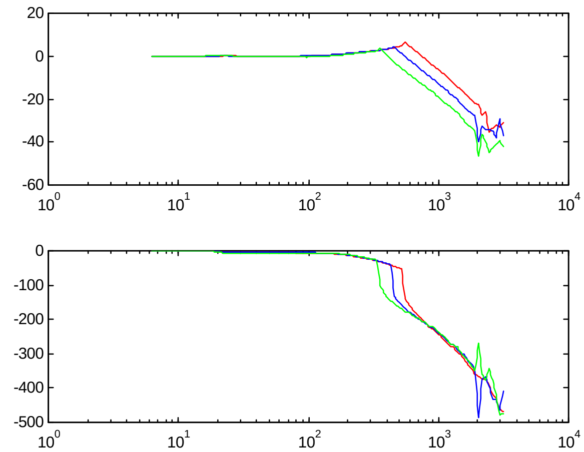

Figure 3.50: The frequency responses of the torque steering actuator.

Clearly, the system responses demonstrates a very high bandwidth of at least 40 Hz. Because each motor used for torque actuation has the same gear train and mounting geometry, it is assumed that the dynamics of each torque motor are identical. Thus the frequency response for the above steering motor and torque motor is assumed to apply to the remaining one steer motor and remaining three torque motors.

In a full-sized vehicle, the bandwidth of differential torque steering is much higher than that of turning the wheels to steer. To simulate this on the Uberquad system, no dynamic prefilter was used on the torque steering system, in essence leaving the motor to act as roughly a 40-Hz torque actuator. On real vehicles, the actuation bandwidth would depend largely on the speed of the ABS or torque control system and associated actuators, in addition to tire dynamics. As mentioned earlier, experimental longitudinal tire dynamics full-sized vehicles have a bandwidth of approximately 40-Hz, which justifies in some limited sense the choice of dynamics for torque control.

3.6.2 4WS4WD Yaw Dynamics at Low Speed (1.2 m/s) + Slow Servos

This section introduces the measured vehicle dynamics measured for the 4WS4WD vehicle at low speed (1.2 m/s). This work was conducted as a continuation of the studies conducted by the previous graduate student. When this experimentation was conducted, there was no consideration of pi-matching. Hence, the actuator dynamics were very slow because poor actuators were being used (without knowledge of their limitations), the wheels on the vehicle had cornering stiffness a factor of 2-4 times too high, and the weight distribution of the vehicle (notably the I_z moment) was arbitrary. To make matters worse, the data collection was initially conducted with the analog arm, which resulted in incredibly poor yaw-rate feedback. With so many caveats on the experimental results, one may question the intent of presenting this data. Ignoring the justification of continuing previous research techniques, many lessons can be learned from this experiment outside the realm of vehicle testing. The feedback, scaling, modeling, and controller development issues solved during this experiment allowed the success of the future vehicle tests.

System identification was first performed on the yaw response using the front wheel as the control input using the multiple bode-plot method previously discussed, resulting in the following fits:

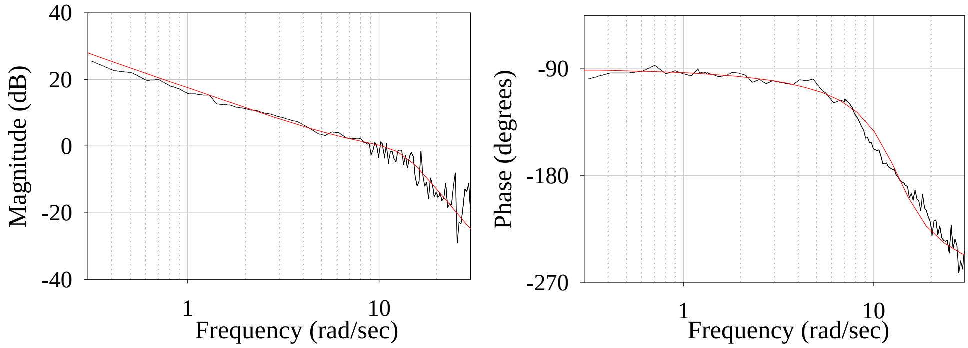

Figure 3.51: The fit of the yaw angle dynamics using the front wheels as the control input.

The above plots were fit for denominators ranging from 2nd to 5th order, and the best fit was found for denominators of 3rd order. The numerator order was then varied from 0th order to 3rd order, and the best fit was found to be at 0th order. The fit was performed using the INVFREQS command in MATLAB, with weighting at the corner frequencies to refine the fit. The solid line in the above plot corresponds to the transfer function:

$$\frac{\psi(s)}{V_f(s)} = \frac{13480}{s \cdot \left(s^2 + 10.3 \cdot s + 180\right)} \tag{3.142}$$

Note that the yaw angle is measured in degrees for this transfer function, which affects the D.C. gain on the transfer function. Also note that the yaw angle was scaled by 1/10 when the yaw position was returned to the DSA, so that the transfer function identified in the above Bode plot was multiplied by 10 to obtain the transfer function from voltage to yaw angle. The poles of this function are:

$$\text{Poles} = -5.13 \pm 12.4\,j \tag{3.143}$$

This represents a system that is slightly oscillatory in the open-loop time-domain response, which is expected.

Consideration of the above model fit shows some discrepancy in the model fit: the actuator dynamics (a DC motor) have 0 zeros and 2 poles, while the vehicle dynamics have one free integrator, two poles in the left-half of the complex plane (LHP), and one minimum-phase zero. Thus we expect the system to have 1 zero, 4 LHP poles, and one free integrator. Instead, the above fit has 0 zeros, 2 LHP poles, and one free integrator. The explanation for this discrepancy is clear when the bicycle model parameters for the system are measured. The bicycle model predicts (from these parameters) that the LHP vehicle poles are at approximately 20-30 rad/sec and 110 rad/sec, and the zero is located at around 30 rad/sec. The actuator dynamics are unknown (because of the rate-limiter), but examination of the actuator bode plots reveals are likely less than 20 radians per second when the combined rate-limiter and linear dynamic effects are combined. Thus, an explanation of the vehicle dynamics is as follows: the 110 rad/sec pole is being “washed out”, there is an approximate pole/zero cancellation between the remaining bicycle model pole and zero, leaving only the actuator dynamics and a free integrator to explain the observed model order.

To obtain the rear-steering dynamics, system identification was again performed as just described using the rear wheel as the control input, resulting in the following fits:

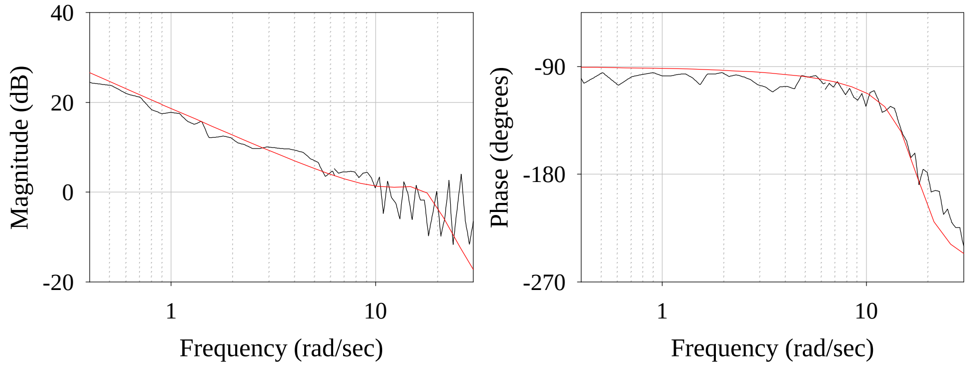

Figure 3.52: The fit of the yaw angle dynamics using the rear wheels as the control input.

Again, the order of the denominator was searched between 2nd and 5th order, and the order of the numerator was searched between 0th and 3rd order, with the best fit as shown below. Also, the results were weighed again at the corner frequencies to produce a more precise fit. The transfer function obtained from the voltage sent to the rear wheels to the yaw angle was found to be:

$$\frac{\psi(s)}{V_f(s)} = \frac{26500}{s \cdot \left(s^2 + 8.50 \cdot s + 310\right)} \tag{3.144}$$

The poles of this transfer function were found to be:

$$\text{Poles} = -4.25 \pm 17.1j \tag{3.145}$$

Again, the resulting poles indicate a time domain response that is slightly oscillatory. Before continuing to the next vehicle, note that the time-domain verification of open-loop dynamics are presented in the controller implementation section later in this thesis (to serve as a comparison between open-loop and closed-loop responses).

3.6.3 4WS4WD at High Speed (3.0 m/s) + Fast Servos

When Buckingham-Pi analysis was conducted on the vehicle, it was discovered that the operating velocities needed to represent a full-sized vehicle were much higher than the testing speeds of 1.2 m/s. It was also discovered that the low-frequency dynamics previously thought to be vehicle dynamics were in fact actuator dynamics. This section details the frequency-domain and time-domain identification of the system at a higher velocity of 3.0 m/s. This velocity corresponds roughly to a full-sized vehicle traveling at 65 mph, or approximately 30 m/s. The low-bandwidth actuators were replaced with the highest-bandwidth (and most expensive!) R/C actuators available.

As detailed in earlier sections, frequency-domain identification was conducted using swept-sine input, allowing 20 cycles for integration and 5 seconds to settle each frequency. The figures below were obtained using 400 separate sweeping frequencies. To obtain a dynamic model of the system, two separate methods were used: a theoretical approach and an input/output approach. To obtain a fit using the theoretical approach, the system was assumed to fit the bicycle model. To obtain a fit using the input/output approach, the system was assumed to be represented by a linear, causal transfer functions from driver input to vehicle state outputs. To fit the frequency response to the theoretical bicycle model, the unknown parameters in the bicycle, namely the cornering stiffness and the z-axis moment of inertia, were varied until a minimum error was found between the model and measured frequency responses. When the minimum error was sought, the actuator dynamics were included in the model, as well as the servo delay of 0.012 seconds. To obtain an a fit using the input/output approach, the frequency response was fit using causal transfer functions from 1st to 10th order until a minimum error was found. The arbitrary input-output transfer function fit was forced to have the same actuator dynamics between the front and rear transfer functions for yaw rate and lateral velocity. The plots below show three fits: the fit using the bicycle model alone (no actuator dynamics), the fit using the bicycle model with the actuator dynamics, and the fit using the input/output approach of using an arbitrary transfer function:

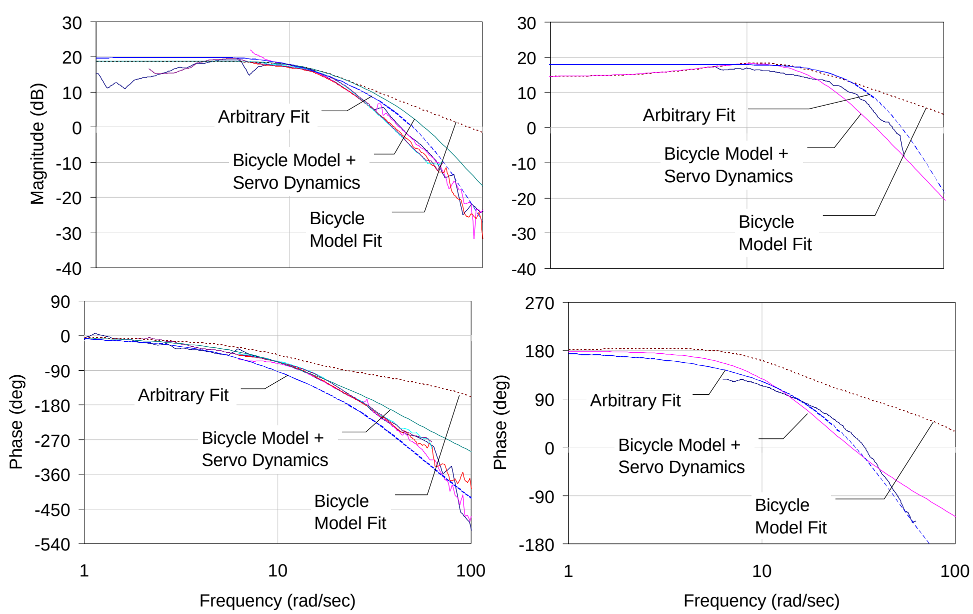

Figure 3.53: Frequency-domain fits of yaw-rate dynamics using the front (left plots) and rear (right plots) wheels as the source for steering inputs.

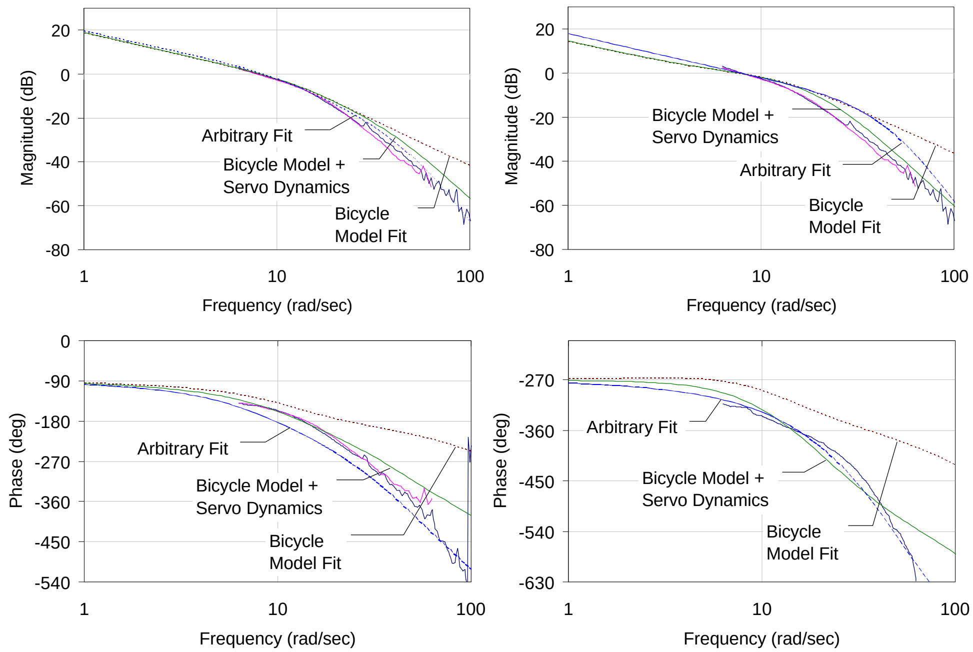

Figure 3.54: Frequency-domain fits of yaw dynamics using the front (left plots) and rear (right plots) wheels as the source for steering inputs.

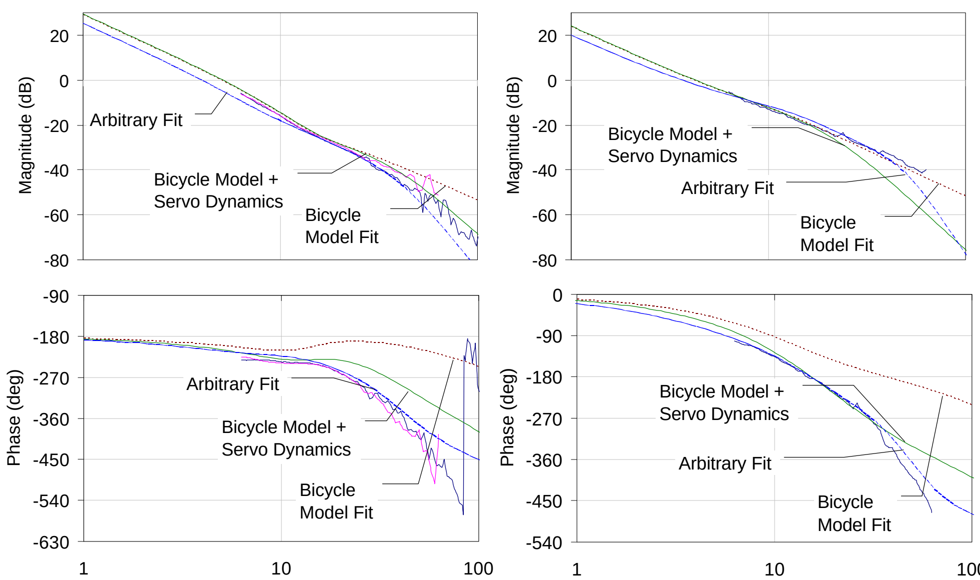

Figure 3.55: Frequency-domain fits of lateral dynamics using the front (left plots) and rear (right plots) wheels as the source for steering inputs.

The identified models for the bicycle model were obtained using the following parameters substituted into the bicycle model transfer functions derived earlier:

V	(velocity)	=	3.0 m/s
m	(mass)	=	4.025 kg
I_z	(z-axis mom.)	=	0.13 kg-m^2

a	(dist. C.G. to front)	=	0.1387 m
b	(dist. C.G. to rear)	=	0.1893 m
$C_{\alpha f}$	(cornering stiffness front tire)	=	20 N/rad
$C_{\alpha r}$	(cornering stiffness rear tire)	=	45 N/rad
Tnomf	(average front wheel torque)	=	0 N-m
Tnomr	(average front wheel torque)	=	0 N-m

This results in the following transfer function for the bicycle model where the actuator is approximated as a simple gain:

$$\frac{\dot{\psi}(s)}{\delta_f(s)} = \frac{42.7 \cdot s + 752}{s^2 + 21 \cdot s + 170.6} \tag{3.146}$$

$$\frac{\dot{\psi}(s)}{\delta_r(s)} = \frac{-131 \cdot s - 752}{s^2 + 21 \cdot s + 170.6} \tag{3.147}$$

$$\frac{\delta_f(s)}{\delta_{f,c}(s)} = 1.99 \tag{3.148}$$

$$\frac{\delta_r(s)}{\delta_{r,c}(s)} = 1.20 \tag{3.149}$$

For the bicycle model with actuator dynamics, the above expressions for yaw rate remain the same, but the actuator dynamics become:

$$\frac{\delta_f(s)}{\delta_{f,c}(s)} = \frac{1.99}{0.000567 \cdot s^2 + 0.0342 \cdot s + 1} \tag{3.150}$$

$$\frac{\delta_r(s)}{\delta_{r,c}(s)} = \frac{1.20}{0.0016 \cdot s^2 + 0.05765 \cdot s + 1} \tag{3.151}$$

Now that frequency-domain identification is complete, a verification of the dynamics is conducted by considering the system responses in the time domain. When practical, time domain verification was conducted with the driver-in-the-loop, that is with someone physically driving the vehicle. The following figures show the time-domain fits both with and without actuator dynamics.

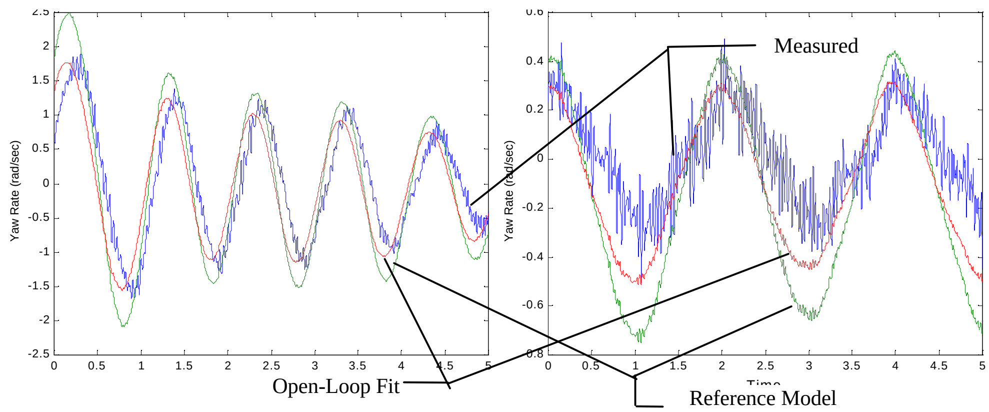

<u>Figure 3.56</u>: Time-domain fits of yaw rate showing the desired model, the predicted model, and measured yaw rate when actuator dynamics are ignored using front steering.

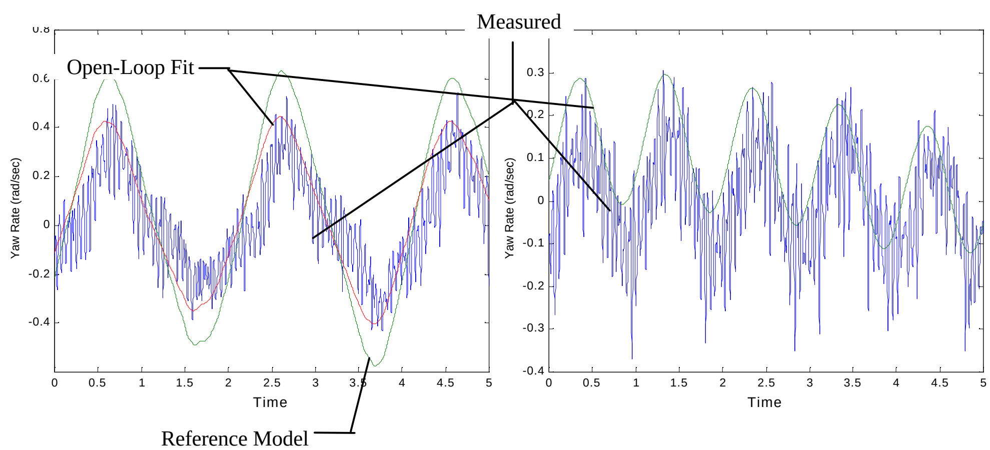

<u>Figure 3.57</u>: Time-domain fits of yaw rate showing the desired model, the predicted model, and measured yaw rate when actuator dynamics are included using front (left) and rear (right) steering.

It can be seen quite clearly from the above time-domain plots that there remains some amplitude and phase error, and that the modeling with actuator dynamics produces a much better fit of the system response. It should be noted that the fit in the frequency domain was obtained by forcing both the front and rear steering dynamics to follow a bicycle model. Hence, the parameters (instead of the poles) are the degrees of freedom. The frequency domain and time domain “fits” are coupled across states and control inputs: the front-steering yaw rate, rear-steering yaw rate, front-steering lateral position, and rear-steering lateral position bode plots all had to be fit simultaneously solely by varying bicycle model parameters. Because only two parameters, cornering stiffness and z-axis moment of inertia, had errors large enough to justify “tweaking” the system away from the measured values to obtain a better fit, therefore the degrees of freedom are only 3 (Iz, Caf, Car) to obtain a fit of 4 bode plots.

A better "fit" would be obtained if the system were not constrained so tightly by the bicycle model dynamics; however, arguments regarding dynamic similitude using the bicycle model would then be unjustified. This "better fit" using arbitrary input/output transfer functions is shown in the above frequency domain plots. For comparison, a controller design based off of these fits was compared to one based off of the bicycle model, and no difference could be seen in their performance. In light of this in for sake of simplicity, the results of this experiment are not presented in this thesis.

Given that the above fits represent a "parameter-based" identification, it is remarkable that the system dynamics did in actually fit quite closely to measured values. This fact in itself justifies and supports the bicycle model as a dynamic model for the system, which in turn justifies to some extent the dynamic similitude arguments presented earlier.

3.6.4 Uberquad at High Speed (3.0 m/s) + DC Motor

The final vehicle identification conducted in this thesis was on the Uberquad vehicle. Again, the state-variable of interest was yaw-rate, and the fits were conducted by varying the bicycle model parameters. The Uberquad was unique in that the transfer function from wheel angle to yaw-rate could be measured during testing in order to generate the bicycle model transfer functions with no actuator dynamics. This greatly simplified the model verification for the Uberquad.

The following figures show the frequency-domain system identification for the Uberquad for the three types of steering input: front steering, rear steering, and torque steering. The torque steering was conducted using the front two motors on the vehicle to both drive the vehicle and provide torque steering. Understandably, this can be quite simply modified into any number of configurations. This particular configuration was chosen out of convenience.

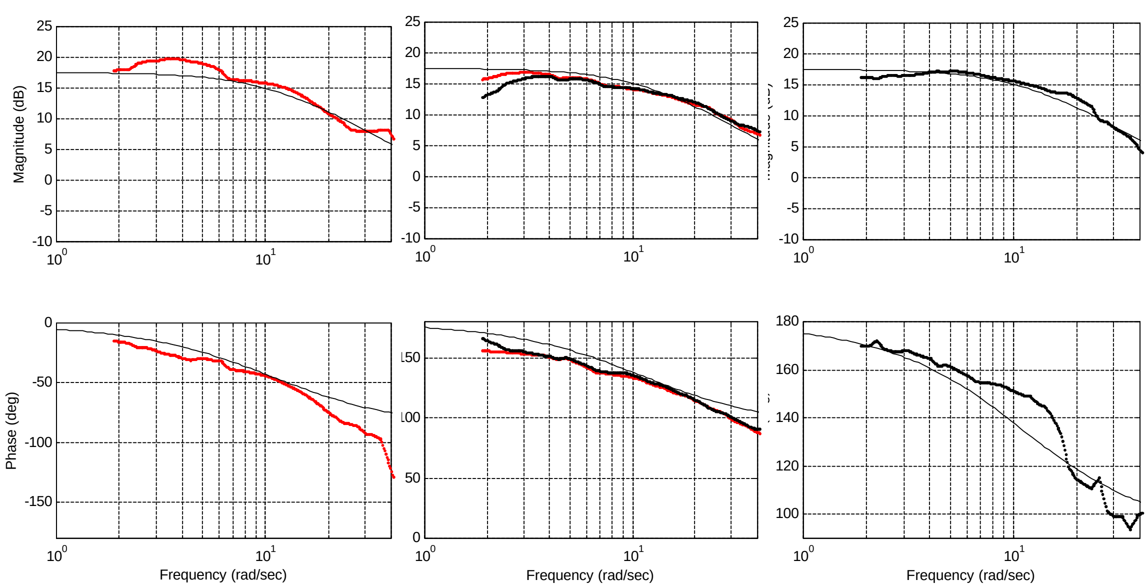

Figure 3.58: Frequency-domain fits for the Uberquad using front (left), rear (center), and differential-torque steering (right).

In order to evaluate the frequency-domain fit, the controller was made to track a sinusoid input to verify the amplitude and phase relationships of the frequency-domain fit. Three different frequencies were examined (only one is shown below): low (1-2 rad/sec), medium(4-5 rad/sec), and high (10 rad/sec). In addition, a square-wave tracking response was recorded for each type of input. A square wave was chosen because square wave tracking tends to emphasize high-frequency model mismatch, and intentionally shows model error during the square-wave steering command. The square wave tracking in essence requires an instantaneous change in yaw rate, which is impossible given that the steering angles for the wheels cannot instantaneously change. Thus, we do NOT expect the square wave responses to match between open-loop model and measured yaw-rate. The sine wave tracking was so well that a square wave tracking signal was a logical method to compare each type of input.

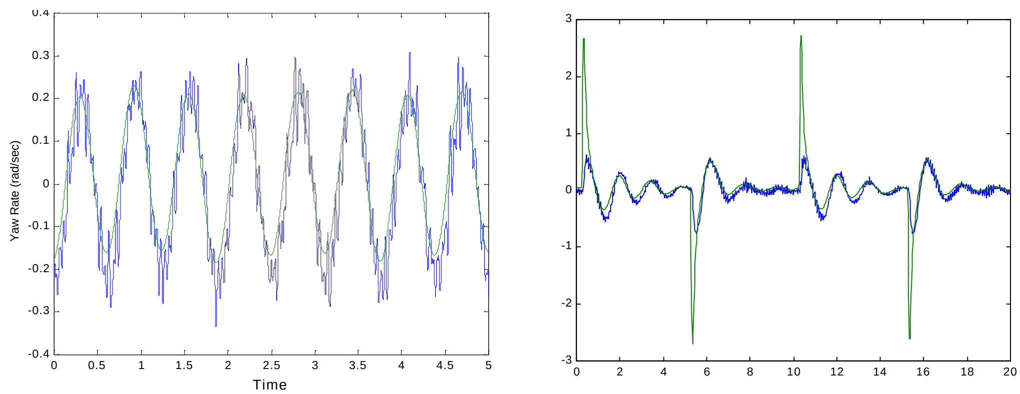

Figure 3.59: Time-domain fits for the Uberquad using front steering under different tracking trajectories: high frequency sinusoid (left) and step input (right).

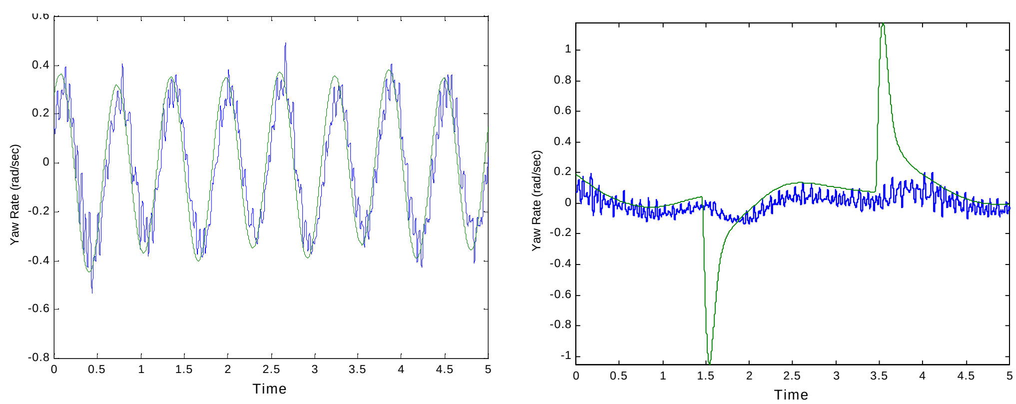

Figure 3.60: Time-domain fits for the Uberquad using rear steering under different tracking trajectories: high frequency sinusoid (left) and step input (right).

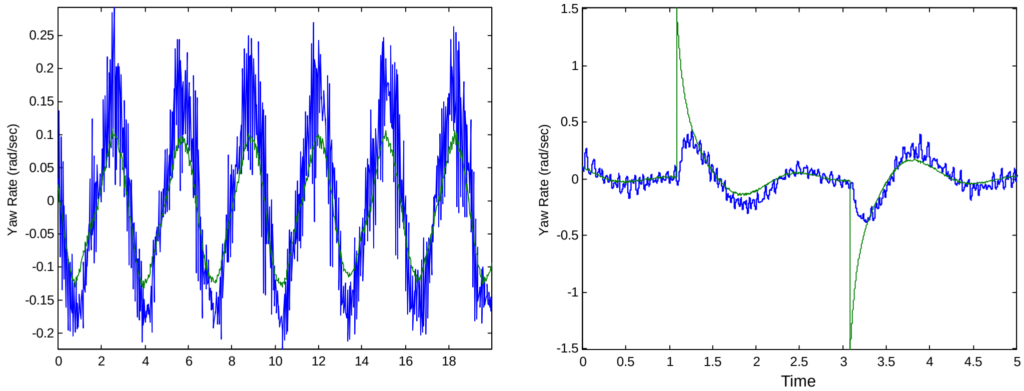

Figure 3.61: Time-domain fits for the Uberquad using differential torque steering under different tracking trajectories: high frequency sinusoid (left) and step input (right).

Several important points must be made about the previous model fits. The bicycle model parameters that gave the best dynamic fits in the frequency domain were nearly identical to the off-line measurements. This was not the case with the 4WS4WD vehicle, where some of the parameters varied from the measured values by as much as 50%. The above responses in both the frequency and time domain fit much closer to the bicycle model than those of the 4WS4WD vehicle. These overall trends suggests that the Uberquad is perhaps a much "tighter" system dynamically, and does not (as much) show the non-linear effects that plagued the 4WS4WD model testing such as rate-limited actuation and dead-zones in the steering linkages.

4 Control Approach

In previous sections, the motivational and theoretical basis for vehicle control was developed. Before continuing to the next natural step of implementation, the concepts and intent of control are first introduced. This chapter is written to provide an overview of the control methodology used in this thesis, and is written toward prospective control students who may be interested in the concept but unfamiliar with the practice of Model Reference Control.

4.1 Alternative Methods

Before delving into one particular control algorithm for pages and pages, alternative methods currently in use are described. The focus of this section is on practicality. It is quite easy to develop a "new" control theory or idea. It is wholly a different matter to ensure that the concept is clear and easily understood, as well as beneficial toward the end of controlling vehicular behavior.

4.1.1 Commercial Methods

Each car manufacturer is working to develop specific controllers for vehicle chassis handling, and with each controller is a new acronym. The first manufacturer to feature commercial yaw-rate or stability control was Mercedes-Benz in the form of the 1996 V-12 S class series. These vehicles were the first to feature the Electronic Stability Program (ESP). With the ESP, a yaw-rate sensor senses excessive side-slip, and compensates the vehicle by applying appropriate braking maneuvers. Based on an article by (VanZanten, Erhardt, and Pfaff 1995), it appears that the control is based on minimizing the sideslip velocity, and is likely a model-following approach based in the transfer function domain, with the feedback control designed using optimal control theory. It appears that the sampling rate is every 40 milliseconds (Arnholt 1995). As one writer notes, a Mercedes so equipped is the closest thing yet to the crash-proof automobile (Sherman 1995a).

Two years after Mercedes introduced their system, ITT Automotive introduced an Automotive Stability Management System (ASMS) that is currently used on the BMW 3-series sedan starting in 1998 (Sherman 1995b). This system also uses yaw rate and lateral acceleration feedback in conjunction with wheel-slip sensors and steering sensors.

4.1.2 2WS

Because of the actuation requirements for 4WS vehicles, some researches are instead focusing on the automation of vehicles using simply 2WS. Peng et al use a Pontiac 6000 vehicle to validate a feedback-type controller, where the error signal is actually previewed slightly. The resulting controller in effect becomes a feedback/feedforward controller (Peng et al. 1994).

4.1.3 Feedforward 4WS

The use of feedforward control was the first method attempted on vehicles with regard to rear-wheel steering. Feedforward control has the advantage a feed-forward control can achieve fast vehicle responses to steering wheel commands, without the lag or error necessary to achieve control input from a feedback system. This advantage is retained even if reduced-order approximations for the plant are used. Additionally, feedforward terms can contain non-linear dynamics simply because they do not affect the closed loop stability (Lee 1997).

4.1.3.1 Proportional Feedforward

Originally researchers were more interested in 4WS because the front and rear steering inputs, when used in conjunction, can in some way decouple the yaw and sideslip degrees of freedom. The simplest method to do this is to use a rear-wheel controller that is a feedforward proportional controller with variable gain. That is, the controller makes the rear wheel angle some ratio of the front wheel angle. One class of simple proportional controllers would be the controllers developed by Sano et al. from 1979 on (Nakaya and al. 1982; Sano 1986; Sano and al. 1979; Sano and al. 1980). In these controllers, the rear steering ratio was a predetermined function of speed where the ratio was determined by minimizing the steady-state side slip angle of the vehicle in the high speed range. The resulting ratio can be expressed as:

$$g = \frac{-b + \dfrac{ma}{C_{ar}L} v_x^{\ 2}}{a + \dfrac{mb}{C_{af}L} v_x^{\ 2}} \tag{4.1}$$

where the above parameters are the standard notation used in the bicycle model (reference 2 and 3 in VSD, p680 1995) and (Cho and Kim 1995; Sano 1986). This method is often referred to as the Vehicle Sped Function (VSF). It is also often expressed as:

$$\gamma = \frac{-\mathrm{b} + \mathrm{E_r v_x}^2}{\mathrm{a} + \mathrm{E_f v_x}^2} \tag{4.2}$$

where E_f and E_r are the steering compliance of the front and rear wheels. In the low speed range, the rear wheels were steered in a direction opposite the front wheels to make the turning radius of the vehicle smaller. To simplify the system, a mechanical link was used to connect the front and rear wheels, which relies on the concept that the driver corrects the steering angles with smaller magnitudes as the vehicle speed increases. With the rear wheel steering in the same direction as the front wheel, the phase lag of the lateral acceleration can be reduced while keeping the vehicle yaw rate response unchanged (Furukawa and Abe 1997).

An alternative approach to maximize vehicle stability is presented by (Cho and Kim 1995) called the Maximum Stability method. At each velocity, root locus diagrams of the closed loop system are made using the front-to-rear steering ratio as the locus parameter. The value that gives the closed-loop pole locations farthest in the left-half plane is then used.

The inherent problems with the proportional feedforward approach are that the controller minimizes only the steady-state sideslip angle. A significant amount of transients may be introduced by use of the rear wheels. Additionally, the lack of feedback can introduce undesirable performance degradation with varying models, road conditions, etc.

4.1.3.2 Proportional + Delay Feedforward

The steady-state methods described previously improve vehicle stability, but the response will still contain undesirable transient dynamics. By applying suitable transient control, the vehicle response can be improved without sacrificing stability (Inoue and Sugasawa 1993). Several authors have observed that the rear-steer command is approximately proportional to the front steering input, but delayed. Cho and Kim (Cho and Kim 1995) use a time delayed rear-steering type of controller where the control law for the rear input is:

$$d_r(t) = g \cdot d_f(t - t_s) \tag{4.3}$$

where gamma is a velocity-scheduled gain, and t_s is a velocity-scheduled time delay. This technique was introduced earlier by (Shibahata and al. 1985). With this method, the phase lag at lower frequencies for yaw rate and lateral acceleration will be reduced, but this effect diminishes in the range of 0.7 – 1.0 Hz. This trend is characteristic of feed-forward types of rear-wheel control (Furukawa and Abe 1997). We see that the use of the time-delay with the proportional term improves the transient effects of the rear steering input, but suffers from the similar drawbacks of purely proportional control.

4.1.3.3 Transfer-Function Feedforward Methods

The use of a time-delayed input to the rear wheels improves performance, but can also introduce undesirable transient performance. There are two basic types of dynamic (non-proportional) rear wheel control: in phase and phase reversal. The method of using a delay always steers the rear wheels in the same phase as the front wheels. However, if we allow the rear wheels to be steered momentarily in the direction opposite of the front wheels, the vehicle will be more responsive (Inoue and Sugasawa 1993). Naturally, this approach requires higher levels of actuation, but the performance improvement is significant. Takiguchi et al. obtained a front and rear steering ratios such that the phase difference between lateral acceleration and yaw rate is zero (Takiguchi and al. 1986). Examination of the relationship between side-slip angle, yaw-rate, and lateral acceleration reveal that this result is identical to the previous work by Sano. However, the concept was expanded by Takeuchi (Takeuchi and al. 1985) when they derived the transient theoretical relationship needed to maintain the body side-slip angle to zero. These results are in complete agreement with work conducted by Fukunaga who reported that by actively steering the front and rear wheels in relation to the steering input, the phase lag between lateral acceleration and yaw rate could be set to zero (Fukunaga and al. 1987).

A paper by (Ahring and Mitschke 1995) notes that if we attempt to make the yaw rate and sideslip angle invariant to vehicle loading and cornering stiffness, then rear-wheel control alone will not work because the system is coupled between these two state variables. Hence, two inputs are needed. Invariance of yaw-rate and side-slip angle with respect to loading and cornering stiffness will only be obtained if the controller has access to the steering input for both the front and rear wheels independent of the driver. Although this is not likely to be adopted in practice (simply because the driver will have no control over the vehicle if the controller electronics fail), their paper does point out limitations on performance achievable by using the rear wheels alone to assist the driver.

4.1.4 Feedback 4WS

The use of feedback for vehicle control has several advantages over purely feedforward control. Perhaps the most important advantage, the use of feedback maintains stable vehicle characteristics during changes in driving conditions (Inoue and Sugasawa 1993). As pointed out by the same author, the use of feedback must achieve the same level of steering input response as feedforward control to be considered. In addition, it can be shown that stability against external disturbances cannot be set independently of driving performance for a purely feedback system (Inoue and Sugasawa 1993). From a standpoint of model following, the zeros of a system are invariant; feedback control cannot affect the zeros of a vehicle model.

4.1.4.1 Proportional Feedback

It is possible to force the vehicle, via feedback, to have neutral steer characteristics. Assuming the bicycle model parameters are known, the bicycle model predicts neutral steer characteristics with feedback gain:

$$\delta_r(t) = C \cdot V_{long} \cdot \dot{\psi} \tag{4.4}$$

with

$$C = \frac{m}{2 \cdot L} \cdot \left(\frac{a}{C_{\alpha r}} - \frac{b}{C_{\alpha f}} \right) \tag{4.5}$$

where V_{long} is the longitudinal velocity of the car, $\dot{\Psi}$ is the yaw rate of the vehicle, m is the mass of the vehicle, L is the length of the vehicle, C_I are the cornering stiffness of the front and rear tires, and a and b are the length from the CG to the front and rear axles, respectively. This model was presented by (Senger and Schwartz 1987), and tested in simulation and compared to other methods by (Sridhar and Hatwal 1992) and found to be the easiest to drive among several parameter-based methods.

4.1.4.2 State Feedback

The performance of the closed-loop system is often examined by incorporating a model of the driver in the control loop. Cho and Kim design an optimal four-wheel steering system via a LQR approach, where the driver is assumed to be modeled as a purely feedback PD-controller with a time delay of 0.2

seconds. Three optimal approaches are considered: minimizing four state variables (lateral error, yaw rate, and derivative of both), minimizing the side-slip velocity (lateral velocity), and minimizing the side-slip velocity and the yaw rate equally. The resulting controller in all cases resembles a state-feedback type of control. Cho and Kim note for their controller that the results of an optimal control structure reveal nearly identical performance as the proportional + delayed feedforward controller, with slightly less oscillation.

4.1.4.3 Nonlinear Control

One option to obtain perhaps the maximum vehicle performance is to account for system nonlinearities (like sliding or strange deformations in the wheel). As an example, Smith and Benton design an emergency controller to maneuver the vehicle as rapidly as possible from one lane into another using a non-linear optimization scheme (Smith and Benton 1996). The purpose of the non-linear scheme is to account for vehicle tire non-linearities during a very aggressive maneuver. The controller attempts to minimize the distance traveled before the vehicle leaves a lane; hence, the tire forces are saturated for much of the maneuver.

Obviously, accounting for tire non-linearities will improve vehicular performance. However, there seem to be two primary issues with using a non-linear model or control. The first is obtaining the model: most controllers based on complex tire dynamics assume that the vehicle has knowledge of the road surface before arriving at the road surface, or can at least achieve robust estimation of road parameters. This has historically been very difficult to achieve. The second issue is design of the controller. It is quite difficult to “tune” a non-linear controller, simply because the system response can be non-intuitive. As a general rule, highly nonlinear controllers tend to be best suited for two extremes: to marginally improve a system that is already under control using linear methods by accounting for known model nonlinearities, or to stabilize a system that is not stabilizable or difficult to approach using linear controllers. For this reason, nonlinear controllers are for the present time avoided in this vehicle research.

4.1.4.4 Driver Out of the Loop – PID

In the paper by (Ahring and Mitschke 1995), a PID regulator is used to control both the front and rear wheels, with a transfer function coupling the two via feedforward terms. The resulting coupling network is sensitive to vibration if the gains are incorrectly chosen; however, the authors are able to obtain a yaw-rate and side-slip response that is invariant to cornering stiffness and vehicle loading given only yaw rate and lateral acceleration feedback. A drawback to this method is that the use of feedback very often introduces the vibration the authors comment on. This vibration is inherent in the coupling between the two free modes because of the poor damping inherent in the bicycle model. This vibration is seen in later experimental testing of the vehicle using a purely feedback type of control.

4.1.4.5 Driver Out of the Loop – Neural Networks

In recent years, non-standard “modern” neural networks have been introduced to control the vehicle. In the paper by (Nagai, Ueda, and Moran 1995), a neural network is trained and used to control a

4WS vehicle. However, the network was trained and tested only in simulation. Because neural networks are inherently sensitive to the method by which they are trained, it is unlikely that this method will be adapted for control of an actual vehicle in the near future without a significant amount of further validation.

4.1.5 Feedforward + Feedback 4WS

In designing feedforward and feedback systems in conjunction, several important aspects must be considered. The division of control tasks between feedforward and feedback control must be clearly defined, including considerations of problems that might arise when all tasks are entrusted to feedback control. The combined use of feedback and feedforward control should not complicate the control system. Finally, controller robustness to external disturbances and model changes should not change significantly with the use of feedforward control as compared to feedback control alone (Inoue and Sugasawa 1993).

The tradeoff decision between feedforward and feedback control is critical with regard to controller implementation. It is possible to examine the merits of each type of controller if we isolate the effect of each term (Inoue and Sugasawa 1993). For this discussion, we choose yaw rate as the state variable of interest; however, any vehicle state can be chosen without loss of generality. The yaw rate of the vehicle is given by:

$$\dot{\psi} = \delta_f \cdot \dot{\psi}_f + \delta_r \cdot \dot{\psi}_r + \psi_{dist} \tag{4.6}$$

where $\dot{\psi}_f, \dot{\psi}_r$ are the relationships (transfer function or time domain) between steering inputs, δ_f, δ_r, and yaw rate output, $\dot{\psi}$. The subscript "dist" notes a disturbance input at the output of the system. From the previous diagram, the rear steering input is:

$$\delta_r = \delta_f \cdot FF + e \cdot FB \tag{4.7}$$

where FF is the feedforward transfer function, FB is the feedback transfer function, and e is the error.

$$e = \delta_f \cdot TF - \dot{\psi} \tag{4.8}$$

where TF is the Target Function for the yaw rate (i.e. the reference model). We can combine these equations to obtain:

$$\dot{\psi} = \frac{(\dot{\psi}_f + FF \cdot \dot{\psi}_r) + TF \cdot FB \cdot \dot{\psi}_r}{1 + FB \cdot \dot{\psi}_r}\delta_f + \frac{\psi_{dist}}{1 + FB \cdot \dot{\psi}_r} \tag{4.9}$$

Let us assume that we can obtained the exact desired yaw rate response by feedforward control. We can then specify that the target function, TF, be:

$$TF = \dot{\psi}_f + FF \cdot \dot{\psi}_r \tag{4.10}$$

The resulting transfer function using this target function is:

$$\dot{\psi} = \underbrace{(\dot{\psi}_f + FF \cdot \dot{\psi}_r)}_{\substack{\text{desired}\\ \text{reference}\\ \text{model}}}\delta_f + \underbrace{\frac{1}{1 + FB \cdot \dot{\psi}_r}}_{\substack{\text{disturbance}\\ \text{rejection}}} \cdot \psi_{dist} \tag{4.11}$$

We thus have completely decoupled the desired reference model from the disturbance rejection characteristics. We can see that if FB can be chosen to invert $\dot{\psi}_r$, then the disturbance rejection term will not contribute any additional dynamic terms into the yaw response.

A feedforward/feedback system was used by Lee (Lee 1997) consisting of a filtered front steer input and proportional yaw rate feedback (using filtered yaw rate):

$$\delta_r = K_\delta \cdot \frac{(1+\tau_1 \cdot s)}{(1+\tau_2 \cdot s)} \delta_f - K_\psi \cdot \dot{\psi} \tag{4.12}$$

From dynamic inversion arguments, it is clear that the above method will work well only if the vehicle response can be adequately described by a first order transfer function.

Basic feedforward and feedback rear-wheel steering controllers are discussed in (Lee, Mariott, and Le 1997). It was found that the vehicles became more responsive (smaller J turn rise time) if the wheels are steered in phase with negative yaw rate feedback. The vehicle becomes less response if the wheels are steering in phase with positive yaw rate feedback.

Several authors, namely Cho and Kim, include driver feedback models in order to examine closed loop stability (Cho and Kim 1995; Cho and Kim 1996). The driver model is feedback based with a delay, with a preview amount of the tracking error proportional to the square of vehicle velocity. The resulting controller can be thought of as a feedforward-feedback system.

Simple mixed feedforward/feedback structures have been tested that are based on the theoretical bicycle model. Sridar and Hatwal suggest the following structure (Sridhar and Hatwal 1992):

$$\delta_r(t) = -\delta_f(t) + C \cdot V_{long} \cdot \dot{\psi} \tag{4.13}$$

with

$$C = \frac{m}{2L} \cdot \left(\frac{b}{C_{\alpha f}} + \frac{a}{C_{\alpha r}} \right) \tag{4.14}$$

The motivation for this form was taken from the paper by (Sato et al. 1983). If we examine the controller, we find it is very similar to the control used in the feedback section to produce neutral steering characteristics.

Shiotsuka et al demonstrated the use of a Neural Network to predict the tire friction for changing mu values and changing velocity. Using this estimator, they iteratively design an optimal controller for both a feedforward and feedback controller. They demonstrate their performance with time-domain simulations (based seemingly on their neural network), and show good performance for high acceleration maneuvers (Shiotsuka, Nagamatsu, and Yoshida 1993).

An excellent paper is presented by the Honda research group where the road friction parameter is estimated based on the yaw rate measurements. Using the estimated friction value, an adaptive feedforward and feedback controller is designed to track a reference model. The feedforward controller is designed to minimize the steady-state and transient vehicle slip angle in spite of changes in friction, while the feedback controller is designed using an Internal Model Control structure to compensate for nonlinearities and achieve robust performance. The feedback gains are then determined used a mu synthesis approach. This paper is distinguished in that the experimental results are validated both in the time and frequency domain on an actual vehicle (Wakamatsu et al. 1997).

Often the questionable assumption is made that the bicycle model parameters are known beforehand for a particular vehicle/roadway combination. With this in mind, the dynamics of the vehicle can be inverted and a controller designed to produce invariant and/or optimal performance. Yaniv uses this approach to achieve speed-invariant performance for a bus with a controller that commands both front and rear wheels (Yaniv 1997).

4.1.6 Mixed Steering and Braking

One method to control the vehicle orientation is to use the torque produced by each wheel during braking or acceleration to generate a yaw moment. This is often referred to as Direct Yaw Control (DYC). If the traction and braking forces are distributed appropriately, the yaw moment and thus the lateral motion can be accurately controlled (Fukunaga and al. 1987). An advantage of the DYC method is that the longitudinal forces of a tire do not saturate as quickly as in the lateral direction (Abe, Ohkubo, and Kano 1996). As was shown in earlier section sections, the tire has a more linear response with higher bandwidth in the longitudinal direction than in the lateral direction. Hence, more precise yaw moments can be generated to control the vehicle lateral motion using DYC rather than RWS. Finally, the system is somewhat fail-safe since DYC is more robust to changing vehicle conditions as the longitudinal forces do not saturate as fast as the lateral forces, and the driver maintains control over the front steering input (Fukunaga and al. 1987) (Nagai, Hirano, and Yamanaka 1997).

We must realize that the use of longitudinal tire forces can influence actuation of longitudinal controllers such as ABS or Traction Control Systems (TCS), thus increasing the complexity of the vehicle dynamics (Fukunaga and al. 1987). Hence, these brake/torque controllers are most often used in accident prevention/ skid control rather than vehicle directional control. The Mitsubishi group has developed a controller method that emphasis comfort (based on minimizing the jerk of the vehicle) that recognizes in some part that driver discomfort must be considered. In their study, the determined that jerk was a key indicator of whether a maneuver was conducted for comfort or for collision avoidance (Hayafune and Yoshida 1990).

It is important at this point to make a distinction between DYC and ABS or TCS systems. TCS/ABS systems should be considered fundamentally different types of vehicle control technology. TCS/ABS control the longitudinal force on each wheel independently to prevent lockup or spin during braking or traction efforts. Even though these systems may stabilize the vehicle lateral motion, they do not actively control the vehicle’s overall motion (Fukunaga and al. 1987). This becomes intuitively clear if the acceleration diagram shown in Chapter 2 is examined.

A model reference tracking controller was developed by Will and Zak of Purdue that utilizes brakes, front steering, and rear steering for control input (Will and Zak 1997). The design of the controller is based on the Lyapunov direct method. The controller is designed using the bicycle model, and validated using step inputs using a higher order (roll and pitch DOF) model. Both feedforward and feedback terms are used; however, the feedforward is simply a direct feedforward command (unity), so the system zeros may deteriorate performance. The resulting control ends up behaving like a sliding-mode control where the reference model trajectory is the invariant manifold. One problem with this control is that the control naturally chatters to maintain tracking with the reference model (Will and Zak 1997).

A Direct Yaw Moment control system based on model following technique using state feedback is described in detail in a paper by Nagai et al (Nagai, Hirano, and Yamanaka 1997). A controller utilizing both feedforward and feedback is designed to achieve model following. The feedforward and feedback terms are decoupled, this providing freedom to design the feedback controller using robust control methods, pole placement, or optimal control. In this paper the authors choose an optimal control technique. As a note, this paper is perhaps one of the closest published work yet discovered in terms of similarity to the thesis work presented here. Another paper using transfer function based Model Reference Control to control the yaw rate and sideslip responses with 4WS and DYC is given by (Abe, Ohkubo, and Kano 1996). Specifically, they show that DYC is more responsive than 4WS because the yaw rate response by DYC is proportional to steering wheel input while the response to 4WS is a first-order lag. A feedforward and feedback controller is used, with the feedforward term intended to produce zero side slip. Simulation studies demonstrated a consistent lag in the yaw rate tracking using 4WS, while the DYC showed good tracking. In addition to yaw rate control, the authors introduce a cooperative control where zero sideslip as well as model-following with the yaw rate. The authors also note that when the tires begin to saturate, the yaw-rate feedback tends to destabilize the system by requiring excessive feedback actuation.

There are very few papers comparing 4WS vehicles with DYC. Notable exceptions are the two papers by Dr. Alleyne where different control input strategies are compared in the steady-state (Alleyne 1997a) and during transient maneuvers (Alleyne 1997b). The strategies compared were Four Wheel Steering, Front Wheel Steering, Four Wheel Brake Steering, Front Wheel Brake Steering, and Rear Wheel Brake Steering. Each of these techniques were evaluated when using an optimal controller design approach (LQ) based on the bicycle model where the metric of comparison was the ratio of the amount of tire usage to the maximum available tire force. It was found that the 4WS is as efficient in it tire usage as front wheel steering, and that rear wheel braking should be avoided. Differential braking was not as efficient as these other two steering methods; however, it is in general preferred for liability reasons (Alleyne 1997b).

One of the few papers dealing with aggressive cornering and acceleration/braking was presented by Shibahata et al from Honda. In this paper, a parameter-based controller based on a stabilizing yaw moment is introduced. Good performance is achieved; however, the controller assumes that the tire model (friction, lag, etc.) is known exactly. The resulting feedforward controller is not discussed, and experimental verification is not presented in this paper. In this paper, a performance curve in the acceleration domain is presented that nearly encompasses nearly all of the acceleration domain (Shibahata, Shimada, and Tomari 1993). Based on the structure of the controller, the concept is sound but many assumptions are made with regard to road friction, tire model, etc. for this controller to be of practical use.

4.2 Introduction to Model Reference Control

Model reference control (MRC) is a control technique where the performance of a system is specified by the performance of another system. The area of Model reference control is well studied, and includes non-linear and time-varying systems . In general, MRC is presented in the context of adaptive control, where an adaptive routine iteratively identifies new plant parameters, and the controller is modified "on-the-fly" to achieve model tracking.

4.2.1 Dead-Beat Control

If the general purpose of MRC is to achieve model tracking, then we must consider the simplest method to do so for a stable, non-minimum phase system. Simply "flip" the transfer function, multiply it through the reference model, and use the resulting transfer function as the new controller. This method is often referred to as model inversion, but it is highly sensitive to modeling errors, and is not suited for non-minimum phase systems. One aspect of control is that a sampled system is always non-minimum phase if the sampling rate is high enough. Clearly, the issues associated with Dead-Beat control tend to outweigh its simplicity. However, in the following derivation of MRC with disturbance rejection, we borrow on the idea of model inversion.

4.2.2 Theory and Implementation of MRC

This section outlines the procedure used to transform the dynamics of the vehicle so that the vehicle performance behaves like a different, reference vehicle. In essence, the Model Reference Controller approach can be looked at as a simultaneous pole AND zero placement approach, with a feedforward term that anticipates the vehicle response. The following derivation is a modification of the derivation provided by Astrom and Wittenmark in their publication, <u>Adaptive Control</u> (Astrom and Wittenmark 1995).

To begin, we consider the general case of a plant that receives a control input u and has a single output y. We assume at this point that the plant is linear; that is, the plant can be represented by a transfer function that is a polynomial of s for both the numerator and the denominator.

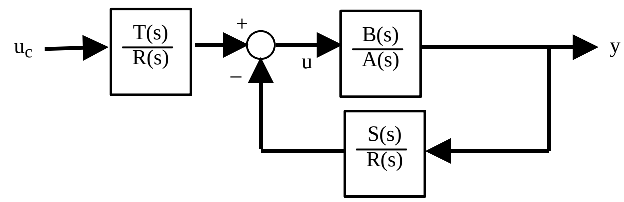

Figure 4.1: The feedback/feedforward structure of the MRC method.

We can represent the output of the plant with the following equation,

$$Y(s) = \frac{B}{A} \cdot U(s) \tag{4.15}$$

Where A and B are the denominator and numerator, respectively, of the transfer function. We would like the plant to behave like:

$$Y(s) = \frac{B_m}{A_m} \cdot U_c(s) \tag{4.16}$$

where A_m and B_m are the desired denominator and numerator, respectively, of the plant, and U_c is the input into the controller. To obtain the desired behavior, we may implement a controller that has both a feedback and a feedforward portion, such as:

$$u = \frac{T}{R} \cdot u_c - \frac{S}{R} \cdot y \tag{4.17}$$

Here T/R is a feedforward transfer function intended to cancel the dynamics of the plant, and S/R is a feedback transfer function to compensate for any error in the feedforward design. If equation for control effort is substituted into the plant equation and solved for y, the following result is obtained:

$$y = \frac{B \cdot T}{(A \cdot R + B \cdot S)} \cdot u_c \tag{4.18}$$

We can see that to obtain the desired closed loop poles, then A_m must be a common factor of (AR+BS). We can also see that if we wish to cancel any zeros of B, we must also include these terms as additional factors of (AR+BS). To understand this more clearly, we can factor B into two portions:

$$B = B^+ \cdot B^- \tag{4.19}$$

Where B^+ contains the terms to be cancelled and B^- contains the remaining terms. Since there is an infinite number of ways to factor out B^+, we must assume that B^+ is monic (i.e. the coefficient of the highest power is 1). In addition, we must assume that B+ is stable and well damped.

One final factor of (AR+BS) is the observer poles of the system. The term (AR+BS) represents the characteristic polynomial of the system, and that the terms $B^{+\cdot}A_m$ may not have the same order as the characteristic polynomial. To increase the order, we include an additional factor of A_o, which represents the observer poles of the system. In general, we want these poles to be much faster than the model poles, A_m. We can combine all of these requirements to obtain the *Diophantine* equation:

$$A \cdot R + B \cdot S = B^+ \cdot A_o \cdot A_m \tag{4.20}$$

If we factor B in the above equation into B^+ and B^-, we can see that B^+ must also be a factor of AR in order for a solution to exist. We know that A will not factor B^+, because if it did factor, then the original formulation of B/A would not be a minimal realization of the plant. Hence, B^+ must be a factor of R.

$$R = B^+ \cdot R_1 \tag{4.21}$$

If we divide the Diophantine equation by B^+, we obtain:

$$A \cdot R_1 + B^- \cdot S = A_o \cdot A_m \tag{4.22}$$

In this modified form of the Diophantine equation, we can provide the conditions that guarantee that there exist solutions that give a proper (in continuous-time) or causal (in discrete time) control law. To do this, we note that the controller must be causal. Thus, we require

$$\begin{aligned} \deg S &\le \deg R \\ \deg T &\le \deg R \end{aligned} \tag{4.23}$$

Note that if R_o and S_o are solutions to the Diophantine equation, then so are

$$\begin{aligned} R &= R_o + QB \\ S &= S_o - QA \end{aligned} \tag{4.24}$$

where Q is an arbitrary polynomial. Since Q is arbitrary, there are an infinite number of solutions to the Diophantine equation. We select the solution that gives the lowest degree controller, which is called the minimum-degree solution. We note that these conditions are:

$$\begin{aligned} &\deg A_0 \ge 2 \cdot \deg A - \deg A_m - \deg B^+ - 1 \\ &\deg A_m - \deg B_m \ge \deg A - \deg B \end{aligned} \tag{4.25}$$

The second inequality is a requirement on the relative degree of the reference model, also known as the pole excess. In order to solve for the T polynomial, we must require that the term B^- divides B_m; otherwise, no solution exists. We can then write:

$$B_m = B^- B'_m \tag{4.26}$$

$$T = A_0 \cdot B'_m \tag{4.27}$$

which allows us to solve for the T polynomial, completing the MRC controller design. There are additional causality conditions in the use of MRC methods that are outside the scope of this thesis work, but these conditions can be found in the adaptive control books referenced in the appendix.

To summarize the terms for future reference:

u: The control input into the plant

u_c: The control input into the controller

B: The numerator of the plant

B+: The factors of B that are to be cancelled to

B_m: The *desired* numerator of the plant

A: The denominator of the plant

A_m: The *desired* denominator of the plant

R: The denominator of the feedforward and feedback transfer functions used in the control

R_1: The portion of R that does not factor B^+

S: The numerator of the feedback transfer function used in the control

T: The numerator of the feedforward transfer function used in the control

4.2.3 Examples of Using MRC on SISO Systems

Model reference controller design is best explained by using examples, and naturally we begin with a SISO system first. As a first approach, we consider the "drive-by-wire" controller where only the front wheels are used for control input. Because of the obvious safety problems associated with this, this method is not implemented, but serves as an example of implementation of MRC methods.

4.2.3.1 MRC for a First Order SISO System

As an example, we will transform the system, $\frac{Y}{U} = \frac{10}{s+5}$ into $\frac{Y}{U} = \frac{2}{s+1}$.

The second transfer function was chosen to match the DC gain of the open-loop plant dynamics. We can immediately note that B = 10, A = s+5, B_m = 2, and A_m = s+1. If we choose the degree of B^+ to be zero, all of the degree inequality requirements are met. If we assume that no observer is desired, then we can choose A_0 to be 1, and B^+ to be 1. Substituting the known values into the Diophantine equation, we obtain:

$$(s+5)\cdot R + 10\cdot S = (s+1) \tag{4.28}$$

If we assume that R and S are simple constants, then there are a sufficient number of equations to solve for R and S. Again, these equations are obtained by equating the coefficients of the each polynomial power of s. Solving these, we obtain S = -0.4 and R = 1. To solve for T, we note that we can solve for B^- from the equation $B = B^-B^+$. We then find B^- to be 10. We then solve for B_m' to be 0.2. Solving for T gives T = 0.2, which completes the MRC design.

To verify the design, we can simply solve for the transfer function of the resulting block diagram, noting that u = T/R*uc – S/R*y. The result confirms the design.

4.2.3.2 MRC for a Particular Second Order SISO System

As an example, we will transform the system, $\frac{Y}{U} = \frac{10\cdot(s+5)}{s^2+s+2}$ into $\frac{Y}{U} = \frac{50}{s^2+3\cdot s+2}$.

Again, we can choose the second transfer function to match the DC gain of the open-loop plant dynamics. We note that B = 10s+50, A = s^2 + s + 2, B_m = 50, and A_m = s^2 +3s + 2. We can see that we must choose B^+ to be (s+5) to cancel the zeros.

At this point, a check of the required degree of the observer polynomial reveals A_o to be of order 0. For convenience, we choose A_o to be 1. Once A_o and B^+ are known, we can solve for T. From the equation $B = B^-B^+$, B^- is found to be 10. Solving for B_m' gives $B_m' = 5$, and so T = 5 since $A_o = 1$.

At this point, the Diophantine Equation can be formulated as:

$$\left(s^2+s+2\right)\cdot\left(r_1\cdot s+r_2\right)+(10\cdot s+50)\cdot\left(s_1\cdot s+s_2\right)=(s+5)\cdot\left(s^2+3\cdot s+2\right) \tag{4.29}$$

By assuming that R and S are first order, then there are a sufficient number of equations to solve for R and S. At this point, many solution steps are skipped in obtaining R and S, but it is found that R = s+5, S = 0.2s, and T = 5. To verify the design, we can plot the response of the system to ensure that tracking is achieved:

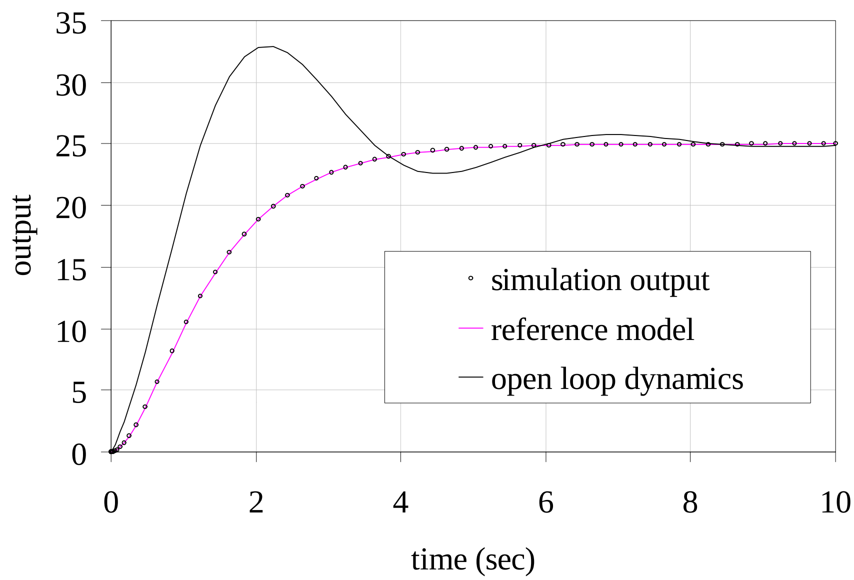

Figure 4.2: The response of the second order MRC design.

4.2.3.3 MRC for the General Second Order SISO Yaw Rate System

The yaw rate dynamics can be represented in a general form as

$$\frac{B}{A}=\frac{b_0}{s^2+a_1\cdot s+a_0} \tag{4.30}$$

If the desired dynamics are represented as:

$$\frac{B_m}{A_m}=\frac{b_{m0}}{s^2+a_{m1}\cdot s+a_{m0}} \tag{4.31}$$

Then the order of the observer that must be used is of minimum 1st order. If the observer is represented as

$$A_o=s+v_0 \tag{4.32}$$

and R, S, and T are represented as:

$$R = s + r_0$$
$$S = s_1 \cdot s + s_0 \qquad (4.33)$$
$$T = t_1 \cdot s + t_0$$

Then each coefficient of R, S, and T can be solved for to be:

$$r_0 = \frac{(v_1 \cdot a_{m1} + v_0 \cdot a_{m2} - r_1 \cdot a_1)}{a_2} \qquad (4.34)$$

$$s_0 = \frac{v_0 \cdot a_{m0} - r_0 \cdot a_0}{b_0} \qquad (4.35)$$

$$s_1 = \frac{(v_1 \cdot a_{m0} + v_0 \cdot a_{m1}) - (r_1 \cdot a_0 + a_1 \cdot r_0)}{b_0} \qquad (4.36)$$

$$t_0 = \frac{b_{m0} \cdot v_0}{b_0} \qquad (4.37)$$

$$t_1 = \frac{b_{m0} \cdot v_1}{b_0} \qquad (4.38)$$

A MATLAB script was developed that solves this specific case of MRC design and all general cases of MRC design by forming the Sylvester matrix and performing the appropriate matrix manipulations to solve for the R, S, and T polynomials.

4.2.4 Sensitivity Functions of MRC Controllers

The purpose of examining sensitivity functions is to determine how the system will perform given a particular error input. To do this, consider the following diagram, which is the MRC system with two error inputs: a disturbance on the input and a disturbance on the output:

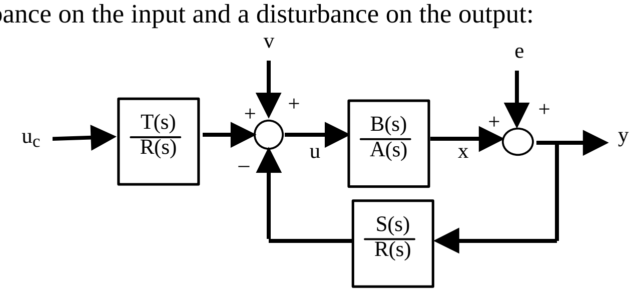

Figure 4.3: The block diagram of the closed-loop system including disturbance terms.

The plant dynamics, output, and control law are given by:

$$Ax(s) = B(u(s) + v(s)) \qquad (4.39)$$

$$y = x + e \qquad (4.40)$$

$$Ru(t) = Tu_c(t) - Sy(t) \qquad (4.41)$$

We can write:

$$Ay = B(u + \nu) + Ae \tag{4.42}$$

Substituting in the control and solving for y gives:

$$\Rightarrow y = \frac{BT}{AR + BS} u_c + \frac{BR}{AR + BS} \nu + \frac{AR}{AR + BS} e \tag{4.43}$$

which, when substituted in equation above, gives a solution for x:

$$\Rightarrow x = \frac{BT}{AR + BS} u_c + \frac{BR}{AR + BS} \nu - \frac{BS}{AR + BS} e \tag{4.44}$$

We can finally solve for the control input, u:

$$\Rightarrow u = \frac{AT}{AR + BS} u_c - \frac{BS}{AR + BS} \nu - \frac{AS}{AR + BS} e \tag{4.45}$$

Note that these equations are presented in (Astrom and Wittenmark 1997). If we examine the above sensitivity functions in detail, we see that portions of the above sensitivity functions are used in the two-input MRC method previously developed.

4.3 Alternative Representation of MRC Loops

The choice of the S and R polynomials is not unique. In fact, the Youla-Kucera Parameterization Theorem states that if $S^0(s)/R^0(s)$ is a stabilizing controller to the system B(s)/A(s), then all rational stabilizing controllers are given by:

$$\frac{S(z)}{R(z)} = \frac{S^o(z) + Q(z)A(z)}{R^o(z) - Q(z)B(z)} \tag{4.46}$$

where Q(s) is stable. Note that the above proof is presented in the z-domain. The details of this proof are presented in Astrom and Wittenmark's, Computer Controlled Systems (Astrom and Wittenmark 1997).

An alternative representation of a Model Reference Controller is also derived where the complete separation between response to command signals and disturbances is obtained. The model structure remains a 2 DOF controller, but robustness properties can be examined in a much more intuitive manner. The structure is as follows:

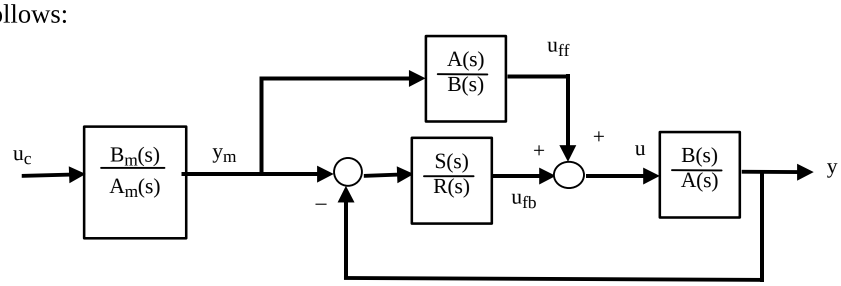

Figure 4.4: The block diagram of the closed-loop system including disturbance terms.

Note that the feedforward term T(s)/R(s) is no longer explicitly in the design, but that the above design is as a consequence not causal. This model structure is commonly seen in the literature with a filter on the feedforward term to guarantee causality.

4.4 *Stability of MRC Methods*

We can see from the above closed-loop diagram that system stability is primarily dependent on the S/R terms. A formal statement of system stability has been obtained by researchers regarding closed-loop stability of the above form. Given a controller in the form:

$$u = \frac{T}{R} \cdot u_c - \frac{S}{R} \cdot y \tag{4.47}$$

It has been proven that the system, if linear, is stable if the difference between the true plant, $\frac{B_0(s)}{A_0(s)}$, and the modeled plant, $\frac{B(s)}{A(s)}$ is bounded by the inequality (Lee 1997):

$$\left|\frac{B(s)}{A(s)} - \frac{B_0(s)}{A_0(s)}\right| \leq \left|\frac{S(s)}{R(s)}\right|^{-1} \tag{4.48}$$

where |a| denotes the modulus of the complex number a. This represents a design tradeoff between closed-loop bandwidth, which is large if S/R is large, and modeling error. If the closed-loop bandwidth is too high, the system may become unstable if the modeling error is too large. If the bandwidth requirement is reduced (by reducing the gain of the system), then the requirement on model accuracy can be relaxed at the sacrifice of tracking performance. This tradeoff historically has been best approached using a robust controller design method (Sun, Olbrot, and Polis 1994; Tamaki et al. 1986) to design the observer polynomial.

4.5 *MRC on Systems with Known Disturbances*

For a vehicle control system, there is always a chance that a controller will fail; therefore, the controller design itself should consider this possibility. If a single input, such as the front wheels, is used for both the controller and for the driver input, any failure in the controller may prevent the driver from being able to steer the vehicle. For this reason, it is more desirable that the driver and controller use separate inputs. To do this, it is possible that a controller steer the rear wheels, while the driver steers the front wheels. Thus, the driver would always have limp-home capability if the controller or sensors fail.

With the driver controlling the front wheels of the vehicle, the vehicle response can be modeled as MRC with a known disturbance. We attempt in this section to obtain a theoretical method to "cancel" the driver input using the rear wheels to obtain the desired reference model. The following diagram pictorially represents the goal of this section:

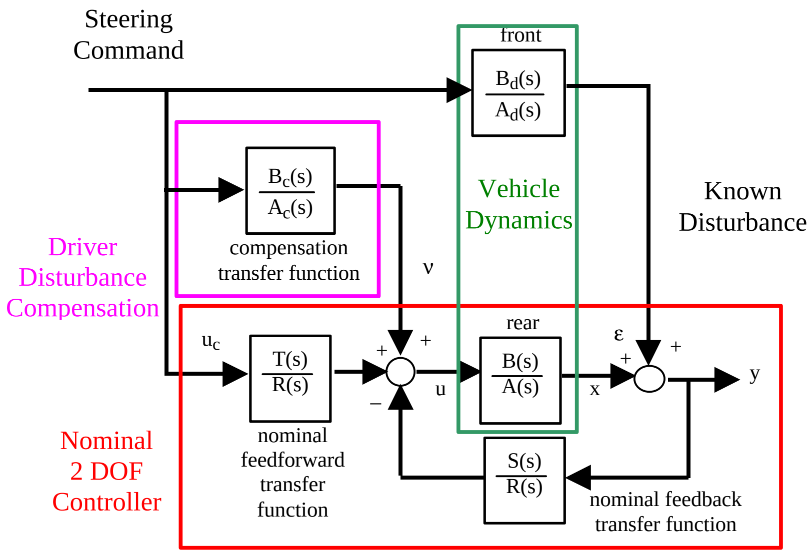

Figure 4.5: The block diagram of the closed-loop system including the driver as a disturbance.

Assume that the output disturbance, ε, can be separated into two parts: known dynamics and unknown disturbances. Assuming a rational, causal transfer function representation for the disturbance gives:

$$\varepsilon(s) = \underbrace{\frac{B_d(s)}{A_d(s)}}_{\substack{\text{known}\\ \text{dynamics}}} \delta_f(s) + \underbrace{\varepsilon'(s)}_{\substack{\text{unknown}\\ \text{disturbance}}} \tag{4.49}$$

The term, δ_f, is defined as the disturbance generator for the known disturbance and in this case is the driver's front steering input. The unknown disturbance term, ε′, contains both unmodeled dynamics of the system as well as external disturbances (e.g. wind) that are not known. Substituting this disturbance into e above gives:

$$\Rightarrow y = \frac{BT}{AR+BS}u_c + \frac{BR}{AR+BS}v + \frac{AR}{AR+BS}\varepsilon + \frac{B_d}{A_d}\frac{AR}{AR+BS}\delta_f \tag{4.50}$$

$$\Rightarrow u = \frac{AT}{AR+BS}u_c - \frac{BS}{AR+BS}v - \frac{AS}{AR+BS}\varepsilon - \frac{B_d}{A_d}\frac{AS}{AR+BS}\delta_f \tag{4.51}$$

For the moment, ignore the output error, ε, in the equation for y above. We wish to cancel the effect of the disturbance (driver input) by use of a control at the input of the plant. To do this, an input disturbance is used to reject the output disturbance. Clearly the choice of v to cancel the disturbance is:

$$v = -\frac{B_d}{A_d}\frac{A}{B}\delta_f \tag{4.52}$$

The controller becomes (note that u_c is the driver front steering input, δ_f):

$$
\begin{aligned}
u &= \frac{AT}{AR+BS}\delta_f + \left(\frac{B_d}{A_d}\frac{A}{B}\right)\frac{BS}{AR+BS}\delta_f - \frac{AS}{AR+BS}\varepsilon - \frac{B_d}{A_d}\frac{AS}{AR+BS}\delta_f \\
&= \frac{AT}{AR+BS}\delta_f - \frac{AS}{AR+BS}\varepsilon
\end{aligned}
\tag{4.53}
$$

We see that we recover the traditional form of the MRC. We now want to formally include the disturbance term into the controller be defining a new control effort, u':

$$
\begin{aligned}
u' &= u + v_{artificial} \\
&= \frac{AT}{AR+BS}\delta_f - \frac{AS}{AR+BS}\varepsilon - \frac{B_d}{A_d}\frac{AS}{AR+BS}\delta_f \\
&= \underbrace{\frac{A_d AT - B_d AS}{A_d(AR+BS)}\delta_f}_{\text{feedforward}} - \underbrace{\frac{AS}{AR+BS}}_{\text{feedback}}\varepsilon
\end{aligned}
\tag{4.54}
$$

This control approach was presented by Brennan and Alleyne this spring (Brennan and Alleyne 1999). This control is somewhat intuitive if we rewrite the output equation ignoring the disturbances and assuming there is no compensation for the front steer input:

$$
y = \frac{\frac{B}{A}\frac{T}{R}}{1+\frac{B}{A}\frac{S}{R}}\delta_f + \frac{B_d}{A_d}\frac{A}{B}\frac{\frac{B}{A}}{1+\frac{B}{A}\frac{S}{R}}\delta_f \tag{4.55}
$$

it is clear that the MRC closed loop structure is kept, but that a feed-forward term has been added. It is therefore natural to use feedforward cancellation to correct the equation and regain the original model structure.

4.6 Simulation Study of Disturbance-Based MRC

To confirm that the above methodology would work on the vehicle, a simulation study was conducted. The plant model used the bicycle model using the measured parameters obtained for the Uberquad, with velocity U = 3.0 m/s, m = 6.52 kg, Iz = 0.18 kg-m^2, a = 0.155 m, b = 0.235 m, Caf = 48, and Car = 32.5. The actuator dynamics were assumed to be second order at 5 Hz with a damping ratio of 0.7 and a gain of 1/1.3 (the gain is due to steering linkage kinematics). To simulate the noise inherent in the yaw-rate measurement, a white-noise signal is added to the yaw-rate output of the state-space model.

To generate a driving command, a PID controller was used to track a square wave reference lateral position. A square wave of amplitude 0.15 meters was fed into a PID lateral position controller whose gains were as follows: P = 0.1 rad/m, I = 0.015 rad/m-sec, and D = 0.07 rad-sec/m. The integral term was limited to +/- 1.5 radians maximum output, and the derivative was obtained by passing the derivative through a first-order filter with a pole at s = 1000 rad/sec. This controller was thus generating a steering command to track a square wave in lateral position.

The steering command was then passed into the a disturbance-based MRC controller, which generated the rear steering command. The following diagram shows the simulation setup:

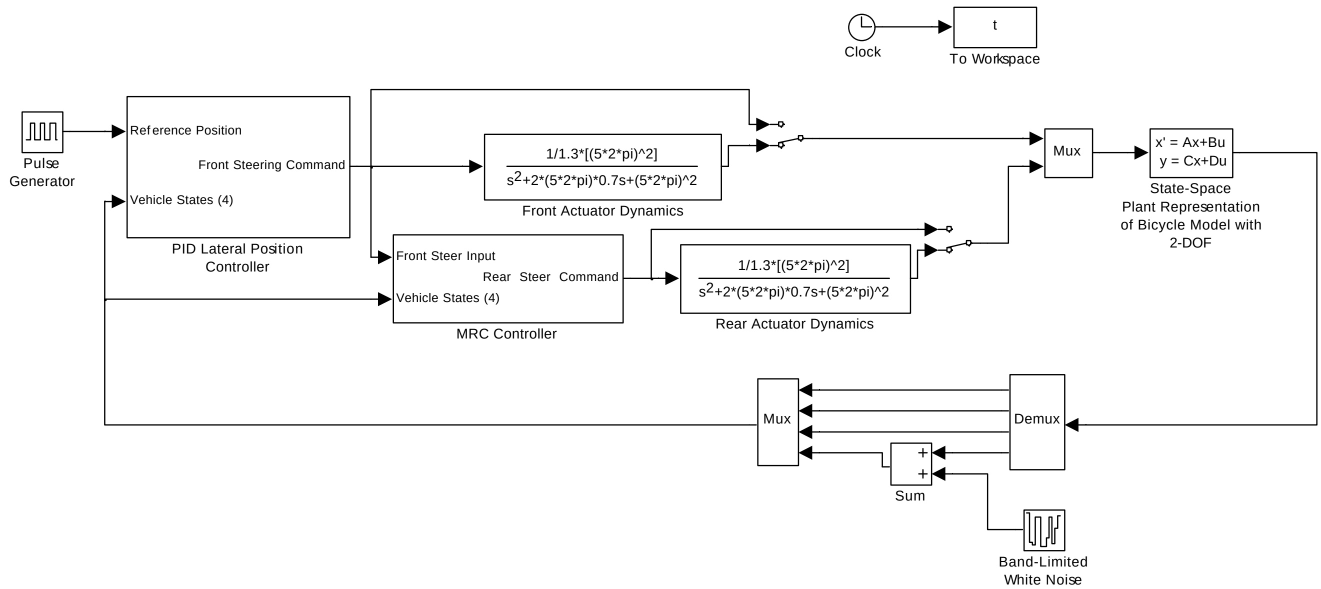

Figure 4.6: The simulation setup to test the disturbance based MRC.

The MRC setup is as follows:

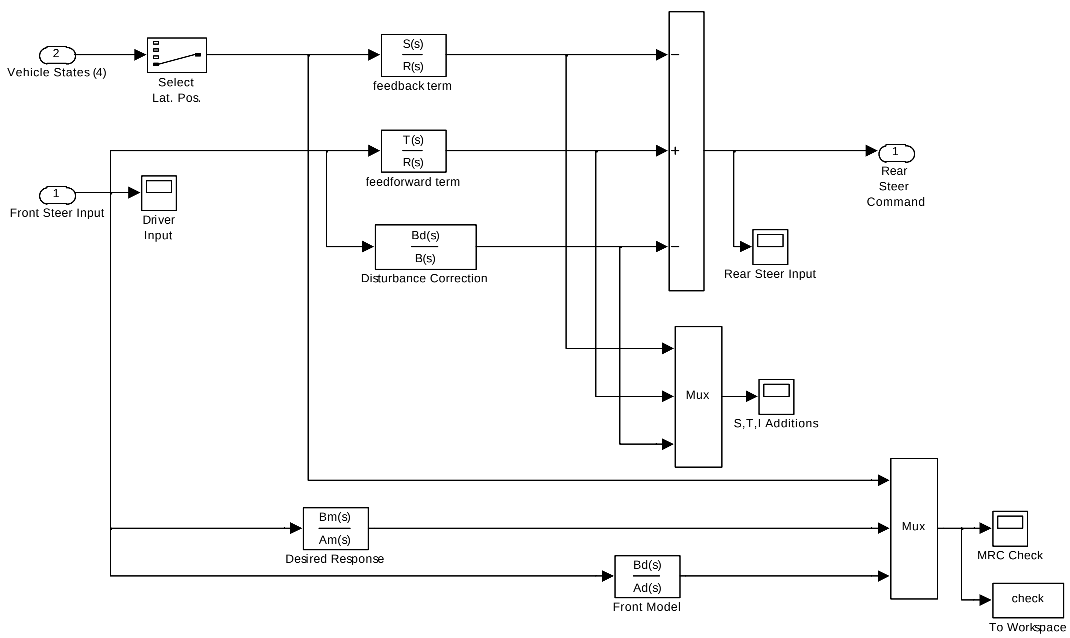

Figure 4.7: The MRC setup to test the disturbance based MRC.

A reference model was chosen to have a higher DC gain than the previous system, faster pole locations, and a cancelled zero. Using the above bicycle model values, the following polynomials were obtained. Note that an observer must be used, and was chosen to be much faster than the bicycle model dynamics:

$$\frac{B_d(s)}{A_d(s)} = \frac{\dot{\psi}(s)}{\delta_{f,c}(s)} = 0.769 \cdot \underbrace{\frac{5 \cdot 2\pi}{s^2 + 2 \cdot 0.7 \cdot (5 \cdot 2\pi) \cdot s + (5 \cdot 2\pi)^2}}_{\substack{\text{assumed}\\\text{actuator}\\\text{dynamics}}} \cdot \underbrace{\frac{81.3 \cdot s + 679.9}{s^2 + 18.97 \cdot s + 90.54}}_{\substack{\text{bicycle}\\\text{mod el}\\\text{dynamics}}} \tag{4.56}$$

$$\frac{B(s)}{A(s)} = \frac{\dot{\psi}(s)}{\delta_{r,c}(s)} = 0.769 \cdot \underbrace{\frac{5 \cdot 2\pi}{s^2 + 2 \cdot 0.7 \cdot (5 \cdot 2\pi) \cdot s + (5 \cdot 2\pi)^2}}_{\substack{\text{assumed}\\\text{actuator}\\\text{dynamics}}} \cdot \underbrace{\frac{-83.47 \cdot s - 679.9}{s^2 + 18.97 \cdot s + 90.54}}_{\substack{\text{bicycle}\\\text{mod el}\\\text{dynamics}}} \tag{4.57}$$

$$\frac{B_m(s)}{A_m(s)} = \frac{\dot{\psi}_{desired}(s)}{\delta_{f,c}(s)} = \underbrace{\frac{5 \cdot 2\pi}{s^2 + 2 \cdot 0.7 \cdot (5 \cdot 2\pi) \cdot s + (5 \cdot 2\pi)^2}}_{\substack{\text{front}\\\text{actuator}\\\text{dynamics}}} \cdot \underbrace{1.5 \cdot 5.776 \cdot \frac{15^2}{s^2 + 2 \cdot 15 \cdot s + 15^2}}_{\substack{\text{mod ified}\\\text{bicycle}\\\text{dynamics}}} \tag{4.58}$$

$$\text{Observer}(s) = s^2 + 2 \cdot 50 \cdot s + 50 \cdot 50 \tag{4.59}$$

$$R(s) = s^3 + 119.2 \cdot s^2 + 4433 \cdot s + 28737 \tag{4.60}$$

$$S(s) = -0.323 \cdot s^3 - 18.07 \cdot s^2 - 488.2 \cdot s - 3785 \tag{4.61}$$

$$T(s) = -30.36 \cdot s^2 - 3036 \cdot s - 75906 \tag{4.62}$$

The resulting vehicle responses with the above controller is as follows. Clear tracking of the desired yaw rate is seen.

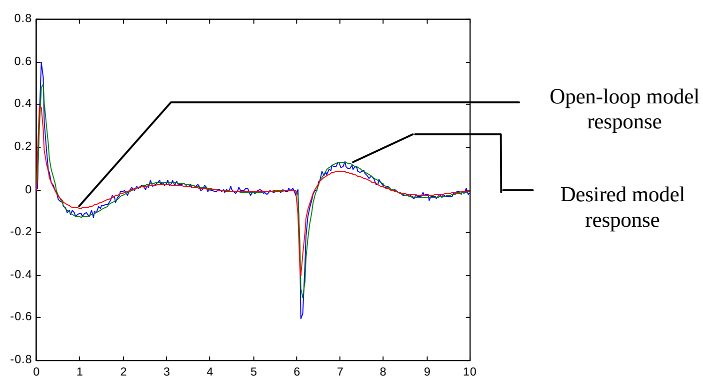

Figure 4.8: The simulation results of the disturbance based MRC with actuator dynamics included in the design.

4.7 History of MRC Methods on Vehicle Control

Previous researchers at this university (Mark DePoorter) have used the MRC method to control the lateral position and yaw angle of a vehicle. However yaw-rate control was first achieved at the Illinois Roadway Simulator during this thesis work. Other researchers have had more success in their implementation of MRC methods for yaw rate control. Specifically, Lee et al at Cal Tech indirectly derives the MRC method (Lee 1997) and uses it for vehicle control. To obtain a model reference controller, they attempt inversion of the plant dynamics using a feedforward term using the feedforward inversion and filter technique described earlier. The authors note that this is only realizable if the relative order of the reference model is larger than that of the plant. They continue their development to show that for non-minimum phase systems, some zero cancellation is required. This is similar to the more formal requirement stated earlier regarding the factorization of the zeros polynomial "B". To examine the controller performance, a cost function is developed and used to evaluate the system.

At Michelin Americas, a Model Reference Adaptive Controller was developed and tested in simulation (Post et al. 1997). The adaptation was used to identify the plant model online. The simulation plant consisted of an ADAMs model with over 200 DOF (however, the authors do not specify if any of these DOF were tire/actuator dynamics).

5 Implementation of Controllers Using the IRS

This section outlines the three sets experiments where Model Reference Control was used to control the yaw rate of a vehicle. The first set of experiments was conducted using the 4WS4WD vehicle at 1.2 m/s. In previous vehicle studies using the IRS, the MRC technique was applied to a vehicle traveling at a low speed of 1.2 m/s using the 4WS4WD vehicle with good results (DePoorter 1997b). As a starting point, these conditions were chosen as appropriate testing conditions simply to replicate previous results with the same vehicle. For the reasons discussed in earlier chapters, it was determined that dynamic similitude was not being achieved, and new operating conditions were more appropriate.

The second set of experiments was also conducted on the 4WS4WD vehicle (after many structural modifications) at the speed of 3.0 m/s. The testing velocity was chosen to represent an "average" full-sized vehicle traveling at about 50 mph. This set of experiments is distinctive from the previous experiments because significant efforts were taken to achieve dynamic matching in the bicycle parameters and in actuator dynamics. In addition, the improved arm feedback system discussed earlier was implemented in this set of experiments.

The third and final set of experiments utilized the Uberquad vehicle operating at 3.0 m/s. Because the Uberquad's parameters are different than the 4WS4WD vehicle, the test represents an average full-sized vehicle operating at approximately 35 mph. The novelty in this final set of experiments was that the vehicle has additional steering capability through torque input. In addition, significant effort was taken to not only achieve bandwidth of actuation but also prevent non-linear dynamics from interfering with the bicycle model.

A summary of each set of experiments follows below. Each summary begins with a description of the open-loop dynamics. Because the open-loop dynamics are used to design the closed-loop controller, the level and type of model mismatch during the system identification can be used to interpret the controller performance in the closed-loop system. In addition, the open-loop responses can be used as a gage against which the closed-loop responses can be compared. Each section then details the MRC methods used to control the plant and the resulting closed-loop performance. Finally, alternative control strategies and sensitivity tests conclude each experiment.

Note that nearly every state plot in this chapter is a yaw rate plot. Because the yaw rate is obtained via numerical differentiation of the yaw signal, which is obtained from encoders, the yaw rate on each plot is the "noisy" data. On each yaw rate plot, an additional plot is given that is a smooth response that (hopefully) is dynamically similar to the measured yaw rate. This response is the output of the model used to predict yaw rate given the same input as the plant. It is important to understand that this "prediction" model is an artificial simplification of the actual plant dynamics. If both the measured and artificial model agree almost exactly in their dynamic response, then it is likely that the predicted model is close enough to the "true" dynamics of the system that controllers can be designed using the simplified artificial model rather than by trial-and-error. In addition to the measured and predicted responses, a third response is often included in the yaw plots that is larger in amplitude (by design) than the predicted response. This "larger" response is the response of the design model, also known as the reference model. The closed-loop responses should track this response perfectly if the controller worked perfectly, and thus can be thought of as a desired closed-loop yaw rate. In summary, three responses are shown on each yaw rate plot: measured yaw rate, a predicted open-loop yaw rate, and a desired closed-loop yaw rate.

5.1 4WS4WD at Low Speed (1.2 m/s) + Slow Servos

These first low-velocity tests were conducted using two methods of vehicle position feedback discussed earlier: the potentiometer arm and the encoder arm. The resulting performance using each feedback technique is quite different due to the differing quality of feedback. First, the testing with the analog arm is discussed and results are given showing the poor quality of the feedback and how this quality hinders controller performance. Next, a discussion of controller implementation results is given for a MRC design using the encoder arms. The dynamics of the system at low speeds were previously found to be:

$$\frac{\psi(s)}{V_f(s)} = \frac{13480}{s \cdot \left(s^2 + 10.3 \cdot s + 180\right)} \tag{5.1}$$

$$\frac{\psi(s)}{V_f(s)} = \frac{26500}{s \cdot \left(s^2 + 8.50 \cdot s + 310\right)} \tag{5.2}$$

These dynamics will be used hereafter as the plant.

5.1.1 Yaw Rate Feedback with Analog Arm Sensing

The first MRC tests at 1.2 m/s utilized an analog arm. Initially, the DC gain of the desired plant dynamics was chosen to be approximately the same as the open-loop plant, so that the driver input command does not change significantly at steady state. From the above equations, the DC gain for the front is 74.9 and for the rear 85.5 deg/volt. As a median value, 80 deg/volt was chosen as a DC gain for the reference model. The pole locations of the desired plant dynamics were chosen to be the same locations previously used by the previous researcher, Mark DePoorter for his system identification, at s = -5 +/- 3j. These poles correspond to slightly less than critical damping, so that there is a slight amount of overshoot. It was found through driving tests that these poles gave a good “feel” to the system. Combining the DC gain and pole locations, the desired yaw transfer function becomes:

$$\frac{\dot{\psi}_{desired}(s)}{V(s)} = \frac{2720}{\left(s + 5 + 3j\right)\left(s + 5 - 3j\right)} \tag{5.3}$$

$$\frac{\dot{\psi}(s)}{V_f(s)} = \frac{2720}{s^2 + 10 \cdot s + 34} \tag{5.4}$$

The MRC design technique produces R, S, and T matrices:

$$R(s) = s + 51.5 \tag{5.5}$$

$$S(s) = -0.0081 \cdot s - 0.5383 \tag{5.6}$$

$$T(s) = 0.1026 \cdot s + 5.1321 \tag{5.7}$$

A comparison between the open-loop and closed-loop responses is shown below:

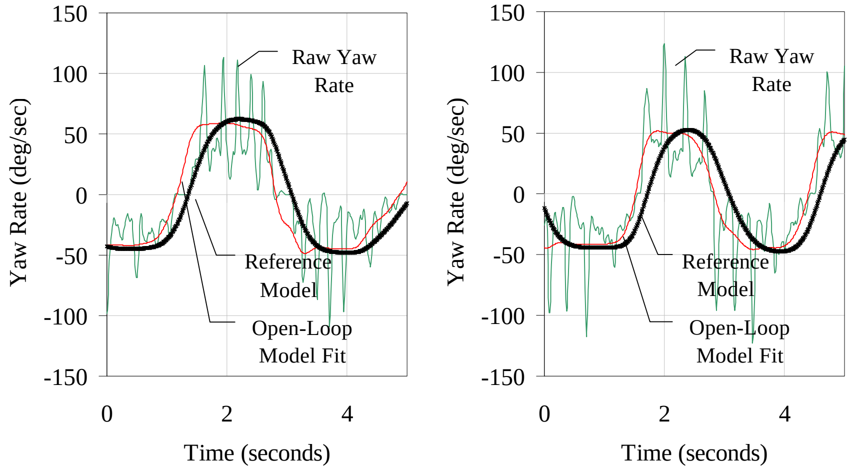

Figure 5.1: The open loop (left) and closed-loop (right) responses of the system.

As seen in the above responses, the amount of noise in the model makes it difficult to distinguish between the predicted model fit yaw rate and the desired model yaw rate. It is even difficult to even determine without prior knowledge which plot represents the closed-loop responses! To obtain a better measured yaw rate, filtering was attempted; however, this introduced a significant phase lag such that the reference model response is indistinguishable from the open-loop model response. It appears that the reference model is too close to the actual model to determine if the controller is working adequately.

The first attempt to implement a model reference controller attempted to control the yaw rate using a MRC design approach and a reference model that was, in retrospect, quite close to the original model. In a second attempt to implement a MRC controller, the reference model was chosen to be significantly different from the original model by increasing the DC gain and moving the pole locations significantly:

$$\frac{\dot{\psi}(s)}{V_f(s)} = \frac{97730}{s^2 + 30 \cdot s + 261} \tag{5.8}$$

The MRC design technique produces R, S, and T matrices:

$$R(s) = s + 71.5 \tag{5.9}$$

$$S(s) = 0.0318 \cdot s - 0.3440 \tag{5.10}$$

$$T(s) = 3.688 \cdot s + 184.4 \tag{5.11}$$

The open-loop and closed-loop responses are shown below:

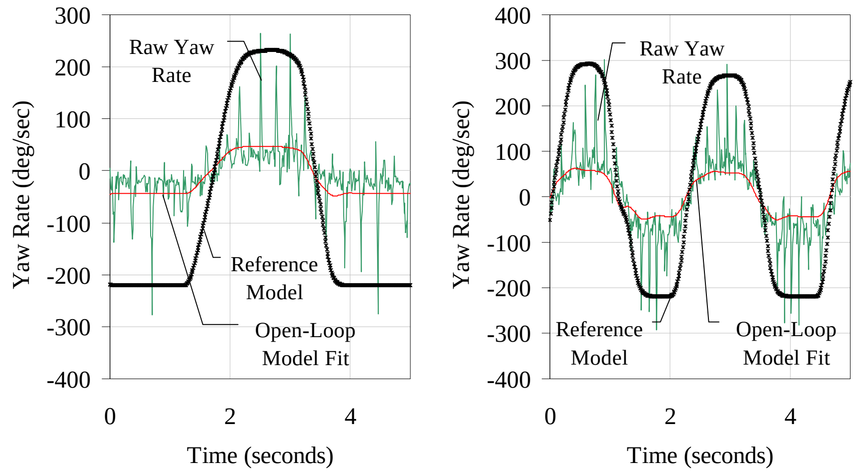

Figure 5.2: The open-loop (left) and closed-loop (right) responses of the system.

As seen in the above responses, again there is a significant amount of noise in the yaw response, but there is a distinct difference between the reference model and the open-loop model responses. Again, a 5 Hz oscillation dominates the yaw rate signal. Comparing the closed and open loop responses, it is clear that the controller is acting to move the yaw rate response closer to the reference model. However, the response is not tracking the desired model (although, the driver noted that the difference between the first design and the second design feels significantly different). Initially, it was expected that the feedback term (S/R) would compensate for this error. If we compare the DC gain of the S/R term for the slow design (= 1.04 E-2) to the fast design (DC gain = 4.81 E-3), it is clear that there is *less* feedback with the faster poles. To have a larger amount of feedback, it appears that either a slower MRC reference model must be selected, or an integrator term must be added to make the response track the reference model. The error seen in the model tracking is likely due to the limitations of the steering actuator. Because the servos used on the vehicle are rate-limited, it is unlikely that they will correctly compensate for a very fast MRC design (where fast refers to pole locations). Regardless of the actuator bandwidth, it is clear that a better feedback signal is needed.

5.1.2 Yaw Rate Feedback with the Encoder Arm

To improve the vehicle yaw-rate feedback, the analog arm was replaced with an arm consisting entirely of encoders. The reference model was again chosen to be:

$$\frac{\dot{\Psi}_{desired}(s)}{V(s)} = \frac{-2720}{(s+5+3j)(s+5-3j)} \tag{5.12}$$

The R, S, and T polynomials again become:

$$R(s) = s + 51.50000 \tag{5.13}$$

$$S(s) = -0.008066038 \cdot s - 0.5383019 \tag{5.14}$$

$$T(s) = -0.1026415 \cdot s - 5.1320755 \tag{5.15}$$

The following figures show the open-loop response of the system using front and rear steering inputs. Overlaid on these plots is the output of the models for front and rear yaw rate response. The yaw rate was filtered using a low-pass differentiator with a cut-off frequency of 70 rad/sec. The yaw angle was filtered using a second order Butterworth filter with a cutoff frequency of 100 Hz. Clearly, the predicted and measured yaw-rate agree.

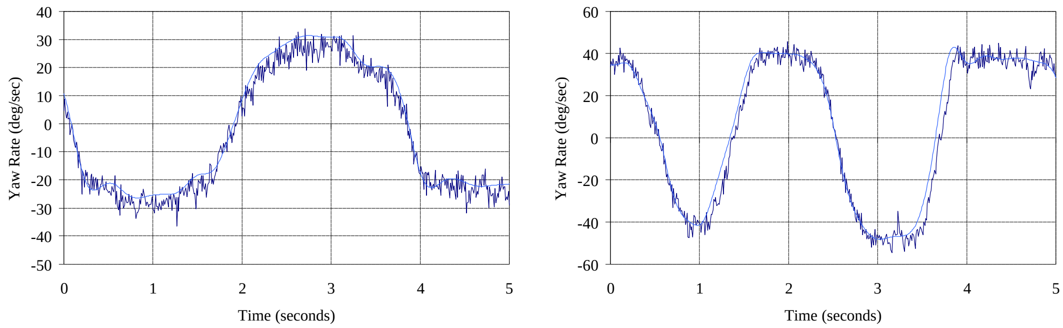

Figure 5. 3: Model fit and yaw rate response in time domain of 4WS4WD vehicle at 1.2 m/s using front (left) and rear (right) steering input.

To compare the performance of the MRC design with existing control strategies for yaw rate control, a P controller was chosen as a metric of comparison. A derivative term is avoided simply because the yaw-rate signal is itself obtained from a derivative. If an additional derivative were taken of this signal, then the noise terms would be quite large. An integral controller is avoided simply because the integration of a small error, such as a calibration error, would cause the car's orientation to be perpetually skewed. The error term that was used for the P controller is the difference between the reference model and measured yaw-rate output. Thus, the P controller is attempting to force model tracking using feedback. The figures below show the vehicle response without a controller, and the vehicle response with a P controller.

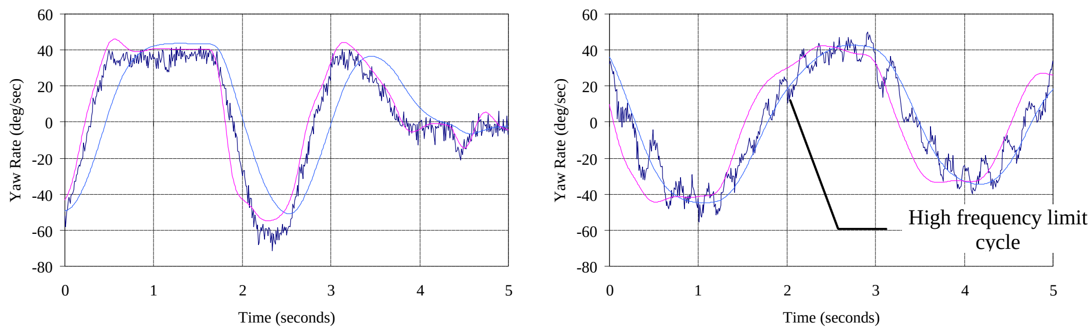

Figure 5.4: The vehicle response with and without the proportional controller, showing a reference model and the open-loop transfer function for front steer.

The P controller obviously improves the model tracking performance, but tracking is only achieved with a high gain. As seen in the above plot, this high gain causes a high frequency yaw oscillation in the vehicle (P gain was 0.03 volts/(deg/sec)).

5.2 4WS4WD at High Speed (3.0 m/s) + Fast Servos

Following the methodology presented at the beginning of the chapter, the open-loop dynamics of the system are examined and compared to the predicted dynamics. The system dynamics for the 4WS4WD system were modeled using two methods: bicycle model with actuator dynamics and bicycle model with no actuator dynamics (only a gain). The following time responses show the time response of the system where no actuator dynamics are included in the system model. The open-loop model without actuator dynamics was previously presented as the following:

$$\frac{\dot{\psi}(s)}{\delta_f(s)} = \frac{42.7 \cdot s + 752}{s^2 + 21 \cdot s + 170.6} \tag{5.16}$$

$$\frac{\dot{\psi}(s)}{\delta_r(s)} = \frac{-131 \cdot s - 752}{s^2 + 21 \cdot s + 170.6} \tag{5.17}$$

$$\frac{\delta_f(s)}{\delta_{f,c}(s)} = 1.99 \tag{5.18}$$

$$\frac{\delta_r(s)}{\delta_{r,c}(s)} = 1.20 \tag{5.19}$$

Resulting in design models of the following:

$$\frac{B_d(s)}{A_d(s)} = \frac{\dot{\psi}(s)}{\delta_{f,c}(s)} = \underbrace{1.99}_{\substack{\text{assumed}\\ \text{actuator}\\ \text{dynamics}}} \cdot \underbrace{\frac{42.7 \cdot s + 752}{s^2 + 21 \cdot s + 170.6}}_{\substack{\text{bicycle}\\ \text{model}\\ \text{dynamics}}} \tag{5.20}$$

$$\frac{B(s)}{A(s)} = \frac{\dot{\psi}(s)}{\delta_{r,c}(s)} = \underbrace{1.20}_{\substack{\text{assumed}\\ \text{actuator}\\ \text{dynamics}}} \cdot \underbrace{\frac{-131 \cdot s - 752}{s^2 + 21 \cdot s + 170.6}}_{\substack{\text{bicycle}\\ \text{model}\\ \text{dynamics}}} \tag{5.21}$$

The responses below show the comparison between the measured yaw rate response and the yaw rate response predicted by the bicycle model when no actuator dynamics are include. The dynamic match shows some modeling errors, with a noticeable and phase and amplitude error in the tracking responses.

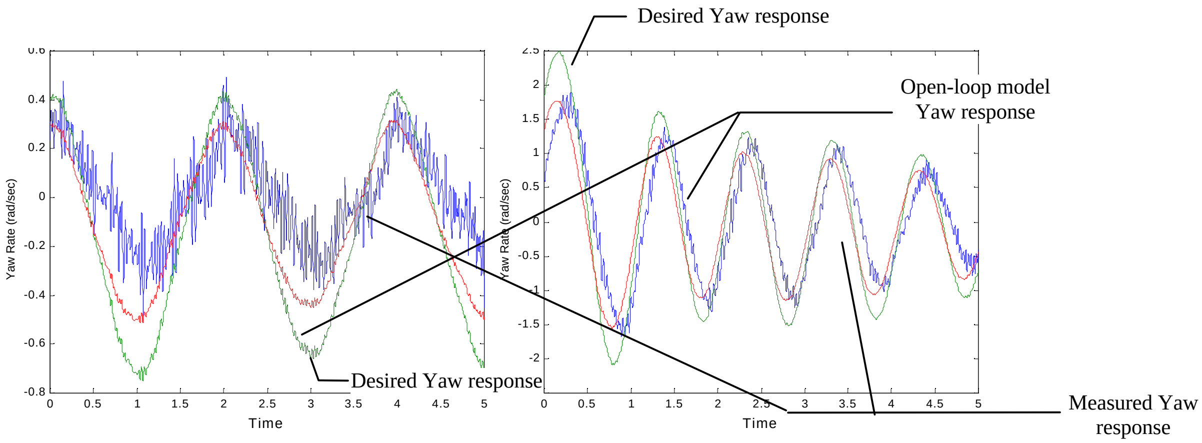

Figure 5.5: The open-loop vehicle response from front steering input without actuator dynamics included in the predicted model.

For a system including actuator dynamics, the above expressions for bicycle model yaw rate remain the same, but the actuator dynamics are no longer represented by a simple gain:

$$\frac{\delta_f(s)}{\delta_{f,c}(s)} = \frac{1.99}{0.000567 \cdot s^2 + 0.0342 \cdot s + 1} \tag{5.22}$$

$$\frac{\delta_r(s)}{\delta_{r,c}(s)} = \frac{1.20}{0.0016 \cdot s^2 + 0.05765 \cdot s + 1} \tag{5.23}$$

Thus, the open-loop dynamics for the model WITH ACTUATOR DYNAMICS become:

$$\frac{B_d(s)}{A_d(s)} = \frac{\dot{\psi}(s)}{\delta_{f,c}(s)} = \underbrace{\frac{1.99}{0.000567 \cdot s^2 + 0.0342 \cdot s + 1}}_{\substack{\text{front}\\\text{actuator}\\\text{dynamics}}} \cdot \underbrace{\frac{42.7 \cdot s + 752}{s^2 + 21 \cdot s + 170.6}}_{\substack{\text{bicycle}\\\text{model}\\\text{dynamics}}} \tag{5.24}$$

$$\frac{B(s)}{A(s)} = \frac{\dot{\psi}(s)}{\delta_{r,c}(s)} = \underbrace{\frac{1.20}{0.0016 \cdot s^2 + .05765 \cdot s + 1}}_{\substack{\text{assumed}\\\text{actuator}\\\text{dynamics}}} \cdot \underbrace{\frac{-131 \cdot s - 752}{s^2 + 21 \cdot s + 170.6}}_{\substack{\text{bicycle}\\\text{model}\\\text{dynamics}}} \tag{5.25}$$

Although the "fit" of each of the two different dynamic representations of the vehicle were presented in Chapter 3, they are presented again here as a means to compare the open-loop and closed-loop performance and to cite possible causes for poor closed-loop model matching. If actuator dynamics are included in the vehicle model, the predicted yaw rate more accurately tracks the measured yaw rate. The improvement in modeling is seen clearly in the responses shown below.

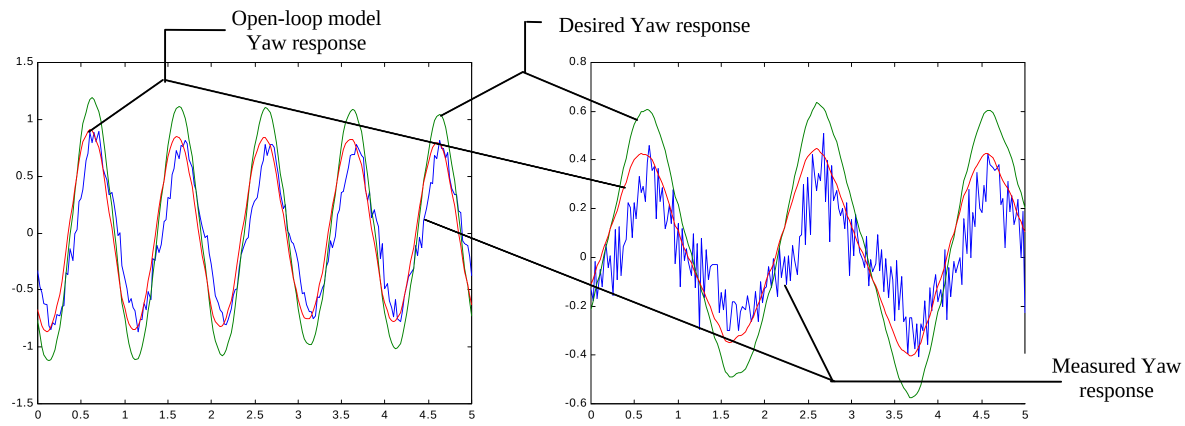

Figure 5.6: The open-loop 4WS4WD response from front steering input with actuator dynamics included.

There remains a small amount of phase lag in the above responses for both the front and rear steering input, regardless of the form of the actuator dynamics. This lag is most likely due to steering linkage nonlinearities present in the 4WS4WD vehicle.

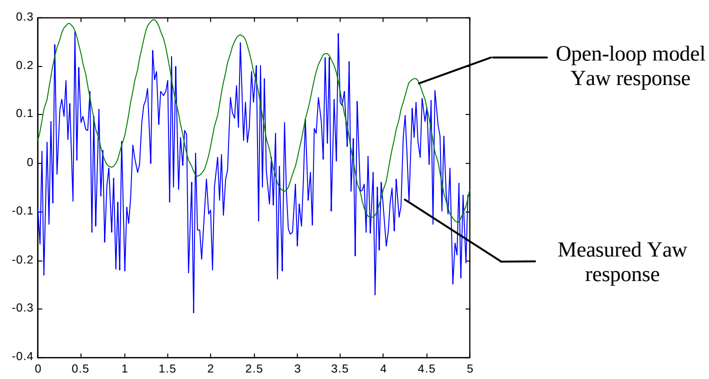

Figure 5.7: The open-loop 4WS4WD response from rear steering input with actuator dynamics included.

A significant deadzone exists by design in the steering actuators (as discussed in the vehicle modeling section of the thesis). This deadzone is most evident in the rear steering linkage, where the measured response has an offset that seems to "drift" up and down (as seen in the above figure). These modeling errors propagate to some extent to the performance of the closed-loop system. Naturally, feedback will (hopefully) tend to account for these modeling errors and unknown disturbances. However this disturbance-MRC control approach, using both a feedforward term and an inversion term, may be more sensitive to modeling error than a purely feedback-based system.

It is important to point out that the improved prediction of the yaw rate by the vehicle model with actuator dynamics was NOT obtained by simply adding more poles to the system to obtain a better fit. Clearly, one can arbitrarily add dynamics to the system to obtain a higher-order representation of the system, but this does not address the physical source for the dynamics. In previous sections, the dynamics of the actuator were identified independent of the vehicle, and were found to be the actuator dynamics presented above. Thus, these dynamics are not added in an arbitrary fashion.

The closed-loop system responses are shown in the figures below, and show a definite tracking of the desired model response. The reference model was chosen to increase the DC gain of the system by a factor of 1.5, move the zero farther into the LHP, and place the poles such that the damping is critical with the same natural frequency of the original system. Two sets of controller responses are given, and they differ in the type of controller. The controller depends on the open-loop model used to design the R,S, and T polynomials. For the open-loop model with no actuator dynamics, the controller polynomials are:

$$\frac{B_m(s)}{A_m(s)} = \frac{\dot{\psi}_{desired}(s)}{\delta_{f,c}(s)} = \underbrace{1.99}_{\substack{\text{front}\\\text{actuator}\\\text{dynamics}}} \cdot \underbrace{1.5 \cdot 752 \cdot \frac{1/20 \cdot s + 1}{s^2 + 26.12 \cdot s + 170.6}}_{\substack{\text{modified}\\\text{bicycle}\\\text{model}\\\text{dynamics}}} \tag{5.26}$$

$$R(s) = s + 5.74 \tag{5.27}$$

$$S(s) = -0.0325 \cdot s \tag{5.28}$$

$$T(s) = -0.528 \cdot s - 10.56 \tag{5.29}$$

For the open-loop model where actuator dynamics are included, the controller requires an observer. The control polynomials are:

$$\frac{B_m(s)}{A_m(s)} = \frac{\dot{\psi}_{desired}(s)}{\delta_{f,c}(s)} = \underbrace{\frac{1.99}{0.000567 \cdot s^2 + 0.0342 \cdot s + 1}}_{\substack{\text{front}\\\text{actuator}\\\text{dynamics}}} \cdot \underbrace{1.5 \cdot 752 \cdot \frac{1/20 \cdot s + 1}{s^2 + 26.12 \cdot s + 170.6}}_{\substack{\text{modified}\\\text{bicycle}\\\text{model}\\\text{dynamics}}} \tag{5.30}$$

$$\text{Observer}(s) = \frac{1}{40^2} \cdot s^2 + \frac{2 \cdot 0.707}{40} \cdot s + 1 \tag{5.31}$$

$$R(s) = 0.391 \cdot s^3 + 35.9 \cdot s^2 + 1580 \cdot s + 7958 \tag{5.32}$$

$$S(s) = -0.152 \cdot s^3 - 7.30 \cdot s^2 - 118 \cdot s - 409 \tag{5.33}$$

$$T(s) = -0.7862 \cdot s^3 - 60.19 \cdot s^2 - 2147 \cdot s - 25159 \tag{5.34}$$

The closed-loop performance of each of the above controllers can be seen in the time-domain yaw-rate plots given below. Note that two graphs are given for EACH controller to show controller consistency (and inconsistencies) under different steering commands.

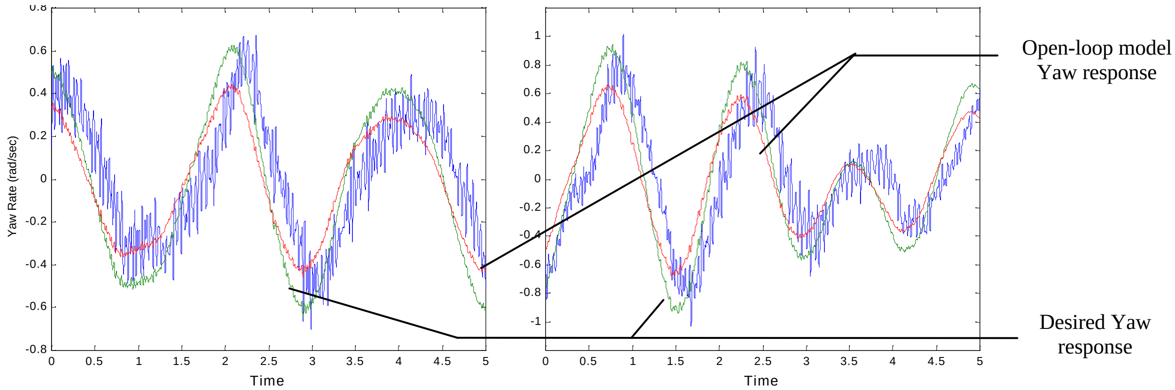

Figure 5.8: The closed-loop 4WS4WD response using disturbance-MRC controller based on a bicycle model with no actuator dynamics.

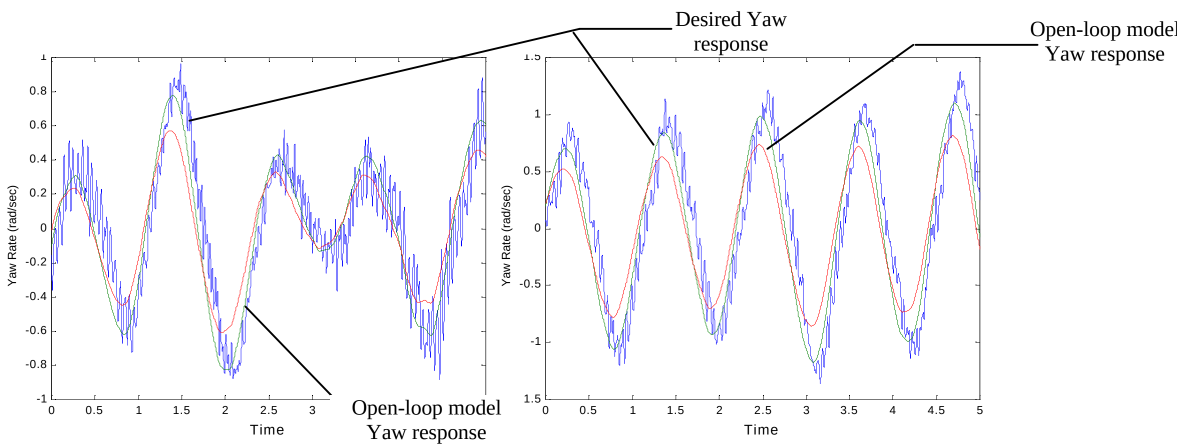

Figure 5.9: The closed-loop 4WS4WD response using disturbance-MRC controller based on a bicycle model with actuator dynamics included.

Clearly, the controller based on the plant with actuator dynamics performs much better than that of the controller without actuator dynamics. If the actuator dynamics are ignored, the controller assumes that the steer command is instantly sent to the wheels, which in fact is not happening. The actuator requires a certain rise time to reach a setpoint. As a result, the controller ignoring this required rise time will overpredict the responsiveness of the vehicle. The measured yaw-rate will thus lag behind the predicted yaw rate, which is precisely what is seen in the controller response for the controller without actuator dynamics above. Clearly, ignoring actuator dynamics can have a severe impact on the closed-loop vehicle performance, so hereafter the discussion will focus on the controller design where actuator dynamics are included.

The above closed-loop responses for the controller that includes actuator dynamics still shows some tracking error, especially where the derivative of the yaw rate is zero (i.e. near the peaks and troughs of the response). Because these areas correspond to where the steering wheels are changing direction, it is likely that this error is due either to the rate-limit non-linearity or the dead-zone non-linearity. If we examine the open-loop responses previously presented, it is clear that a similar model-mismatch is seen in the open-loop responses. If these non-linearities are the source of the tracking error, than it is unlikely that the performance will be improved significantly further with linear controllers.

As demostrated earlier in the thesis, the bicycle model is very sensitive to velocity. As a consequence, the vehicle controller should also be sensitive to velocity. To determine how sensitive the controller was to velocity, controller responses were obtained at 2.0 m/s and 3.5 m/s. The results of these tests are shown below.

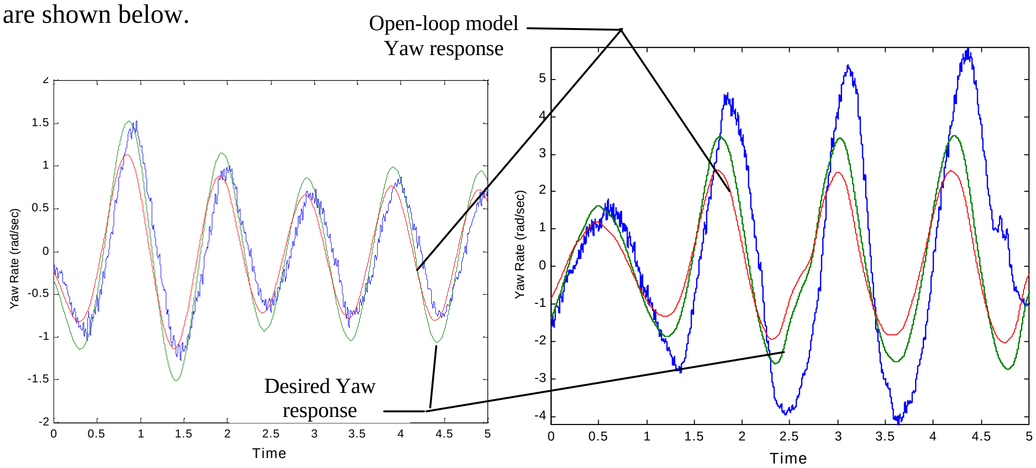

Figure 5.10: The closed-loop 4WS4WD response using disturbance-MRC controller based on a bicycle model with actuator dynamics (identified at 3.0 m/s) tested at 2.0 m/s (left) and 3.5 m/s (right).

At lower speeds, the bicycle model predicts that the poles of the vehicle dynamics are faster and more damped, and at higher speed the poles are slower and less damped. Thus, a controller based on the pole locations at 3.0 m/s will under-predict the vehicle responsiveness at 3.0 m/s. Thus, the vehicle will be "easier" to turn at lower speeds, and more difficult to turn at higher speeds. This is observed in the above plots: at low speeds, the car's yaw rate changes at much lower steering inputs resulting in "undershooting" of the desired response. At high speeds, the car's yaw rate changes much more slowly than expected by the controller, resulting in large "overshooting" of the desired response.

To compare the MRC method to other controllers currently in use commercially, the above controller with actuator dynamics is compared to a proportional controller. The MRC and proportional controllers can be chosen to have arbitrary feedback gains, therefore for comparison purposes the feedback gains of both systems were chosen to be the same. Thus, the proportional controller gain was selected to be the DC gain of the S/R term (the feedback term) in the MRC design: -0.05138 volts/m. The resulting P-controller responses are given below:

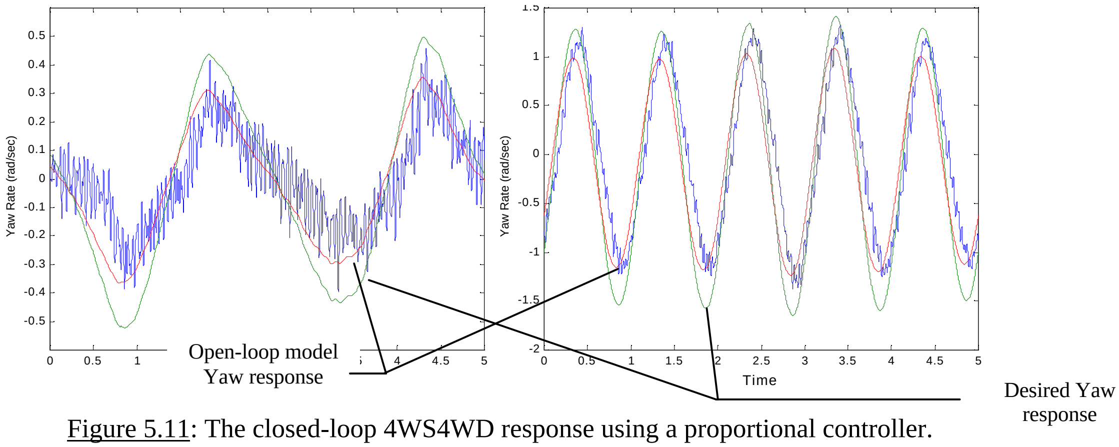

Figure 5.11: The closed-loop 4WS4WD response using a proportional controller.

The proportional controller is seen to exhibit very poor tracking performance. Better performance could be achieved by increasing the gain, but the same could be said regarding the MRC approach. One problem with increasing the gain is that potential instability could develop with large changes in the plant model. A high-gain controller would not be advisable given the previous discussion regarding how the model may change with vehicle speed.

An interesting result of one of the experiments was the production of stable limit cycles which is an indication of plant non-linearities. The following test was conducted where bicycle model with actuator dynamics were used in the MRC controller design. This MRC controller was used in series with a position regulating controller. A constant lateral position was fed into a PID lateral position controller (in order to regulate the car to zero), and thus this PID controller produced a steering command. This steering command was then is fed into the MRC controller as a driver signal. The following stable limit cycle begins:

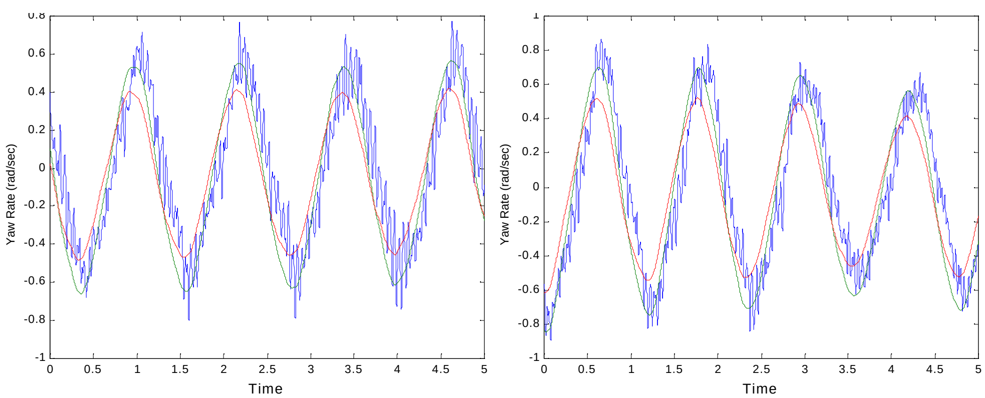

Figure 5.12: The stable limit cycle observed when the MRC controller is used in series with a lateral position-regulating PID controller.

Limit cycles occur only in systems with non-linearities. This suggests that the 4WS4WD vehicle possesses a non-linearity with enough dynamic influence on the closed loop performance to perpetuate the above oscillation. With this in mind, careful attention was paid to the design and construction of the Uberquad vehicle to prevent any deadzones or rate limiting effects. The results of this effort will clearly be seen in the closed-loop performance of this newer vehicle.

5.3 Uberquad at High Speed (3.0 m/s) + DC Motors

The third and final experiment presented in this experiment examined the closed-loop performance of the Uberquad vehicle when a disturbance-based MRC controller is used. As discussed in Chapter 3, the Uberquad has three methods of steering the vehicle: front wheel steering (like a normal vehicle), rear wheel steering, and differential torque steering.

In this thesis, the two front wheels are used to apply the differential torque between the front two wheels. Again, several different combinations of wheels can be used to produce differential torque steering. The merits and advantages of each could easily be investigated; but are beyond the limited scope of this master's thesis. Future work on this area will surely follow shortly after this thesis is completed.

Open-loop vehicle responses are presented in Chapter 3 for the Uberquad, but for comparison an open-loop, front-steering-only response is included below:

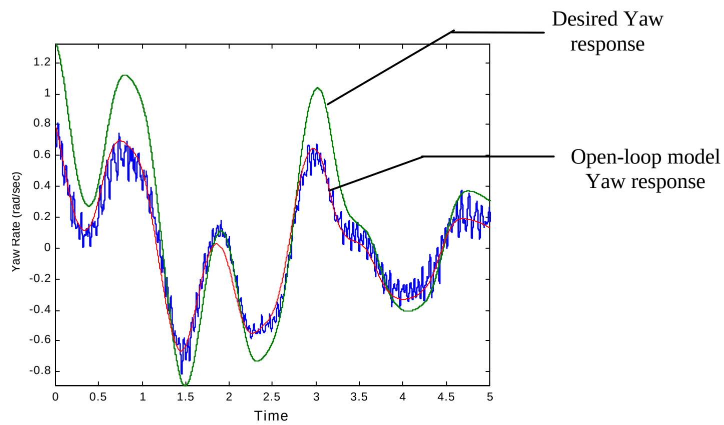

Figure 5.13: The open-loop vehicle response for the Uberquad vehicle using only front steering input.

Before implementing any controller, we observe that the open-loop fit for the Uberquad vehicle is much more "consistent" than that for the 4WS4WD vehicle. Very little error is observed between the open-loop predicted dynamics and the measured dynamics; thus, we expect the controller designed using this open-loop model to perform quite well.

Two controllers are designed for the Uberquad. The first is an MRC controller where the vehicle is made to act like a desired model where the driver had control of the front wheels, and the rear wheels are steered to provide control input. The controller is designed using the disturbance-MRC method described in Chapter 4, where the front steering is the disturbance, and the rear wheel steering is used to track the reference model.

The second controller described in this thesis for the Uberquad also attempts to force the vehicle to track a reference model while the driver is driving the front wheels, except that the controller provides control input via a differential torque signal sent to the two front wheels. Chapter 3 details the identification of the differential torque dynamics both theoretically and experimentally. For this controller, the driver again acts as a disturbance input, while the differential torque is used to track the reference model.

To design the R, S, and T polynomials for each of the above controllers, the open-loop dynamics are again introduced. These polynomials in the Laplace variable s are obtained from the bicycle model by substituting the following measured parameters: U = 3.0 m/s, m = 6.52 kg, Iz = 0.18 kg-m^2, a = 0.155 m, b = 0.235 m, Caf = 48 N/rad, Car = 32.5 N/rad, d = 0.05 m, r = 0.0385 m. The resulting transfer functions are as follows:

$$\frac{\dot{\psi}(s)}{\delta_f(s)} = \frac{81.3\cdot s + 679.9}{s^2 + 18.97\cdot s + 90.54} \tag{5.35}$$

$$\frac{\dot{\psi}(s)}{\delta_r(s)} = \frac{-83.47 - 679.9}{s^2 + 18.97\cdot s + 90.54} \tag{5.36}$$

$$\frac{\dot{\psi}(s)}{\Delta T(s)} = \frac{7.10\cdot s + 58.4}{s^2 + 18.97\cdot s + 90.54} \tag{5.37}$$

$$\frac{\delta_f(s)}{\delta_{f,c}(s)} = 0.769\cdot\frac{5\cdot 2\pi}{s^2 + 2\cdot 0.7\cdot(5\cdot 2\pi)\cdot s + (5\cdot 2\pi)^2} \tag{5.38}$$

$$\frac{\delta_f(s)}{\delta_{r,c}(s)} = 0.769\cdot\frac{5\cdot 2\pi}{s^2 + 2\cdot 0.7\cdot(5\cdot 2\pi)\cdot s + (5\cdot 2\pi)^2} \tag{5.39}$$

$$\frac{\Delta T(s)}{\Delta T_c(s)} = 0.667\cdot\frac{10\cdot 2\pi}{s^2 + 2\cdot 0.7\cdot(10\cdot 2\pi)\cdot s + (10\cdot 2\pi)^2} \tag{5.40}$$

The resulting observer, R, S, and T polynomials for the rear steering control input are as follows:

$$\frac{B_d(s)}{A_d(s)} = \frac{\dot{\psi}(s)}{\delta_{f,c}(s)} = 0.769\cdot\underbrace{\frac{5\cdot 2\pi}{s^2 + 2\cdot 0.7\cdot(5\cdot 2\pi)\cdot s + (5\cdot 2\pi)^2}}_{\substack{\text{assumed}\\\text{actuator}\\\text{dynamics}}}\cdot\underbrace{\frac{81.3\cdot s + 679.9}{s^2 + 18.97\cdot s + 90.54}}_{\substack{\text{bicycle}\\\text{mod el}\\\text{dynamics}}} \tag{5.41}$$

$$\frac{B(s)}{A(s)} = \frac{\dot{\psi}(s)}{\delta_{r,c}(s)} = 0.769\cdot\underbrace{\frac{5\cdot 2\pi}{s^2 + 2\cdot 0.7\cdot(5\cdot 2\pi)\cdot s + (5\cdot 2\pi)^2}}_{\substack{\text{assumed}\\\text{actuator}\\\text{dynamics}}}\cdot\underbrace{\frac{-83.47\cdot s - 679.9}{s^2 + 18.97\cdot s + 90.54}}_{\substack{\text{bicycle}\\\text{mod el}\\\text{dynamics}}} \tag{5.42}$$

$$\frac{B_m(s)}{A_m(s)} = \frac{\dot{\psi}_{desired}(s)}{\delta_{f,c}(s)} = \underbrace{\frac{5\cdot 2\pi}{s^2 + 2\cdot 0.7\cdot(5\cdot 2\pi)\cdot s + (5\cdot 2\pi)^2}}_{\substack{\text{front}\\\text{actuator}\\\text{dynamics}}}\cdot\underbrace{1.5\cdot 5.776\cdot\frac{15^2}{s^2 + 2\cdot 15\cdot s + 15^2}}_{\substack{\text{mod ified}\\\text{bicycle}\\\text{dynamics}}} \tag{5.43}$$

$$\text{Observer}(s) = s^2 + 2\cdot 50\cdot s + 50\cdot 50 \tag{5.44}$$

$$R(s) = s^3 + 119.2 \cdot s^2 + 4433 \cdot s + 28737 \tag{5.45}$$

$$S(s) = -0.323 \cdot s^3 - 18.07 \cdot s^2 - 488.2 \cdot s - 3785 \tag{5.46}$$

$$T(s) = -30.36 \cdot s^2 - 3036 \cdot s - 75906 \tag{5.47}$$

And the resulting observer, R, S, and T polynomials for the differential torque steering MRC are as follows:

$$\frac{B_d(s)}{A_d(s)} = \frac{\dot{\psi}(s)}{\delta_{f,c}(s)} = 0.769 \cdot \underbrace{\frac{5 \cdot 2\pi}{s^2 + 2 \cdot 0.7 \cdot (5 \cdot 2\pi) \cdot s + (5 \cdot 2\pi)^2}}_{\substack{\text{assumed} \\ \text{actuator} \\ \text{dynamics}}} \cdot \underbrace{\frac{81.3 \cdot s + 679.9}{s^2 + 18.97 \cdot s + 90.54}}_{\substack{\text{bicycle} \\ \text{mod el} \\ \text{dynamics}}} \tag{5.48}$$

$$\frac{B(s)}{A(s)} = \frac{\dot{\psi}(s)}{\Delta T_c(s)} = 0.667 \cdot \underbrace{\frac{10 \cdot 2\pi}{s^2 + 2 \cdot 0.7 \cdot (10 \cdot 2\pi) \cdot s + (10 \cdot 2\pi)^2}}_{\substack{\text{assumed} \\ \text{actuator} \\ \text{dynamics}}} \cdot \underbrace{\frac{7.10 \cdot s + 58.4}{s^2 + 18.97 \cdot s + 90.54}}_{\substack{\text{bicycle} \\ \text{mod el} \\ \text{dynamics}}} \tag{5.49}$$

$$\frac{B_m(s)}{A_m(s)} = \frac{\dot{\psi}_{desired}(s)}{\delta_{f,c}(s)} = \underbrace{\frac{5 \cdot 2\pi}{s^2 + 2 \cdot 0.7 \cdot (5 \cdot 2\pi) \cdot s + (5 \cdot 2\pi)^2}}_{\substack{\text{front} \\ \text{actuator} \\ \text{dynamics}}} \cdot \underbrace{1.5 \cdot 5.776 \cdot \frac{15^2}{s^2 + 2 \cdot 15 \cdot s + 15^2}}_{\substack{\text{mod ified} \\ \text{bicycle} \\ \text{dynamics}}} \tag{5.50}$$

$$\text{Observer}(s) = s^2 + 2 \cdot 90 \cdot s + 90 \cdot 90 \tag{5.51}$$

$$R(s) = s^3 + 155.3 \cdot s^2 + 3726 \cdot s + 20714 \tag{5.52}$$

$$S(s) = -5.18 \cdot s^3 + 4.98 \cdot s^2 + 529.4 \cdot s + 48141 \tag{5.53}$$

$$T(s) = 103.1 \cdot s^2 + 18542 \cdot s + 834384 \tag{5.54}$$

After designing the controllers, their performance was tested in the time domain with a driver-in-the-loop (DIL) performance aggressive lane change maneuvers. The following time responses show the controller performance for each of the two controllers:

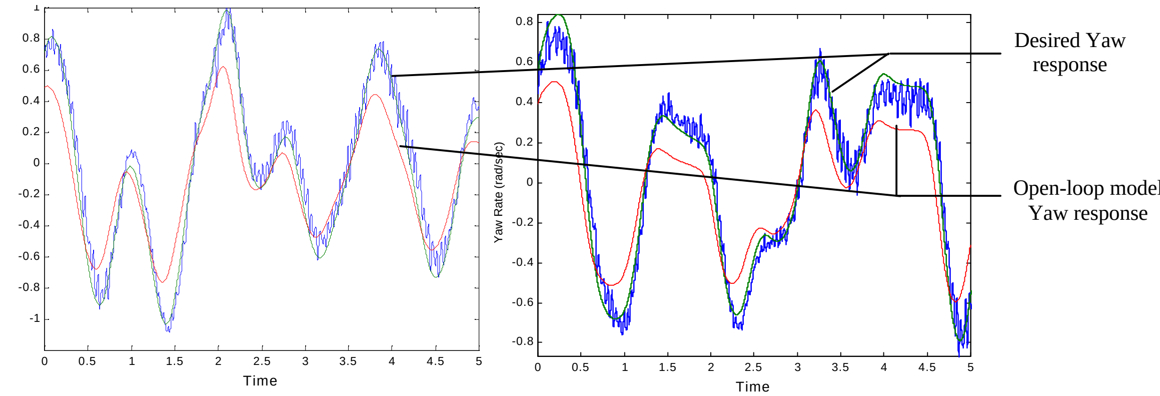

Figure 5.14: The closed-loop disturbance-MRC responses for the Uberquad vehicle with a driver controlling the steering angle of the front wheels, and the controller controlling the steering angle of the rear wheels.

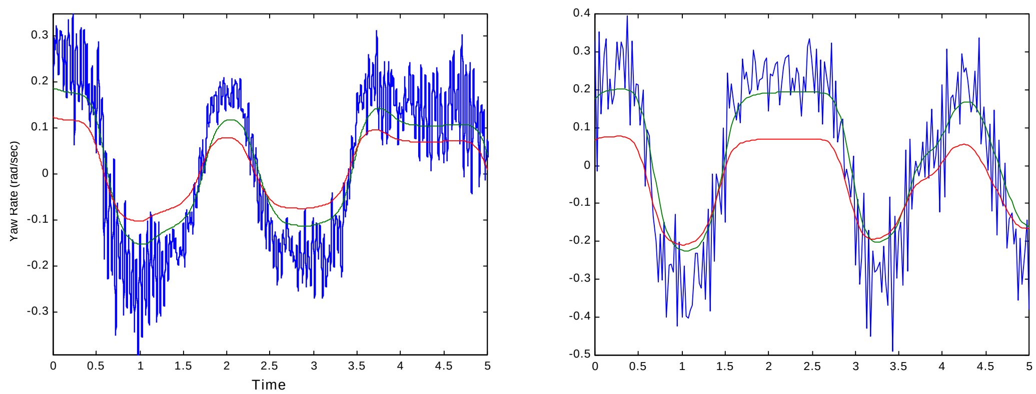

Figure 5.15: The closed-loop disturbance-MRC responses for the Uberquad vehicle with a driver controlling the steering angle of the front wheels, and the controller controlling the differential torque input into the two front wheels.

If we compare the closed-loop performance of the Uberquad with rear-wheel control and that of the 4WS4WD vehicle with similar control, we see the performance of the Uberquad is much better than that of the 4WS4WD vehicle. This improvement is most likely due to more linear steering actuator dynamics, and to decreased dead-zone in the steering linkages. In summary, very good tracking is achieved with the rear-wheel steering controller.

The torque controller displays a significantly larger amount of noise in during the implementation of the torque control. This noise is likely a result of either two sources: physical vibration of the system which is addition additional noise to the yaw-rate measurement, or feedback of the noisy yaw-rate measurement into the wheel torque resulting in a feedback loop. To determine which of these two possibilities was in actuality the cause, an experiment was conducted: The MRC torque steering command was passed through a low-pass filter to determine if the yaw rate measurement improved. The following diagrams show a before and after yaw rate response:

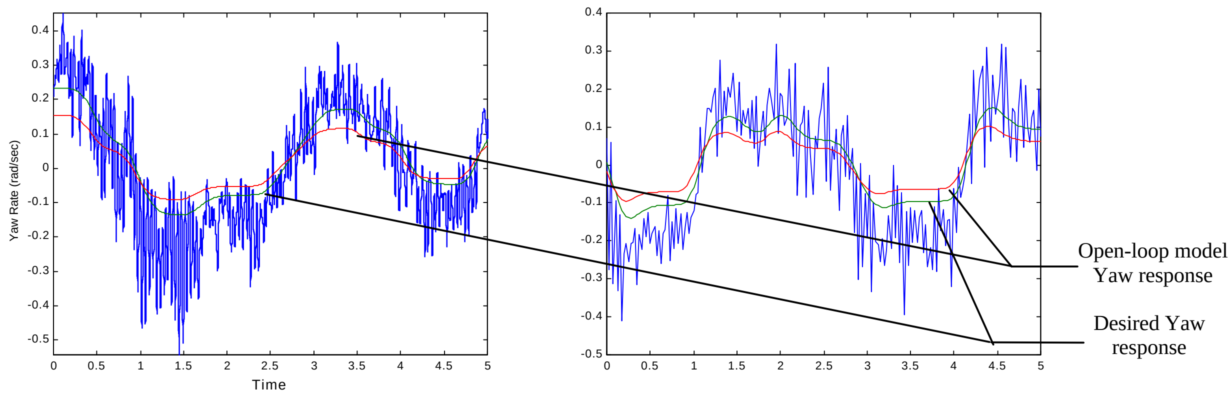

Figure 5.16: Yaw rate responses using MRC before (left) and after (right) the control signal is passed through a second-order low-pass filter with poles at 90 rad/sec.

No significant difference can be seen in the above two plots, implying that the feedback term was not introducing the yaw rate noise. We note that additional filtering could be achieved by decreasing the bandwidth of the filter, but the filter dynamics contribution would begin to significantly affect the controller design.

Experimental testing showed that the torque-steering controller was much more abusive to the vehicle wheels than rear-wheel steering. This is somewhat intuitive, since the wheels are no longer rolling at the same velocity as the vehicle when a differential torque is being applied. The wheels of the vehicle were visibly abraded after only a few hours of testing, and "tire dust" coated the tire area and the treadmill equipment. Other authors have noted at least a 5 to 10 factor increase in wheel wear when using torque steering (Li, Potter, and Jones 1998). From this observation, it is clear that torque steering is not suited to day-to-day steering of the vehicle, and should be reserved for only emergency maneuvers.

One final test was conducted with the Uberquad was to determine how well the controller would perform if the road surface conditions abruptly changed. A real-world example would be accidentally driving over a patch of ice on the road. If the torque steering is intended to be used in emergency situations, then it is appropriate to test this controller under these conditions. As any driver is aware, the automobile accident rate is much greater during inclement weather conditions. Generally, these accidents are caused by changing road surface conditions that can decrease a tire force from aquaplaning or skidding, or increase a tire force due to increased water drag (Hight et al. 1990).

As the vehicle travels over a area of changing road friction, the cornering stiffness of the vehicle and the slip coefficient of the tire will simultaneously decrease. In this dangerous situation, the left side of the vehicle experiences less tractive forces than the right side, resulting in a net moment turning the vehicle OFF the road. The driver’s natural tendency is to compensate by turning the wheel further toward the road. If the vehicle re-enters the roadway in this configuration, the vehicle in general receives a big destabilizing disturbance as the left-side tires again regain traction. At this point, the driver usually over-reacts and steers the vehicle off the road.

Experimentally, it has been suggested that the torque control may be more robust to split-mu types of roadway changes because the torque steering moment is less dependent on road friction than steering forces. To test this idea, the following experiment was planned: one half of the treadmill surface was covered with a very light coat of water. The vehicle was made to track a sawtooth signal that led onto the slick area, and the resulting yaw rate response was recorded. The following diagram shows the experimental setup:

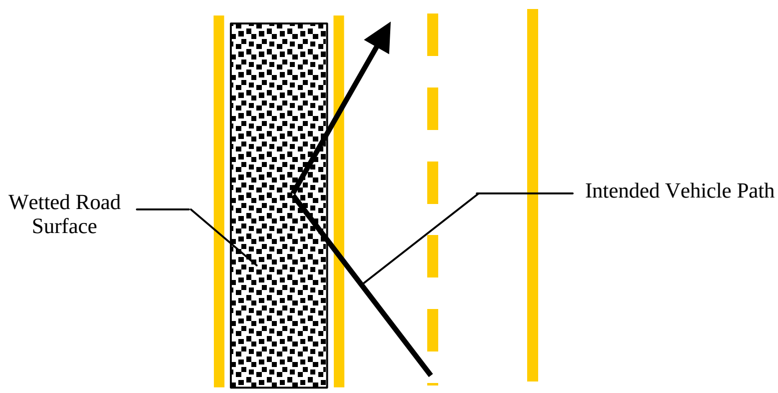

Figure 5.17: The experimental setup used to test the controller sensitivity to changing road friction.

For consistency of results, a PID controller was used to regulate the car to a reference position on the track, and the steering output from this controller was fed into the wheels directly, or into the MRC controller. This allowed us to prevent the driver “experience” from interfering with experimental interpretation of the data. The driver was used to set the setpoint of the regulating PID controller. The driver would turn the wheel far to the left, forcing the vehicle to drive partially on the slick area, and then the driver would release the wheel (which is spring-loaded to return to the center-line of the treadmill) to force the vehicle back onto the center of the road. The following plot shows the results of this experiment *before* the left-half side of the road was wetted.

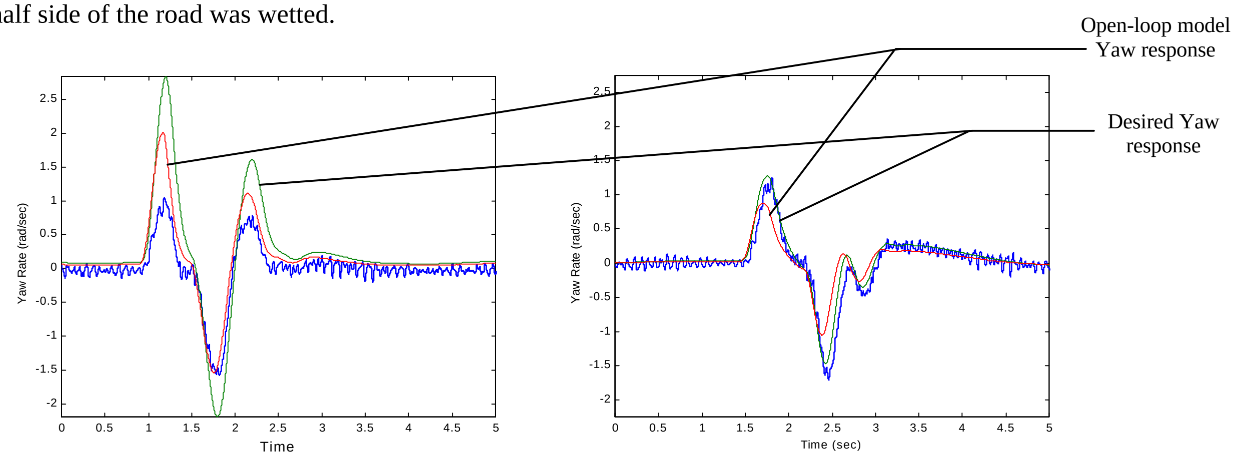

Figure 5.18: Yaw rate responses with no control (left) and with rear-steer MRC (right) on a dry road surface.

With the MRC off, the “recovery” gives two significant positive yaw-rate peaks, showing the results of over-correction by the artificial driver. Note that both controllers slightly over-correct EVEN WHEN THE ROADWAY IS DRY.   With the MRC on, clear model tracking is seen. Because the vehicle model is more damped, there over-correction by the artificial driver. Again, an artificial driver was used because it was discovered that after several trials the human driver “learned” how to handle the vehicle in this recovery maneuver and thereby biased the results. The above “dry” runs were used as a comparison to the following “wet” maneuvers. Again, two figures are presented of the same situation to show variability between experiments.

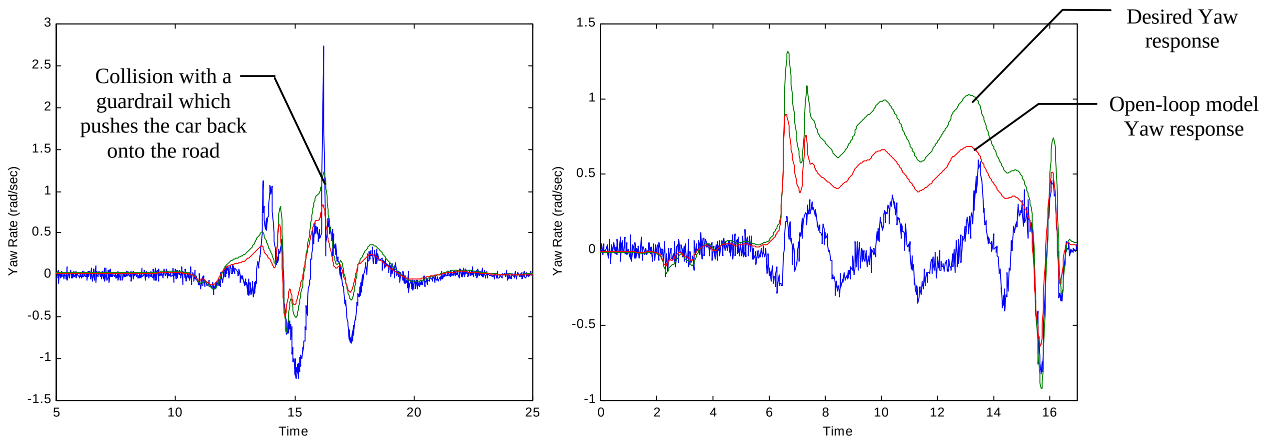

Figure 5.19: Yaw rate responses on a wet surface for an artificial driver with no MRC assistance.

Both figures show SEVERE model mismatch, indicating that the vehicle is no longer handling as it should. In the figure on the left, an impact yaw-rate spike is seen as the vehicle hits a guard-rail, thus turning the vehicle back onto the road where the computer “driver” corrects the vehicle orientation and recovers control. The figure on the left shows a severe and prolonged mismatch between desired and actual yaw rate. In this case, the left side of the vehicle “hydroplaned” and caused a destabilizing moment on the vehicle. The computer “driver” compensated by turning the wheels back onto the road, but for approximately 5 seconds this steering correction was only enough to prevent further spinning. We see from the above plot where the vehicle regains control and the vehicle responses again start to match predicted model responses. Both situations would represent very dangerous accidents at approximately 40 mph in a real vehicle.

The following figures show the driving results for the MRC controller. Although difficult to quantify, the rear-steering MRC did show a noticeable improvement in recovering from the destabilizing road-friction moment. The reason for this is that the MRC controllers employ yaw-rate feedback, and thus can detect a significant mismatch between commanded and measured yaw rate. Two figures are presented of the same situation to show variability between experiments.

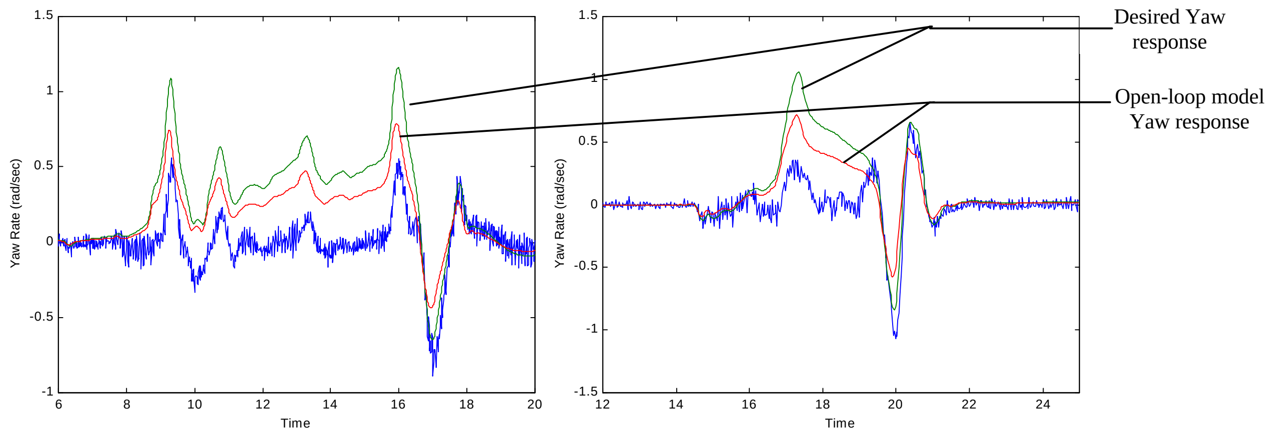

<u>Figure 5.20</u>: Yaw rate responses on a wet surface using rear-steering MRC driver assistance.

Again, severe model-mismatch is observed in these driving situations. The worst-case situation observed with rear-steer MRC is shown above on the left. If we compare this situation with the similar situation without MRC, we see that the MAGNITUDE of dynamic mismatch is not as large. The average MRC error for the duration of the side-skid is 0.4 radians/sec, where for the non-MRC case it is approximately 0.6 radians/second. Whether this change is statistically valid would require testing beyond the scope of this thesis.

As a final test, the rear-steer MRC was replaced with torque-steer MRC, with the following results:

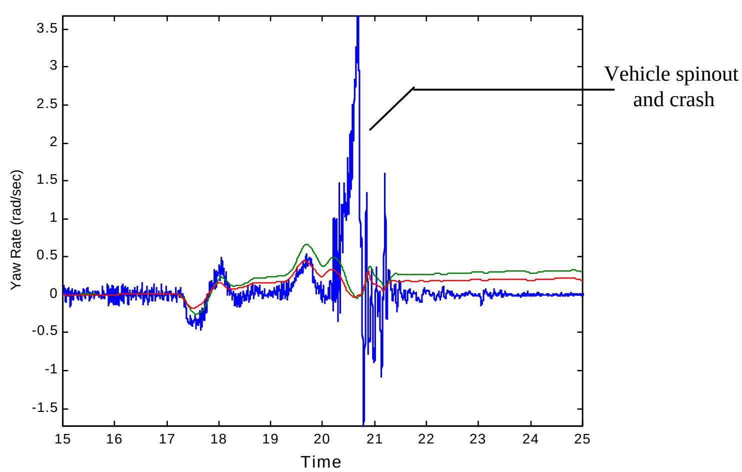

<u>Figure 5.21</u>: Yaw rate responses on a wet surface using rear-steering MRC driver assistance.

causing a collision with the guardrail. The vehicle also lost forward tractive velocity, thus causing the vehicle to drift backward off the treadmill and eventually crash off the treadmill. It became immediately evident that modification of the wheel torque controller would be needed to appropriately test this controller. Two issues remain to be addressed. First, in all the testing presented in this thesis, the vehicle is made to remain stationary on the treadmill as the treadmill maintains a constant velocity. This method was clearly unsuitable for the differential torque steering tests presented here, simply because the vehicle did not have enough tractive force to maintain forward velocity. As the vehicle began to drift backward, the wheel slip increased dramatically as the vehicle attempted to maintain longitudinal positioning on the treadmill. The obvious solution to this is to set the Uberquad to run at a constant velocity and use the treadmill to "track" the vehicle. However, this requires a time-consuming redesign of the longitudinal controller.

A larger problem with the longitudinal wheel slip is that significant wheel spinout no longer correctly simulates real-world vehicles where ABS and TCS (traction control systems) prevent such type of spin-out. Clearly, some type of wheel-slip controller is necessary to use in conjunction with torque-MRC to provide adequate testing of the algorithm. Unfortunately, the time and experimental requirements for this type of controller are beyond the limited scope of this master's thesis, and must remain for future students.

6 Conclusions and Future Work

Because of the amount of material covered in this thesis, even the conclusions must be subcategorized. There were three sections of experiments conducted for this thesis work, and each experiment set deserves a conclusive summary independent of the other experiments. After providing these summaries, then general conclusions are given summarizing the whole of vehicle testing and various aspects of the IRS experiments. Recommendations for future work are then given.

6.1 Experiment-Specific Conclusions

6.1.1 4WS4WD vehicle at 1.2 m/s

In the field of control, the scapegoat of poor controller performance is inevitably poor actuation or poor feedback sensors. Unfortunately, the biggest issues confronted in performing closed-loop control of the 4WS4WD vehicle at these low speeds regarded the quality of the feedback sensors and actuators. Regarding the feedback sensors, the previous student was unable to perform yaw rate control of the vehicle because the encoder arm used by the this student simply did not have enough resolution. The replacement of the encoder arm with the analog sensing arm corrected this problem, but the analog arm simply "wore-out" too quickly for usefulness in vehicle testing. The final arm redesign, using high-resolution, impact isolated encoders appears to be the most economic and reliable method of obtaining vehicle position measurements.

The vehicle testing at 1.2 m/s showed that the MRC method appeared to work quite well, until the dynamics of the steering actuator was investigated. The usefulness of the results of this test became questionable after discovering that the actuator dynamics were the dominant dynamics of the system. This error in design underscores the necessity of selecting the proper actuator beforehand, and testing the dynamics of the system piecemeal to determine which dynamics will dominate the overall response of the system.

The results of the low speed controller were compared to a high-gain proportional controller, with the resulting tracking becoming adequate but producing a noticeable and persistent oscillation. At the time of the test, it was assumed that the system was simply borderline unstable, but later testing (at higher speeds) showed a definite limit cycle in the system. It is possible that the oscillation seen in the proportional controller responses could be the result of a limit cycle set up by a steering linkage deadzone known to exist in the system.

6.1.2 4WS4WD vehicle at 3.0 m/s

In the tests conducted using the 4WS4WD vehicle at higher velocity, the steering actuators were replaced with high-speed (the fastest available) R/C servos. An order-of-magnitude improvement was seen in the actuator responses, both in the time and in the frequency domain. As a result, the dynamics observed in the vehicle testing are conclusively those of the bicycle model. The time responses were fit by varying parameters in this model slightly away from the values that were measured off-line, and the resulting controller based on the bicycle model and actuator dynamics proved to work quite satisfactorily.

An area of investigation in this set of experiments regarded the quality of closed-loop performance if actuator dynamics are ignored. Controller designs with and without actuator dynamics demonstrably showed that neglecting actuator dynamics significantly deteriorates the closed-loop performance. It was also noted that increasing the model order *arbitrarily* to possibly encompass more unmodeled dynamics was detrimental to the system performance in closed-loop. It was then concluded that the mismatch in time and frequency domain system measurements was not likely due to unmodeled *linear* dynamics (at least, within the range of testing), but most likely due to nonlinear rate-limiting and backlash effects seen in the steering actuator and steering linkage respectively. During this set of experiments a stable limit cycle was observed in the system, suggesting once again the presence of large, unaccounted-for nonlinearities in the system. This phenomenon remains a topic for future study.

To emphasize the dependence of vehicle dynamics on velocity, an experiment was conducted where the velocity was varied away from the design velocity. It was discovered that slower velocities caused the controller to undershoot the reference velocity significantly, while faster velocities had the opposite effect. Thus, we conclude that (as expected) the vehicle dynamics are quite sensitive to vehicle velocity.

6.1.3 Uberquad at 3.0 m/s

Without regard to the nature of the experiments conducted using this vehicle, it was immediately clear that the new vehicle with DC motor steering actuation and direct-link steering was much more consistent and predictable in its performance. This aside, several important conclusions can be made regarding MRC techniques on this vehicle. It is clear that the MRC approach can affect vehicle response regardless of whether torque or steering input is used. However, better tracking is achieved with rear steering input. It was also discovered that torque steering was remarkably detrimental to the life of the tires and to the quality of the feedback. Differential torque driving induces noticeable vibrations in the vehicle which may not be suitable for situations outside of emergency recovery maneuvers. Additionally, the torque-steering controller was much more abusive to the vehicle wheels than rear-wheel steering. This suggests that torque steering is not suited to day-to-day steering of the vehicle, and should be reserved for ONLY emergency maneuvers.

Regarding emergency maneuvers, the slip sensitivity tests conducted on the Uberquad shows promising results using yaw-rate feedback versus open-loop driving. The preference between rear steering or torque steering remains questionable. In addition, the “best” controller for this type of testing is also debatable. Fortunately, the repeatability and convenience offered by the use of the Illinois Roadway

Simulator will allow detailed observation of vehicle dynamics in the future to answer these and many other questions.

6.2 General Conclusions

Throughout this thesis, the Model Reference Controller approach was used in a modified form where the driver input was treated as a disturbance. Three sets of experiments conducted on effectively 3 different vehicles showed that this technique worked quite well, but was sensitive to model changes. This was expected and predicted in the controller development. In addition, it was discovered that the best method to "test" the controller was to not only change the pole locations but also the DC gain of the original model to obtain the design model. This change facilitated comparisons between open-loop and closed-loop performance.

The original intent of the MRC was to create an affordable and easy-to-use testbed for vehicle dynamics studies. To this end, the use of off-the-shelf R/C components was originally considered to be preferential over other systems. However, several aspects of these systems has in retrospect proved to be quite difficult to "design around" in terms of yaw-rate control: they have a unique communication system that introduces a random but quantized delay of 12-24 milliseconds, the R/C actuators operate nearly rate-limited at all times, and contain an inherent dead-zone, and the steering linkages are prone to dead-zones as well. Eventually, this methodology of using R/C components was abandoned for yaw rate control. However, these systems remain useful for platooning studies, or with control applications not requiring such a high level of model fidelity and actuator performance.

The use of a fixed vehicle and moving roadway surface for experimentation has proved to be quite useful. Many aspects of the testing conducted in this thesis were greatly simplified by the use of a moving roadway and stationary vehicle, including the use of a position sensing arm, the ability to perform a frequency response, and the ability to use a constant, stable, but external power source to power the vehicle. These advantages, unforeseen at the outset of this thesis, have proved to be quite beneficial for the successful measurement and control of vehicle dynamics.

A central issue addressed in part in this thesis has been the validity of scale vehicle testing. A body of research concerning scale aircraft and scale sea-vessel studies has been extended to scale vehicle studies via the Buckingham Pi Theorem of dynamic similitude and dimensional analysis. Central to the use of this theorem is the assumption that scale vehicles AND full sized vehicles are both modeled by the bicycle model. Previous researchers have addressed the modeling of full sized vehicles, but the experiments conducted and described in this thesis have proved via dynamic measurements that the bicycle model is a very good first approximation to the scale vehicle dynamics. With the verification of the bicycle model to describe vehicle dynamics, the dynamic scaling issue can be reduced to matching of dimensionless parameters between two different systems. These parameters were derived in this thesis and the associated matching conditions were used to determine optimal testing conditions to run vehicle simulations. One issue remains: what vehicle parameters to use. The variability of dimensionless parameters among published data is very large. Thus, the problem of vehicle scaling is less a problem of whether scaling can be achieved but instead deciding what vehicle to scale to. The formation of pi-groups allows parameter-based scheduling of controller gains; given the bicycle model parameters for a particular vehicle, a controller can update the controller gains appropriately.

An important lesson presented in this thesis has been the ability to model different portions of the vehicle/treadmill system separately. It has been remarkable how well these submodels, when combined, have predicted the performance of the system as a whole. This approach is not always successful, especially in systems where the subsystems are interdependent. The fact that the subsystems are not quite as interdependent provides a simple means of changing different aspects of the vehicle to answer questions central to vehicle performance. How large does an actuator have to be to achieve robust tracking? What type of lateral resolution is needed to maintain stable, automated vehicle? These and other questions are easily answered on this system, but remain for future researchers to tackle.

Using the Illinois Roadway Simulator has provided a unique opportunity to study dangerous vehicle dynamics. This researcher is unaware of any scale or full-sized experimental testing conducted at high speeds in split-mu conditions. This researcher is also unaware of any studies where repeated vehicle crashes are encouraged and repeated under controlled conditions to determine the best steering compensation. It is precisely these unstable dynamics that vehicle automation controllers must address to find utility in the general marketplace.

6.3 New Control Avenues

Many sections of this thesis have hinted as possible future research topics. The following discussion is simply a short summary of some of the most likely topics to be examined in the near future.

In two of the three vehicle tests, limit-cycle behavior was observed. What particular aspects of the vehicle construction are causing these limit cycles? Will they exist on full-sized vehicles under tight automation? What improvements or controllers will prevent them from occurring?

The differential torque used to steer the Uberquad in this thesis was implemented by applying a differential torque via the two front tires. A different design may have been to use the two rear tires, or all four tires, or combinations/weightings of each. What is the optimal configuration to use? Which method will least saturate the tire and thus provide the most robust performance under changing road conditions? Can tire slip/saturation be used as a method to "schedule" different wheel torque configurations?

On the Uberquad, two different steering controllers were presented: MRC using differential torque steering and MRC using rear wheel steering. Which method is most suited for highway driving (likely rear-wheel steering) and which method is most suited for emergency maneuvers (differential torque?). Is there some method to weight or schedule the use the each controller if both types of steering are available? With two steering motors and six torque motors available, it appears that there are 6 degrees of controller "freedom" even though some are redundant in terms of the control space. Would it be suitable to force additional control constraints, such as requiring that each wheel have equal net wheel usage, or minimizing sideslip angle?

With the ability to "steer" with the rear wheels and with torque input, it would be possible to determine on-line the cornering stiffness of the system. Many studies have included estimation procedures for determining road friction (Ray 1998). Much of the focus has been to use neural networks to determine tire parameters (Pasterkamp and Pacejka 1997a). One concept is to use the longitudinal slip of the tire to estimate the road friction (Yamazaki, Furukawa, and Suzuki 1997). Utilizing this measurement, it should be possible to develop controllers that are more robust and possibly adaptive to changing road conditions. Assuming that the amount of torque input were known, the torque input could be used as a known disturbance that the front-wheel-steering controller would reject. The cornering stiffness could then be estimated, in a similar manner to how the cornering stiffness was measured for the Uberquad vehicle.

Surpassing parameter estimation, is there some method to adaptively identify and control the plant dynamics? Can the MRC methodology be extended for this physical system to the realm of Model Reference Adaptive control? Would there be enough persistence of excitation to identify the vehicle dynamics? Would additional sensing, such as on-board accelerometers, improve the controller performance?

With two vehicles now available and running, the possibility for two vehicle platooning is now present. Catch and avoid maneuvers could then be demonstrated on the vehicle system. In addition, new platooning ideas such as an advanced optical towbar (where photo-resistors can be used to measure lateral AND longitudinal displacements between vehicles) can be tested.

Would it be possible to attach a motor to the steering wheel and provide direct driver feedback as the nature of driving conditions? For instance, if the vehicle tires are near saturation, the steering wheel can be jittered very quickly to warn that such conditions exist. An interesting concept has been presented in the literature of using the steering wheel to “nudge” the driver to assist in the steering of the vehicle (Yuhara et al. 1997). General Motors has suggested on-board monitoring of drivers to determine safety and driver performance issues (Kamal 1990).

With a driver-in-the-loop, but not in the vehicle (!), very interesting human behavior studies can be conducted. Some authors have spent considerable effort obtaining models of driver behavior (Cho and Kim 1995; Cho and Kim 1996), including using neural networks to simulate a driver input (MacAdam and Johnson 1996). An implementation example would be in attempting to identify the state of the driver (i.e. sleepiness or drunkenness) based on vehicle state measurements and driver inputs. This type of analysis would go past simply recording driver actions: corrective actions could be taken if significant and persistent driving errors are observed (like the driver is having a heart attack… or using a cell phone).

The remaining research avenues using the Illinois Roadway Simulator are extensive. It will likely be some other student to answer some of the above questions and open new doorways. It is the hope of this author that the work presented in this thesis will serve as a good stepping stone for their endeavors.

Appendix 1 - A Summary of Published Vehicle Control Articles

	General Control Issues					Control Specifications Given In/As						Type of Control			Method of Control Input			Domain Used for Control Design			Method Used to Design Control Law						Validation: Domain			Validation: Plant				
Reference	Based on Bicycle Model?	Bicycle Model Values Given?	Incorporates a Driver Model?	Driver Controls Front Wheels?	Acceleration Region	Time Domain (Overshoot,SS Error	Freq. Domain (Bandwidth, Phase)	Classical (Pole Locations)	Parameter (understeer gradient)	Reference Model / Training Data	Author's "Feel"	Uses Feedforward	Uses Feedback	Uses Target Yaw Rate Function	Controller Operates Front Wheel	Rear Steering	Brake/Torque Steering	Linear Control (Transform Domain)	Linear Control (State Space)	Parameter Space Design	Optimal Control (LQR/LQG)	Sliding Mode Control	Nonlinear Control	Adaptive Control	Parameter Solution / Inversion	Fuzzy Control/Neural Networks	Time Domain	Frequency Domain	Parameter Domain	Simulation Model	Order	Includes Tire Lag	Includes Actuator Dynamics	Actual Vehicle
Inoue and Sugasawa, 1993	X			X	1						X	X	X	X		X				X		not	specified				X				not specified			X
Li, Potter, and Jones, 1998	No			N/A	1					X		X	X				X	X		X					X		X			X	14	?		
Kleine and Van Niekerk,1998	X		X		1	X	X								X	X			X	X					X		X			X	3			
Cho and Kim, 1995	X	X	X	X	1	X		X					X			X			X		X						X			X	2			
Smith and Benton, 1996	X	X			5				X				X			X			X		X						X			X	8	X		
Nagai et al, 1995	X	X			5					X		X	X		X	X		X					X			NN	X	X		X	?	X		
Ahring and Mitschke, 1995	X	X		*	5				X			X	X		X	X				X					X		X			X	3			
Palkovics, 1992	X	X			1					X		X	X	X	X	X			X		X						X	X		X	2			
Sridhar and Hatwal, 1992	X	X			1				X			X	X			X	X			X	X				X		X			X	2			
Peng et al, 1994	X	X			1	X					X	X	X		X				X		X						X			X	11	X	X	X
Hayafune and Yoshida, 199	X				1	X	X					X	X		X			X			X						X			X	NS			X
Smith and Starkey, 1994	X	X			5	X						X			X				X		X						X			X	8	X		
Shiotsuka et al, 1993	X	X			5					X		X	X		X	X				X	X			X	X	NN	X			X	NN			
Shibahata et al, 1993	X				4,5,6				X			X					X			X					X				X	X	NS			X
Alleyne, 1997	X				1	X							X		X	X	X		X		X						X			X	7			
Nagai et al, 1997	X	X			1,5					X		X	X	X		X	X		X		X						X			X	NS	X		
Will and Zak, 1997	X	X			1					X		X	X		X	X	X		X			X					X			X	4			
Cho and Kim, 1996	X	X	X	X	1	X		X				X	X			X			X				classical control				X		X	X	NS			
Yaniv, 1997	X	X			5		X		X				X		X	X			X	X	X				X		X		X	X	2			
Wakamatsu, 1997	X				5					X		X	X								X		X	X			X	X		X	NS			X
Lee et al, 1997	NS			X	1,5	X						X	X			X				X					X		X			X	NS			X
Lee, 1997	X	X			1					X		X	X		X	X		X							X		X			X	3		15 Hz, 1st order	
Abe, 1996	X	X	X		1,5					X		X	X			X	X													X	13			
Alleyne, 1997	X	X			1	X							X		X	X	X		X		X						X			X	7			

* Driver input is augmented with control input

NN - Neural Network

NS - Not Specified

Appendix 2 - Instructions on Operating the IRS

1. Open up MATLAB and ensure that you are in the directory of your model.
2. To build the model, drag-and-drop the custom Simulink blocks for the encoder boards, digital I/O, analog output, and analog input into your Simulink diagram where appropriate.
3. Use the Wincon "build" command to compile the Simulink diagram into C-code, and download the resulting code to the Wincon server.
4. Ensuring that the car and the treadmill are off, start the code and open up the "digital input" display to observe the calibration pulses from each position encoder. Zero the arm by moving each link to the "zero" position and ensuring that the digital input goes high for each joint encoder. The zero positions are: straight ahead for the yaw encoder, 90 degrees for the middle link encoder, and straight ahead for the ground link encoder.
5. Check the calibration by moving the treadmill forward and backward. Ensure that the yaw angle does not change significantly. Lifting up the vehicle and moving it around to ensure linear arm response is also sometimes useful.
6. Stop the controller.
7. Turn on the vehicle power by turning on the amplifies for the Uberquad, or by switching on the power at the vehicle for the 4WS4WD vehicle. If the 4WS4WD vehicle is used, turn on the transmitter power by plugging in the power supply and flipping the power switch on the front of the transmitter.
8. Turn on the treadmill by holding down the "Start/Stop" switch for half a second, and hitting the "Run" switch. The start-stop switch powers on a relay switch that is activated when you hit the run switch. You should hear a very distinctive click when hitting run as the relay for 220 volts engages magnetically. If the switch does not engage, simply try again.
9. Make sure that you set the operating speed to be zero at the start. Run the car by starting the Wincon server!

Bibliography

Abe, Masato, Naoto Ohkubo, and Yoshio Kano. 1996. A Direct Yaw Moment Control for Improving Limit Performance of Vehicle Handling - Comparison and Cooperation with 4WS. *Vehicle System Dynamics Supplement* 25:3-23.

Ahring, E., and M. Mitschke. 1995. Comparison of All-Wheel Steerings in the System Driver-Vehicle. *Vehicle System Dynamics* 24:283-298.

Alleyne, Andrew. 1997a. A Comparison of Alternative Intervention Strategies for Unintended Roadway Departure (URD) Control. *Vehicle System Dynamics* 27:157-186.

Alleyne, Andrew. 1997b. A Comparison of Alternative Obstacle Avoidance Strategies for Vehicle Control. *Vehicle System Dynamics* 27:371-392.

Arnholt, Mike. 1995. It's ESP - Mercedes/Bosch system tames those slippery roads. *WARD's Auto World,* April, 53-4.

Astrom, Karl J., and Bjorn Wittenmark. 1995. *Adaptive Control*. 2nd ed. Reading, Massachusetts: Addison-Wesley.

Astrom, Karl J., and Bjorn Wittenmark. 1997. *Computer-Controlled Systems: Theory and Design*. Edited by T. Kailath. 3rd ed, *Prentice Hall Information and System Sciences Series*. Upper Saddle River, New Jersey: Prentice Hall.

Bakker, E., L. Nyborg, and H. B. Pacejka. 1987. Tyre Modeling for Use in Vehicle Dynamics Studies. Paper read at Int. Congress and Exposition, at Detroit, MI.

Bakker, E., H. B. Pacejka, and L. Lidner. 1989. A New Tyre Model with an Application in Vehicle Dynamics Studies. *SAE Trans. J. of Passenger Cars, SAE paper #890087* 98.

Bekker, M.G. 1969. *Introduction to Terrain-Vehicle Systems*. Ann Arbor: The University of Michigan Press.

Brennan, Sean, and Andrew Alleyne. 1999. Driver Assisted Yaw Rate Control. Paper read at American Controls Conference, June 2-4, 1999, at San Diego, CA.

Buckingham, E. 1914. On Physically Similar Systems; Illustrations of the use of dimensional equations. *Physical Review* 4:345-376.

Bundorf, R. T. 1968. A Primer on Vehicle Directional Control. Warren, Michigan: General Motors Technical Center.

Chen, Kan, and Robert D. Ervin. 1990. Socioeconomic Aspects of Intelligent Vehicle-Highway Systems. *Supplement to SAE International* SP-833 (Automated Highway/Intelligent Vehicle Systems: Technology and Socioeconomic Aspects):51-58.

Cho, Young H., and J. Kim. 1995. Design of Optimal Four-Wheel Steering System. *Vehicle System Dynamics* 24:661-682.

Cho, Young H., and J. Kim. 1996. Stability Analysis of the Human Controlled Vehicle Moving Along a Curved Path. *Vehicle System Dynamics* 25:51-69.

Clark, D. C. 1960. The Turning Behavior of Articulated Track-Laying Vehicles. Warren, Michigan: U.S. Army Land Locomotion Laboratory.

Danner, M., K. Langwieder, and W. Schmelzing. 1985. Aspects in optimizing car structures and passenger protection by a comprehensive analysis of car-to-car and car-to-object collisions. *Society of Automotive Engineers* Paper # 850514.

d'Entremont, Kenneth L. 1997. The Behavior of Tire-Force Model Parameters Under Extreme Operating Conditions. *Supplement to the SAE International* SP-1228 (Research into Vehicle Dynamics and Simulation - 1997):17-26.

DePoorter, Mark. 1997a. Development, Experimentation, and Control of a Small Scale Vehicle Dynamics and Control Laboratory. M.S., Mechanical and Industrial Engineering, University of Illinois at Urbana-Champaign, Urbana.

DePoorter, Mark. 1997b. The Illinois Roadway Simulator. Masters, Mechanical and Industrial Engineering, University of Illinois at Urbana-Champaign, Urbana, Illinois.

DePoorter, M., S. Brennan, and A. Alleyne. 1998. Driver Assisted Control Strategies: Theory and Experiment. Paper read at 1998 ASME International Mechanical Engineering Congress and Exposition, Nov. 1998, at Anaheim, CA.

Doniselli, Carlo, Giampiero Mastinu, and Massimiliano Gobbi. 1996. Aerodynamic Effects on Ride Comfort and Road Holding of Automobiles. *Vehicle System Dynamics Supplement* 25:1996.

Dugoff, H. , P. S. Fancher, and L. Segel. 1970. An Analysis of Tire Traction Properties and Their Influence on Vehicle Dynamic Performance. *SAE Transactions* 79 (SAE Paper No 700377):341-366.

Edwards, Scott. 1998. *Programming and Customizing the Basic Stamp Computer*. New York: McGraw-Hill.

Ellis, John. 1989. *Road Vehicle Dynamics*. 2nd ed. 4815 Provens Dr., Akron, O.H.: Author.

Emori, R. I. 1969. *"Automobile Accident Reconstruction". UCLA Motor Vehicle Safety Contract Final Report*. Vol. Report No. 69-51, *UCLA Motor Vehicle Safety Contract Final Report*. LA: UCLA Schools of Engineering and Medicine.

Evans, Leonard. 1991. *Traffic Safety and the Driver*. New York: Van Nostrand Reinhold.

Fancher, P., J. Bernard, C. Clover, and C. Winkler. 1997. Representing Truck Tire Characteristics in Simulations of Braking and Braking-in-a-Turn Maneuvers. *Vehicle System Dynamics Supplement* 27:207-220.

Fenton, R.E., and et al. 1976. On the Steering of Automated Vehicles: Theory and Experiment. *IEEE Transactions on Automatic Control* AC-21 (3):306-315.

Fukunaga, Y, and et al. 1987. Improved Handling and Stability Using Four-Wheel Steering. Paper read at 11th Technical Conference on Experimental Safety Vehicles, at Washington D.C.

Furukawa, Yoshimi, and Masato Abe. 1997. Advanced Chassis Control Systems for Vehicle Handling and Active Safety. *Vehicle System Dynamics* 28:59-86.

Furukawa, Y., and et. al. 1989. A Review of Four-Wheel Steering Studies from the Viewpoint of Vehicle Dynamics and Control. *Vehicle System Dynamics* 18:1-186.

Hayafune, Kazuya, and Hiroaki Yoshida. 1990. Control Method of Autonomous Vehicle Considering Compatibility of Riding Comfort and Vehicle Controllability. *Supplement to SAE International* SP-833 (Automated Highway/Intelligent Vehicle Systems: Technology and Socioeconomic Aspects):35-40.

Heydinger, G.J., W.R. Garrot, and J.P. Christos. 1991. The Importance of Tire Lag on Simulated Transient Vehicle Response. SAE Paper No 910235.

Heydinger, G. J, W. R. Garrot, and J.P. Christos. 1994. The Dynamic Effects of Tire Lag on Simulation Yaw Rate Predictions. *ASME Journal of Dynamic Systems, Measurement and Control* 116 (June):249-256.

Hight, Philip V. , Jeffrey B. Wheeler, Timothy J. Reust, and Norman Birch. 1990. *The Effect of Right Side Water Drag on Vehicle Dynamics and Accident Causation*. Vol. Accident Reconstruction: Human, Vehicle, and Environmental Factors, *Society of Automotive Engineers*. Warrendale, PA: Society of Automotive Engineers.

Higuchi, A., and H. B. Pacejka. 1997. The Relaxation Length Concept at Large Wheel Slip and Camber. *Vehicle System Dynamics Supplement* 27:50-64.

Horinouchi, Katsutoshi, Takashi Yonekawa, Tamio Kanou, Seisyu Utsumi, and Yoshihisa Nagahara. 1997. Handling Analysis with Vehicle Dynamics Simulator. *Supplement to SAE International* SP-1228 (Research into Vehicle Dynamics and Simulation - 1997):181-191.

Huber, L., and O. Dietz. 1937. Pendelbewegungen von Lastkraftwagenanhangern..." (Snaking of truck trailers). *VDI* 16.

Hyde, Alvin S. 1992. *Crash injuries: how and why they happen. A primer for anyone who cares about people in cars*. Key Biscayne, Florida: Hyde Associates, Inc.

Inoue, H., and F. Sugasawa. 1993. Comparison of Feedforward and Feedback Control for 4WS. *Vehicle System Dynamics* 22:425-436.

Jansen, S.T.H., and J.J.M. VanOosten. 1995. Development and Evaluation of Vehicle Simulation Models for a 4WS Application. *Vehicle System Dynamics* 24:343-363.

Kamal, Mounir M. 1990. A General Motors' Perspective on Intelligent Vehicle/Highway Systems. *SAE Supplement* Automated Highway/Intelligent Vehicle Systems: Technology and Socioeconomic Aspects (SP-833):1-16.

LeBlanc, David J., Gregory E. Johnson, Paul J. Th. Venhovens, Garth Gerber, Robert DeSonia, Robert D. Ervin, Chiu-Feng Lin, A. Galip Ulsoy, and Thomas E. Pilutti. 1996. CAPC: A Road-Departure Prevention System. *IEEE Control Systems Magazine* December:61-71.

Lee, Allan Y. 1997. Matching Vehicle Responses Using the Model-Following Control Method. *Supplement to the SAE International* SP-1228 (Research into Vehicle Dynamics and Simulation - 1997):57-69.

Lee, Allan Y., Alan T. Mariott, and Nhan T. Le. 1997. Variable Dynamic Testbed Vehicle: Dynamics Analysis. *Supplement to SAE International* SP-1228 (Research into Vehicle Dynamics and Simulation - 1997):39-55.

Legouis, T., A. Laneville, P. Bourassa, and Payre G. 1986. Characterization of Dynamic Vehicle Stability Using Two Models of the Human Pilot Behavior. *Vehicle System Dynamics* 15:1-18.

Leister, G. 1997. New Procedures for Tyre Characteristic Measurement. *Vehicle System Dynamics Supplement* 27:22-36.

Li, W., T. E. C Potter, and R. P. Jones. 1998. Steering of 4WD Vehicles With Independent Wheel Torque Control. *Vehicle System Dyanamics Suppliment 28* 29 (28):205-218.

Lugner, P. 1977. The Influence of the Structure of Automobile Models and Tyre Characteristics on the Theoretical Results of Steady-State and Transient Vehicle Performance. Paper read at The 5th VSD-wnd IUTAM syumposium, at Vienna, Austria.

Lugner, P. 1982. *Horizontal Motion of Automobiles-Theoretical and Practical Investigations, The Dynamics of High Speed Vehicles*. New York: Springer-Verlag.

MacAdam, C.C. 1981. Application of an Optimal Preview Control for Simulation of Closed-Loop Automobile Driving. *IEEE Transactions on Systems, Man and Cybernetics* SMC-11 (6):393-399.

MacAdam, Charles C., and Gregory E. Johnson. 1996. Application of Elementary Neural Networks and Preview Sensors for Representing Driver Steering Control Behavior. *Vehicle System Dynamics* 25:1-30.

Marquard, E. 1937. Untersuchung der Federungeigenschaften von Kraftfahrzeugen an Modellen (Study of suspension Models of Motor Vehicles). *ATZ* 17.

Mastinu, G., S. Gaiazzi, F. Montanaro, and D. Pirola. 1997. A Semi-Analytical Tyre Model for Steady- and Transient-State Simulations. *Vehicle System Dynamics Supplement* 27:2-21.

McKenna, K. J. 1974. A Variable Response Vehicle - Description and Applications. Paper read at Joint Automatic Control Conference, June 19-21, at Austin, Texas.

McMahon, Thomas A., and John Tyler Bonner. 1983. *On Size and Life*. New York: Scientific American Books, Inc.

Nagai, Masao, Yutaka Hirano, and Sachiko Yamanaka. 1997. Integrated Control of Active Rear Steering and Direct Yaw Moment Control. *Vehicle System Dynamics* 27:357-370.

Nagai, Masao, Etsuhiro Ueda, and Antonio Moran. 1995. Nonlinear Design Approach to Four-Wheel-Steering Systems Using Neural Networks. *Vehicle System Dynamics*:329-342.

Nakaya, H. , and et al. 1982. Effects of Vehicle Yaw and Lateral Acceleration Response on Drivers Control Performance. Paper read at Proc. of FISITA 19th International Congress, at Melbourne.

NHTSA. 1986. *1986 addendum to The economic cost to society of motor vehicle accidents*. Edited by N. H. T. S. Administration. Washington, DC: Document DOT HS 806 342.

Nuttal, C. J. 1951. Preliminary Study of the Turning Characteristics of Articulated Tracked Vehicles. Hoboken, N.J.: Experimental Towing Tank, Stevens Inst. of Technology.

Nwagboso, Christopher O. 1993. *Automotive Sensory Systems*, *Road Vehicle Automation Series*. London: Chapman & Hall.

Okuno, Akihiro, Atsushi Kutami, and Kenji Fujita. 1990. Toward Autonomous Cruising on Highways. *SAE International Supplement* Automated Highway/Intelligent Vehicle Systems: Technology and Socioeconomic Aspects (SP-833):7-16.

Pacejka, H. B., and I.J.M. Besselink. 1997. Magic Tyre Model with Transient Properties. *Vehicle System Dynamics Supplement* 27:234-249.

Pasterkamp, W. R., and H.B. Pacejka. 1997a. Application of Neural Networks in the Estimation of Tire/Road Friction Using the Tire as a Sensor. *Supplement to SAE International* SP1228 (Research into Vehicle Dynamics and Simulation - 1997):1-8.

Pasterkamp, W. R., and H. B. Pacejka. 1997b. The Tyre as a Sensor to Estimate Friction. *Vehicle System Dynamics* 27:409-433.

Pavlics, F. 1966. Locomotion Energy Requirements for Lunar Surface Vehicles. *SAE* (No. 660149).

Peng, H., and M. Tomizuka. 1990a. Lateral Control of Front-Wheel-Steering Rubber-Tire Vehicles. In *California PATH Report*.

Peng, H., and M. Tomizuka. 1990b. Vehicle Lateral Control for Highway Automation. Paper read at Proceedings of the 1990 ACC Conference, at San Diego, CA.

Peng, H., and M. Tomizuka. 1993. Preview Control for Vehicle Lateral Guidance in Highway Automation. *ASME Journal of Dynamic Systems, Measurement and Control* 115 (December):679-686.

Peng, Huei, Webin Zhang, Masayoshi Tomizuka, and Steven Shladover. 1994. A Reusability Study of Vehicle Lateral Control system. *Vehicle System Dynamics* 28:259-278.

Post, J. W., R. J. Burke, M. V. Drexel, and J. D. Robertson. 1997. An Adaptive Control Model for Lateral Path Following with Closed-Loop Handling Simulations. *Supplement to SAE International* SP-1228 (Research into Vehicle Dynamics and Simulation - 1997):217-231.

Ray, Laura R. 1998. Estimation of Nonlinear Tire Forces and Road Friction for Modeling and Control. Paper read at Advances in Automotive Control 1998 - Proceedings of 2nd IFAC Workshop, 26 February - 1 March 1998, at Mohican State Park, Loudonville, Ohio.

Roelofsen, P. 1995. Active Rear Wheel Steering. M.S., Dept. of Mechanical and Marine Technology, T.U. Delft.

Roos, G., R. Rollet, and R.F.C. Kriens. 1997. Numerical Simulation of Vehicle Behavior during Straight Line Keeping on Undulating Road Surfaces. *Vehicle System Dynamics* 27:267-283.

Rymiszewski, A. J. 1965. Improving Wheeled Vehicle Water Speed by Means of Wheel Shrouding. Warren, Michigan: U.S. Army Land Locomotion Laboratory.

Salaani, Mohamed Kamel, Jeffrey P. Chrstos, and Dennis A. Guenther. 1997. Parameter Measurement and Development of a NADSdyna Validation Data Set for a 1994 Ford Taurus. *Supplement to SAE International* SP-1228 (Vehicle Dynamics and Simulation 1997):99-108.

Salaani, Mohamed Kamel, Gary J. Heydinger, and Dennis A. Guenther. 1997. Validation Results from Using NADSdyna Vehicle Dynamics Simulation. *Supplement to SAE International* SP-1228 (Vehicle Dynamics and Simulation 1997):109-118.

Sano, S. 1986. Four Wheel Steering System with Rear Wheel Steer Angle Controlled as a Function of Steering Wheel Angle. *Society of Automotive Engineers* Paper #860625.

Sano, S., and et. al. 1979. The Effect of Improved Vehicle Dynamics on Drivers Control Performance. Paper read at The 7th International Conference on Experimental Safety Vehicles, at Paris.

Sano, S., and et al. 1980. Influence of Vehicle Response Parameters on Drivers Control Performance. Paper read at FISITA 18th International Congress, at Hamburg.

Sato, H., A. Hirota, H. Yanagisawa, and T. Fukushima. 1983. Dynamic Characteristics of a Whole Wheel Steering Vehicle with Yaw Velocity Feedback Rear Wheel Steering. Paper read at I. Mech. E. Conference Publications, at London.

Segal, L. 1956. Theoretical Prediction and Experimental Substantiation of the Response of the Automobile to Steering Control. *Proceedings of the Automobile Division of the Institute of Mechanical Engineers* 7:310-330.

Senger, K. H., and W. Schwartz. 1987. The Influence of a Four Wheel Steering System on the Stability Behavior of a Vehicle - Driver System. Paper read at the 10th IAVSD Symposium, Aug. 24-28, at Prague, Czechoslovakia.

Serway, R. A. 1990. *Physics for Scientists and Engineers, 3rd Ed.* 3rd ed. 2 vols. Vol. 1. Fort Worth: Saunders.

Sherman, Don. 1995a. Mecedez/Bosch ESP. *Automotive Industries*, April, 84-88.

Sherman, Don. 1995b. Stable as she goes. *Automotive Industries* 175 (May):63.

Shibahata, Y., and et al. 1985. Effects of rear suspension steer properties on handling and stability. Paper read at JSA Conference (in Japanese).

Shibahata, Y., K. Shimada, and T. Tomari. 1993. Improvement of Vehicle Maneuverability by Direct Yaw Moment Control. *Vehicle System Dynamics* 22:465-481.

Shiotsuka, T., A. Nagamatsu, and K. Yoshida. 1993. Adaptive Control of 4WS System by Using Neural Network. *Vehicle System Dynamics*:411-424.

Shladover, S. E., and et al. 1978. Steering Controller Design for Automated Guideway Transit Vehicles. *ASME Journal of Dynamic Systems, Measurement, and Control* 100 (March):1-8.

Sledge, Nathaniel H., and Kurt M Marshek. 1997. Comparison of Ideal Vehicle Lane-Change Trajectories. *Supplement to SAE International* SP-1228 (Research into Vehicle Dynamics and Simulation - 1997):233-255.

Smith, Dirk E., and Robert E. Benton. 1996. Automated Emergency Four-Wheel-Steered Vehicle Using Continuous Gain Equations. *Vehicle System Dynamics* 26:127-142.

Smith, Dirk E., and John M. Starkey. 1994. Effects of Model Complexity on the Performance of Automated Vehicle Steering Controllers: Controller Development and Evaluation. *Vehicle System Dynamics*:627-645.

Smith, Dirk E., and John M. Starkey. 1995. Effects of Model Complexity on the Performance of Automated Vehicle Steering Controllers: Model Development, Validation and Comparison. *Vehicle System Dynamics* 24:163-181.

Sridhar, J., and H. Hatwal. 1992. A Comparative Study of Four Wheel Steering Models Using the Inverse Solution. *Vehicle System Dynamics* 22:1-17.

Steeds, W. 1960. *Mechanics of Road Vehicles: A Textbook for Students, Draughtsmen, and Automobile Engineers*. London: Iliffe & Sons, Ltd.

Sugasawa, F., N. Irie, and J. Kuroki. 1992. Development of a Simulator Vehicle for Conducting Vehicle Dynamics Research. *International Journal of Vehicle Design* 13 (2):159-167.

Sun, J., A. W. Olbrot, and M. P. Polis. 1994. Robust Stabilizations and Robust Performance Using Model Reference Control and Modeling Error Compensation. *IEEE Transactions on Automatic Control* 39 (3):630-635.

Takeuchi, S., and et al. 1985. Analysis of Transient Response Test. *Journal of JSAE (in Japanese)* 39 (11).

Takiguchi, T. , and et al. 1986. Improvement of Vehicle Dynamics by Vehicle-Speed Sensing Four-Wheel Steering System. *Society of Automotive Engineers, #860624*.

Tamaki, K., O. Kiyoshi, K. Ohnishi, and K. Miyachi. 1986. Micro-processor Based Robust Control of a DC Servo Motor. *IEEE Control Systems Magazine*:30-36.

Tomizuka, Masayoshi, and Karl J. Hedrick. 1995. Advanced Control Methods for Automotive Applications. *Vehicle System Dynamics* 24:449-468.

Tousi, S., A.K. Bajaj, and W. Soedel. 1988. On the Stability of a Flexible Vehicle Controlled by a Human Pilot. *Vehicle System Dynamics* 17:37-56.

Tousi, S. et al. 1991. Finite disturbance Directional Stability of the Vehicles with Human Pilot Considering Nonlinear Cornering Behavior. *Vehicle System Dynamics* 20:21-55.

VanZanten, Anton T. , Rainer Erhardt, and Georg Pfaff. 1995. Control of Vehicle Dynamics - Mercedes-Benz AG's ESP. *Automotive Engineering*, May, 87-93.

Wakamatsu, Kiyoshi, Yoshimitsu Akuta, Manbu Ikegaya, and Nobuyoshi Asanuma. 1997. Adaptive Yaw Rate Feedback 4WS with Tire/Road Friction Coefficient Estimator. *Vehicle System Dynamics* 27:305-326.

Weir, D. H., and D. McRuer. 1970. Dynamics of Driver Vehicle Steering Control. *Automatica* 6:87-98.

Whitcomb, D. W., and W. F. Milliken. 1956. Design Implications of a General Theory of Automobile Stability and Control. *Automobile Division, The Institute of Mechanical Engineers*:83-107.

Will, Anthony B., and Stanislaw H. Zak. 1997. Modeling and Control of an Automated Vehicle. *Vehicle System Dynamics* 27:131-155.

Yamazaki, S., O. Furukawa, and T. Suzuki. 1997. Study on Real Time Estimation of Tire to Road Friction. *Vehicle System Dynamics Supplement* 27:225-233.

Yaniv, Oded. 1997. Robustness to Speed of 4WS Vehicles for Yaw and Lateral Dynamics. *Vehicle System Dynamics*:221-234.

Yuhara, Naohiro, Shinichiro Horiuchi, Tomoko Iijima, Kazutaka Shimizu, and Nobuyoshi Asanuma. 1997. An Advanced Steering System with Active Kinesthetic Feedback for Handling Qualities Improvement. *Vehicle System Dynamics* 27:327-355.

Zakin, Ya. H. 1959. O pritchine vozniknovenya pritsepov (The cause of instability of trailers). *Avtom. Promyshlennost (Russian Automotive Industry Journal)* 11.

Zegelaar, P. W. A., and H. B. Pacejka. 1997. Dynamic Tyre Responses to Brake Torque Variations. *Vehicle System Dynamics Supplement* 27:65-79.